The Non-destructive Testing of Adhesive Joints for Environmental Degradation

by:

Keith Adrian Vine

Supervisors:

Prof. P. Cawley

Prof. A.J. Kinloch

A thesis submitted for the degree of Doctor of Philosophy of the University of London.

Department of Mechanical Engineering

Imperial College of Science Technology and Medicine

University of London

Exhibition Road, London, SW7 2BX

August 1999

Abstract

This thesis presents the results of an investigation aimed at producing a non-destructive test for determining environmental degradation of adhesive joints. One of the biggest factors preventing the more widespread use of adhesive joints is the adverse effect that wet environments have on their performance coupled with the lack of a reliable non-destructive technique for assessing the extent of this reduction in performance. This thesis has attempted to determine the suitability of ultrasonic techniques for detecting environmental degradation, specifically of aluminium epoxy joints typical of those used in the aerospace industry. Degradation of this type of joint is one of the factors that may determine the serviceability of many ageing aircraft. It was also hoped that a greater understanding of the mechanisms of degradation would be attained.

Ultrasonic techniques were identified as being the most promising for assessing the degradation of adhesive joints, with normal and oblique incidence techniques being used. Mechanical tests and surface analysis techniques were also used to quantify and explain the degree of degradation that specimens had undergone in a hot wet environment.

Several possible mechanisms of water ingress were identified. The most readily identified of these was through edge disbonds, which was easily detected using ultrasonic methods. Diffusion of water through the epoxy layer was also seen to occur and could be predicted, but could not be related to a loss of toughness. With the epoxy used for this work water diffusion through the epoxy layer could not be detected non-destructively. Evidence was also seen for the penetration of water through flaws in the epoxy layer and this was thought to be the mechanism responsible for a loss in toughness across large areas of some of the specimens. Small spot disbonds were seen to form around flaws in the epoxy layer. Detection of these small spots and the flaws in the epoxy layer was possible non-destructively, but only given sufficient spatial resolution. There was also some evidence to suggest that there was water ingress along the interface in some specimens. It was concluded that the most suitable technique for inspecting adhesive joints for environmental degradation is high frequency, highly focused normal incidence ultrasound.

Acknowledgements

There are a large number of people that I need to thank for the invaluable help and support that have I been given during the course of this thesis. There are all the members of the N.D.T. group who have made the last few years so enjoyable, including (in no particular order) Andrew Chan, Bruce Drinkwater, Michel Castaign, David Alleyne, Paul Wilcox, Brian Pavlacovic, Mark Evans, Brent Zeller, Mike Lowe, Roger Dalton, Pierre Marty, Arnaud Bernard, Christophe Aristegui, Jon Allin, Malcom Beard, Thomas Vogt, Rob Long, Stephane Baly, Olivier Diligent and Carolin Gatelier.

Particular thanks needs to go to my two supervisors, Professor Peter Cawley and Professor Tony Kinloch for invaluable guidance and the reading of this thesis.

Special thanks also go to my parents and more especially Sally for their help in proof reading of this thesis but more importantly for their constant support.

I would further like to thank the technicians of the adhesive lab, Peter Savage, Scott Innes and Tom Robinson for wonderful technical support along with Nick Tailor. Thanks also to Dr. Watts for generously allowing the use of his facilities and Steve Greaves at the University of Surrey for all of his help with the XPS work. Finally thanks also to Dr. Bruce and DERA for their financial support and technical discussions.

Table of contents

List of Figures

List of tables

1. Introduction

1.1 The advantages of adhesive bonding

Adhesive bonding has been used in engineering for many years, in particular in the aerospace industry. There are several reasons for the rapid expansion in application of adhesive bonding over the last century. There are many benefits in the use of an adhesive bond over other fastening techniques [1, 2]. Amongst these can be listed the weight saving that a bonded structure can command in comparison with a structure employing mechanical fastening methods. Adhesive bonding also allows the joining of dissimilar materials, can avoid the potentially damaging effects of heat, is well suited to joining thin sheets and benefits from a uniform distribution of stress over the whole area of the joint. There is also the chance to improve the aesthetics and performance of structures that are bonded due to the unobtrusive nature of a bonded joint e.g. the bonding of wing skins as opposed to rivets. These advantages can combine to allow the design of structures which would otherwise be very difficult without adhesive. The construction of honeycomb sections is an excellent example of this in which extremely stiff yet light weight panels can be produced.

The developments in adhesive bonding can be seen to be linked with that of polymers, as almost all structural adhesives employed over the last five decades have been polymer based. Synthetic polymers offer the essential characteristics for producing a load bearing assembly. They are applied in an essentially liquid form, which allows the adhesive to make intimate contact with both substrates, and then during cure the polymer cross links to form a relatively tough material capable of carrying the loads imposed by the structure. They can also offer advantages in the assembly of structures allowing easy automation, and in the automotive industry for example, the adhesive cure can be incorporated into the same process step as the paint curing.

1.2 The disadvantages of adhesive joints

With so many potential reasons in favour of adhesive bonding there are issues which need to be addressed before all of these benefits can be realised in a wider range of applications. Principal amongst these is the poor performance of adhesive bonds in the presence of moisture. This effect is evident as a reduction in the adherence between the adhesive and the adherends. This reduction in durability has been recognised for many years, and much has been done to rectify this problem. In the case of bonding of aluminium this has involved increasing use of sophisticated surface treatments of the aluminium prior to bonding. The subject of environmental degradation of adhesive joints is covered in great detail by Kinloch [1], with many contributions from other authors covering all aspects of joint degradation.

The effect of moisture may be very small in terms of changes to the adhesive and the adherends but the effect on the overall strength of the joint can be disastrous. This means that the physical manifestation of moisture in adhesive joints can be extremely small and it is this which results in another reason for the impeded use of adhesive bonding: the lack of suitable technique for detecting the strength reduction in adhesive joints due to moisture. It is this problem that this thesis attempts to address.

Non-destructive techniques for the inspection of structures to ensure their integrity both during manufacture and their service life form an essential part of engineering today. A reliable non-destructive testing (NDT) technique allows for less over-engineering of components, which drives down cost by using less material and in the case of any moving machinery increases efficiency with all the benefits that this brings. As mentioned above, the problem with the durability of adhesive joints lies at or around the interface of the adhesive and adherend, as opposed to any change in the bulk of either material. This is where the problem for any current NDT technique lies.

1.3 Current NDT techniques and application to adhesive joints

There are a large number of NDT techniques which cover a broad range of inspection problems, and new techniques are evolving rapidly. However, of these existing techniques, few have shown any significant promise for the detection of weak interfacial strength in an adhesive joint. This section will briefly discuss techniques

that are available and in development, and examine their applicability to adhesive joints, and most particularly to the question of poor adhesion [3-5].

Table 1.1 lists a range of potential NDT techniques, many of these techniques have some application in the inspection of bonded structures, with associated advantages and disadvantages. However in determining the suitability of a given technique for the inspection of an adhesive joint we must be aware of the potential defects that we are likely to encounter and how sensitive a given technique is to each type of defect. The range of defects that may be encountered in adhesive bonding vary from total absence of adhesive to poor interfacial strength between the adherend and adhesive. Between these extremes are problems within the adhesive layer such as cracking, porosity or voiding and poor mechanical properties of the adhesive such as

Technique	**Potential for inspection of adhesive joints**
X-ray[6]	Some
shearography[7]	detection of disbonds
thermography[8]	as above
holography[9]	as above
ultrasonics[3]	excellent, the most commonly used
microwave[10]	poor
visual	poor
radar	poor
dye penetrant	none
MRI[11]	detection of state of cure and possibly presence of moisture
eddy current[12]	poor
dielectric[13]	detection of state of cure and possibly presence of moisture
neutron radiography[6]	properties/presence of adhesive
mechanical impedance [14]	poor
IR spectroscopy[2]	moisture detection

Table 1.1 Summary of N.D.T. techniques available.

those due to incomplete cure. We may also wish to detect variations in the bondline thickness. The performance of some bonds is highly dependent on the presence of a suitable pre-treatment of the adherend. For example the durability of a bond between aluminium adherends is highly dependent on the formation of an oxide layer on the aluminium prior to bonding. This then gives a very broad range of attributes required of a non-destructive test to detect all of these possible problems. The common trade off between sensitivity/accuracy and speed must also be considered. If these potential defects are split into categories ranging from the grossest, missing or misplaced adhesive to the most subtle, weak interfacial strength, we can determine the suitability of the range of techniques at our disposal and the benefits that each technique has.

For the problem of missing adhesive there is the broadest range of techniques available, and it is the compromise between time, resolution and money that affects the technique used. Techniques that have been proven to be suitable for this include ultrasonics, thermography, shearography, holography, neutron radiography and X-ray. X-rays are not best suited to many of the problems associated with adhesive bonding for one main reason. A photographic exposure made using X-rays primarily shows variation in the permeability of the sample to X-rays. When bonding metals there is a huge contrast between the permeability of the metal and the adhesive in the joint. However the absence of adhesive can be detected by using a high contrast penetrant. Similar to X-ray radiography is neutron radiography, but in this case the X-ray source is replaced with a neutron source. This has the advantage that there is much less contrast between metals and adhesive, making adhesive loss easier to detect, and like X-ray, large areas can be inspected in a single exposure. The big disadvantage lies in the cost and risk associated with the neutron source. A detailed article on the use of X-ray and neutron radiography for the inspection of aircraft structures was produced by Smith [6].

Themography is particularly suited to the detection of voiding or missing adhesive when thin adherends are being used. This has been shown to be particularly effective for the detection of core/skin disbonds in honeycomb panels [15]. The sensitivity of thermography varies with the depth of the defect, becoming less sensitive the deeper the defect. The biggest advantage is its ability to inspect relatively large areas in a single shot, making it very useful as rapid screening tool. The use of thermography is investigated by Reynolds [8]. Very similar advantages and disadvantages exist for both shearography and holography. However these methods detect variations in the deformation of a structure when a stress is applied. This

requires relatively large defects to ensure detection, and also becomes less sensitive with thicker adherends [16] [7].

Probably the most common way of inspecting adhesive joints has been by using ultrasonic techniques [5]. In general a normal incidence approach has been used. More detailed description of ultrasonic testing will follow in further chapters, but there are several advantages and disadvantages that can be identified. Amongst the advantages are the fact that missing, voided or misplaced adhesive can be easily detected and in typical aerospace joints the resolution that can be achieved is sub millimetre. However it is the disadvantages which have often left people seeking a more convenient alternative. The primary disadvantage is that the structure that is to be tested needs to have ultrasound coupled to it. This is usually done with water coupling, either by immersion or water jets. This makes the testing of porous materials extremely difficult. The other major problem is the time taken, as with conventional ultrasonics the probe needs to be moved over every part of the structure to be tested. On large structures this can be extremely time consuming.

When we move to problems within the bulk of the adhesive the number of techniques that are suitable is reduced considerably. We are left with a few techniques with some proven suitability and others which are still in development. The main problem that is likely to affect the performance of a joint in this area results from poor curing of the adhesive. Most reliable for detecting this is shear wave ultrasonics. This is due to the curing of an adhesive resulting primarily in an increase in its shear modulus [17], which rises from zero with the adhesive in liquid form. However, the Young's Modulus of the adhesive also rises during cure, allowing normal incidence techniques to be applied to this problem [18], with the advantages of convenience, particularly if spatial information is required. Other possible techniques include Magnetic Resonance Imaging (MRI) and dielectric measurements. MRI is able to detect changes in the relaxation time of polar molecules, which is related to the state of cure of the adhesive [11]. However it is neither cheap nor convenient. Dielectric measurements are capable of detecting both water absorbed in the adhesive and free water at the interface [13]. One of the problems with dielectric measurements is that the entire joint is treated as a capacitor, so results obtained are an average over the whole joint. Therefore changes in a small, but significant, area of the joint could easily be missed. Detecting poor cohesive properties in the adhesive can be thought of as primarily as a process or quality control procedure, ensuring that the joint has been made correctly.

1.4 Detecting weak interfaces

The problem of poor interfacial properties is the one that has had a large amount of research devoted to it [19-23], and still has no reliable techniques available. The majority of research in this area has concentrated on ultrasonics in various forms, the reasons for which will be discussed in more detail. However there are many difficulties associated with determining the interfacial integrity of an adhesive joint. There is a large amount of experience within the adhesive community as to what will produce a good bonds, and what conditions are liable to give poor bonds. The production of durable bonds in the case of aluminium joints is governed largely by the pre-treatments; this covered in detail by Brewis [24]. However there is limited knowledge as to exactly what changes within an adhesive joint to reduce its interfacial integrity and produce interfacial failure when in an as-made condition the joint would fail cohesively. It is clear that the presence of moisture is key in the deterioration of the interfacial toughness of a bond [25], but the exact mechanisms by which water reduces the bond strength are unclear. This is partially due to the difficulty in examining the interface of the bond prior to failing the joint, for obvious reasons. After the interface of the joint has been exposed to the environment, changes to its chemistry and morphology can occur rapidly. This a problem where a reliable N.D.T. technique could help in the understanding of the mechanisms of strength loss in adhesive joints and possibly be used to improve the durability of bonds. However it is clear that the presence of moisture in an adhesive joint is one the key factors in reducing the bond performance. The measurement of joint performance is largely concerned with the toughness of the joint as opposed to the absolute strength of the bond, where toughness can be described as the ability of the joint to resist crack growth.

Many N.D.T. techniques have concentrated on the detection of water in an adhesive joint. The presence of water in joints can be divided into two types; there is the presence of free water, either at the interface or trapped in voids in the epoxy, or there is water that has been adsorbed by the adhesive. There is a range of techniques that can be used for the detection of water in joints, ultrasonic techniques, dielectric measurements and MRI are amongst the most common [2] [13]. All of these techniques have the potential of allowing some measure of the amount of water that has entered an adhesive joint; however that alone is no measure of the integrity of the bond. The performance of these different techniques may well vary with different adhesives. For example the effect of water on an unmodified epoxy resin can be negligible when using ultrasound [26], but adhesives such as FM1000 show a large

increase in attenuation during the absorption of water (see Appendix B). Moreover if we are to understand the effects of water on an adhesive bond then simply detecting the presence of water is not sufficient. It would be most beneficial to use a technique that allows some measurement of the interfacial properties to be made. Given that an adhesive joint is produced to carry stress, ultrasonics techniques appear to stand alone as an N.D.T. technique which actually gives a measure of the ability of an interface to carry stress (the stresses generated for ultrasonic N.D.T. are extremely small but a measurement of a mechanical connection is made). It also allows interrogation of an interface which is not directly accessible. In the case of bonded aluminium structures the durability of the bond is determined largely by the oxide layer which is produced prior to the forming of the bond. Ultrasonic methods allow the measurement of the elastic constants of this layer [27] [28], although there are physical limits to the thickness of layer that can be measured when using the thickness of adherend that is typically used in an adhesive joint. These limits will be discussed in more detail in Chapter 2.

1.5 The effect of surface preparation

The improvements that can be obtained in the performance of an adhesive joint through variations in the way the aluminium surface is prepared prior to bonding have been recognised for many years. (It is the bonding of aluminium that we are concerned with for the purposes of this thesis). The better pre-treatments no doubt stem from the experience with the use of aluminium before bonding was an issue, when anodising was used to improve the corrosion resistance of aluminium [24] . This became more important with the introduction of higher strength alloys which are more prone to corrosion. Many of these treatments have since been optimised for bonding, giving us the range that sees common use today. These range from simply degreasing the surface (i.e. cleaning), through grit blasting, etching to anodising. The following descriptions largely follow those given by Alberiici [29].

1.5.1 Clean and degrease

Cleaning and degreasing of the surface to be bonded is the simplest form of pre-treatment, and the simplest form of bonding of any kind requires that the surfaces to be bonded are clean and free from grease or contamination. However this is rarely considered sufficient for any form of structural bond of aluminium, and can be expected to produce a joint that will fall apart rapidly if left in any moist environment.

1.5.2 Grit blast

Grit-blasting is primarily a pre-treatment that is designed to improve the mechanical performance of a joint by increasing the surface area of the bond. Figure 1.1 shows the surface of grit blasted aluminium. It is immediately obvious that grit blasting the surface has increased the area. However it has been reported that it is possible for the surface to be so contorted that adhesive may not be able to fully wet the surface [30]. However this pre-treatment is not to be recommended when the joint is to be exposed to moisture rich environments [24], but is often used in conjunction with the surface preparations which are described next.

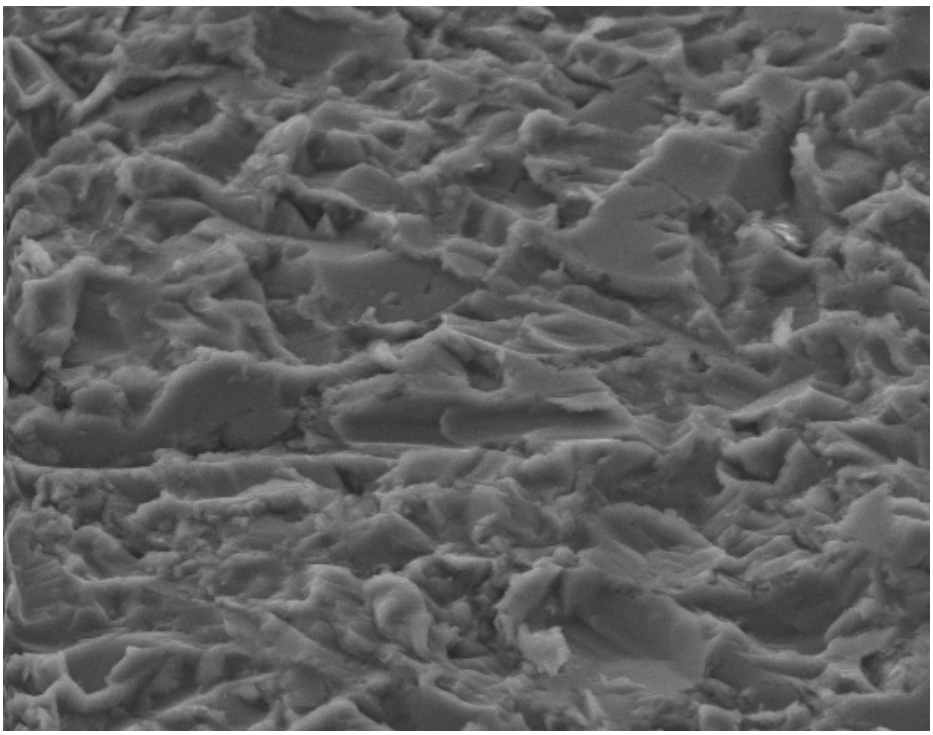

Figure 1.1 aluminium grit blast surface.

1.5.3 Chromic acid etch

This etch process is primarily used to remove the original less stable oxide layer; it replaces it with a very thin and more stable oxide layer (~30nm thick), which consists of a shallow pore within a shallow blister, with whisker-like protrusions between adjoining cells, see Figure 1.2. This morphology is thought to produce reasonable interlocking between the oxide and the adhesive, albeit on a very small scale [30]. This process involves a thorough cleaning of the aluminium prior to the etching which consists of 30 minutes in chromic acid at 68° C. It is during the

following rinse that the oxide is built up, although only to the extent of a few hundredths of a micron. This oxide layer, unsurprisingly, gives relatively poor corrosion resistance. The exact processing conditions for this pre-treatment are given in Appendix A. This a European etch standard, and is similar to the Forrest Products Laboratory etch that is used in the USA.

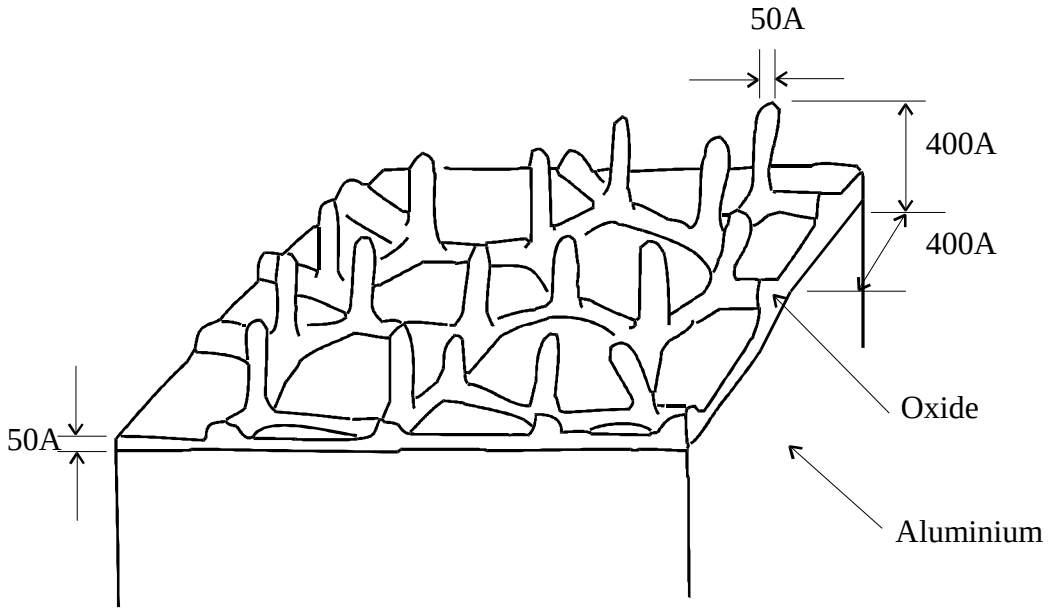

Figure 1.2 Schematic of CAE oxide structure, after [31].

1.5.4 Chromic Acid Anodise

This is the pre-treatment used primarily by the European aerospace industry. This treatment produces a dense oxide layer around 3.5μm thick, with narrow pores. This process was originally chosen for its good corrosion resistance. However when it was being used more for bonding applications then the process was optimised to produce as open a pore structure as possible. A schematic of this oxide layer is shown in Figure 1.3. There is thought to be little keying between the adhesive and this oxide [29]. The advantages of this layer are that it has good corrosion resistance, and produces an interface which is difficult for water to penetrate along.

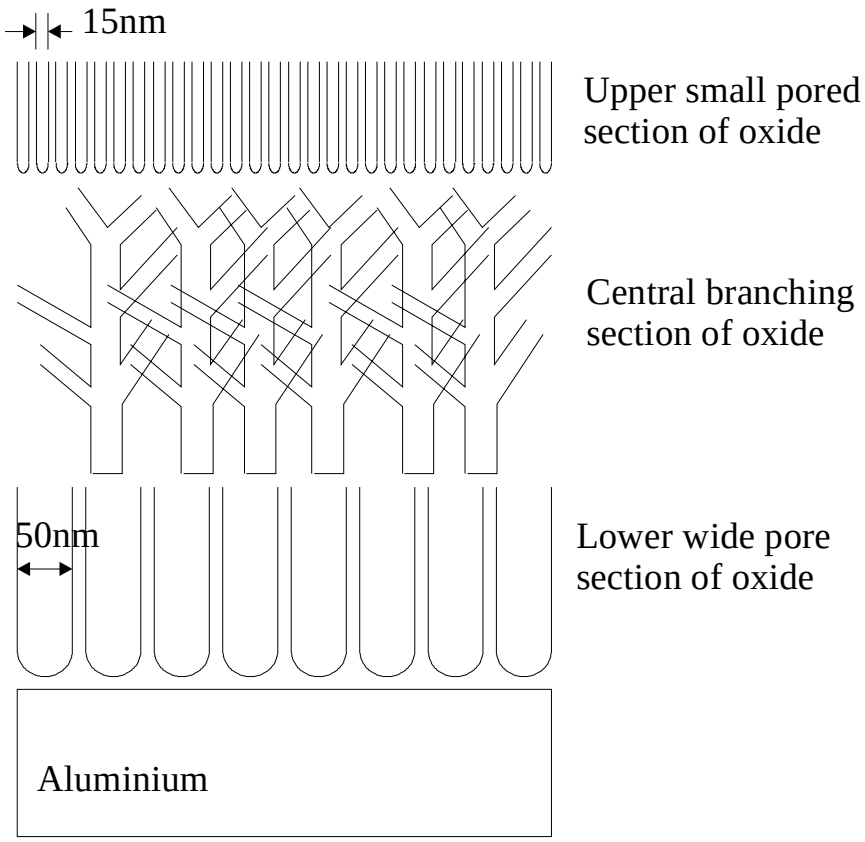

Figure 1.3 schematic of CAA oxide layer, after [32].

1.5.5 Phosphoric Acid Anodised

This treatment was developed by Boeing in the late 1960's and 1970's to improve upon other anodic films, which they considered unsuitable for bonding primary structure. Initially the PAA film may appear to be unsatisfactory because it is a very thin and open film which was known to be a poor corrosion inhibitor. However its success may come from its very open structure, which allows for very good interlocking with the adhesive. The structure of this oxide is in many ways similar to that produced by the FPL etch, but it is considerably thicker (0.4 - 0.6μm), see Figure 1.4. It has been shown that primers and epoxies can penetrate well down into this porous oxide [31]. One of the advantages of this treatment is that is less sensitive to the anodising conditions than the CAA, making it easy to apply in industry. There is also the advantage that polarised light can be used as an inspection technique immediately after anodization as an easy check on the uniformity of the anodic film [24]

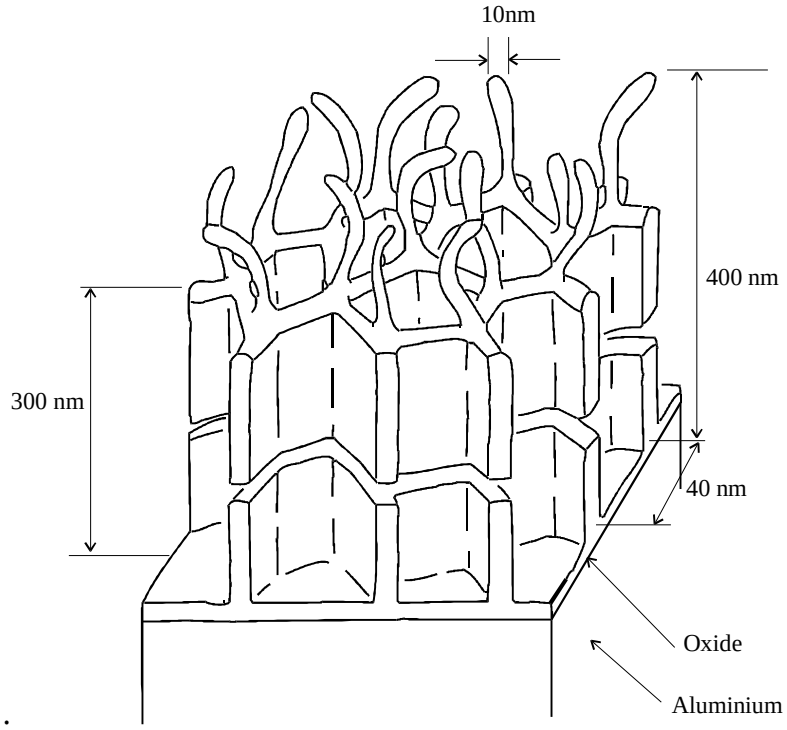

Figure 1.4 Isometric of PAA oxide layer, after [31].

1.6 Effect of pre-treatment on durability

Much work has been done by the adhesives community to assess the effect of pre-treatment on durability. There are large amounts of data that show the effect that various pre-treatments have on a range of durability tests [32] [1] [29]. It is clear from this durability data that if a joint is to have any significant life in a harsh environment then anodisation is essential, but even the more simple etch treatments give a significant improvement to joint durability. Simple grit blasting has little effect on the longevity of a joint, except for the fact that it may start off with a higher strength than an untreated aluminium surface due to the large increase in surface area available for bonding[24]. The oxide layer which will still be present in this case is that naturally occurring on aluminium. There are at least two reasons for the poor durability of grit blasting. The naturally occurring oxide layer is less stable than those produced by anodising or etching, being more susceptible to corrosion. However this alone is not sufficient. For corrosion to start there must be a supply of oxygen and water. The amount of water thought to be necessary is very small [33], but some work has suggested that the extremely contorted surface of a grit blast aluminium can be too contorted to allow for complete wetting by the adhesive. This incomplete coverage of

a less corrosion resistant oxide layer is then the most likely reason for the poor durability of simple grit blast aluminium joints.

This then suggests that to produce a durable bond we need to produce a stable oxide layer and ensure that any polymer covering completely wets the surface, preventing the free passage of water to the interface. This is exactly what both the etch and anodise treatments aim to do. They all have in common the fact that they produce an open oxide structure, with the most significant difference being the oxide layer thickness. The importance of the epoxy penetration into the oxide layer is highlighted by the PAA treatment which produces a highly open oxide structure, which left open will corrode much more rapidly than other anodised surfaces, but has good durability when used in adhesive joints (particularly when a primer is used, which ensures that the pores in the oxide are filled [31] [24]). This is also the reason that a CAA surface is not sealed prior to bonding, which it would be if the treatment were simply for corrosion protection. Sealing of an oxide layer is done by dipping in boiling water, which produces excess oxide which fills over the top of the pores, preventing water from entering the oxide layer. (This is how coloured surfaces are produced, a coloured dye being sealed into the oxide layer).The corrosion protection offered by the oxide layer cannot be the only consideration as it has been found that joints made with pre-treatments like sulphuric anodising have poorer performance, and this is due to the brittleness of the oxide layer, as failure will occur within the oxide layer, regardless of whether the specimen is wet or dry [24].

1.7 Effect of water

There are many potential effects that water may have on a adhesive joint, affecting the adhesive, adherend and the interface between them. Some of the effects are well understood, whereas others are less clearly defined. It is particularly those that affect the interface that are not so well defined.

The effects of water on adhesives will vary with the type of adhesive, but we will consider only epoxy resins of the type used in the aerospace industry. Adhesives absorb water and this can change their mechanical properties. The rate at which they absorb water can be measured in water uptake experiments, and this allows the amount of water that has entered a joint to be calculated assuming Fickian diffusion [34]. Generally water will plasticise the adhesive, toughening it [25]. The diffusion rates for different adhesives vary enormously, as will the change in their mechanical

properties. Whether these changes will be detectable ultrasonically needs to be verified for each type of adhesive. However the absorption of water into the adhesive has been seen as an increase in attenuation (appendix B). Also as the mechanical behaviour of polymers is highly non-linear [35], changes in low rate mechanical properties cannot always be expected to map across to the strain rates that are used in ultrasonic testing. Water can also cause cracking or crazing of the adhesive and induce swelling stresses [36].

Absorption of water by the adhesive is only one transport mechanism for water to enter a joint. It is not clear that a saturated adhesive layer at the adhesive/adherend interface is sufficient to cause any weakening of the bond, but it is possible for water to cause weakening of the interface by displacing the epoxy [1] or causing hydration of the oxide, with the hydrated oxide being considerably weaker than the original oxide. Also any voiding at the interface maybe sufficient for free water to accumulate and this can lead to corrosion and disbonding. The behaviour of free aluminium/oxide surfaces is well documented and the changes that can be expected in the presence of moisture are clear [37]. Davies and Venables describe the hydration of a chromic acid etched surface, [31] whereby the hydration of the oxide layer is sufficient to weaken the aluminium/oxide bond, and so the failure of the joint is through the aluminium/oxide interface. They also report that the hydrated oxide thickness is three times that of the original oxide layer. This hydration process changes the oxide from Al_2O_3 to crystallites of boehmite ALOOH. This can easily happen at the edges of the joint, where corrosion can start on the uncovered aluminium surface and undercut the bond. It is for this reason that edges of joints that are to be exposed to harsh environments are always protected against corrosion. However similar problems will result if there are paths for free water along the adhesive or interface. This can be water wicking along a carrier film in the adhesive or along a poorly wetted interface or by capillary action along cracks or crazes in the adhesive. There is also a need to ensure adequate protection of the bulk adherend as failure in the adherend can be a problem in highly corrosive environments, such as salt spray [1].

Leidheiser [33] identifies more than ten mechanisms through which a polymer coating can become “unstuck”. However nearly all of these mechanisms have in common the fact that they require water for the de-adhesion process to commence. He also suggests that water will often travel along preferred pathways in the adhesive, as opposed to a uniform advance, and that these pathways may be left by the removal of solvents during cure of the polymer.

It is clear that water can have a wide variety of effects on an adhesive joint, and these are likely to vary from small scale changes due to water entering at microscopic flaws, or they may be changes to the mechanical properties of the bulk adhesive due to the adsorption of water.

1.8 Aims

The problem that we set out to solve at the beginning of this thesis is as follows; a non-destructive technique is sought that can be used to reliably determine the extent of degradation that an adhesive joint has suffered from exposure to harsh environments. Specifically we are concentrating on the bonding of aluminium as is typically used in the aerospace industry and would be applicable to the large numbers of aircraft that have used adhesive bonding since the end of the second world war. As part of solving this problem it will be necessary to develop an understanding of the mechanisms that are involved in the degradation of bonds by harsh environments which includes mechanisms of water transport through the adhesive and along the interface, and the effect that the moisture may have on the bond between the adhesive and adherend. It is hoped that a greater understanding of the mechanisms of degradation of adhesive joints will be gained from this work.

1.9 Outline of Thesis

Chapter 2 discusses the different experimental techniques that have been used in this project. This includes a detailed study of ultrasonic methods that had been developed prior to this work. Also included in this chapter is a detailed description of the specimens, covering the materials and processes used and the type of environment used for degrading them. The mechanical tests that have been performed on bonds are also described, along with the analysis of the raw data used to obtain fracture toughness values for both specimens that had been degraded and those stored dry. This is followed by a description of the surface analysis techniques that have been used to quantify the changes that have occurred to the specimens as a result of environmental effects.

Chapter 3 looks at the results that have been obtained from the two-layer specimens. (This specimen type is a single aluminium plate with an epoxy layer cast on it and is designed to degrade quicker than a conventional sandwich joint.) The

results are divided into three sections; the ultrasonic results, mechanical test results and results obtained from analysis of the failure surfaces. The chapter concludes with a summary of the two-layer specimen results.

The results obtained from a more conventional three-layer specimen are presented in Chapter 4. The results are presented in the same order as used in the preceding chapter. The end of the chapter has a summary of all of the results obtained from the three-layer specimens.

A detailed analysis and discussion of the results that have been presented in the previous two chapters is given in Chapter 5. This is where the results from the three major areas of investigation are drawn together to produce a coherent view of the degradation process that the specimens have undergone. The connections that exist between the results obtained from the two specimen types are also discussed.

Conclusions are presented in Chapter 6. Much of this concerns the mechanisms of degradation that have been identified from this work. The implications of these mechanisms are presented and a best approach for the non-destructive examination adhesive joints is proposed.

2. Specimens and Experimental Techniques

2.1 Introduction

The first part of this chapter describes the specimens that were used for this work. One of the prime considerations for the specimens was that the results obtained from the non-destructive test would be as clear as possible, leaving as little probability of misinterpretation as possible. It was also hoped that the specimens would give clear results as to the mechanisms by which degradation occurred, which influenced their design. The following sections describe the experimental techniques that were used. These are discussed in the same order that they were applied to the specimens. First are the non-destructive testing techniques (almost exclusively ultrasonic). The ultrasonic techniques have been divided into three sub-categories; first is normal incidence reflection coefficient measurements; second is oblique incidence reflection coefficient measurements; third is scanning of the specimens, which is essentially giving spatial information about the first two techniques. This is followed by the mechanical tests that have been used to measure the toughness of the interfaces of the specimens after exposure to a harsh environment, and also for those that have been stored dry. Finally there are surface analysis techniques, that have been used to determine the reasons for any change in toughness observed between specimens, or defects detected ultrasonically.

2.2 Specimen Design

2.2.1 Consideration from previous work

Previous work by Pialucha [38] [26] used a specimen design shown in Figure 2.1. This had been chosen so that water would gain access to the interlayer via diffusion through the epoxy layer. This allows for relatively accurate assessment of the amount of water in the epoxy adjacent to the interface. These specimens featured a circular epoxy region, of diameter 100mm and 2mm thickness cast on a 4.5mm thick

aluminium plate. Various oxide layers had been produced on the aluminium ranging from the extremely thin layer produced by etching, through CAA and PAA described earlier, to sulphuric acid anodised samples with oxide layers in the 10's of μm thickness range.

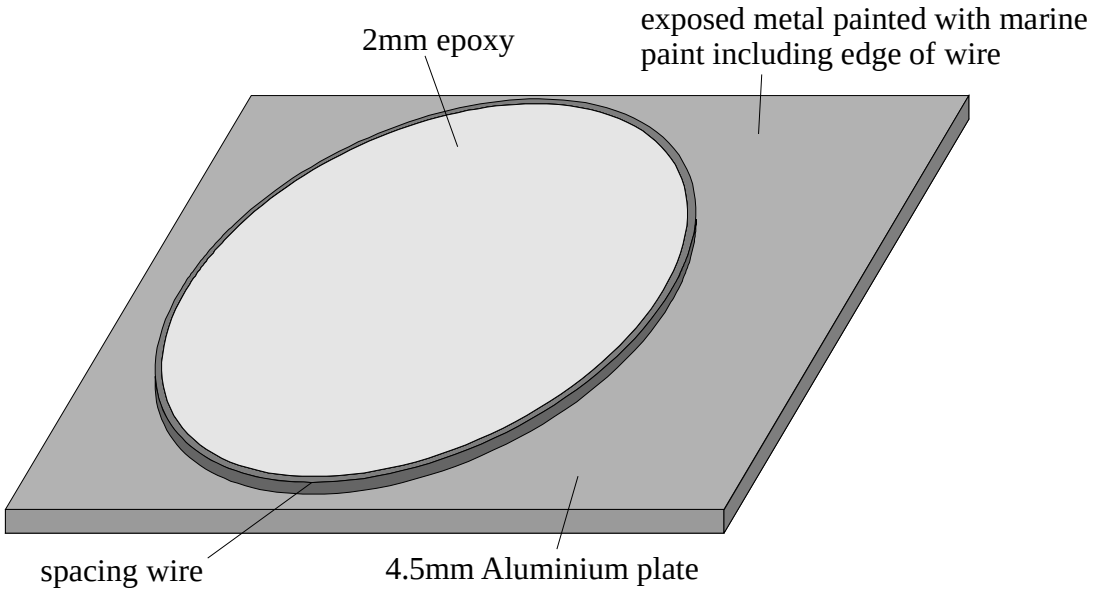

Figure 2.1 Two-layer sample used by Pialucha

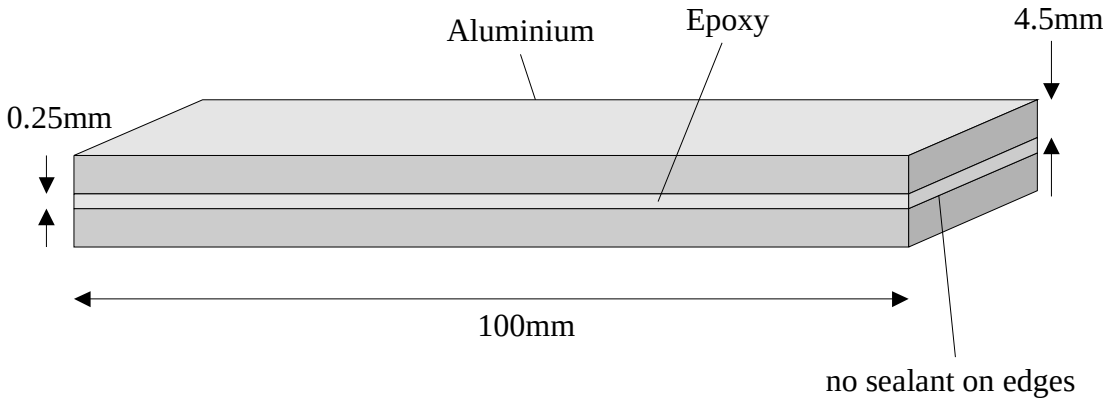

Figure 2.2 Three-layer sample used by Pialucha

However monitoring of these samples after considerable time immersed in water showed no signs of change in the reflection coefficients that were being monitored. There was also no visible sign of change at any position on these specimens, across the entire range of pre-treatments used. At the same time as these 2-layer specimens were made there were also a range of 3-layer specimens made, using the same epoxy and pre-treatments as the 2-layer specimens. These are shown in Figure 2.2.

These 3-layer specimens were exposed to the same conditions as the 2-layer specimens and in the same period that produced no change in the 2-layer specimens many of these 3-layer specimens had fallen apart. The main difference between these specimens was that the 3-layer samples were not sealed along the edge, allowing water direct access to the interface. In light of these results it was considered necessary to produce specimens where water was able to gain access to the interface in the same manner as the 3-layer specimens used by Pialucha. It was also desirable to have a specimen that allowed ultrasonic inspection to the very edge of the bondline.

2.2.2 Two-layer specimen design

The overall design of the two-layer specimens was motivated by several different ideas. We wished to determine the degree to which having unsealed edges would affect the failure rate of the specimen and to what extent we would be able to detect ultrasonically the differences that the unsealed edge would introduce. This would be facilitated by having an overlap of adherend from the bondline so that an ultrasonic scan could probe to the edge of the adhesive. However it was felt that this may influence the way in which degradation progressed and so to make the specimen more representative of an in-service joint, flush adherend/adhesive edges were also incorporated. This led to four different edge conditions being incorporated in the specimen, shown in Figure 2.3. The plate size was chosen to give ample separation between the edges so that effects caused by the different edge conditions could be separated. The 2mm epoxy layer thickness was chosen for two reasons. Being 2mm thick allows plenty of separation between ultrasound reflections from within the specimen, making the reflection from the aluminium/epoxy interface easy to isolate. This is more of a consideration for the oblique incidence technique than for normal incidence for reasons that will be discussed in the following sections. The aluminium

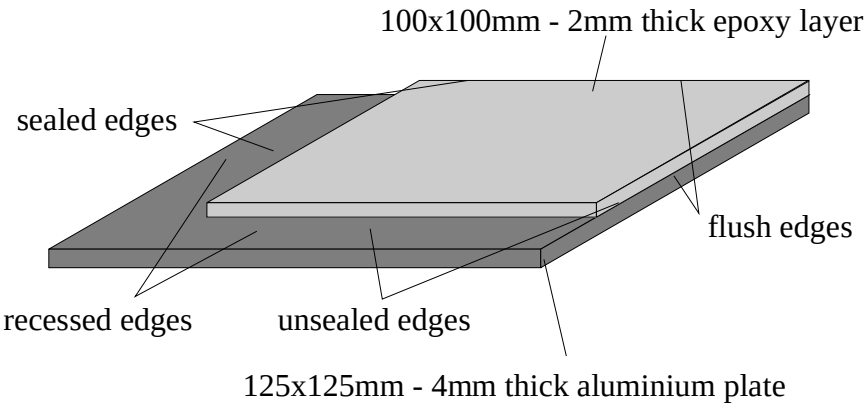

Figure 2.3 Two-layer specimen design.

plate thickness was chosen at 4mm to suit the focal length of the highest frequency focused probe available to use at the time. There were also considerations for the mechanical tests and the flatness of the specimen which influenced the thickness of the aluminium, and these are discussed in the relevant sections.

2.2.3 Two-layer specimen manufacturing method

The earliest specimens of this type were produced by simply clamping a metal template with a 100x100mm square hole to the aluminium plate and pouring in the degassed epoxy to a depth exceeding 2mm. Two edges of the plate were then machined to produce the flush adherend/adhesive interface, and the epoxy layer was machined back to 2mm uniform thickness. The edges to be sealed were then painted with a two-part marine paint. Several of these early specimens with simple degrease pre-treatments showed problems with this manufacturing method. When the adhesive started to debond it bowed markedly, suggesting that there was considerable residual stress. It was also felt that it would be difficult to produce consistent specimens because of the difficulty of machining such a brittle epoxy, with the possibility of introducing minor flaws that could affect the performance of the specimen. Also, when using more durable pre-treatments the edge machining would remove the protective oxide layer, thus allowing undercutting corrosion to accelerate the failure of the specimen and so not be a true comparative test of the durability of the pre-

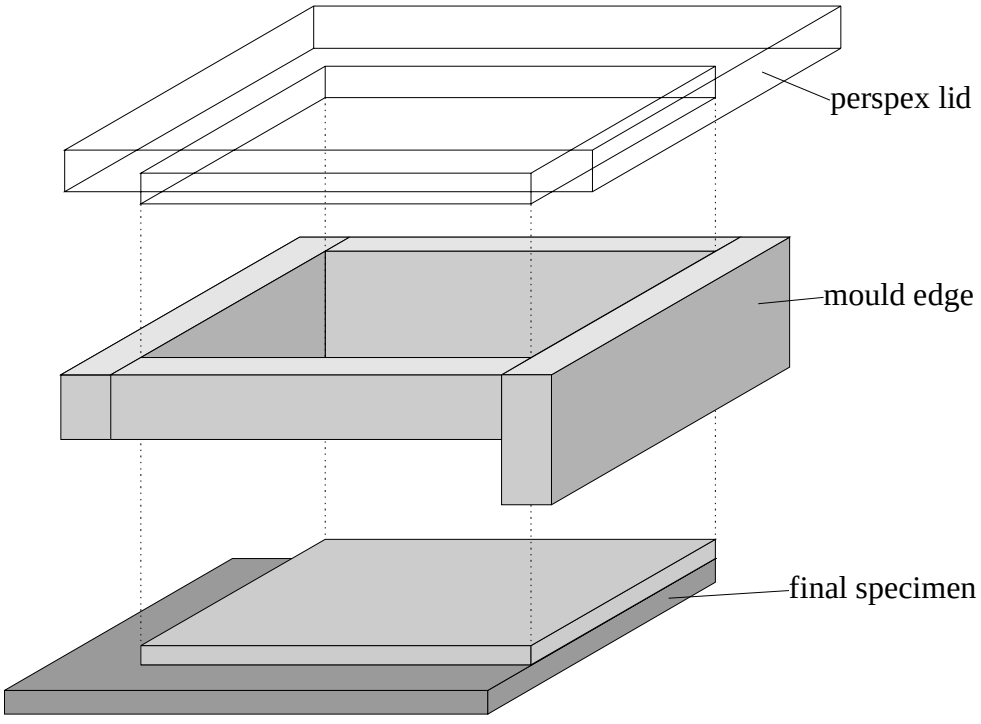

Figure 2.4 Mould used to manufacture two-layer specimens.

treatments.

To overcome these problems a new method was used. This involved producing a mould into which the epoxy was poured, with the aluminium adherend forming one side of the mould cavity. This is shown in Figure 2.4. The mould edge and the perspex lid were coated with mould release prior to the epoxy being poured. A vent hole was made in the perspex lid so that excess epoxy and trapped air would escape as the lid was pressed down onto the mould edge. After 24 hours of curing at room temperature the specimen was removed complete and required no machining. The finish of the free epoxy surface of the specimen was determined by the finish of the mould cavity side of the perspex lid, which was kept polished. This generally left the specimen with an epoxy layer clear enough for a good visual assessment of the interface.

2.2.4 Three-layer specimen design

The three-layer specimens incorporated many of the same ideas that were present in the two-layer specimens. The different edge conditions were kept the same i.e. there were two sealed edges and two unsealed, with one of each of these having a flush adherend/adhesive edge and the other a recessed adhesive layer. The major difference, apart from the presence of the second aluminium adherend, was that the epoxy layer thickness was reduced to 0.2mm, which aimed to be more representative of a structural adhesive joint. A schematic of a three-layer specimen is shown in Figure 2.5. The CFRP shims were used during joint manufacture both to control the bondline thickness and to generate the recessed edges. The specimens were made by laying silicon gel covered CFRP shims on the surface of the lower adherend as shown in Figure 2.5, pouring the epoxy onto the lower adherend and slowly bringing the top adherend down onto the epoxy, carefully squeezing air out to the edges. The shims were covered in silicon gel both to act as mould release so that the shims could be removed after the epoxy had cured, and also to hold the shim in place and prevent epoxy seeping under it. Later specimens used a slight variation on this design by having the two main shims on opposite sides, thus removing the need for the third smaller shim. The sealing of the recessed edges was more difficult with the three-layer specimens due to the small gap between the adherends. A thinner marine primer was used into which the sealed recessed edge was dipped to allow penetration of the primer into the gap. The sealed edges were then painted with the same two-part marine paint that was used for the two-layer specimens.

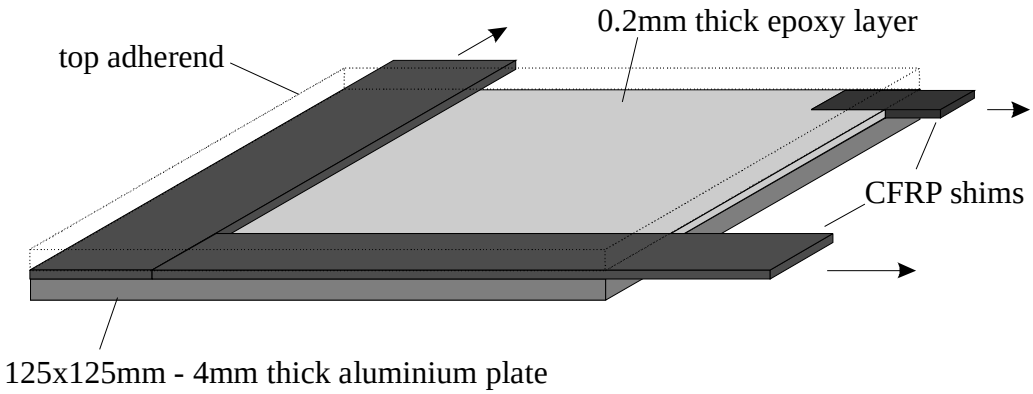

Figure 2.5 Three-layer specimen manufacture.

2.2.5 Materials

The materials chosen for this work were kept the same as those used by Pialucha [26]. This was primarily so that the considerable amount of data about these materials could be used, avoiding the need to repeat all the ultrasonic characterisation and water uptake experiments. The aluminium alloy used was L157, an aerospace grade alloy. The adhesive was a two-part liquid adhesive from Ciba-Geigy, epoxy resin AY103 and hardener HY951. Pialucha [26] performed mass gain experiments for sheets of resin immersed in water to calculate diffusion rates for this adhesive [34]. The diffusion coefficient calculated from Pialucha's water uptake experiment was $2.035.10^{-13}$ m^2s^{-1}, which compares well with the values measured by Althof which can be found in [25]. The diffusion coefficient relates the amount of substances diffusing across an area in a given time to the concentration gradient. Figure 2.6 shows the water concentration distribution curves taken from Crank [34]. For a given size of adhesive joint the curves shown represent the variation in water concentration with increasing time for increasing values of Dt/l^2. The x axis of this graph represents the position within the adhesive joint with an overlap length of 2l. The y axis shows the amount of diffused water as a ratio, normalised to saturated adhesive. From these, Figure 2.7 was calculated which shows the ratio of water at the interface of a two-layer specimen immersed in water, with a 2mm thick epoxy layer, the ratio being normalised to that of a fully saturated layer. The diffusion path in the three layer specimens can be considered as one dimensional if diffusion between the centre of one edge and the centre of the specimen is considered, with the distance from the edge of the specimen to the centre being 50 mm.

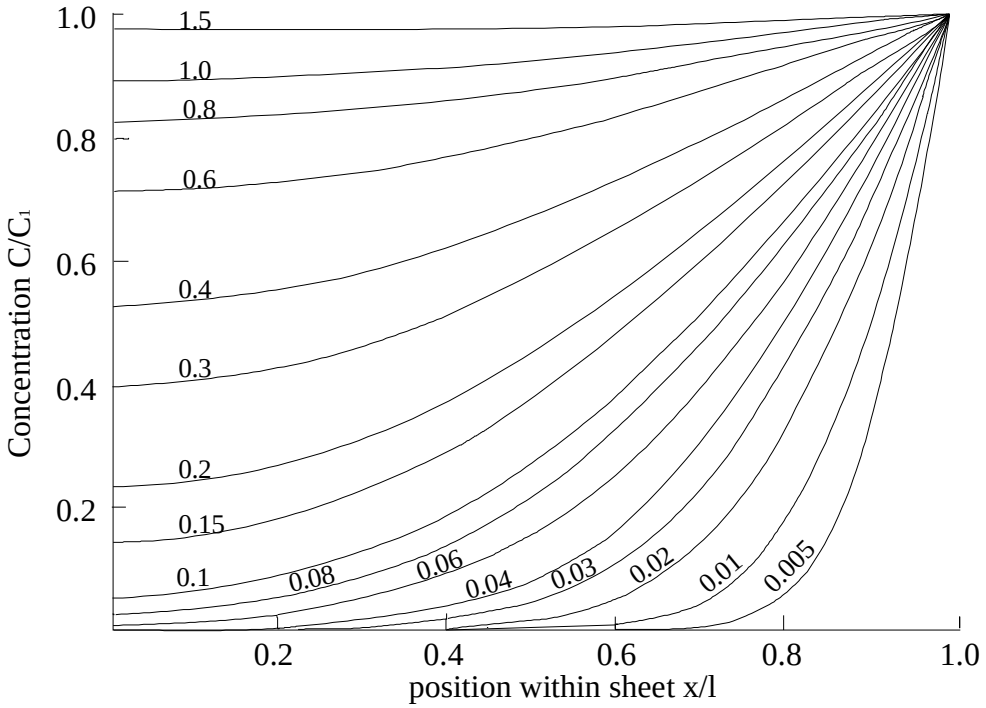

Figure 2.6 Water concentration distribution curves for one-dimensional diffusion of water into adhesive sheet, numbers on curves represent values of Dt/l^2 where D is the diffusion coefficient, t is time and l is the diffusion length [34].

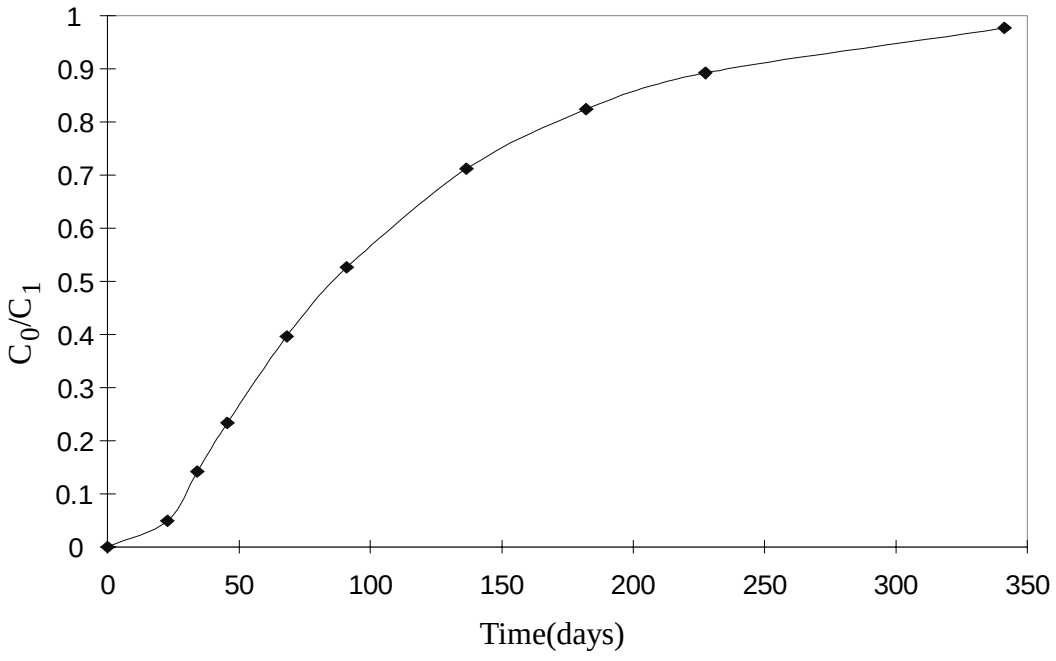

Figure 2.7 Water concentration at aluminium/epoxy interface for a 2mm thick epoxy layer as a function of time [26].

2.3 Non-destructive testing techniques

This section discusses the various ways in which ultrasound can be used to interrogate adhesive joints to determine their integrity. All forms of ultrasonic testing rely on the ability of a material to transmit stress waves. Ultrasound is sound with a frequency above 20kHz. Two types of wave may propagate in a bulk material; longitudinal waves, where the particle displacement in the material is in the direction of the wave propagation, and shear waves, where the particle movement is at 90º to the direction of propagation; shear waves will only propagate in materials that can support a shear stress, i.e. solids and viscous fluids. Away from the boundaries of a material it is only these two types of wave that need to be considered. When the boundaries of the structure are to be considered then the wave propagation can change its form and waves can travel along the boundary e.g. Rayleigh waves, or in structures of a thickness of the same magnitude as the wave length of the sound being considered, plate/rod/bar waves are seen[39]. Combinations of all of these types of wave propagation are used for non-destructive testing.

2.3.1 Normal incidence reflection coefficient measurements

The reflection of ultrasound from the interfaces between materials represents the simplest of scenarios in the application of ultrasonic techniques. An ultrasonic wave will travel uninterrupted in a material until a meets a change in the acoustic impedance of that material. The amplitude of the wave will be reduced if the material is attenuative. The acoustic impedance of a material is defined as the product of the density and the acoustic velocity. This holds for both longitudinal and shear waves. The reflection coefficient of the reflected wave can be shown to follow the relationship [40],

$$R_{12} = \frac{z_2 - z_1}{z_2 + z_1} \tag{2.1}$$

where R_{12} is the reflection coefficient of the wave reflected from the boundary between materials 1 and 2, and z_1 and z_2 are respectively the acoustic impedances of materials 1 and 2. The reason for the use of a coupling medium when using ultrasound can be seen from (2.1). If we consider trying to couple ultrasound into a metal structure where the acoustic impedance is 17×10^6 $kgm^{-2}s^{-1}$ (assuming the properties of aluminium shown in Table 2.1), using only air where the acoustic impedance is 430 $kgm^{-2}s^{-1}$ then the amount of energy transmitted into the structure is virtually zero. This

is why water is frequently used as a coupling medium as its impedance is within one order magnitude of that of many engineering materials. The simplest use of ultrasound to inspect materials was to monitor the transmission of an ultrasonic wave through a material, since in the presence of a defect the amplitude of signal transmitted would be reduced. This could be done either for through transmission or using a single probe in pulse echo, where the amplitude from the back wall or additional reflector (typically glass) would be monitored. The problem of coupling shear waves into a structure is slightly more difficult as a fluid cannot be used as it will not support shear. There are two ways in which shear measurements can be made; using a contact shear probe or via mode conversion of longitudinal waves at a boundary. The mode conversion method will be discussed in more detail in the following section. Contact shear probe measurements are done using a viscous substance, such as honey or molasses, to couple the shear waves to the structure. This is not ideal for repeatable measurements as there are inconsistencies in the coupling layer, and it also lacks the convenience of allowing easy movement of the probe [41].

Material	**Density (kg/m^3)**	**Longitudinal Velocity (m/s)**	**Shear Velocity (m/s)**
air	1.25	350	-
aluminium	2820	6330	3120
aluminium oxide	3896	10400	6490
epoxy resin	1170	2610	1100
water	1000	1483	-

Table 2.1 Acoustic properties of materials relevant to the ultrasonic inspection of adhesive joints.

This simple derivation for the reflection of ultrasound from a single interface does not include the effects of attenuation, but this has very little effect on the accuracy of the result. It also gives rise to a reflection coefficient which is independent of frequency. However this is not true when we consider the case of the reflection from multiple layers when the duration of the signal in time is comparable to the transit time for the wave across the layers. This is very much the case for an adhesive joint, where even if we only consider a three layer system, the thickness of the epoxy layer often means that we cannot distinguish clear reflections for each of the layers of

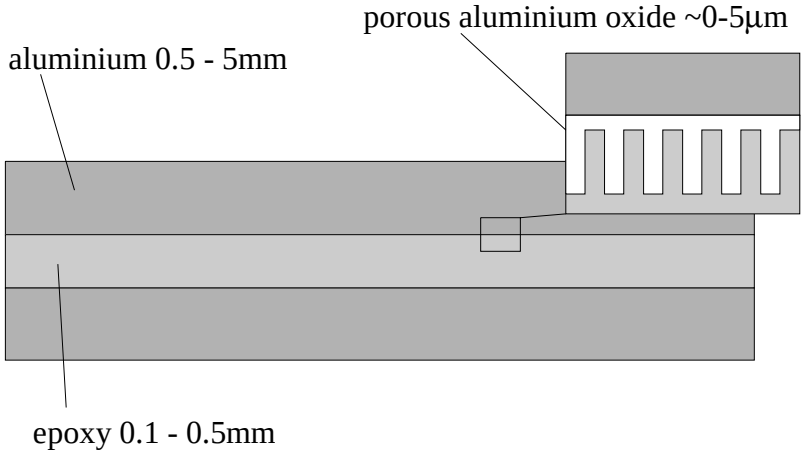

Figure 2.8 Schematic of aluminium/aluminium joint showing oxide and epoxy layers

the system. If we include the oxide layer which exists between the epoxy and the aluminium then we have five layers in our system as shown in Figure 2.8. As we have seen in chapter 1 this oxide layer is often intentionally made porous, and during manufacture the epoxy may enter the pores, resulting in a micro-composite layer [42]. If we use an ultrasonic pulse of short enough duration we are able to isolate the reflection from the epoxy/aluminium interface, and so we can make predictions of the reflection coefficient from the interface based upon the bulk properties of the aluminium and epoxy, which we can treat as semi-inifinite, and the properties of our micro-composite layer, including its thickness [43].

Material Property of Layer	**Oxide layer (water in pores)**	**Oxide layer (epoxy in pores)**
Density (kg/m^3)	2480	2515
C_{33} (GPa)	166	180
C_{11} (GPa)	130	140
C_{13} (GPa)	29	45
C_{55} (GPa)	35	36
E_{33} (GPa)	156	157
$E_{11} = E_{22}$ (GPa)	107	110
$G_{13} = G_{23}$ (GPa)	35	36
$G_{12} = G_{21}$ (GPa)	42	44

Table 2.2 Properties of oxide layer, [44].

Table 2.2 shows the mechanical constants calculated by Zeller et al.[44] (the accuracy quoted for these figures is ± 10% except for C55 which is defined as the lower bound), for an oxalic acid anodised oxide layer. This form of anodising was chosen as it allows oxides of very similar properties to be produced to PAA, with easier control of the thickness of oxide produced. The properties shown are for an anisotropic model of the oxide layer with the 33 direction being normal to the adherend surface i.e. parallel to the direction of the pores. Figure 2.9 shows the predicted frequency response for a 10 μm thick oxide with epoxy filled pores using the properties shown in Table 2.2. For comparison, the reflection from an aluminium/epoxy interface is included. The detail for the model used for this prediction is explained in section 2.3.2. This shows that for a 10 μm oxide layer there is a 15% increase in the reflection coefficient at around 210 MHz, compared to an interface that has no oxide layer. There are two important observations that can be made from this prediction; the oxide layer is at least three times thicker than that produced by any of the standard pre-treatments described in Chapter 1 and it is not possible to propagate 210 MHz through more than a few hundred microns of aluminium (certainly not through the 1-2 mm that would be required for a typical aircraft structure). If we scale the frequency that would be required for a normal incidence measurement with the thickness of the oxide layer, then for a 1 μm oxide

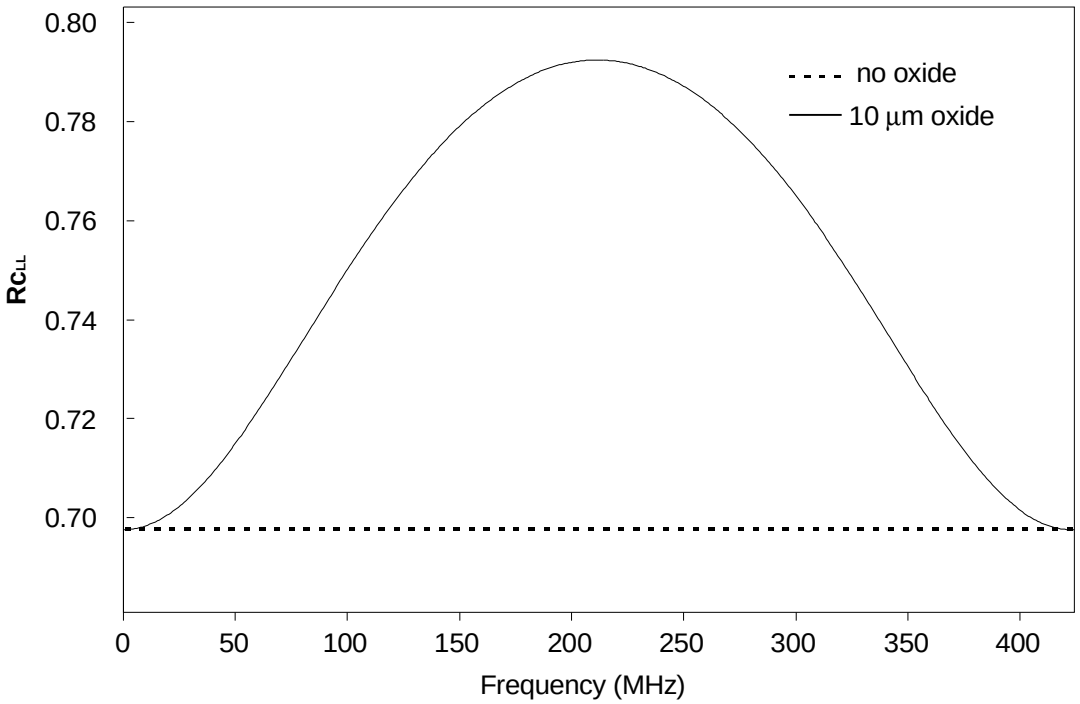

Figure 2.9 Predicted frequency response for 10 μm oxide layer with epoxy filled pores between half spaces of aluminium and epoxy.

layer we would need a frequency of 2.1 GHz to define the maximum of the normal incidence reflection coefficient.

Other approaches have been used to study the reflection of ultrasound from interfaces. Tattersall [45], models an imperfect interface between two solids as a spring. This has the result of producing a frequency dependent reflection coefficient from two surfaces. Baik and Thompson [46] have shown that the reflection of ultrasound from the contact between two rough surfaces can be modelled using a spring model. He shows that variation in the interfacial stiffness can be measured using normal incidence ultrasound, and that this is related to the degree of contact between the two surfaces. Similar results are shown by Lavrentyev for the case of a thin layer and varying degrees of contact [47]. However Alers [48] found that the reflection of ultrasound from the interfaces in a range of different types of bonds did not correlate well with their strength. Later work by Pilarski [49] reports good correlation between the reflection of ultrasound at normal incidence from the interface between lucite and epoxy with the strength of the bond using an approach based on measurement of interfacial stiffness. The interface of the bond between the P.M.M.A. and epoxy was modelled as a spring and variations in the spring constant were used to simulate variations in the quality of the bond with an infinite stiffness to simulate a perfect bond and zero to simulate no bond. The variability of results based on the spring model for predicting adhesive joint strength suggests that results may be highly system dependent, with many variations in both preparation of bonds and the manner in which their strength is measured. The success of these methods appears to be related to the correlation between the extent of contact between the adherend and adhesive.

Nagy [20] demonstrated the ability of a highly focused, high frequency normal incidence transducer to detect weak kissing bonds (where the adhesive and adherend are in intimate contact but show no adhesion) that remained undetected by conventional ultrasonic bond testers. Using highly focused transducers two focal zones are produced when the transducer is focused below the surface of adherend; one for the longitudinal waves and the other for mode converted shear waves. It was the use of shear reflection that Nagy showed was able to detect very weak kissing bonds.

2.3.2 Oblique incidence reflection coefficient measurements

Several authors have identified oblique incidence as offering considerable improvements in sensitivity to the interface properties of adhesive joints [50-53],

when compared to normal incidence techniques. Oblique incidence ultrasound has been shown to be capable of detecting oxide layers with thickness down to around 10 μm [38]. The oblique incidence method relies on mode conversion of an incident wave at an interface, splitting the incoming wave into a longitudinal wave and a shear wave. When an oblique incidence longitudinal wave is incident on a surface the transmitted signal will be split into both longitudinal and shear waves. When these waves hit the bottom of the specimen there will again be mode conversion, giving rise to a total of four possible reflected waves, as shown in Figure 2.10. These are longitudinal longitudinal (LL), longitudinal shear (LS), shear longitudinal (SL) and shear shear (SS). The LS and SL will arrive at the same time and position but all the other waves will be separated in both time and space. This makes it possible to maximise and isolate each of the signals by varying the position of the receiver and also gating the signals in the time domain.

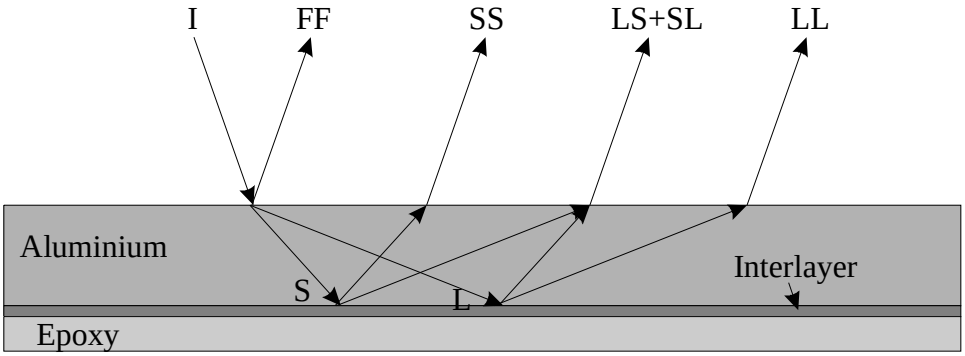

Figure 2.10 Mode conversion of oblique incidence longitudinal wave into four possible reflected waves.

In order to determine the sensitivity of the oblique incidence method the response of the interlayer to ultrasonic waves was modelled using a program developed by Lowe and Pialucha based on the transfer matrix technique [54, 55] [44]. This allowed predictions to be made for the response of complex multilayered systems to the input of either longitudinal or shear waves at any frequency and angle. This enables theoretical system responses to be calculated either for frequency sweeps at a single angle, or angle sweeps at fixed frequency. These predicted curves can then be used to assess the best combination of angle and frequency for the greatest sensitivity to any given layer properties. The interlayer of adhesive joints was originally modeled as an isotropic layer. A more representative model of the interlayer is achieved by modelling it as a transversely isotropic layer, with mechanical moduli calculated using the method developed by Nielsen [56] for composite materials. The interlayer can be considered as analogous to a fibre reinforced resin, with the oxide being like the resin

and the pores being like the fibres. Similar modelling of the oxide layer has been successfully used by Wang and Rokhlin [23, 57] [58]. They have also shown similar success for predicting the response of oblique incidence ultrasound to these porous oxide layers.

Reflection coefficients for the four possible reflections are shown in Figure 2.11 and Figure 2.12. Two curves are shown in each case, one for a 10μm oxide layer between semi-infinite half spaces of aluminium and epoxy, with the oxide properties taken from Table 2.2 [44], and the other for an aluminium/epoxy interface at a frequency of 10MHz. The prediction used the anisotropic model, and the material properties used are shown in Table 2.2. The anisotropic layer is modelled using four material constants C11, C13, C33 and C55 and the density. The epoxy and aluminium layers are treated as isotropic, with density and longitudinal and shear velocities being taken from Table 2.1. The predictions are shown for a frequency of 10MHz. The oxide layer is thicker than would usually be seen for an in-service joint, but was chosen to increase the separation between the curves. Even so there is no obvious separation between the curves shown in Figure 2.11 (a) and (b), and it is not until we have an incident shear wave (Figure 2.12a and b) that we see a clear distinction between the reflection coefficients from the interfaces with and without an oxide layer present. An initial view is that both the shear shear (SS) reflection coefficient Rc_{SS} and the shear longitudinal (SL) reflection coefficient Rc_{SL} offer considerably more sensitivity to the presence of the oxide layer than either of the longitudinal incident reflection and indeed normal incidence reflections. However there are several reasons for not choosing to use $Rc_{SL.}$ From Figure 2.10 it can be seen that the SL and LS exit the aluminium plate at the same position, and will also occur at the same position in time. This makes them impossible to separate. It can also be seen that the maximum separation between the two Rc_{SL} curves is at a high angle of incidence. It is preferable to use the SS reflection at an angle of 32°, where the separation between the curves is greatest. There is also the added benefit of this being above the longitudinal critical angle, which means that there will only be a single reflection from the interface, making signal identification considerably easier. Rose reports advantages in using 32° shear waves for detecting weak interfaces in aluminium epoxy specimens[53], where a scanning technique using shear waves was able to identify areas of poor bond that conventional normal incidence could not.

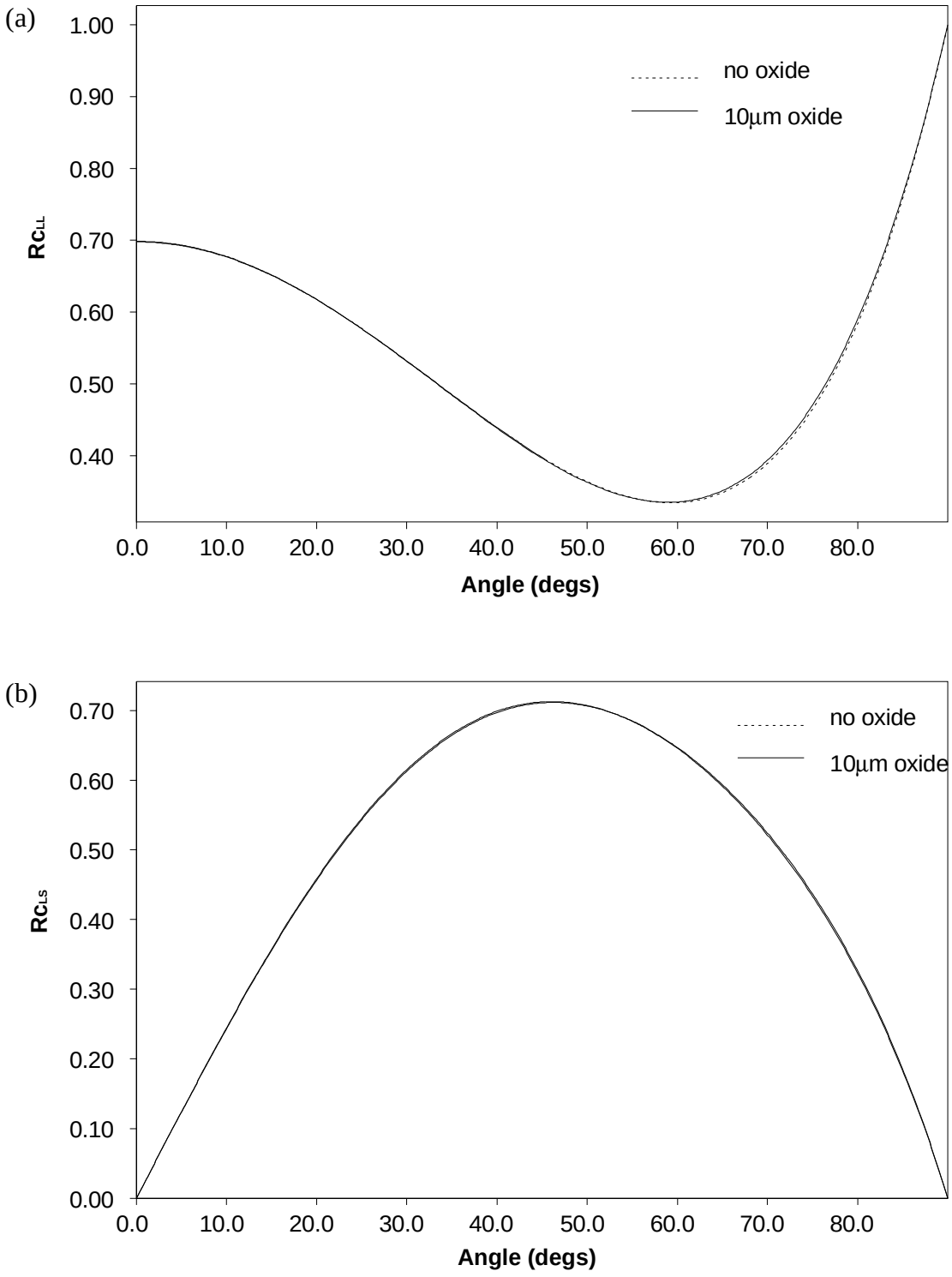

Figure 2.11 Predictions of reflection coefficients from a aluminium/10μm oxide layer/epoxy system compared with aluminium/epoxy showing (a) the LL response and (b) the LS response.

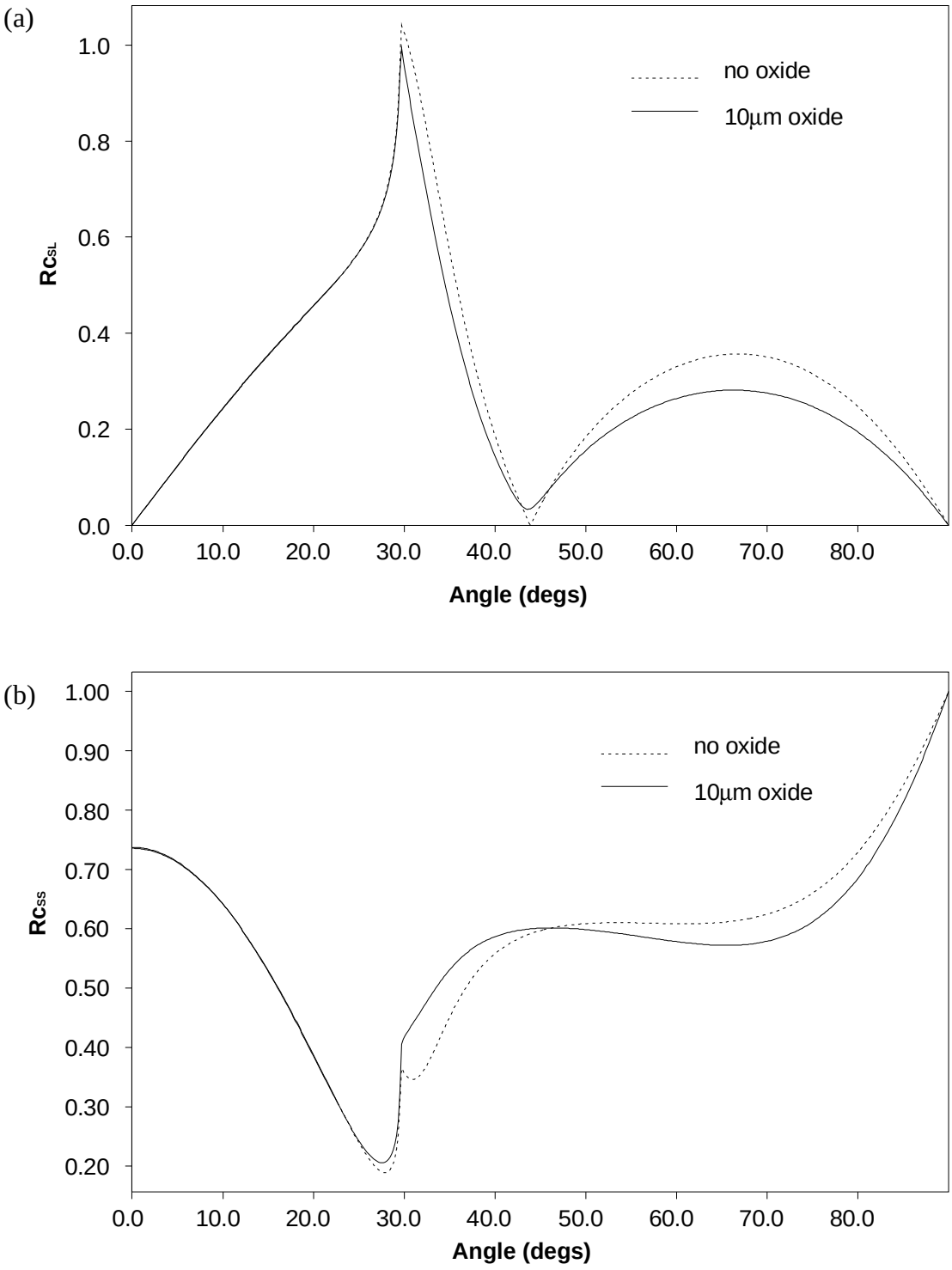

Figure 2.12 Predictions of reflection coefficients from a aluminium/10μm oxide layer/epoxy system compared with aluminium/epoxy showing (a) the SL response and (b) the SS response.

To improve the sensitivity the centre frequency has been increased from 10MHz as used by Pialucha to 20MHz. Oblique incidence reflection coefficient measurements have been made with a pair of 20MHz transducers on the same samples

used by Pialucha and have shown reasonable agreement with his experimental curves using 10MHz transducers. These measurements are shown in Figure 2.13 along with the predicted reflection coefficient for a 5μm thick oxide layer with the same properties as used for the previous oblique incidence reflection coefficient predictions. In this case the thickness of the oxide layer was chosen to fit the experimental results. This figure shows good agreement, both for the continuity of results obtained by Pialucha and also for the agreement with theory. This shows that doubling the frequency doubles the difference in reflection coefficient obtained compared to the case of no oxide being present. (All of the results shown are normalised with respect to a bare aluminium/epoxy interface, hence the appearance of Rc_{SS} >1.)

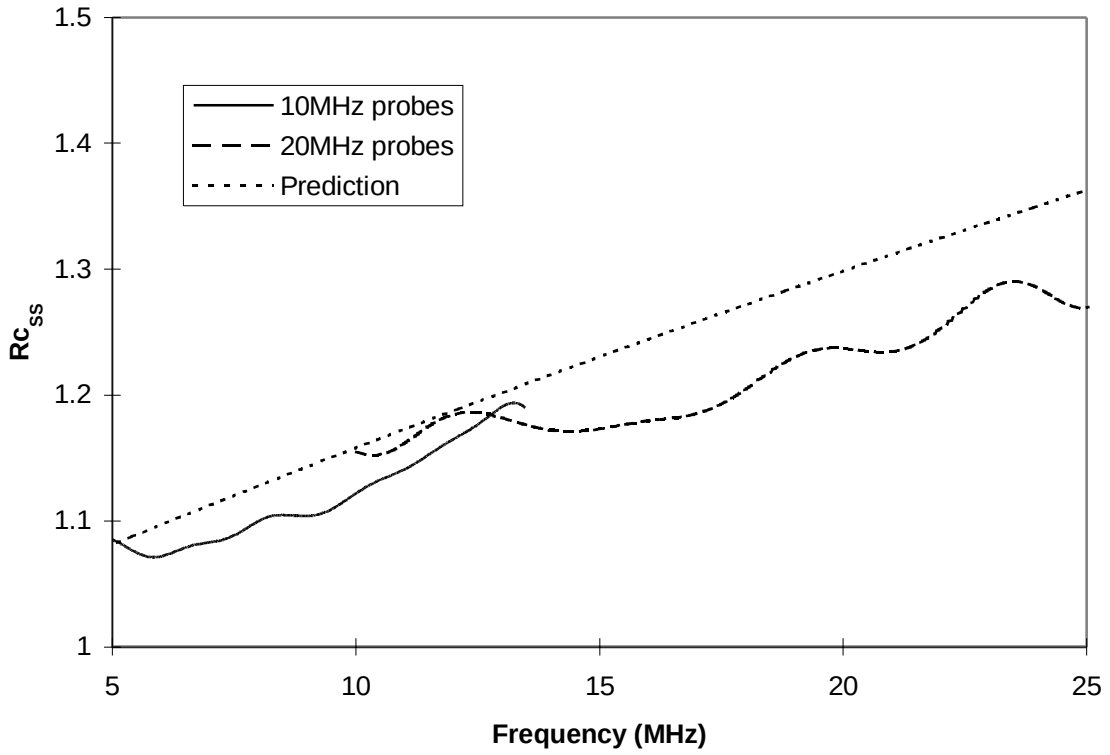

Figure 2.13 SS reflection coefficient measurement at 32° from one of Pialucha's specimens, showing measurements made with 10MHz and 20MHz probes along with predicted frequency response for a 5μm oxide layer.

More extensive work to determine changes in the physical properties of oxide layers using both normal and oblique incidence techniques and acoustic microscopy has been done by Zeller [59]. This work is taking a more direct approach to measuring the oxide properties by measuring exposed oxides, or oxides covered by a very thin overlayer, enabling much higher frequencies to be used for a more accurate measure of oxide properties and has also included the use of high resolution T.E.M. improving

the level of information. It is this work that has generated the material properties used for the predictive modelling with the results published in [44].

2.3.3 Scanning

This has been the major technique used for the screening of specimens. The previous sections have covered the sensitivities of both normal and oblique incidence techniques, and these sensitivities are still valid when we consider a scanning probe system. However previously when discussing sensitivities we have considered that the defect will be of a greater planar extent than the footprint of the probe being used. When we consider the form that environmental attack might take for an adhesive joint it becomes clear that spatial information about the joint is paramount. Corrosion under an organic coating is highly unlikely to proceed in a uniform manner under the entire coating but will generally initiate at microscopic flaws, which subsequent corrosion causes to expand and produce further unbonding of the coating. Similar patterns have been identified as prevalent in adhesive joints, and it is through such a mechanism of degradation that the Aloha Airlines Boeing 737 lost a large section of fuselage roof [60], resulting in Figure 2.14. The failure of this lap joint was identified as being caused by a number of sub-critical sized corrosion sites in the bondline.

Figure 2.14 Photograph of Aloha Airlines 737, which suffered from a failure of the main fuselage lap joint.

This leads to slightly different considerations when we try to optimise our probe arrangements for scanning as opposed to point measurements. For this purpose there are two reasons for using focused transducers. The first is that a focused

transducer will give higher spatial resolution than can be obtained using a planar probe. The second benefit becomes clear when the use of collimated beams for scanning is considered. Planar probes are extremely sensitive to alignment, and even when scanning nominally flat plates the variation in signal can make defect detection difficult. The explanation for this sensitivity to alignment can be quickly explained if we consider the angular misalignment required to produce a 2π phase change for an incident ultrasonic wave across the face of a transducer, see Figure 2.15. A piezoelectric transducer produces an output proportional to the sum of the displacements across its surface. When there is a complete wavelength of misalignment across the face of an ideal piston transducer the output will be zero. The transducers used for the oblique incidence reflection coefficient measurements had a centre frequency of 20MHz and an element diameter of 6mm. Therefore the misalignment angle for complete cancellation of signal can be seen to be:

$$\theta = \tan^{-1}\frac{\lambda}{D} \qquad (2.2)$$

where λ is the wavelength in water, and D is the transducer element diameter. At 20 MHz the wavelength in water is 0.0742 mm, resulting in a misalignment angle of 0.708°. This applies for oblique incidence scanning as well as normal incidence.

This is not quite the case as there is a distribution of energy across the face of a plane probe which is approximately Gaussian so the phases at the edge of the transducer will not be as large an amplitude as the centre. However the approximation is of the correct magnitude for determining the sensitivity to misalignment.

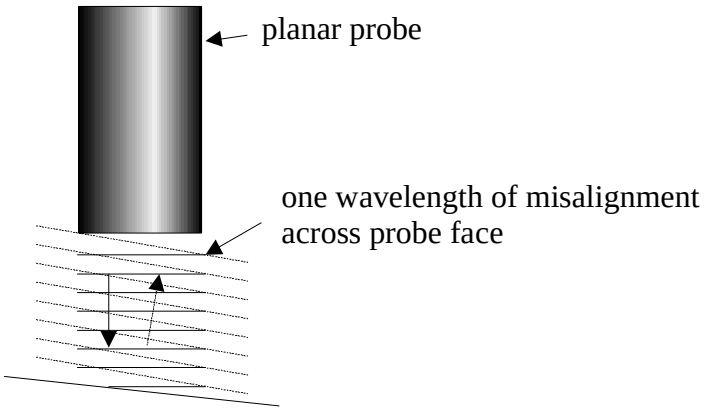

Figure 2.15 Probe misalignment

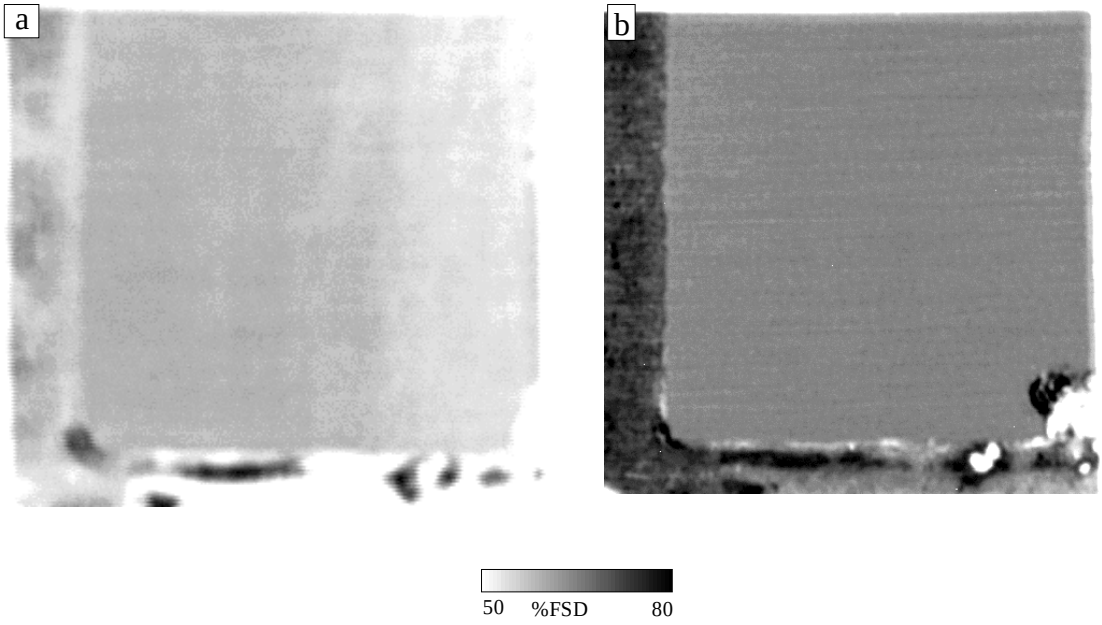

Figure 2.16 Comparison of oblique incidence scans performed with (a) unfocused 20MHz probes and (b) focused 10MHz probes from a two-layer CAA specimen.

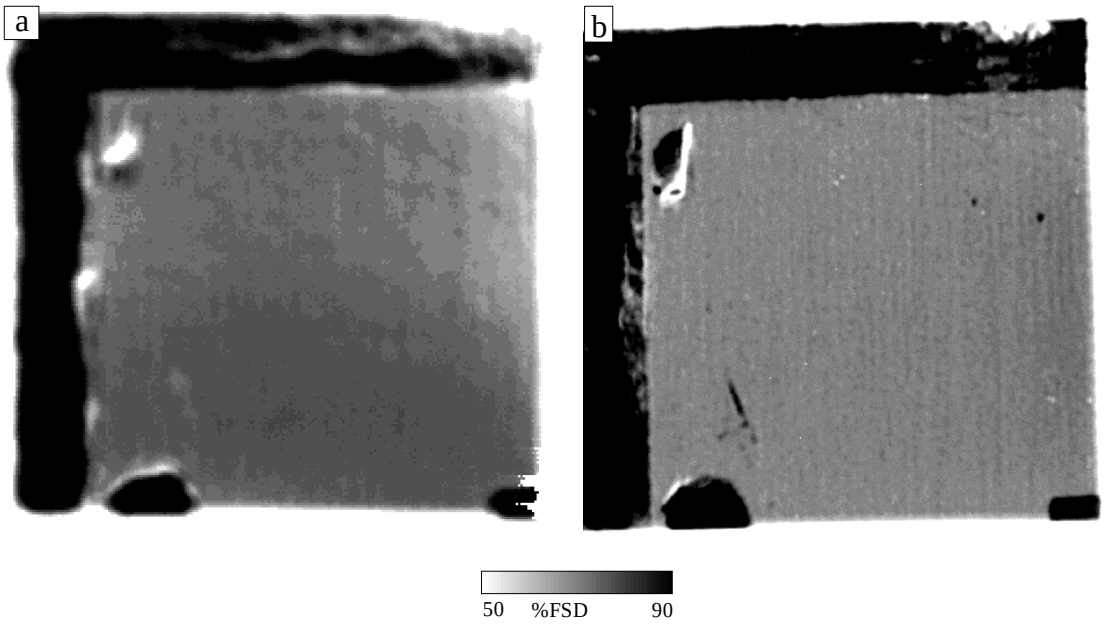

Figure 2.17 Comparison of oblique incidence scans performed with (a) unfocused 20MHz probes and (b) focused 10MHz probes from a three-layer PAA specimen.

Figure 2.16 and Figure 2.17 show how using focused probes can dramatically reduce the variation in signal amplitude across a specimen. These figures are included purely to demonstrate the effects of varying probe type, and a full explanation of these results and the features shown in the scans are discussed in Chapters 3 and 4 respectively for the two and three-layer specimens. However both of these figures

clearly show both the improved resolution that focused probes produce and also the more consistent amplitude of the reflection from the bondline. From Figure 2.16 we can see that the amplitude of the reflected signal varies by approximately 15% from the left to right edges using plane probes, but this variation disappears using the focused probes. A similar variation can be seen in Figure 2.17 between the lower edge and the top right corner of the specimen. We can also see two small voids in the upper right corner of the specimen when using the focused probes but there is no evidence of these in the scan using plane probes.

As well as the improvements in sensitivity to misalignment other considerations include how small a focal spot can be produced for a given frequency. The diameter of the focal zone is described by

$$f_d = \frac{2R\lambda}{d} \tag{2.3}$$

[41] where R is the radius of curvature of the focal plane, λ is the wavelength and d is the probe diameter. To maximise the resolution we need to minimise the focal length and wavelength and maximise the probe diameter. The constraint on focal length is determined by the thickness and velocity of sound in the adherend. In the case of the 4mm thick aluminium adherends used for this work a focal length of 25mm was used, remembering that the focal length is shortened according to Snell's law when focusing through a material interface.

If we use a simple ray analysis we can see that the edge ray of a 4mm diameter, 25mm focal length probe will be incident on the aluminum surface at,

$$\theta_i = \tan^{-1}\left(\frac{D/2}{f_l}\right) \tag{2.4}$$

where D is the diameter of the probe, and f_l is the focal length, resulting in an incident angle of 4.6°. Using Snell's law,

$$\frac{c_i}{c_r} = \frac{\sin(\theta_i)}{\sin(\theta_r)} \tag{2.5}$$

the refracted angle in the aluminium is 19.8°, when c_i and c_r are the velocities in the water and aluminium respectively. If we assume that the diameter of the probe is the

diameter of the beam incident on the surface of the aluminium we see that the point of focus in the aluminium is at a depth of,

$$d_f = \frac{(D/2)}{\tan(\theta_r)} \qquad (2.6)$$

This results in a depth of focus of 5.56mm. However it is not realistic to scan with the full diameter of the probe being incident on the surface of the aluminium (i.e. in contact) as the probe face is recessed in the casing. Scanning a stepped wedge of aluminium showed that the maximum thickness of aluminium that could be scanned allowing sufficient clearance of the probe from the surface was 4mm

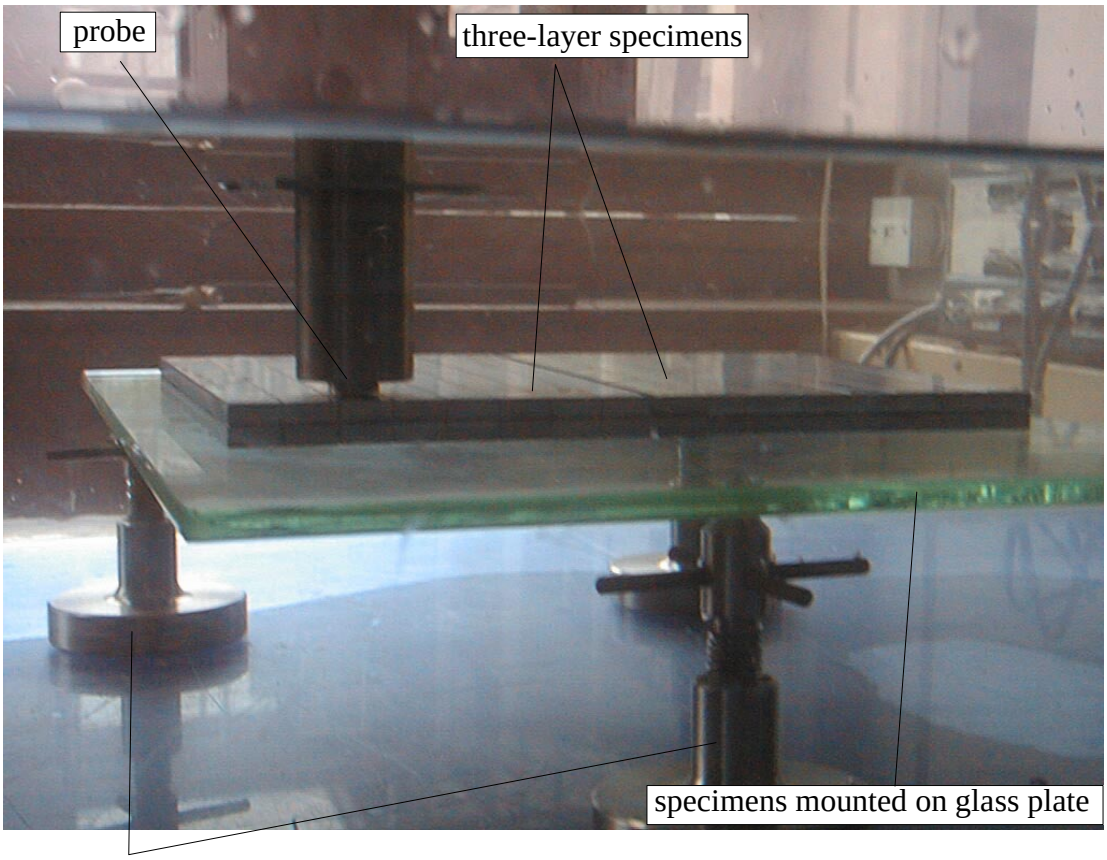

Figure 2.18 Photograph showing position of probe for scanning 4mm adherends with 50MHz focused probe.

The other benefit of minimising the focal length is that at frequencies in the tens of MHz range the attenuation in water becomes significant, so keeping the water path length to a minimum maintains a maximum frequency giving as short a

wavelength as possible. From (2.4) it can be seen that the probe diameter affects the diameter of the focal zone. The diameter of probe that is used also has obvious physical constraints, with a very small diameter probe having no focusing effect, and a hemispherical probe impossible to focus below the specimen surface. The compromise used for the normal incidence scans was a 25mm focal length, 4mm diameter 50MHz centre frequency probe.

The compromise that is needed for scanning at oblique incidence is slightly different. For a point measurement at oblique incidence (area interrogated being determined by the size of probes used) a single angle on the reflection coefficient versus angle curve could be selected when using planar probes. However as has been discussed planar probes are not best suited for scanning. We therefore need to find an area on the reflection coefficient versus angle curve where we maintain good sensitivity to the interlayer properties over a range of angles. If we re-examine the predictions shown in Figure 2.11 and Figure 2.12 with the intention of finding a suitable setup for scanning we can quickly see that the SS reflection is still the most promising, when using angles just above 32°, which is the longitudinal critical angle.

The probes used to validate the idea of using focused probes to reduce the sensitivity to misalignment were 10MHz with a focal length of 75mm and an element diameter of 9mm. These probes will result in a range of angles being incident on the surface of the aluminium. If we continued to use a 32° shear wave angle then some of the waves from the transducer would be incident below the longitudinal critical angle. From these curves it was decided that an angle of 37.4° shear in aluminium was most suitable, as shown in Figure 2.19.

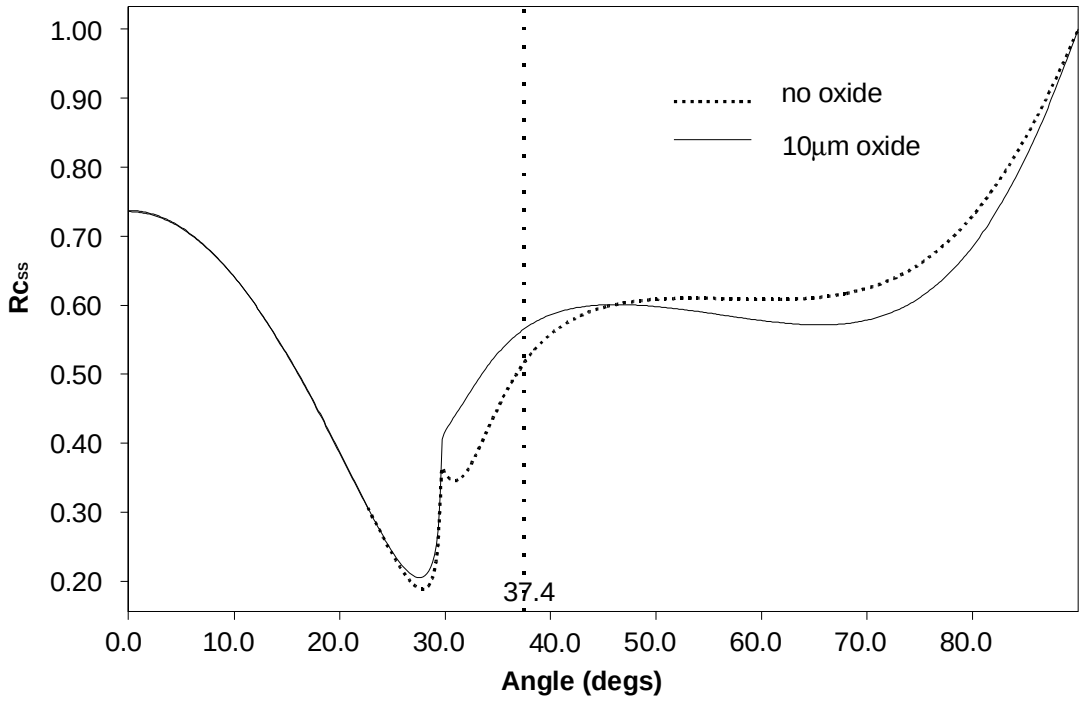

Figure 2.19 Variation of SS reflection coefficient with angle for the case with a 1μm oxide layer compared with the case for no oxide layer, showing angle chosen for oblique incidence scans.

This gives good sensitivity to the presence of the oxide layer, but moves the angle a little further away from the longitudinal critical angle. This ensures that small changes in alignment during scanning will not result in the appearance of any LL or SL+LS reflections, thus giving more complicated time domain signals. The probable interference between mode converted signals would make scanning very difficult, certainly for 3 layer specimens, where the bondline thickness is around 0.3mm. It is also desirable for the angle to be as near to normal as possible in order to produce a sharp focal zone; if the angle of incidence is too oblique then the focal spot becomes very elongated, giving poorer resolution scans. The specimen design used also meant that there would be the possibility of water moving along the interface of the specimen and so predictions were made to determine the sensitivity of this probe arrangement for the detection of a thin water layer.

Figure 2.20 shows the variation in the SS reflection coefficient when there is a 100nm water layer present between the oxide layer and the epoxy. The same properties of oxide were used as for Figure 2.11 and Figure 2.12. It can be seen from this figure that there is a difference in reflection coefficient at 37.4° which was highlighted as suitable for the oblique incidence scans, although this difference is greater as the angle approaches the longitudinal critical angle. Figure 2.21 shows the variation of the SS

reflection coefficient with frequency at an angle of 37.4° for the same case shown in Figure 2.20. This shows that the sensitivity to a thin water layer is maintained down to very low frequency, and consequently at 20MHz the sensitivity to the presence of a water layer is good down to very thin layers.

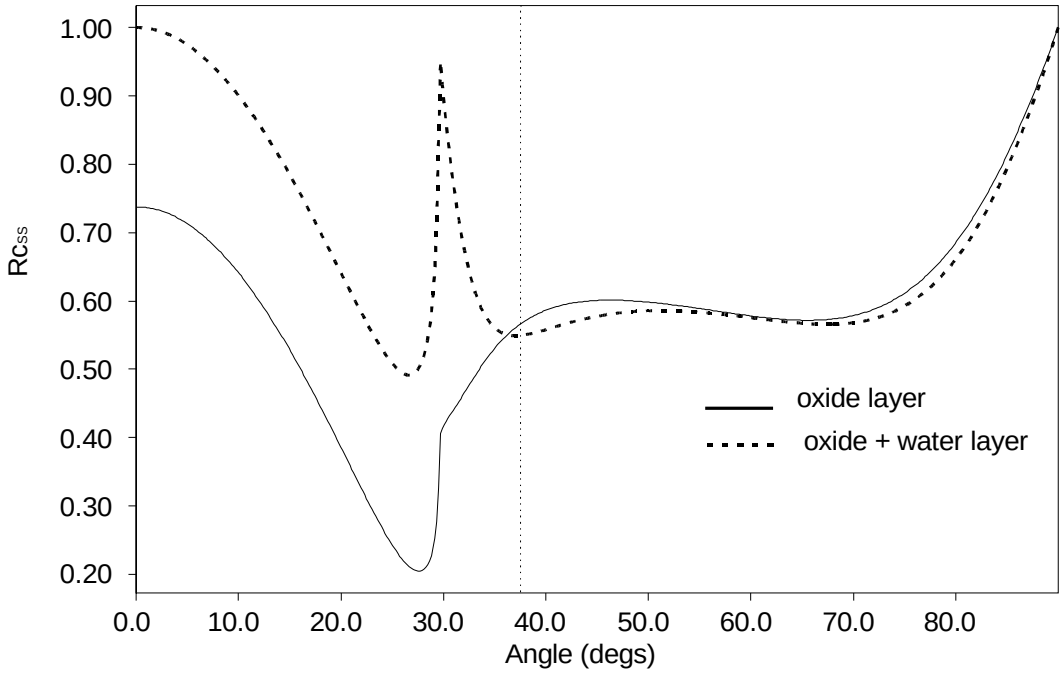

Figure 2.20 Predicted SS response for two cases, solid line is for aluminium/10μm oxide/epoxy and the dashed line is for aluminium/10μm oxide/100 nm water/epoxy, showing reflection coefficient against angle for a frequency of 10MHz.

These considerations resulted in the use of a pair of 20MHz, 50mm focal length 6mm diameter probes for the oblique incidence scans, set to 16.81° from the normal. Using Snell's law 16.81° in water results in 37.4° shear angle in aluminium. As will be seen from the results at this frequency there is a noticeable amount of material noise, significant enough for the rolling direction of the aluminium to be apparent. The scattering of shear waves in the aluminium seems to be greater than that of longitudinal waves. To a certain extent this expected as the shear velocity is around 50% of the longitudinal velocity, and so the wave length is correspondingly shorter. The other factor is that the path through the adherend is longer for an obliquely incident wave. However this produces fewer wave lengths at 20MHz oblique than at 50MHz normal, suggesting that the shear scattering is higher than longitudinal waves. This realistically limits the upper frequency limit for oblique incidence to around 20MHz

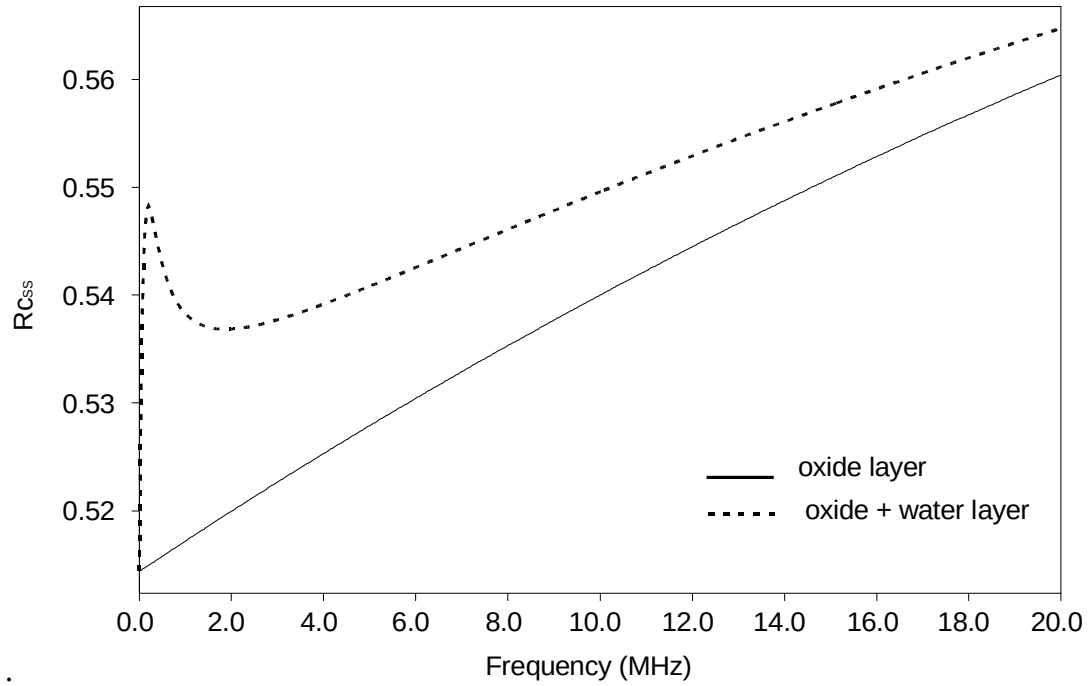

Figure 2.21 Predicted SS response for two cases, solid line is for aluminium/10μm oxide/epoxy and the dashed line is for aluminium/10μm oxide/100 nm water/epoxy, showing reflection coefficient against frequency for an angle of 37.4°.

2.3.4 Visual inspection

Although often ignored as a non-destructive testing technique in certain cases visual inspection can be one the most reliable and rapid techniques available. This was used for rapid screening of two layer specimens, where a transparent adhesive layer enabled the interface to be clearly visible. Small changes, sub-millimeter, can be distinctly visible. However determining the exact depth of defects seen through the epoxy layer is not possible, and so it is not possible to discriminate between defects at the epoxy/aluminium interface and those a little distance into the epoxy layer.

2.4 Mechanical Tests

Several different testing regimes were considered for this work. One of the key considerations was that we wished to produce results that could contain spatial information for comparison with the results obtained from the ultrasonic measurements. The first idea tested was to section the specimen into 10mm squares

and use a simple “butt-test” to produce a grid of results, shown in Figure 2.22. However this proved to be extremely sensitive to any misalignment between the stubs that the specimen was glued between, particularly due to brittle nature of the adhesive being used. This also a required a large amount of machining resulting in a large loss of material and the possibility of introducing damage to the interface of the joint ruining the results.

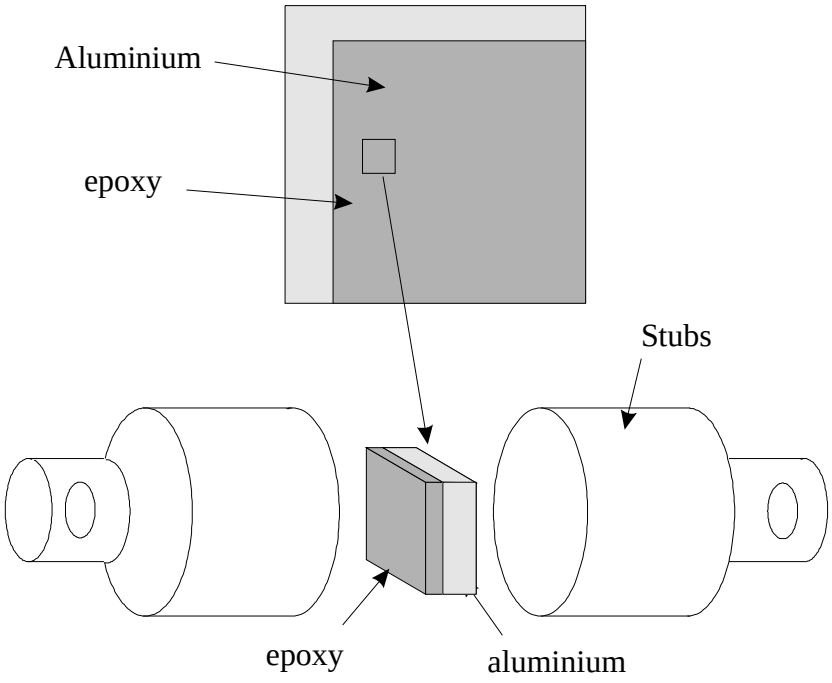

Figure 2.22 First method used for testing the mechanical performance of specimens.

The method that was chosen used a peel test, where the specimens were cut into strips. The resolution obtained is then determined by the width of the strips cut from the specimen and the accuracy with which the crack length could be measured. This was also partially influenced by the way in which the specimen failed. When a highly brittle failure occurred then measurement were made at the point at which the crack jumped. When the crack grew in a continuous manner measurements were taken at no more than 5mm intervals.

For the two layer specimens the sample to be tested was cut into 10mm wide strips. The width of the strip cut is a compromise between the spatial resolution and the amount of material lost in the cut. 10mm strips gave eight useable samples from a 100mm square specimen. Each of these strips had their edges fly cut and then sprayed with a thin layer of white paint which allowed for clear crack definition using a video microscope for measuring the crack length. The strips were then bonded to a stiff steel plate. This is shown schematically in Figure 2.23.

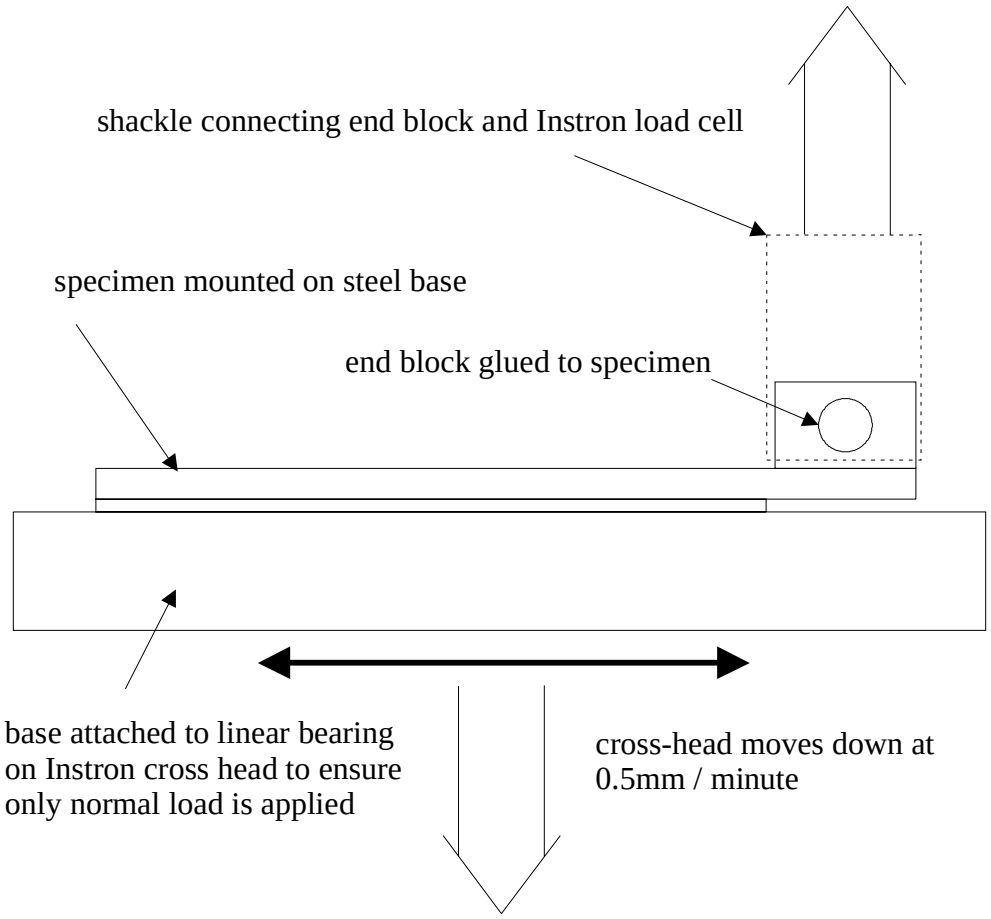

Figure 2.23 Two-layer mechanical specimen test set-up.

Bonding to a base stiffer than the peel arm results in the crack propagating along the interface even when the specimen has not been exposed to water [61]. The peel arm of these specimens was sufficiently stiff to avoid plastic deformation of the adherend during the test. This meant that the elastic energy stored in the arm is dissipated in the fracture of the bond, making analysis considerably easier. The sample was then mounted in a Instron (displacement control) tensile test machine. The test was recorded using a video microscope, giving crack length at any given time. The output from the Instron was then also plotted against time, allowing crack length and load to be known at any time. Sudden changes in load, such as final failure or the crack jumping gave significant events that could be seen both from the video and also on the load time graph, which allowed verification of the synchronisation of the video clock and the Instron output. The two events were generally accurate to within one second.

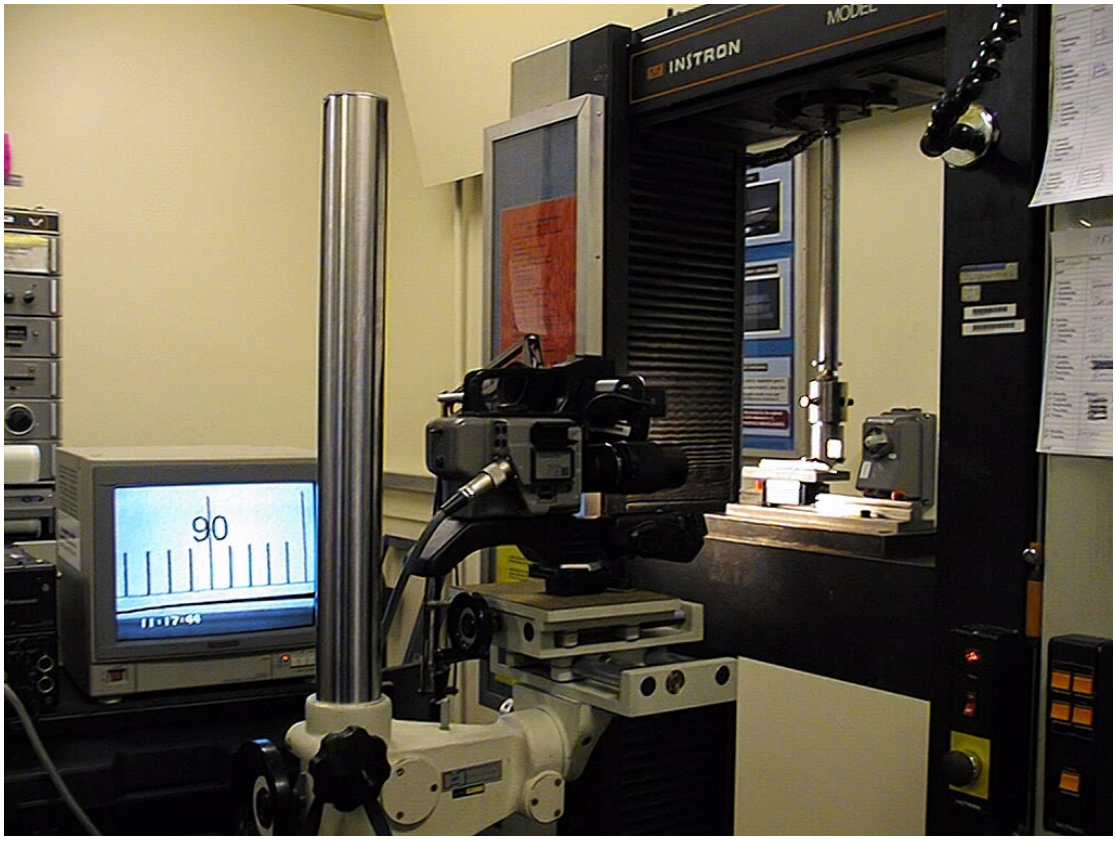

Figure 2.24 Photograph showing mechanical test arrangements.

Therefore for each strip we have load against crack length. To calculate the fracture energy released the following equation was used [62].

$$G_c = \frac{6a^2P^2\delta}{b^2t^3E} \qquad (2.7)$$

where a is the crack length, P is the load, δ is used to correct for the stiffening of the end block, b is the specimen width, t is the thickness of the adherend and E is the Young's modulus of the adherend. This equation assumes that all of the energy dissipated in breaking the bond is stored in a single peel arm. This can be verified by stopping a test and reversing the cross-head displacement. If the test is elastic for the peel arm the specimen should unload along the same load displacement curve as during loading.

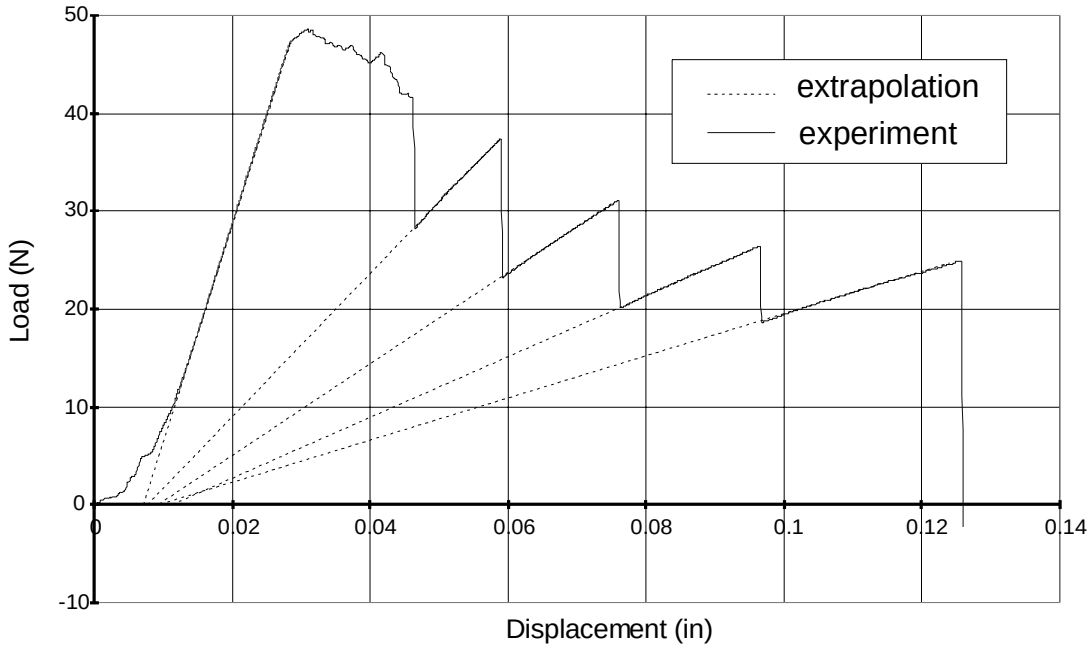

Figure 2.25 Load displacement graph from mechanical test of three-layer specimen, extrapolation of curve back to zero load shown for a number of position during crack arrest.

Figure 2.25 shows the load displacement graph obtained from a three-layer mechanical test. At several points during this test the crack stopped growing, and a linear increase in the load was observed. These linear portions of the curve have been extrapolated back to zero load, and these all show near identical displacements at zero load. (This displacement being the slack in the shackles at the start of the test.) This shows that there has been no plastic bending of the adherends during the test, allowing (2.8) to be used.

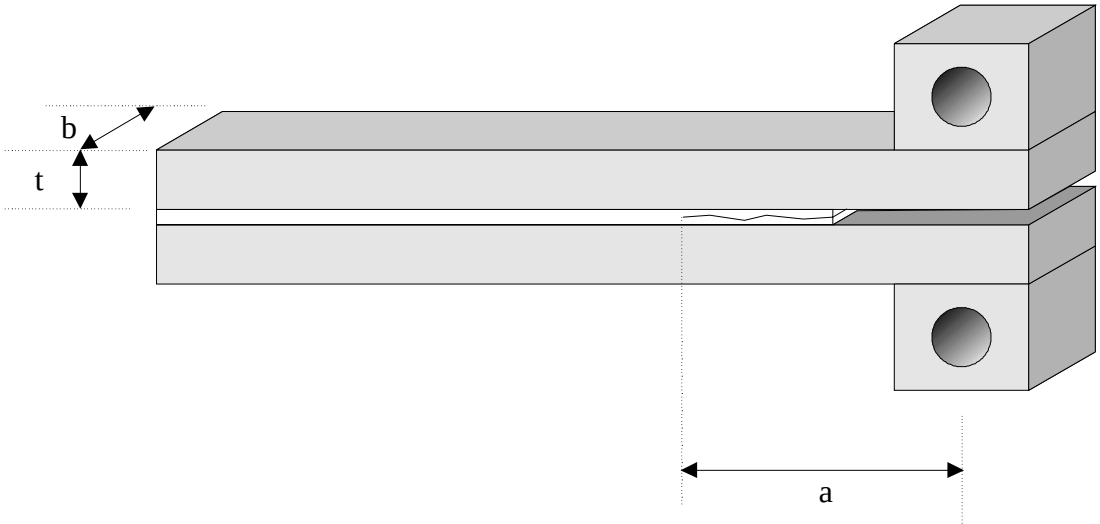

Figure 2.26 Three layer mechanical test specimen

Figure 2.26 shows a schematic of the 3-layer mechanical test specimen. The method for mechanically testing the three-layer specimens is much the same, without the need for bonding the specimen to anything. In this case each strip cut from the original specimen is symmetrical about the bondline. The stress through the bondline is symmetrical which will generally produce a cohesive failure if the interfaces of the joint are as tough as when they were produced. It is possible to use a similar approach to that used for the two-layer specimens to produce a failure along the interface even for the undegraded specimens, but this approach was not generally used. This was done for one dry three-layer specimen to verify that the dry interfacial fracture energy was higher than the cohesive failure energy. The reason for, and results from, this test are discussed in detail in Chapter 4 section 4.4.3. The testing procedure used was the same as that described above, producing crack length versus load. In this case the fracture energy is calculated from

$$G_c = \frac{12a^2P^2\delta}{b^2t^3E} \qquad (2.8)$$

with the only difference between 2.8 and 2.9 being the multiplier, where in the two layer specimen the energy is stored in one arm, but in the three layer specimen it is stored in two arms.

2.5 Surface Analysis

Surface analysis has been done to allow an exact description of changes that have occurred in the interface regions of the adhesive joint specimens after exposure to moisture. This is to include both changes in morphology and chemical composition. A number of techniques have been used including optical and electron microscopy, used to study morphological changes and EDX (energy dispersive x-ray spectroscopy) and XPS (x-ray photospectroscopy) to study changes in the chemical composition.

There is no single technique that can supply all of the information that we may require, so these techniques are largely complementary. Optical microscopy is of little use for examining aluminium oxide layers, but does have the advantage of being very quick and convenient, and allows a rapid investigation of things that maybe visible by eye, but not identifiable. It should also allow for the sizing of defects. It also gives useful information prior to using electron microscopy, for locating and identifying defects when seen at the much higher magnifications of an electron microscope. For

detailed examination of joint failure surfaces electron microscopy is essential. There are two primary forms, SEM (scanning electron microscopy) and TEM (transmission electron microscopy). Both of these techniques allow for images to be produced with sub-micron resolution, although TEM images can be considerably higher resolution, with SEM having the advantage of less demanding sample preparation.

2.5.1 SEM

In scanning electron microscopy, (SEM) an electron beam is scanned across the surface of the sample. When the electrons strike the sample, a variety of signals are generated, and it is the detection of specific signals which produces an image or a measure of the elemental composition of the specimen [63] [31]. The three signals which provide the greatest amount of information in SEM are the secondary electrons, backscattered electrons, and X-rays.

Secondary electrons are emitted from the atoms occupying the top surface and produce a readily interpretable image of the surface. The contrast in the image is determined by the sample morphology. A high resolution image can be obtained because of the small diameter of the primary electron beam.

Backscattered electrons are primary beam electrons which are 'reflected' from atoms in the solid. The contrast in the image produced is determined by the atomic number of the elements in the sample. The image will therefore show the distribution of different chemical phases in the sample. Because these electrons are emitted from a depth in the sample, the resolution in the image is not as good as for secondary electrons.

Interaction of the primary beam with atoms in the sample causes shell transitions which result in the emission of an X-ray. The emitted X-ray has an energy characteristic of the parent element. Detection and measurement of the energy permits elemental analysis (Energy Dispersive X-ray Spectroscopy or EDX). EDX can provide rapid qualitative, or with adequate standards, quantitative analysis of elemental composition with a sampling depth of 1-2 microns. X-rays may also be used to form maps or line profiles, showing the elemental distribution in a sample surface. However in general a conducting surface is required, so for polymers a gold coating is generally used. The resolution of images produced is dependent on the surface conductivity and accelerating voltage used, with the best images being produced using a high kV electron gun. At high kV the beam has a greater penetration depth, with the

penetration being proportional to the material density. This means that thin polymer coatings appear transparent to the electron beam.

2.5.2 XPS

XPS is an abbreviation for X-ray Photoelectron Spectroscopy [64] [31]. When light strikes an atom an electron may be ejected if the energy of the light is high enough. When X-rays strike a solid electrons are always ejected from the near-surface region of the solid. If the energy of the ejected photoelectron is measured, its Binding Energy can be calculated, which is the energy required to remove the electron from its atom. From the binding energy the following can be determined: the elements from which it is made, the relative quantity of each element and the chemical state of the elements present. Modern XPS instruments can also produce images or maps showing the distribution of the elements or their chemical states over the surface. A good instrument would have a spatial resolution of a few microns. Electrons can only escape from the solid if they originate close to the surface. If they originate from too deep within the bulk of the solid then they will be reabsorbed or suffer inelastic collisions. The information available from XPS is, therefore, highly specific to the surface of the material (1-3 nm) . The measurements must be made in ultra-high vacuum (uhv) to allow the photoelectrons to travel from the surface of the sample to the detector without striking a gas atom. Many XPS spectrometers have other analytical techniques associated with them for example: Auger Electron Spectroscopy (AES), Secondary Ion Mass Spectrometry (SIMS), Ultraviolet photoelectron spectroscopy (UPS).

2.6 Summary

This chapter has described the specimens used, and all of the techniques that have been used to obtain the results that are presented in the following two chapters. The reader should now have a detailed understanding of how the specimens were produced, including both material and the processes used. The methods used to obtain the results have also been described in detail. Some of the explanations have used data from the actual specimens to demonstrate the technique; these results are presented and discussed in detail in the relevant chapter. We have seen that the theoretical predictions for the response of the interlayers present in adhesive joints to ultrasound suggest that the use of the oblique incidence technique should offer a considerable improvement in sensitivity to the properties of these layers over the more conventional

normal incidence use of ultrasound. The mechanical tests that are used to quantify the performance of the specimens has been presented, along with some validation of the choice of analysis. We have also examined the range of techniques that are available to examine the failure surface of the specimens to explain the mechanical test results. The next two chapters contain all of the results, with Chapter 3 containing all of the two-layer specimen results and Chapter 4 containing the results from the three-layer specimens.

3. Two-layer Specimen Results

3.1 Introduction

This chapter contains all of the results that have been obtained from the two-layer specimens, with the results from the three-layer specimens being presented in the following chapter. The results are subdivided so that the specimens are discussed by the pre-treatments that they received prior to bonding. Then, for each specimen, the results are presented in approximately chronological order, with the ultrasonic results progressing from the initial scans through to the final scans before the specimens were sectioned prior to mechanical tests. Then the results of the mechanical tests are presented followed by the surface analysis. Many of the early specimens were used to validate the experimental techniques and produced useful results, though without progressing through all the mechanical tests and surface analysis.

It is worth explaining the difference in appearance in some of the ultrasonic results that are presented. The earliest scans were done using an older scanning system, which used a 4-bit gated peak detector. This gives a smaller dynamic signal range that can be presented on a scan compared with the newer scanning system. The later scans were produced using signals captured using a 1GHz digitiser card, and then peak detected in software. This makes the thresholds applied to the signals less critical, allowing the full range of signals to be displayed on the scan. The 4-bit digitised scans frequently have some parts of the signal missing as they are outside the limits which are necessary to highlight the detail in the main region of interest in the scan. The majority of the results have been obtained using the newer system. It should also be mentioned that for all of the ultrasonic scans presented the level of grey shown in the scan is proportional to the signal amplitude, with black being the highest and white being lowest. The maximum and minimum levels to be displayed have been chosen to highlight as much detail as possible. For all of the scans the reflection from the interface of interest has been gated. All of the normal incidence scans have been produced using the same 50MHz, 1 inch focus polymer probe. The pulser that was used changed at the same time as the scanning system; this resulted in a slightly higher frequency and more broadband signal, but the effect on the scans is minor. The

oblique incidence scans were obtained using 20MHz focused probes except in the case of some of the earlier scans which used either 20MHz unfocused probes or 10MHz focused probes but these cases are specifically labelled.

The original purpose of using a two-layer specimen design was to provide a specimen which was as simple as possible for inspecting ultrasonically and had a large free epoxy surface which would allow water to arrive at the interface after diffusion through the epoxy in a uniform manner. The 2mm epoxy thickness would prevent the epoxy at the interface from saturating too quickly; see the diffusion calculations presented in Chapter 2. However the fact that these specimens had a clear epoxy covering meant that they could easily be inspected visually to see if there were gross changes, and this acted as a guide as to how frequently they would be inspected ultrasonically. They were also used as a guide for the inspection of the three-layer specimens, which obviously could not be inspected visually, but were not expected to degrade any quicker than the two-layer specimens and indeed probably much slower due to the length of the diffusion path from the free edges to the centre of the specimen. The relative rates at which joints made with different pre-treatments can be expected to degrade is well documented [24], and so much of the early effort was concentrated on the least durable treatments. The following results are ordered by the expected durability.

3.2 Grit blast

3.2.1 Normal incidence ultrasound

Figure 3.1 shows the results obtained from the normal incidence scans of a 2-layer grit blast specimen. The figure label details how many days the sample has been immersed in water at 50° C for each of the scan images presented. The scale at the bottom of the figure shows the signal amplitude associated with the grey scale of each image. It is shown as a percentage of the maximum measurable by the digitiser. Anything above the upper limit is shown in black, and white below the lower limit. This is kept largely the same for all of the specimens, with the oblique incidence scans using a different set of limits.

Examining this figure quickly shows that the most obvious change to occur with increasing exposure to hot water is the growth of disbonds from the unsealed edges, and these advance rapidly toward the centre of the specimen. From the initial

scan there is an area of white speckle. This is due to surface roughness. The scattering from roughness is inversely proportional to the wavelength of the ultrasound [65, 66]. This roughness was present on the plate when it was received, and the grit blasting process makes it difficult to see when examining the plate by eye. The effect of roughness can be seen when looking at the reflections from the disbonded regions of the sample; as time progresses corrosion roughens the surface, and the reflected signal amplitude drops.

However there is other more important information that can be gained from this figure. After 27 days in water there are several changes to be noted. The marine paint that was used to seal two of the edges can be seen. Rapid corrosion of the free unsealed edge can be seen, with large corrosion pits appearing. With the short wavelength and small spot size being used the surface roughness seen on these samples could be imaged by monitoring the time of the reflection of the interface signal, which would generate a surface profile. However for the purposes of this work the change in the interface is so gross that it is of little interest. We can also see that there is some disbonding initiating from the flush unsealed edge, which is the largest significant change.

Closer observation shows that there are some small dark spots appearing under the epoxy. These are apparently quite randomly distributed, with no apparent difference being seen with proximity to sealed or unsealed, flush or recessed edges. Unfortunately many of these small defects are more easily seen on the computer screen than the printed figure. Some of these small spots have been highlighted on subsequent scans but close scrutiny of the scan from 27 days shows some sign of them. There are also blurred lighter shaded lines visible; these are due to scratches on the top surface, produced during removal of the protective coating. The protective coating is necessary to prevent gross corrosion of the free surface which would prevent detailed scanning, as has been discussed in Chapter 2.

As the exposure time increases the general trend is for many of the features seen after 27 days of exposure to increase in extent. The number, of what are termed micro defects, (those which are isolated from adjacent defects and occur throughout the specimen) increases. These take two forms, small spots which are generally detected when their size is around 0.5mm diameter or bigger and line defects, which in many cases lead to the development of small corrosion spots. Again their detectability appears to be size limited. There are also darker areas appearing within the centre region of the specimen, which visual examination suggests are clusters of

extremely small disbonds. We can also see that roughening of the unsealed recessed edge by corrosion causes total loss of the signal after 67 days in water (there is still easily detectable reflection from the interface in this area but it is lower than the minimum that is assigned a grey level in these scans).

Figure 3.2 shows higher resolution scans taken from the same sample after 223 days in water. This figure shows that it is possible to detect defects that are less than 1mm diameter, with detail considerably below this being evident (~0.1mm), although this is smaller than could be reliably detected. It is important to note that although the scan pitch is as small as 0.025mm for the finest scan, the focal spot size of the probe remains unchanged for all of the normal incidence scans. Changing the scan pitch from 0.1 to 0.025mm primarily helps by giving some spatial averaging, making smaller defects easier to identify but no sharper.

3.2.2 Oblique incidence ultrasound

Figure 3.3 shows the same sample and the same exposure times, but for this figure the oblique incidence technique has been used. In general the results are much the same as those obtained at normal incidence, with several important differences. There are improvements over the high frequency normal incidence results in that there is lower sensitivity to roughness, which has made defect identification easier in places. This can be seen particularly in the lower right hand corner where roughness had produced much scattering on the normal incidence scan. This is also true for roughness of the top surface, as there are no signs of an influence from top surface scratches on any of the scans. However this reduced sensitivity to roughness is accompanied by a reduction in sensitivity to small defects. Whereas in the normal incidence scan there was the appearance of many small spots none of these can be seen in the oblique incidence scans. There are areas of the specimen where dark shaded areas can be seen, which appear to correspond to clusters of very small defects. (see Figure 3.4) This is very much what would be expected from a normal incidence scan produced using a lower frequency, being less well focused and less sensitive to surface finish.

It is important to note the consistency of the signal from the interface of this specimen. It had been hoped that the oblique incidence results would give greater sensitivity to subtle changes in the interfacial properties of the joint. However the predictions that this is based upon still requires the detection of small variation in the signal amplitude. We can see from this figure that from the initial scan that there is

significant signal amplitude variation across the sample, over short distances, which give the scans a grainy appearance. This appears to be due to the rolling of the plate, giving an uneven grain structure. This signal variation will then increase the size of the reflection required from an area of degradation before we can successfully identify it from a scan.

3.2.3 Comparing scans with the visual assessment of the specimen

Figure 3.4 shows the comparison of the normal incidence and oblique incidence scans with a photograph of the specimen taken after 223 days in water. The advantages of using a clear adhesive can be seen from this figure, as there is a huge amount of detail in the photograph. Examination of the specimen by eye is preferable to examination of a photograph as identifying marks which are on the free epoxy surface and those which are under the epoxy layer becomes easier. It also enables the visual assessment of the extent to which corrosion under the epoxy has made it bulge, giving some idea of the stress that is being applied to the interface. However comparison of the scans and the photograph gives a good idea of how much detail each of the scanning techniques is detecting and how much is being missed. It is interesting to see from the photograph that one of the most affected areas of the specimen is in the lower right, which can be seen from the initial normal incidence scan of the sample is where there was a great deal of roughness at the interface. It can also be seen that although the normal incidence scan detected many more micro-defects than the oblique incidence there is even more detail to be seen in the photograph.

However there is a distinction to be made between the visual and the ultrasonic images. Visual assessment of the specimen alone is not sufficient to predict the appearance of the normal incidence scan, based on defect size. We can see that some defects of visually similar appearance do not appear the same in the normal incidence scan. Part of this may be because the ultrasound is only sensitive to defects at the interface. This could mean that although visually similar, some of these defects are distinguishable by the amount they disturb the interface. When the specimen is inspected visually we see the defects in plan view, and the extent of the defect that is seen is largely independent of the depth. Therefore some of these defects may be predominantly contained in the epoxy and thus appear small (or not at all) on a scan produced by monitoring the interface.

3.2.4 Mechanical tests

Figure 3.5 shows the comparison of the failure surface from the same 2-layer grit blast specimen with the final normal incidence scan. The strips that have been cut for the mechanical tests are clear, and these strips have been overlaid onto the ultrasound image. The right-most strip has not been tested as preparing the edge of the strip was felt to be too difficult due to the amount of disturbance to the epoxy layer because of the large disbond present. However this shows that the presence of the epoxy gives greater contrast to many of the micro-defects compared to the strips where the epoxy has been removed, though in general the appearance of the failure surface is very similar to that seen when the epoxy layer was in place. i.e. the right most strip shows a strip which still has the epoxy layer in place, whereas the other seven strips are shown after the mechanical test in which the epoxy is removed.

One of the most interesting things can be seen from Figure 3.5 is that the defects that were clearly visible from the normal incidence scan are distinguishable on the failure surface due to the presence of a covering layer of epoxy. This might lead to the curious conclusion that prior to the mechanical testing of this specimen the defects detected were failure within the epoxy, albeit very close to the interface otherwise they would not have been detected on an interface scan. A large amount of the detail seen on the failure surface is present on the scan. However it is a different matter to predict the failure surface that would be obtained with only the scan to base the prediction on. The mechanical tests for this specimen provided only three successful strips due to a number of problems. These primarily were problems synchronising the load displacement data from the testing machine with the video recording of the crack growth. However the results obtained have been included in Table 3.1.

Figure 3.6 (b) shows a micrograph of this specimen, together with a small section of the failure surface shown in the previous figure. This S.E.M. picture shows one of the lines that was visible by eye from the specimen. The highly contorted surface generated by grit-blasting is evident. Also evident is a line of epoxy covering the surface. This suggests that the what was visible prior to destructive testing of this specimen was a defect in the epoxy layer and not at the interface. Whether the flaw was a complete disbond or a line of weaker epoxy is not obvious from the results obtained so far. However it is evident that such a flaw may well allow water to penetrate the joint. This figure also shows a difference in the appearance of the failure surface either side of the line. However high resolution S.E.M. images from areas either side of the line failed to show any differences.

3.2.5 Additional grit blast specimen

Due to the lack of satisfactory results from the mechanical tests on the previously discussed specimen, another pair of grit blast specimens were produced. These were left in water for a single, longer period, with periodic visual inspection being carried out to ascertain the extent of disbonding. After 145 days the sample was removed from water, scanned and then sectioned for mechanical tests. At the same time as one of the specimens was in water another, made at the same time, was left in a dry oven at 50°C for the same period as the wet sample was in water. This enabled the effects of temperature alone to be determined, so that comparison between the wet and dry specimens was entirely due to the presence of moisture.

Figure 3.7 shows the comparison of the final scans from the wet and dry samples with photographs of the failure surfaces. As was seen with the previous grit blast sample there is good agreement between what is seen on the scan and the failure surface. This sample did not suffer from the same amount of roughness as the previous sample, making the identification of the small scale disbonds much easier. It requires detailed examination of the failure surface to see all of the detail which is apparent from the scan of the sample. There is less edge disbonding on this sample, probably due to the exposure time being approximately half that of the previous specimen. The time that it takes for a disbond to initiate also has a large effect on the apparent disbond rate, when the disbonded area is considered as a function of overall exposure time. This has been seen more graphically on other specimens (see two-layer PAA specimen discussed later in this chapter) where as many as 200 days pass before significant disbonding is detected, but once started the disbonding progresses at a uniform rate. Visual inspection of the failure surfaces indicates that both wet and dry specimens failed at the interface, with no significant amount of epoxy visible on either specimen. This is to be expected due to the asymmetric nature of the mechanical test as previously discussed in Chapter 2.

Figure 3.8 shows both the failure surface and the results obtained from the mechanical tests. Comparing the wet and dry mechanical test results there is an obvious drop in toughness from the dry to the wet specimen. By simply averaging the toughness values obtained from the mechanical tests this equates to a drop from 60.9 Jm^{-2} for the dry specimen to 28.0 Jm^{-2} for the wet specimen. This is relatively uniform with the standard deviation for the whole specimen being ± 7.23 Jm^{-2}. However the right-most strips appear to have degraded more than the rest of the specimen, the average for strips two to five is 32.8 Jm^{-2} with a standard deviation of

±4.0 Jm^{-2}, and for strips six to eight the average is 20.9 Jm^{-2} and a standard deviation of ±4.8 Jm^{-2}. Strips six to eight are on the side which is closest to the unsealed recessed edge. It can also be seen that the strips on this side of the specimen fail at shorter crack lengths due to the gross edge disbonding that can be seen both from the failure surface and from the ultrasonic scan of the specimen. However there is no obvious drop in G_c as the crack approaches these disbonds. This highlights one of the difficulties of the mechanical tests in that the disbonds were generally present at the flush edged end of the specimen, and the crack had to be initiated at the overlapping end. Therefore the crack approached the disbond through the last attached piece of epoxy, and the final failure was always some distance from the end of the specimen making a measure of G_c for the final 5-10mm of the specimen impossible.

3.2.6 Failure surface analysis

Figure 3.9 shows the XPS binding energy graph obtained from a section taken from the adherend side of the early wet 2-layer grit-blast specimen. After mechanical tests the epoxy layer remained attached to the large metal base plate that each strip of the specimen had been bonded to. The epoxy was extremely brittle making it difficult to remove from the base plate and so XPS results have all been obtained from the adherend side of the failure surface. The data shown in Figure 3.9 presented in this form is primarily useful for explaining how the quantified surface analysis results that are going to be presented next are obtained. The light grey curve shows what has been labelled as “survey” and this is used to quickly identify what elements are present on the surface of the sample. Chapter 2 gives a more detailed explanation of the technique. From this curve, and after examining survey spectra from a number of different samples, nine significant different elements were identified as being present. The survey however is not accurate enough for making a quantified analysis of the elements present. To do this a finer sweep is made over the range of energies covered by the peak of interest. When the size of the peak is low for a given element several sweeps are made so that the an average can be taken to reduce the noise. Once all of the peaks have been well defined the area under each is calculated and this is then used to calculate the ratio of each of the elements present. The finer resolution scans from each of these elements is overlaid onto the survey. The same experimental procedure is used for all of the samples tested but in some cases the quantity of certain elements is too low to quantify and these are simply left as zero.

The surface analysis data from the wet sample is not particularly useful taken in isolation. However it becomes much more significant when the results are

compared with those obtained from the dry sample. One of the advantages of the mechanical tests performed on the two-layer specimens is that even the dry samples undergo visually an apparently interfacial failure. This allows comparison of wet and dry interfaces to be made. Direct comparison of the spectra obtained from the wet and the dry specimens is not ideal due to the enormous difference in the size of the peaks from the fundamental elements such as oxygen and carbon compared with those from sodium and chlorine etc.

Figure 3.10 shows a graph comparing the quantified results from two sections taken from the grit blast specimen shown in Figure 3.5, and one section taken from a dry two-layer specimen. The two sections that were taken from the wet sample were chosen as representative of the two fundamentally different areas of the failure surface. One of the areas is labelled as “defects” which was taken from an area with a large number of dark spots and lines visible to the eye, and the other section, labelled as “no defects”, was taken from what appeared to the eye as a clean grit-blast surface. The elements that have been chosen can be loosely split into two groups: those that can be expected in a dry sample and those which are the results of contamination. Those which can be expected in a dry sample could also be divided into those due to the adherend and those due to the adhesive, with the aluminium and oxygen being present due to the adherend (with the ratio depending on pre-treatment), carbon and nitrogen being due to the adhesive. In some cases we may also see sodium, chlorine and calcium with these being carried in by water.

If we first consider the results from the dry sample compared with those from the wet specimen, we can see that the biggest differences are in the concentrations of the aluminium and silicon, and that there are no signs of either sodium or chlorine. To a lesser extent we can see that the oxygen concentration is slightly higher and the carbon is a little lower. Comparing the results for the two sections taken from the same wet sample we can see that the sample labelled defect, which was taken from an area which had visible surface contamination is closer in the elemental surface concentrations to the dry sample result than the sample labelled as no defect. It is worth remembering that the XPS results are obtained over an area 5x1mm. The “no defect” area appeared to be relatively uniform, whereas the “defect” area was a cluster of dark spots, and so the surface analysis results are an average of the elemental concentrations of both the dark spots and the clean area in between. The no defect area shows signs of sodium, chlorine and calcium and lower concentrations of aluminium and oxygen. This suggests that there has been contamination by water on the clean wet sample, but perhaps we are seeing more aluminium oxide in the defect areas. However

the differences between the “clean” and “dirty” areas is small, as are the quantities of sodium and chlorine making in difficult to draw absolute conclusions from this analysis. These results can be discussed in more detail once the surface analysis results from the other specimens have been considered.

3.2.7 Summary of results from grit-blast specimen

The grit-blast specimens discussed in this section have shown many defects. As was discussed in section 1.5 it can be expected to be the least durable of all of the pre-treatments used. Thus the defects seen here can be used as a base line against which to judge the other specimens. The defects that have been seen can be divided into several types

- edge disbonding - easily detected disbonds (both visually and using either ultrasonic technique) which subsequently corrode and the disbond spreads further into the sample, the rate of growth of these disbonds is most clearly seen in Figure 3.1.

- small spots - these have occurred across a large portion of the specimen, but have generally been to a greater extent closer to the edges of the specimen, particularly in the corners. These defects can be sub-divided into those that have been seen from visual inspection and those also detected ultrasonically. It is interesting to note that the most clearly ultrasonically detected small spots appear on the failure surface with a epoxy coating, this is seen in Figure 3.5.

- line defects - these were seen to a great extent on the initial grit-blast specimen, and can also be divided between those only detected visually and those also seen ultrasonically, these can be seen from Figure 3.4 and Figure 3.5. Microscopy from a section of one of these lines has shown it be a covering of epoxy left on the failure surface.

The small spots and line defects have loosely be termed micro-defects as there detection appears to be largely determined by the resolving power of the technique used for detection.

The mechanical tests of these specimens have shown that there has been a significant toughness loss across the whole of the wet specimen when compared to the dry, but the loss has been greatest in the strips taken adjacent to the unsealed edge, see

Figure 3.8. There has not been any evidence of a greater loss of toughness adjacent to the large edge disbonds, but this may partially be a factor of the mechanical test.

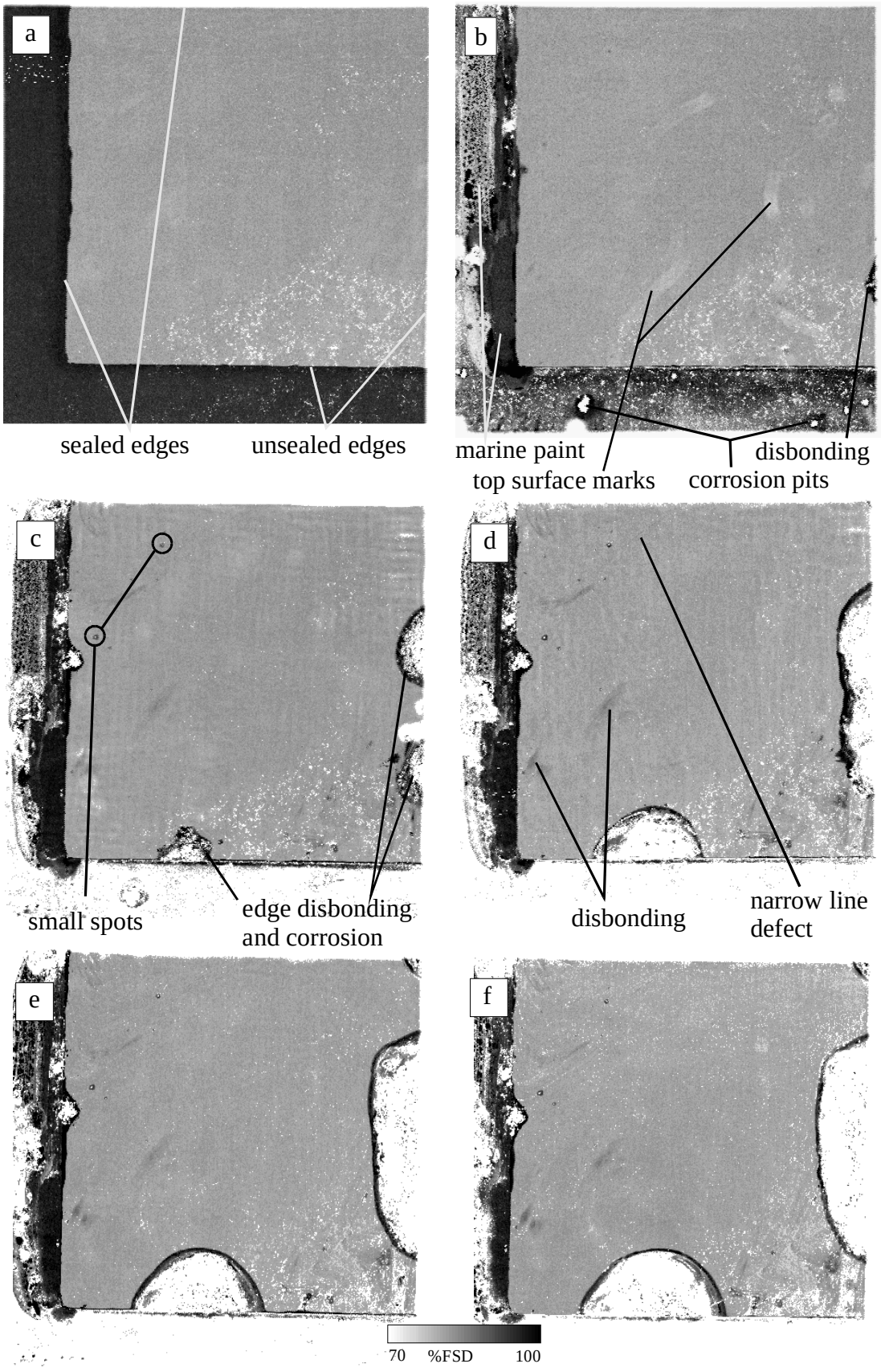

Figure 3.1 Normal incidence scans from grit-blast specimen after (a) 0 days (b) 27 days (c) 67 days (d) 117 days (e) 173 days and (f) 223 days.

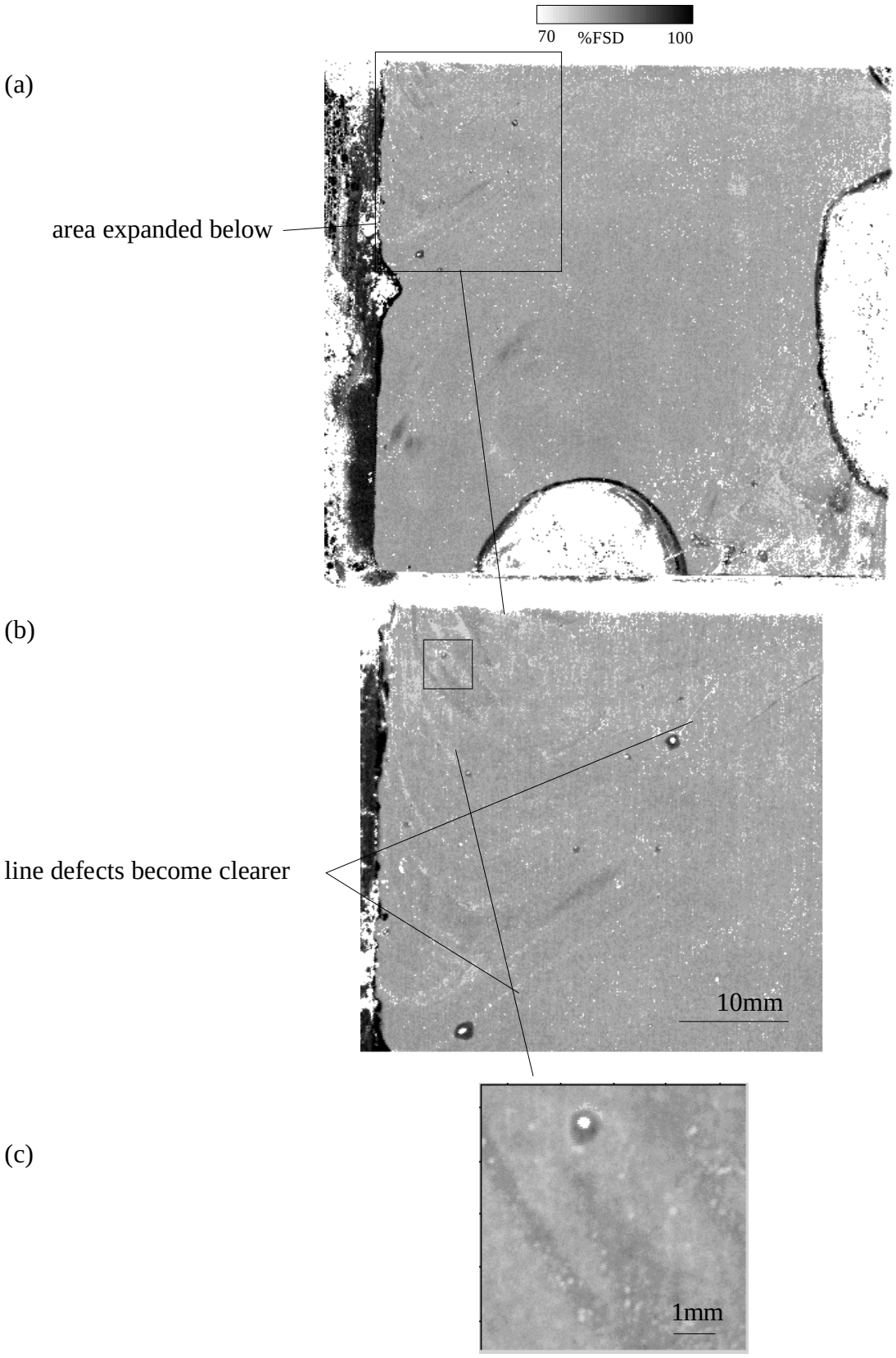

Figure 3.2 Finer resolution scans from grit-blast specimen after 223 days in water (a) 0.25 mm scan pitch: (b) 0.1 mm scan pitch: (c) 0.025 scan pitch.

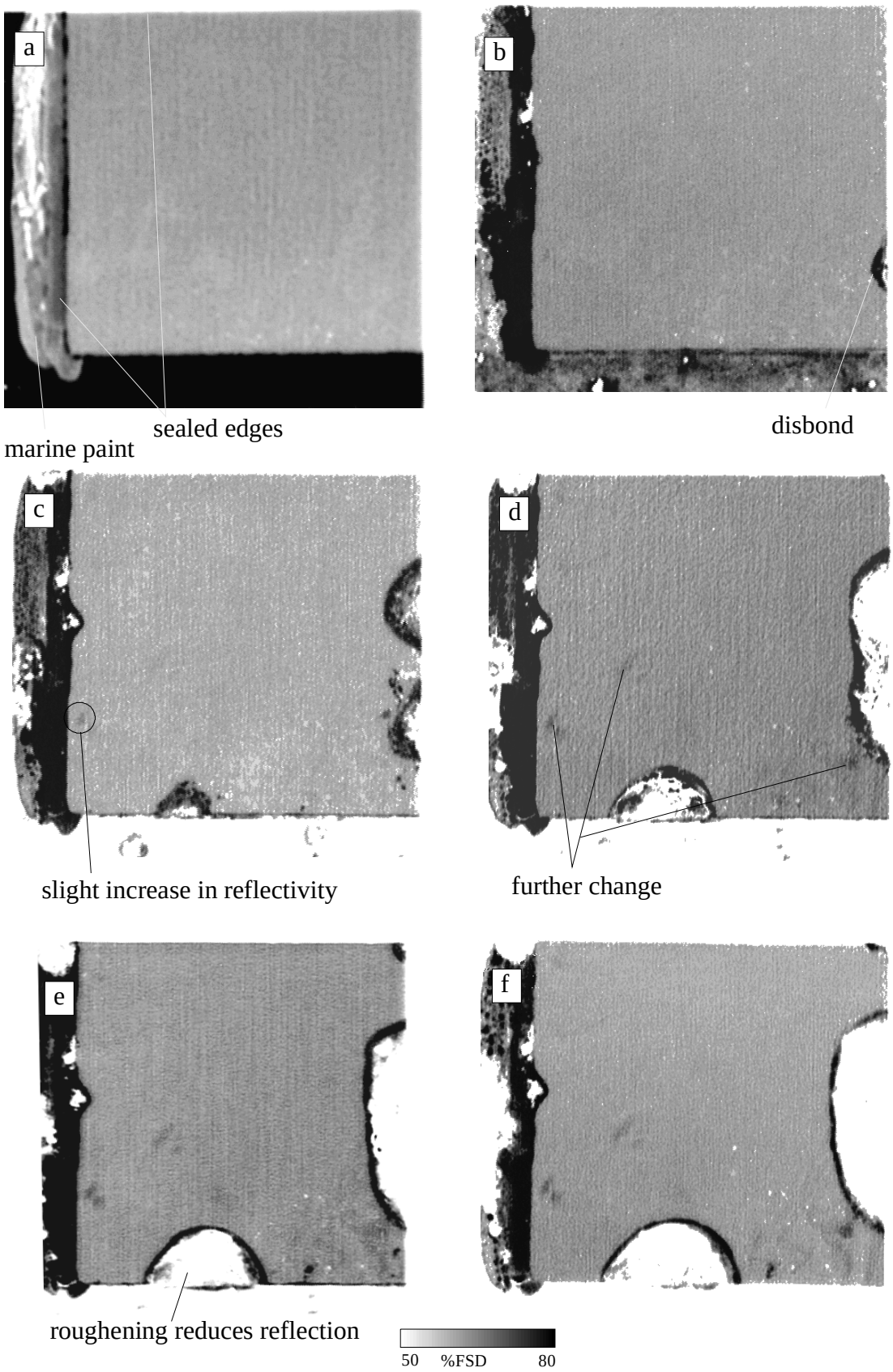

Figure 3.3 Oblique incidence scans from grit-blast specimen after (a) 0 days (b) 27 days (c) 67 days (d) 117 days (e) 173 days and (f) 223 days.

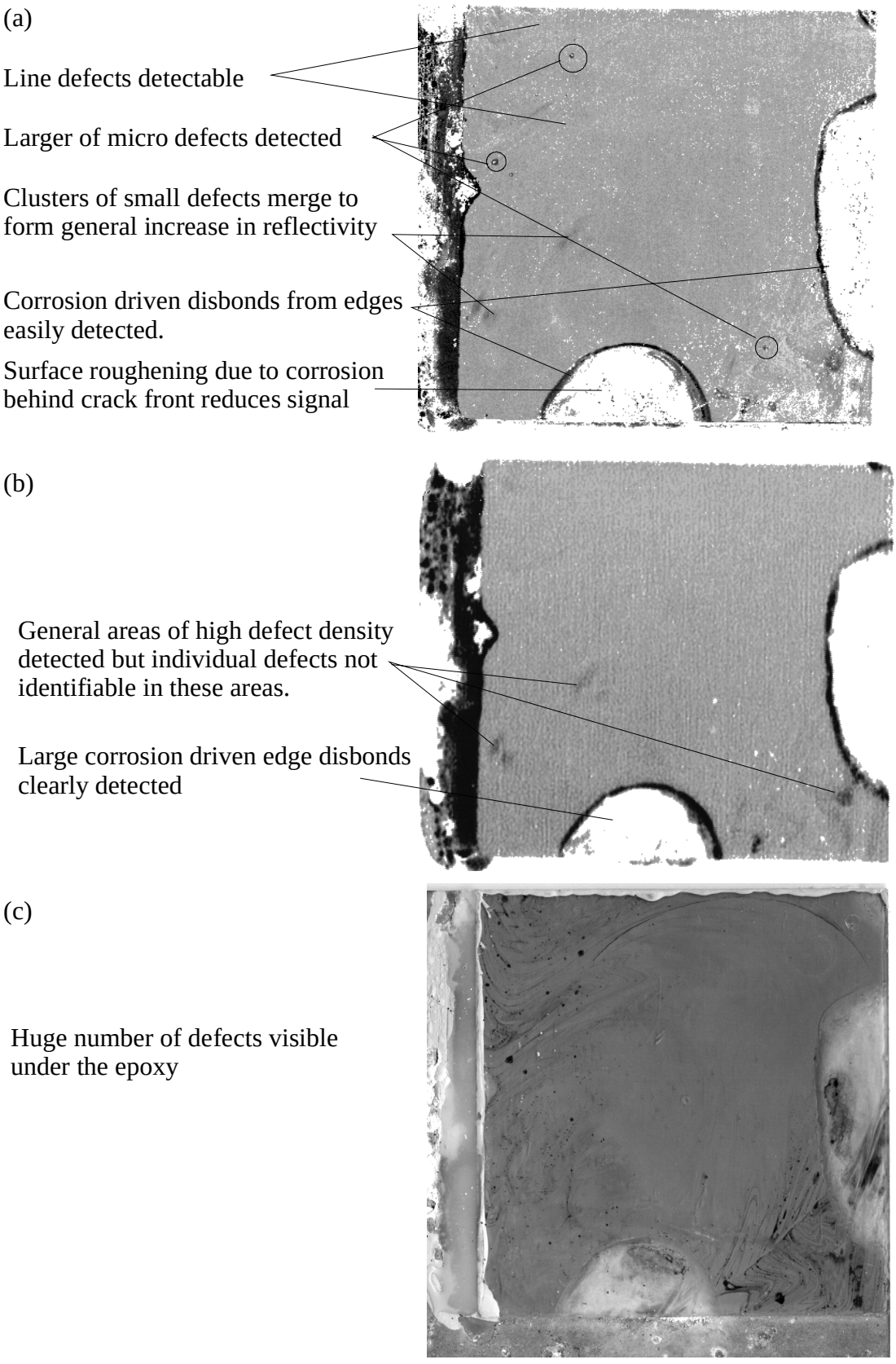

Figure 3.4 Comparison of (a)normal and (b) oblique incidence scans with (c) a photograph from a 2-layer grit-blast specimen after 223 days in water.

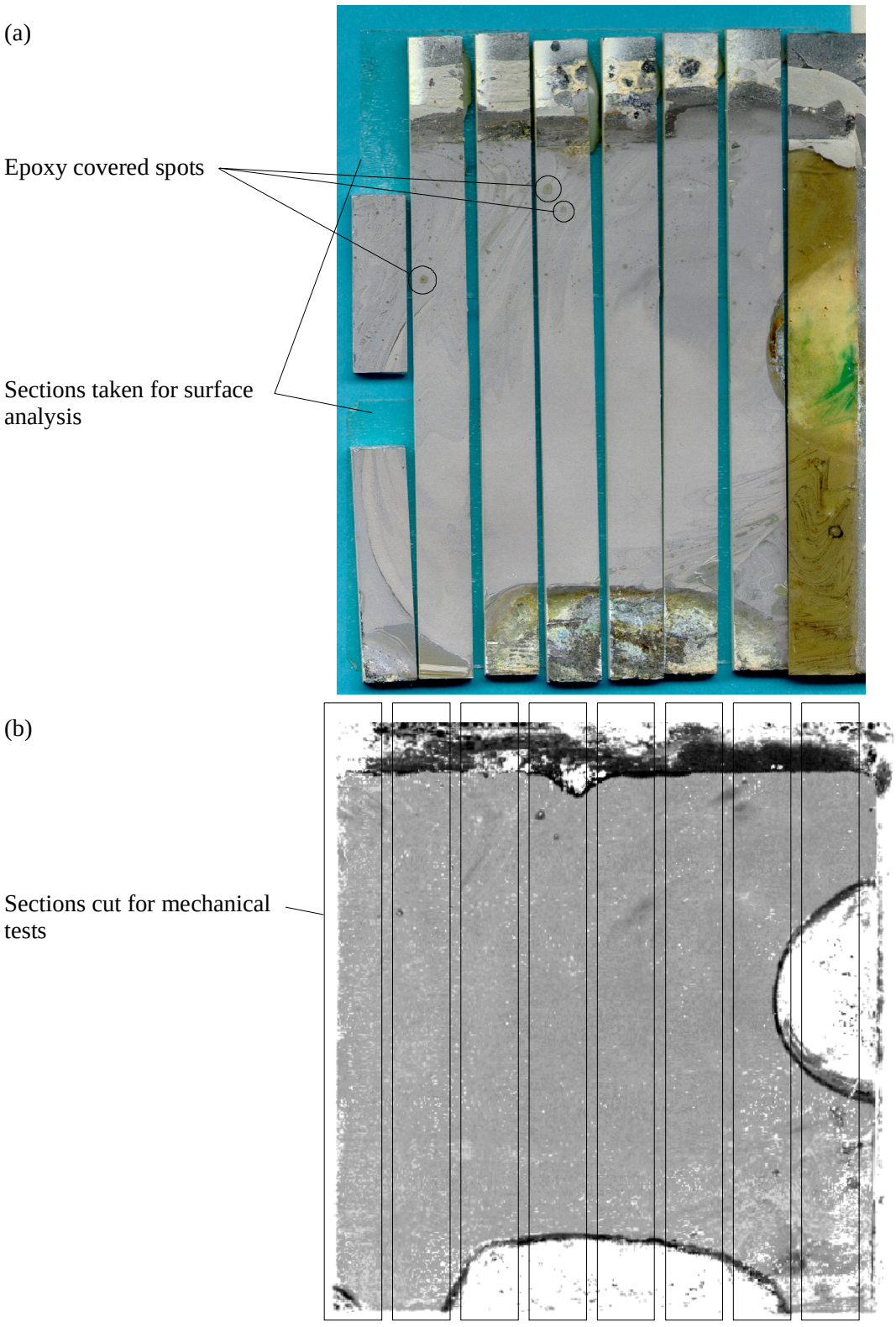

Figure 3.5 Initial 2-layer grit-blast specimen after 223 days in water showing comparison of (a) failure surface and; (b) normal incidence scan.

(a)

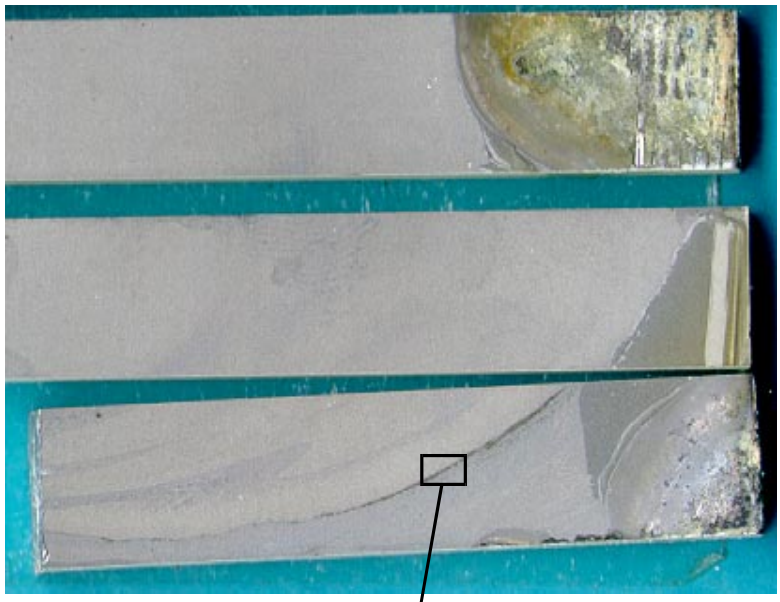

(b)

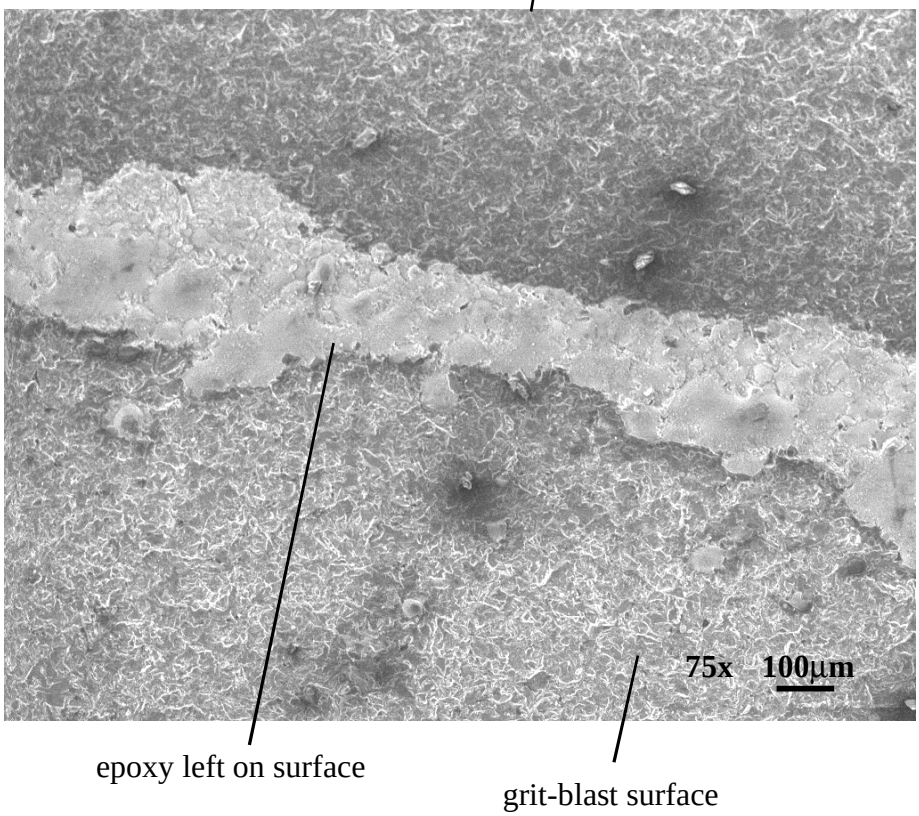

Figure 3.6 Failure surface from two-layer grit-blast specimen showing (a) macroscopic view and (b) S.E.M. micrograph.

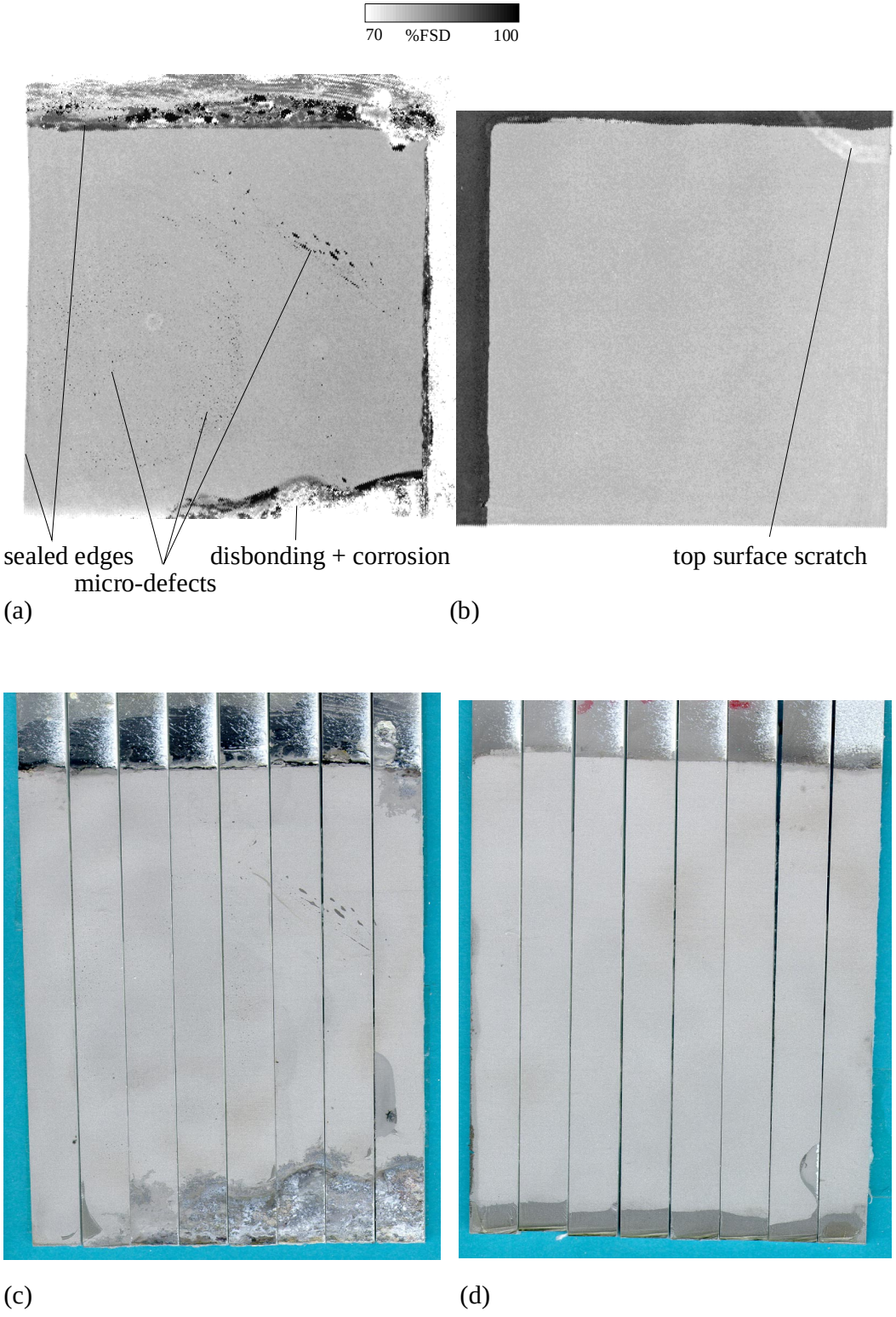

Figure 3.7 Comparison of normal incidence scan from 2-layer grit-blast specimen after; (a) 145 days in hot water and; (b)145 days in oven at 50°C with failure surface from; (c) wet specimen and; (d) dry specimen.

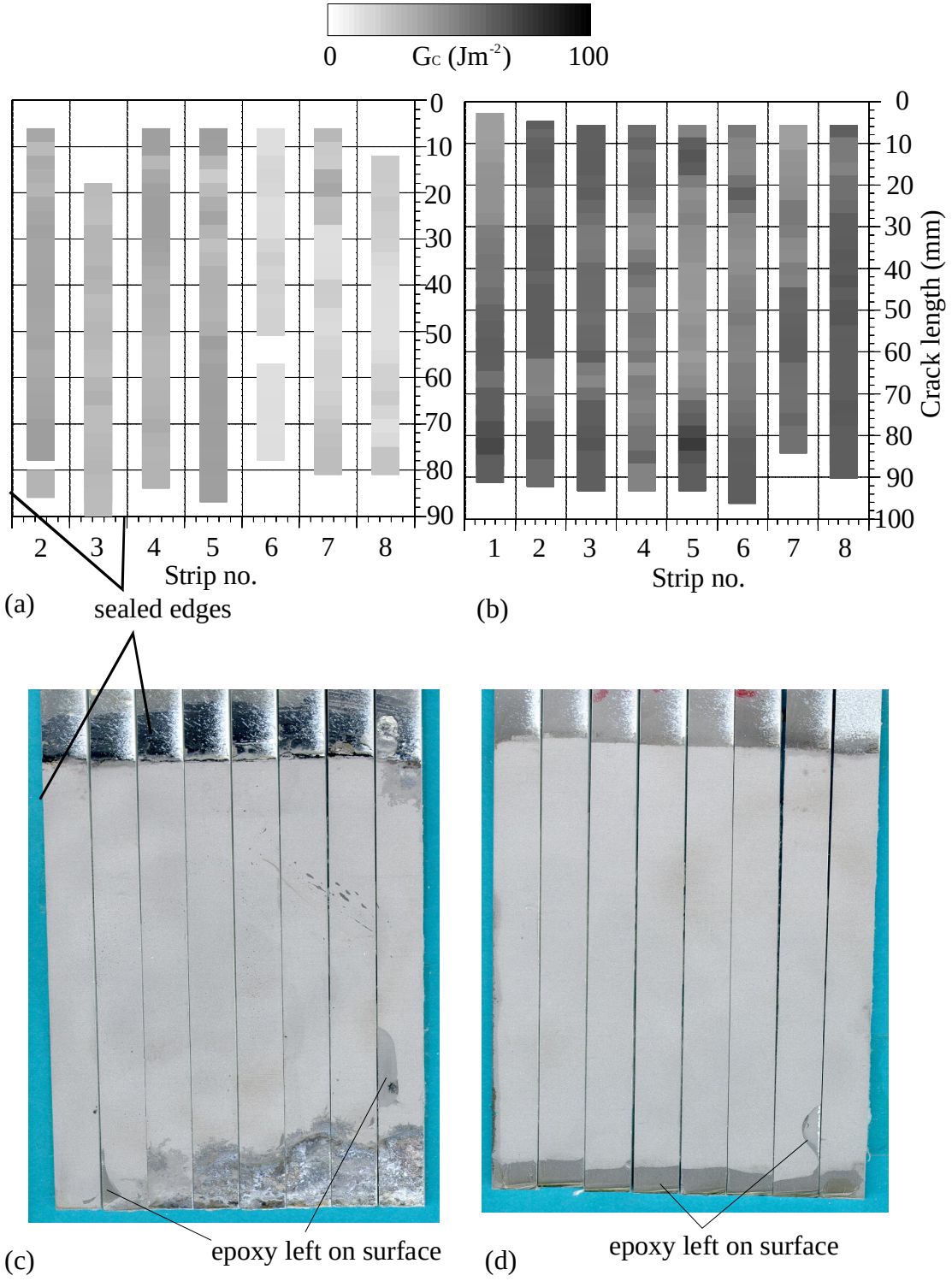

Figure 3.8 Comparison of mechanical test results from 2-layer grit-blast specimen after; (a) 145 days in water and; (b) 145 days in dry oven with failure surface from; (c) wet and; (d) dry grit-blast specimens.

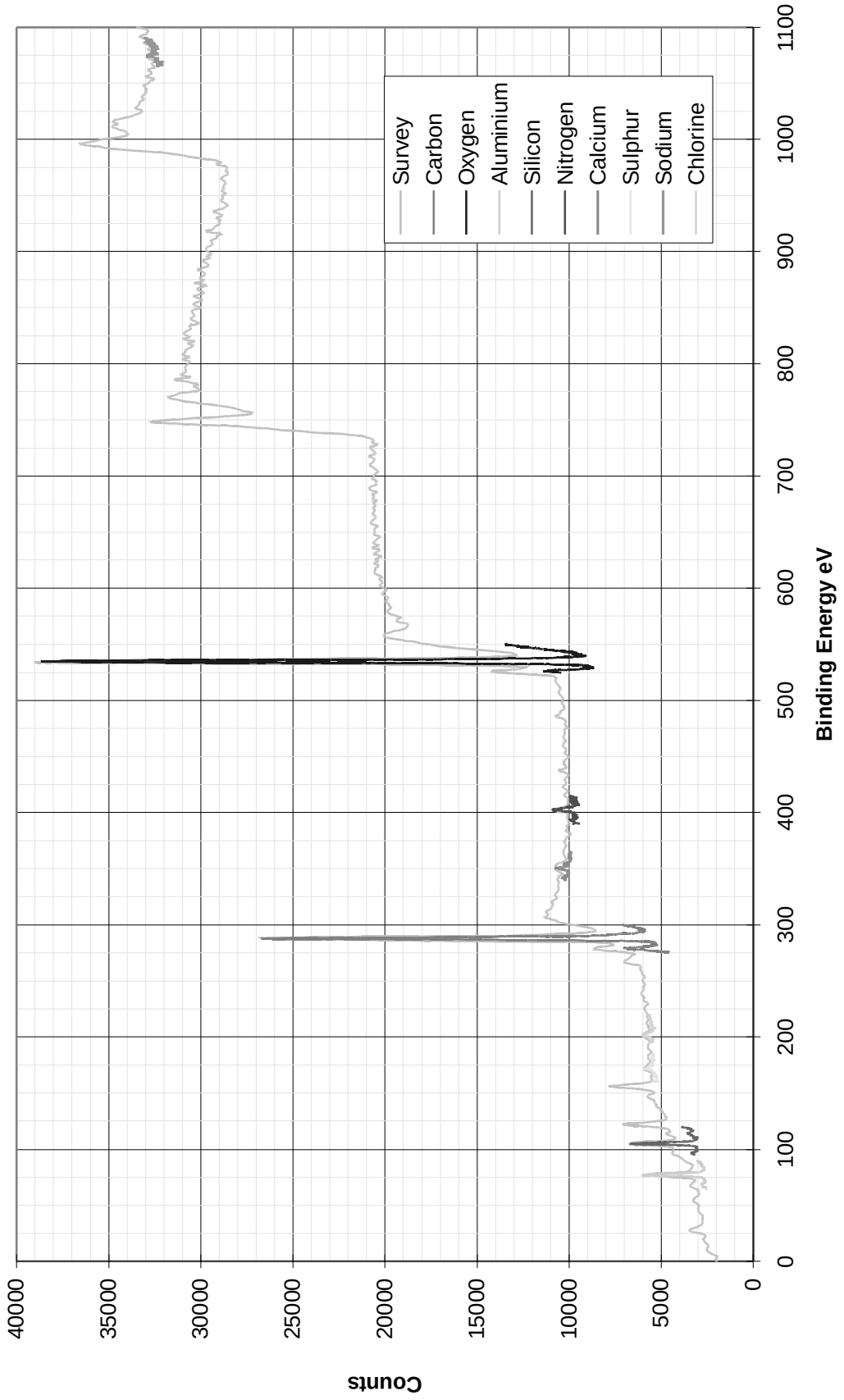

Figure 3.9 XPS result from adherend side of 2-layer grit-blast specimen, coarse sweep data is shown in grey with more accurately obtained data overlaid in colour.

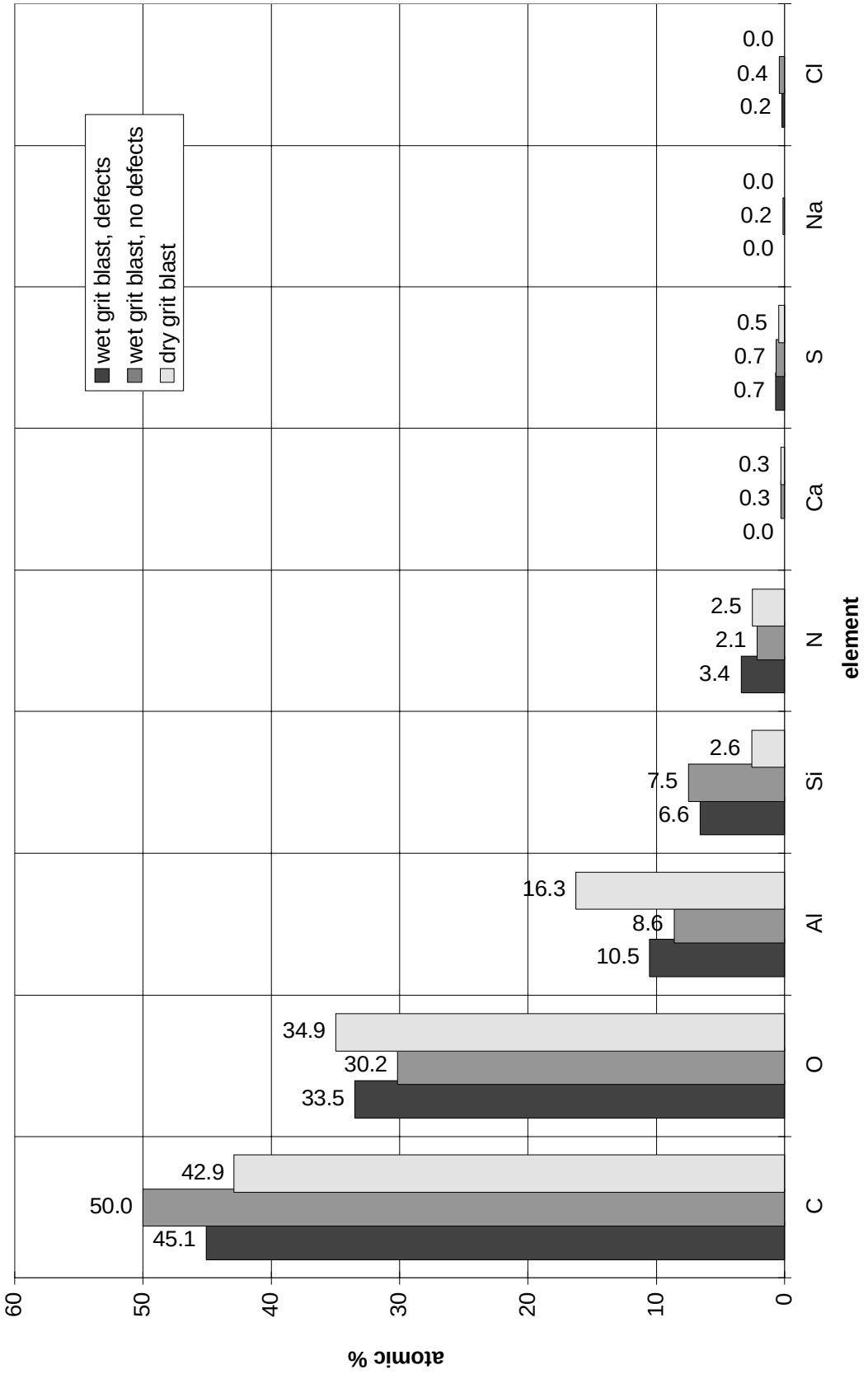

Figure 3.10 Comparison of quantified XPS results from the adherend side of both wet and dry 2-layer grit blast specimen.

3.3 Chromic Acid Etch

3.3.1 Normal incidence ultrasound

Figure 3.11 shows the normal incidence scans obtained from a two layer chromic acid etch sample with increasing exposure to water. The results from this specimen are in many ways similar to those seen from the grit blast specimens discussed in the preceding sections. The initial scan from this sample has a square overlaid on it to show the area covered by a thick layer of epoxy. The areas outside of this that appear the same are areas of spew adhesive, not more than 0.5mm thick. We can also see some roughness down the left hand edge of the specimen, appearing as white flecks on all of the scans. As time increases we see both the development of large disbonded regions initiating at the unsealed edges, as well as the appearance of micro-defects. However in this case the number and extent of micro-defects is much smaller than seen on the grit blast specimen. The edge corrosion appears to be similar in the rate at which it progresses compared with the grit-blast specimen, indeed slightly faster for this CAE sample. The largest of the micro-defects have been circled for clarity. It can be seen that these micro-defects become more detectable with time. The line defects which were visible take longer before they appear on the scans (see Figure 3.15 for example of this). Again there is evidence of some pitting of the free aluminium surface, which is seen as the pale shadows on some of the scans, labelled as top surface marks.

Figure 3.12 shows the last two scans from this sample with higher resolution scans of some of the micro-defects. The defects that are shown in these scans are very clear given sufficient resolution, however there are other defects, particularly line defects that are only visually apparent but not detectable with ultrasound. This may be because what we see with the eye on these specimens is sometimes contained at least partially within the epoxy and may not be present at the interface. This is similar to the grit blast specimen discussed in the previous section, where the failure surface highlighted the differences between the visual appearance and the result from the normal incidence scan.

3.3.2 Oblique incidence ultrasound

Figure 3.13 shows the oblique incidence scans taken from the same CAE sample. These scans clearly show the gross edge disbonding; however the micro-defects are not as apparent as on the normal incidence scans. Very close examination

of these scans shows some evidence of the micro-defects, however they are difficult to identify without first seeing the normal incidence scan or examining the sample visually. The reason for the difficulty in identifying these small defects is two fold; firstly there is the fact that the focal spot of the pair of probes is considerably bigger than the 50MHz normal incidence probe, which will blur the image, making small defect detection difficult. However there is also far more scattering from the aluminium grains than is seen at normal incidence. This is evident in the form of banding on the images which appears to show the rolling direction of the aluminium plate from which the samples were cut, as was seen with the grit blast specimen. This banding can be discounted as merely an artefact of scanning as it appears with the probes and scan direction arbitrarily aligned, and will appear the same size regardless of the scan pitch. This is illustrated in Figure 3.14 which shows a higher resolution scan along with the last two scans taken from the specimen. The reason for this increased scattering from the oblique incidence scans may partly be explained due to the shorter wavelength of shear waves compared to longitudinal waves, and the fact that as they are travelling obliquely their path is longer in the aluminium than a simple normal incidence scan. However the lower frequency of the oblique incidence technique results in a similar number of wavelengths being propagated in the aluminium by both techniques. This suggests that shear waves are scattered more than longitudinal waves. These scans still fail to show any real sign of micro-defects.

It is a curious point that the oblique incidence scans show pitting to the top surface in a rather different manner to the normal incidence scan. At normal incidence the beam is nearly 5mm diameter as it passes through the top surface, resulting in a large blurred shadow on the image of the lower interface. With the pair of probes used for the oblique incidence scans the beam diameter on entry to the plate is smaller, but both the entry and exit beams will pass any pit on the top surface at some point in the scan. This results in a smaller disruption at a single point of the scan, but a single pit will cause two shadows to appear on the final scan. Hence top surface pitting is identifiable as it will always produce a pair of shadows on the final image. This also highlights the distance between the entry and exit points of the beam into the plate, which shows how much of the scan will be lost around edges, as either entry or exit points being over the edge of the plate results in no signal.

3.3.3 Comparing scans with the visual assessment of the specimen

Figure 3.15 shows a comparison of the final scans produced from this sample for both normal and oblique incidence with a photograph of the specimen. This figure

is convenient for showing the limits of detectability for the different techniques. It is clear that the number of narrow lines that can be seen from the photograph is far greater than seen from either scan. It is only the widest of the lines which appear in the scans.

The normal incidence scan shows that thin layers of spew adhesive appear the same as the bulk adhesive, whereas in the oblique incidence scan, because of the longer wavelength, the spew is distinguishable from the bulk. This can be understood by considering the layers spew adhesive as generating two signals, one from the top and one from the bottom of the layer. At higher frequencies the signal duration is short and there is sufficient separation between these reflections for them not to interfere. Therefore the peak detection which is performed to produce the image will find the same amplitude for the reflection from the interface of the aluminium and epoxy for both thin regions of spew adhesive and the bulk adhesive. However the fact that very thin layers appear the same as the bulk suggests that any defects located a small distance into the epoxy layer will not be apparent from the scan. This is in many ways a problem that will only occur with this geometry of specimen, as with a true joint there will only be a thin epoxy layer, and reasonable images can be produced scanning through the epoxy layer to the second aluminium epoxy interface, which will show defects within the epoxy layer, size allowing. This problem could be overcome by collecting full wave forms and using this to give information from some depth behind the interface, but this was not consider to be relevant as we are interested in the properties of the interface.

This CAE sample had seen very serious degradation as can be seen from the area of disbonding. It was decided not to expose this specimen to any further degradation. Before the specimen had been sectioned for mechanical tests the epoxy layer bowed and peeled itself almost completely away from the aluminium. This indicated that there was residual stress in the epoxy layer. It also suggests that the interface was not particularly tough across the majority of the specimen.

3.3.4 Additional CAE specimens

To enable calculation of fracture toughness values for this type of specimen with CAE pre-treatment another pair of specimens was produced. The normal incidence scans of these samples are shown in Figure 3.16, along with a photograph of the failure surfaces after mechanical tests. The biggest difference between the wet sample in this case and the one discussed previously is the lack of any micro-defects,

and this is accompanied by a slower rate of edge disbonding. There is also more pitting of the top surface of this sample. The more severe disruption to the top surface here will have been contributed to by the fact the periods between inspection for this sample were longer than on previous samples. Prior to scanning the top surface protection is rubbed off and any corrosion cleaned away. With short periods between scans this usually prevented any serious corrosion on the top surface.

Examining the failure surface does not produce any other significant information, with the surface appearing uniform, except for the large corrosion patch along the lower edge of the sample, which is also clearly visible from the scan. The failure appears to be uniformly interfacial. The failure surface from the dry sample is less uniform, with many areas having epoxy remaining on the surface. Figure 3.17 shows the comparison of these failure surfaces with the fracture toughness values from the mechanical tests. Generally the mechanical tests from these two layer specimens have produced continuous smooth crack growth. However in the case of the dry specimen shown here the crack growth was very unstable with many sudden jumps. This is evident from the mechanical test results by the number of gaps in the data and the large fluctuations in measured toughness. Comparing the wet and dry samples there appears to be excellent toughness in the bonded regions of the wet sample, appearing to surpass the dry sample in many places. This however may be misleading due to the large fluctuations in the toughness for the dry sample. The fact that the failure surface of the dry sample shows large areas of the specimen covered in epoxy suggests that the interfacial toughness of this specimen was excellent.

Comparison of the wet CAE sample with dry grit blast sample still suggests that the wet CAE sample has not suffered from significant degradation over the remaining bonded regions. The average fracture toughness for the wet specimen was 99 Jm^{-2} with a standard deviation of ± 17 Jm^{-2}. The fracture toughness of the dry sample was 103 Jm^{-2} with a standard deviation of 78 Jm^{-2}. This high variability of the results for the dry sample is due to the instability in the crack growth, with the crack jumping and stopping.

3.3.5 Failure surface analysis

Due to the nature of the failure of the dry CAE sample, which left large clearly identifiable layers of epoxy on the adherend side of the failure, a comparison of surface analysis results for the wet and dry CAE sample is of little use. When there are clearly large areas of the sample covered by epoxy, the surface analysis will simply

detect that there is an epoxy covered surface. Figure 3.18 shows the XPS result from the wet CAE sample. Taken in isolation there is less significance to be placed on the results than when compared with a dry sample. However it can be seen that there are no traces of calcium or sodium present, and these are key elements for identifying the presence of bulk water at the interface. This for a specimen which had been immersed in water long enough to have significant levels of water at the interface, but where the mechanical test results show no drop in toughness. This is suggesting that the presence of moisture in the epoxy alone is not sufficient for degradation of the bond.

The result from the wet CAE specimen has been compared with the XPS results obtained from the dry grit-blast specimen. This shows more carbon on the wet CAE specimen, but less aluminium and oxygen. This suggests that the wet CAE specimen has a thin covering layer when compared with the wet grit-blast specimen. This is most likely a thin epoxy layer, suggesting that the failure was in the epoxy, albeit very close to the aluminium interface. (Any significant thickness of epoxy would completely hide the aluminium.) This difference is locus can also be related to the higher toughness of the wet CAE specimen. Again this result will be discussed further once the XPS results from all of specimens have been presented.

3.3.6 Summary of results from CAE specimens

The results presented in this section have included two different wet CAE specimens. The first specimen gave results very similar to the wet grit-blast specimen. Comparing the types of defects it can be seen that:

- edge disbonds - appear very similar to the grit-blast specimen, although the rate of growth was slightly higher on the CAE specimen

- small spots - far fewer spots were seen on the first CAE specimen compared with the grit-blast specimen, this includes both those detected visually and those also detected with ultrasound.

- line defects - there were tens of lines defects on this specimen, the majority of these were near the edges of the specimen, but some occurred through the central regions of the specimen.

- In general the occurrence of micro-defects was smaller on the first CAE specimen than the grit-blast specimen.

•No fracture toughness measurements were made from the first wet CAE specimen, but it can be implied from the fact that the epoxy layer peeled away from the aluminium under residual stresses that the specimen had undergone significant toughness loss.

The second CAE specimen was noticeably different.

- edge disbonds - grew at a much slower rate than both the wet grit-blast and CAE specimens

- small spots - were not observed on this specimen, either visually or ultrasonically.

- line defects - were not observed on the specimen, either before or after the mechanical tests.

- The fracture toughness measured on this specimen was considerably higher than both the wet and dry grit-blast specimens, and also showed no loss in toughness compared with the dry CAE specimen.

- The XPS results from the second wet CAE specimen, when compared with the dry grit-blast specimen, showed the failure to be further from the aluminium and this can be associated with the greater toughness.

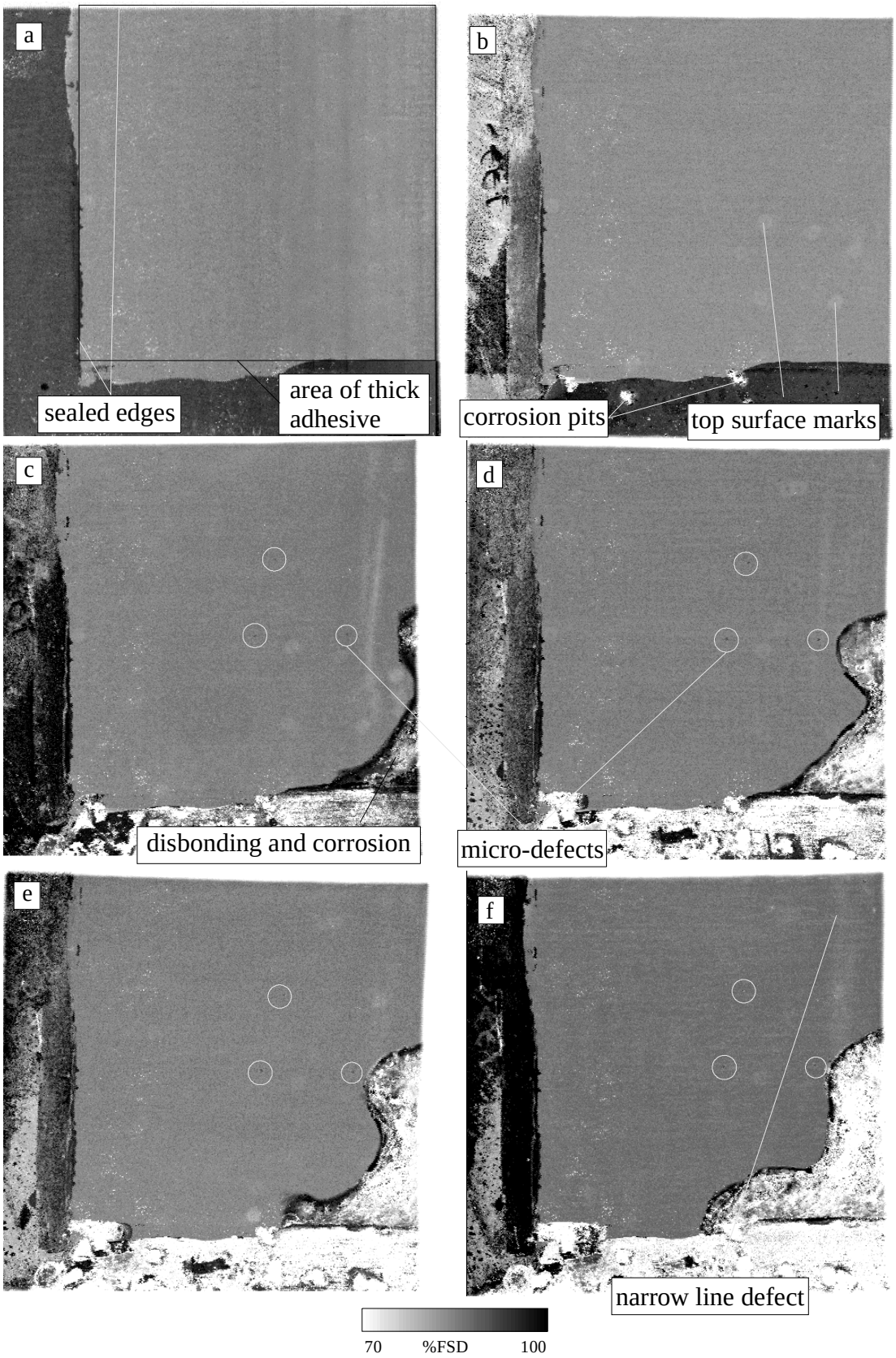

Figure 3.11 Normal incidence scans from 2-layer CAE specimen after (a) 0 days (b) 15days (c) 32 days (d) 60 days (e) 81 days and (f) 117 days.

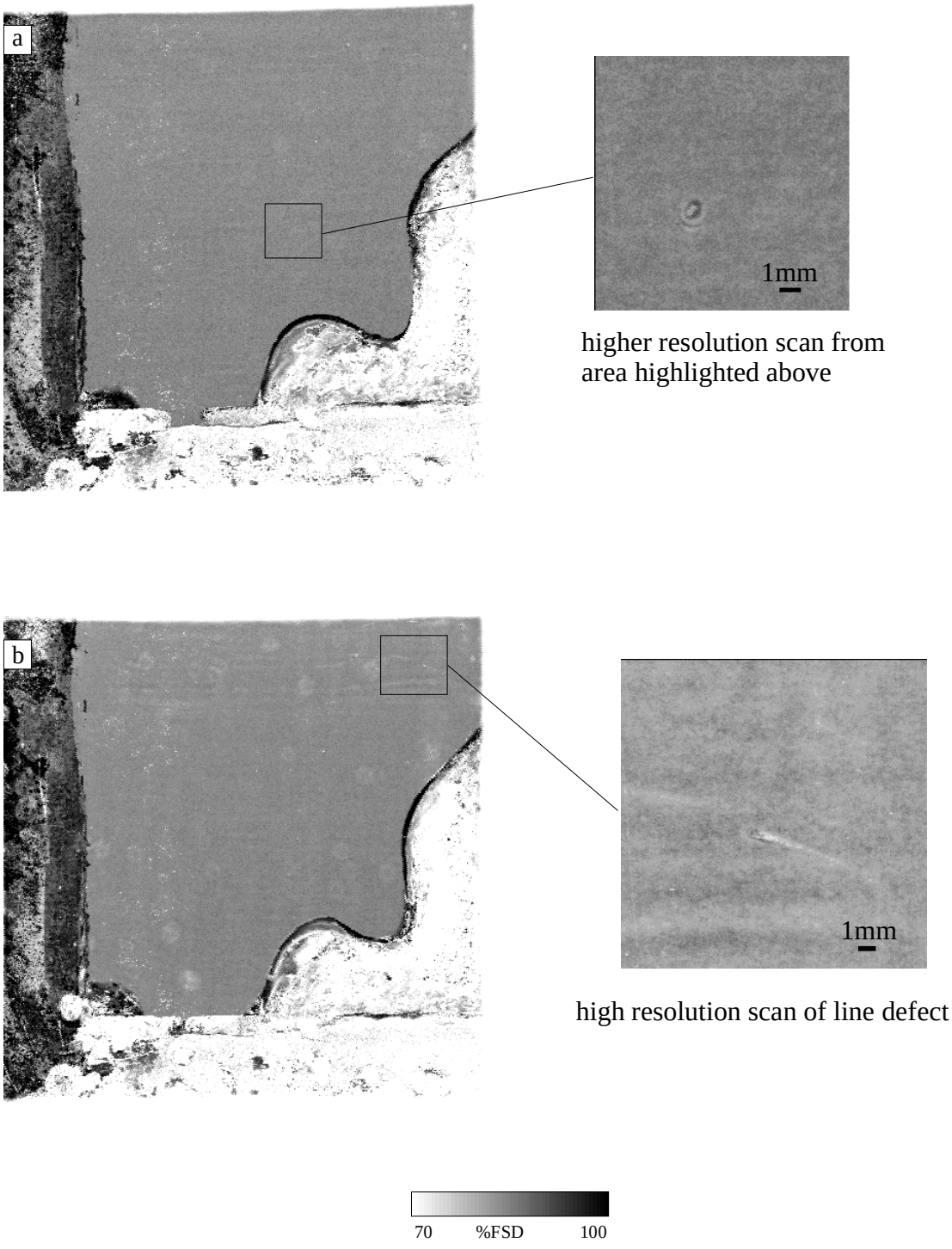

Figure 3.12 Normal incidence scans from 2-layer CAE specimen after (a) 154 days with inset high resolution scan of micro-defect and (b) 194 days with high resolution scan of line defect.

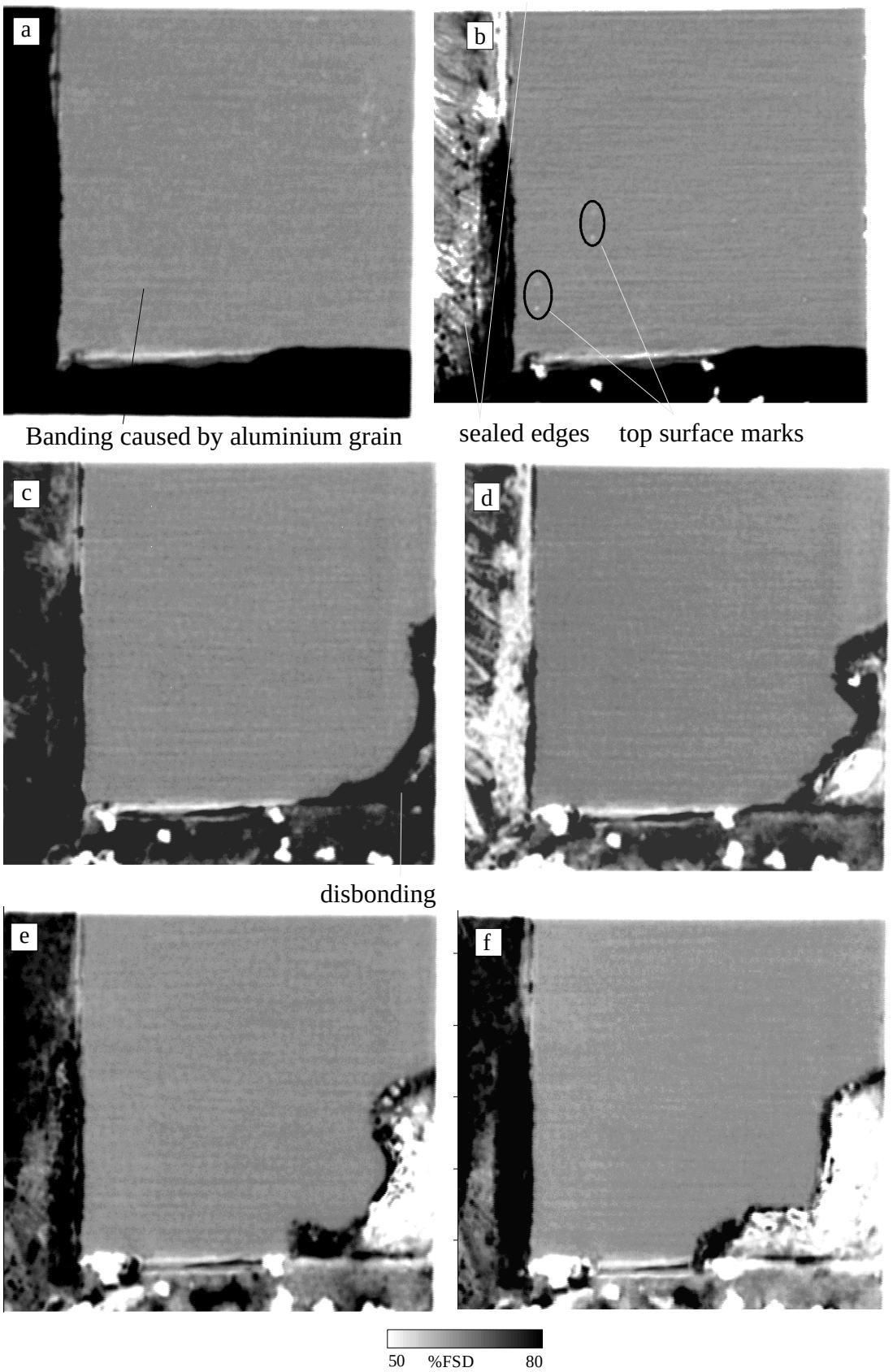

Figure 3.13 Oblique incidence scans from 2-layer CAE specimen for exposure times of (a) 0 (b) 15 (c) 32 (d) 60 (e) 81 and (f) 117 days.

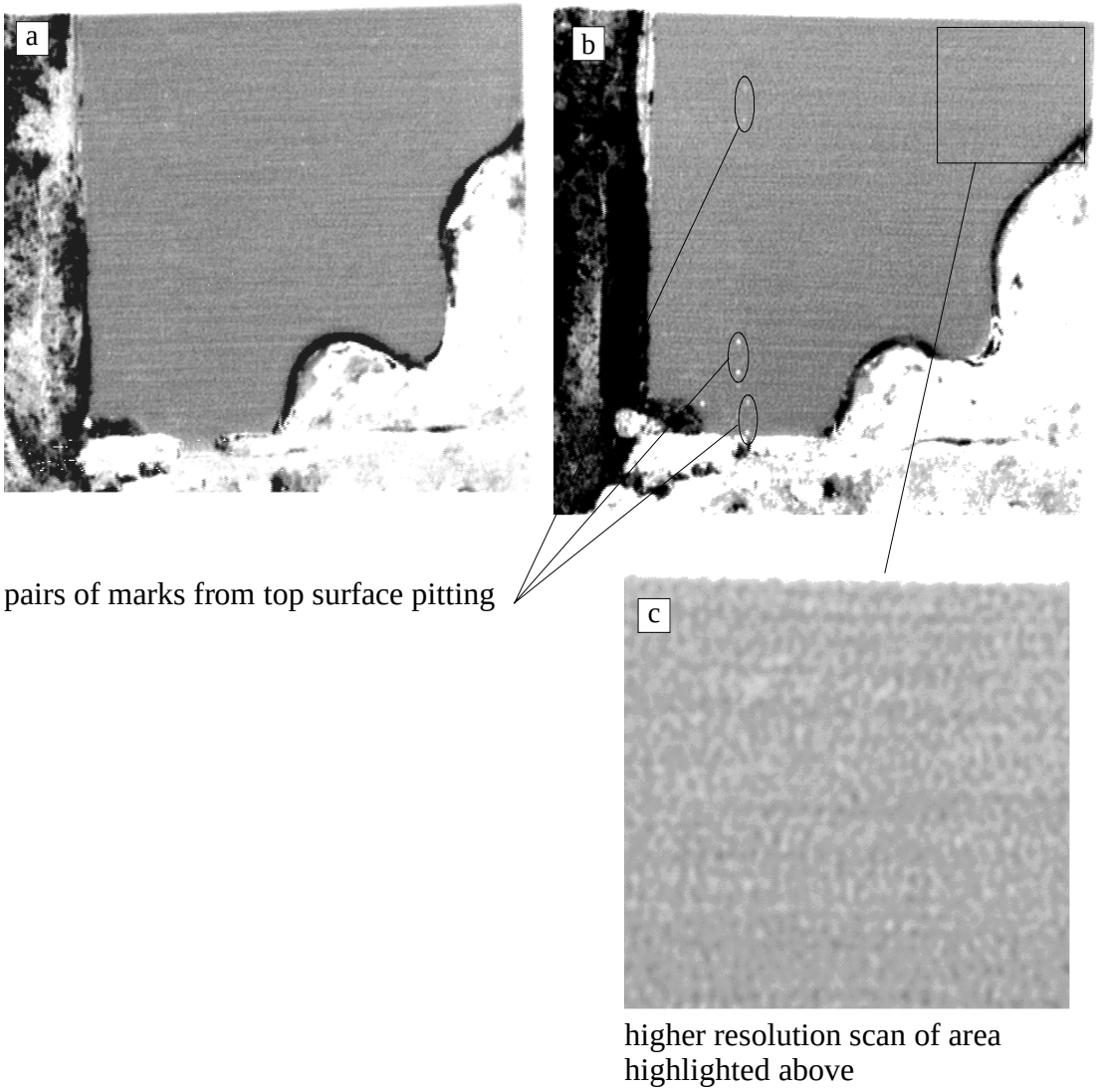

Figure 3.14 Oblique incidence scans for 2-layer CAE specimen for exposure times of (a) 154 and (b) 194 days and (c) high resolution scan of highlighted area of scan after 194 days.

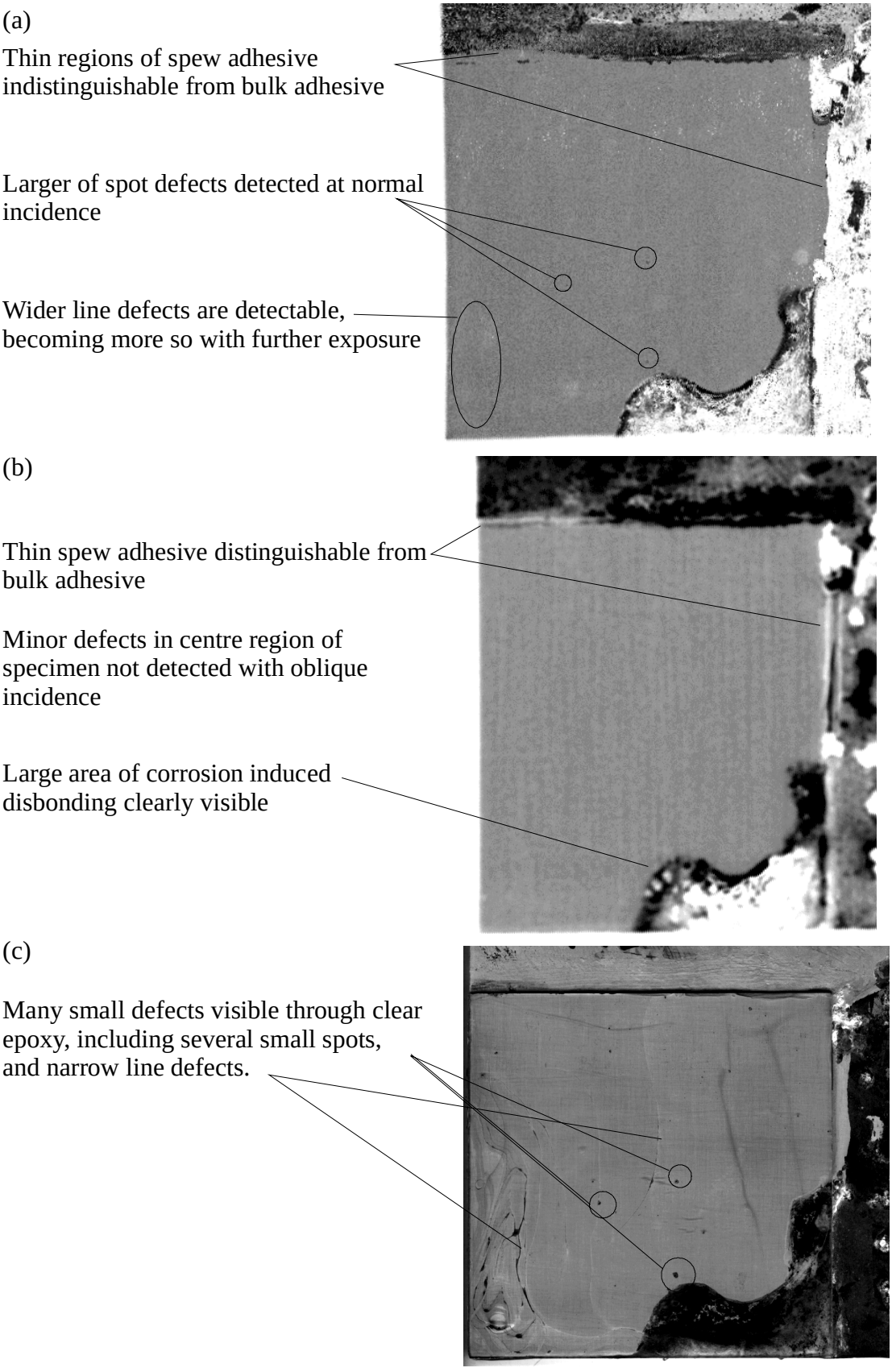

Figure 3.15 Comparison of (a) normal and (b) oblique incidence scans with (c) photograph from 2-layer CAE specimen.

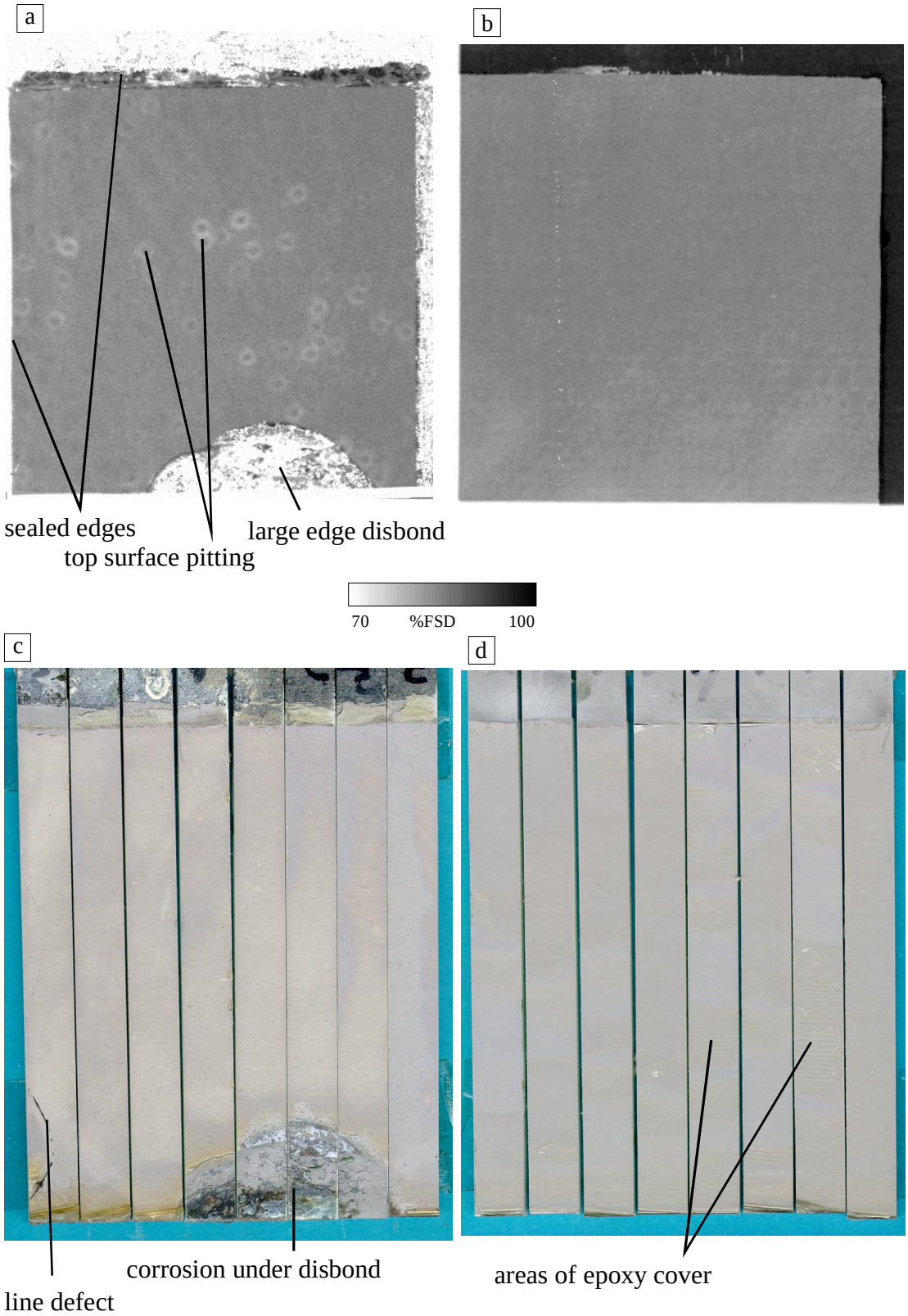

Figure 3.16 Comparison of final scans from (a) wet specimen after 185 days in water and (b) dry specimen with failure surface of (c) wet specimen and (d) dry specimen for 2-layer CAE specimens.

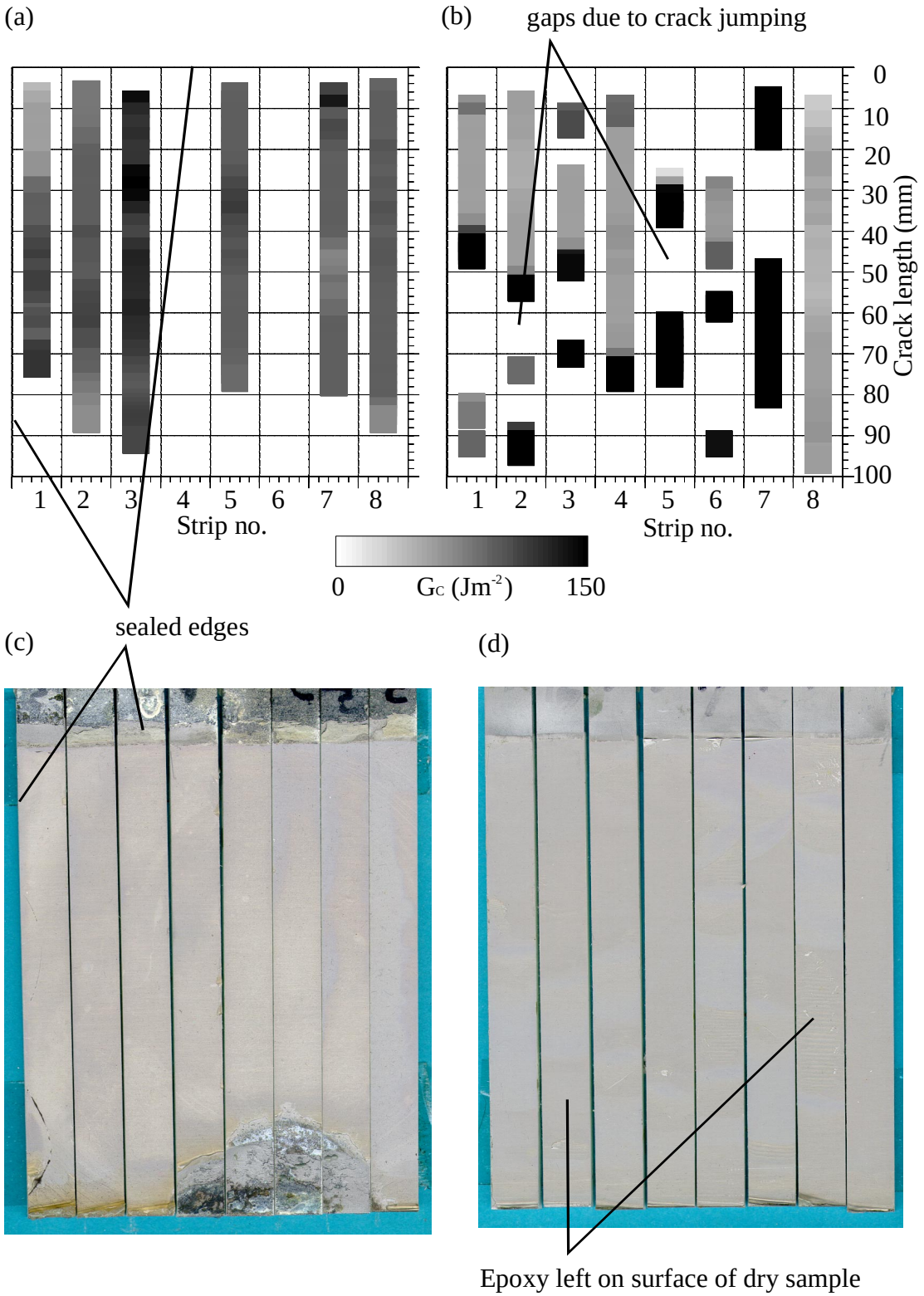

Figure 3.17 Comparison of mechanical test results for (a) wet and (b) dry 2-layer CAE sample and failure surface from (c) wet and (d) dry sample.

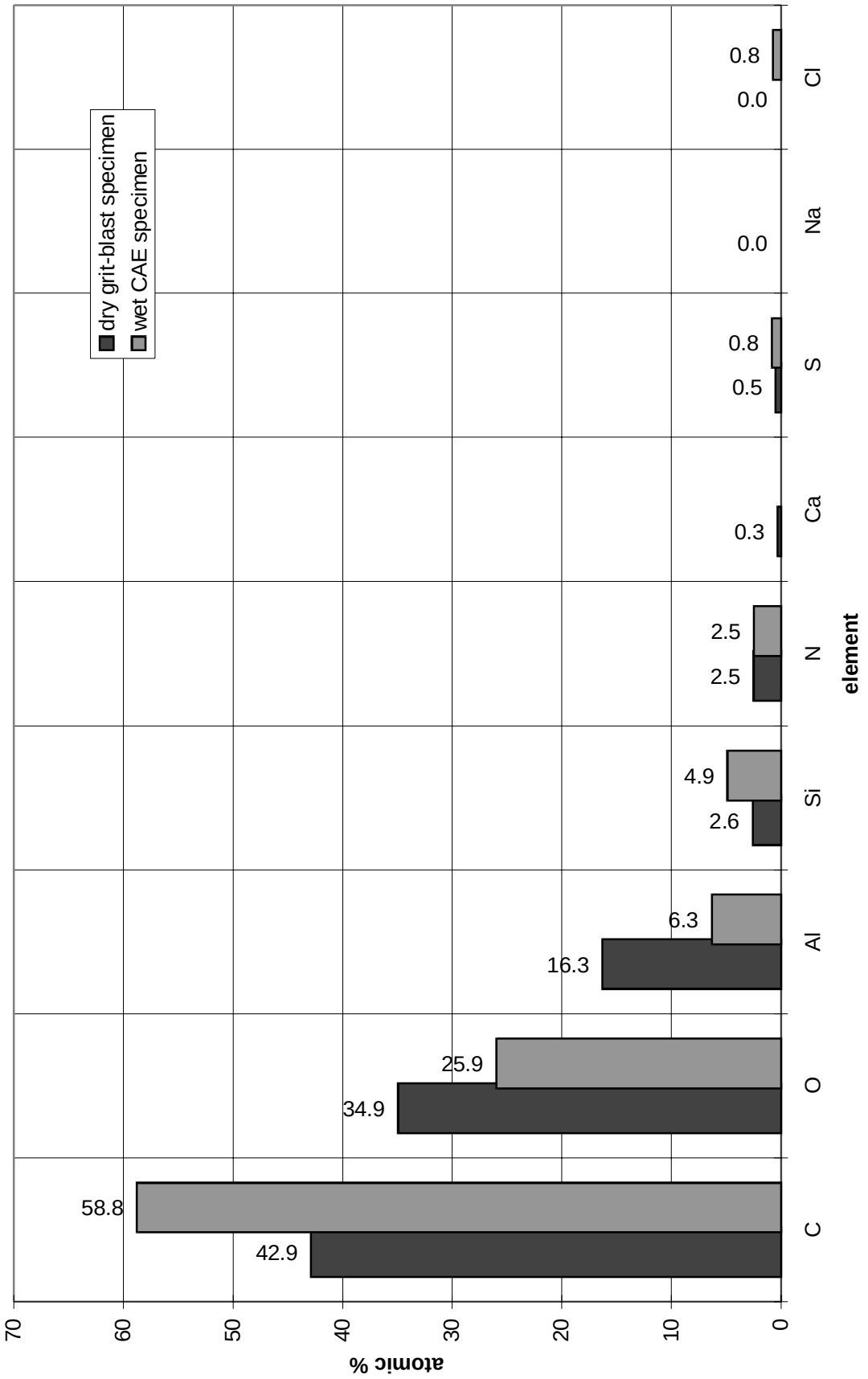

Figure 3.18 XPS results from wet CAE specimen.

3.4 Phosphoric Acid Anodise

3.4.1 Normal incidence ultrasound

Figure 3.19 shows the results for the first five normal incidence scans from a two layer PAA specimen. From the first scan after immersion several features are apparent. There are the appearance of two small defects. There are also a few white spots along the right hand side of the scan. This is caused by corrosion to the top surface along this edge. This highlights one of the difficulties with these specimens. We wish to have an unsealed flush edge on the specimen, but we are also required to seal the top surface to prevent corrosion. It has been difficult to ensure that there is no sealant covering the interface of the aluminium and epoxy along the edge while ensuring sufficient protection to the top surface. The micro-defects that have appeared in this case are both close to edges, with one being adjacent to a sealed edge. However for the first 180 days in water there is relatively little change to this specimen. This is in line with what can be expected for an anodised specimen in comparison with the grit blast and simple etch specimens seen so far.

Figure 3.20 shows the same specimen for exposure times up to 393 days. The most obvious change is the appearance of a large disbond starting from the flush unsealed edge. In the following scans it can be seen that this expands, with a second disbond developing along the same edge. Figure 3.19 and Figure 3.20 show that it takes some time for the edge disbonds to initiate but once they have they grow rapidly. This may be explained by the anodic layer which extends down the edge of the specimen, giving it better corrosion protection than bare aluminium. Figure 3.20 also shows that the micro-defects that were apparent in Figure 3.19 change their appearance, almost completely disappearing before reappearing as white specks. Initially as straight faced disbonds they behave as reflectors, however with time they develop into pits which scatter the ultrasound, reducing the amplitude of the received signal. The higher resolution scan in Figure 3.20 shows what appears as a small defect which subsequently is engulfed by a large disbond. By the final scan there is no change in the appearance of micro-defects with the edge disbonds growing steadily.

3.4.2 Oblique incidence ultrasound

Figure 3.21 shows the oblique incidence scans from the specimen discussed above for exposure up to 181 days, with Figure 3.22 showing the remaining scans from the same specimen. The results from this specimen are much the same as have

been seen from previously presented specimens. Compared with normal incidence results we can see that it takes longer for the small defects to be detected at oblique incidence. The edge disbonds appear the same with either form of scanning and this can be seen in Figure 3.22. As with the normal incidence scans we see that the edge disbonds appear black near the crack front as this is a clean disbond and behaves as a good reflector, but as time passes corrosion roughens the surface, reducing the signal level. Comparing the normal and oblique results we see that at normal incidence the loss in signal due to roughness occurs sooner than at oblique incidence. Figure 3.22 also shows a higher resolution scan of the same area that was highlighted in the normal incidence scan (Figure 3.20). There are no signs of the defect seen at normal incidence when the oblique incidence technique is used.

3.4.3 Comparison of scans with visual assessment of the specimen

For ease of comparison the final normal and oblique scans are shown together with a photograph of the specimen after 393 days in water, Figure 3.23. Comparing the normal incidence scan with the photo it can be seen that there are many apparently interfacial marks on the specimen which appear as white spots on the scan. This suggests that they are acting primarily as scatterers. This makes identification more difficult as there are more mechanisms of loss which will reduce the amplitude of the reflected signal as opposed to mechanisms which will increase the amplitude of the reflected signal. However this is better than the results obtained using oblique incidence technique which shows virtually no signs of any of these small defects.

3.4.4 Mechanical tests

Figure 3.24 shows the failure surface from this specimen after mechanical testing along with the final normal incidence scan as well as the corresponding results from a PAA specimen kept in a desiccator for the same period that the wet sample was in water. The failure surface for the wet specimen appears very similar to the photograph of the specimen before the mechanical test shown in Figure 3.23. However it is clear that only the larger of the interfacial marks appeared on the scan with there being many more on a much smaller scale. This figure also shows the distinct colouring that phosphoric anodised surfaces have. This is particularly striking for the dry sample which has areas of very different colour. Figure 3.25 shows the mechanical test results along with the failure surface for both the wet and dry samples. Comparison of the mechanical test results for these two specimens show a significant drop in toughness for the wet specimen. This is a relatively uniform toughness drop, but with some indication that the toughness drop is greater along the unsealed edge.

The average fracture toughness for the dry sample is 55 Jm^{-2} with a standard deviation of ±17 Jm^{-2}, while for the wet specimen the average is 30Jm^{-2} with a standard deviation of ±7 Jm^{-2}. Comparing the mechanical test result for the dry specimen with its failure surface there is some indication that the colouring of the surface is related to the toughness, with the redder areas appearing to be slightly less tough, although this is by no means absolute.

3.4.5 Failure surface analysis

Figure 3.26 shows the quantified XPS results from four different sections taken from both the wet and dry PAA specimens discussed in the previous paragraph. The quickest result to explain is the reason for the colour differences seen on the failure surface of the dry specimen. Marked as PAA red and PAA green on the graph the key to the difference is in the percentage of aluminium showing from the analysis. The red areas show much less aluminium and oxygen present at the surface, while showing higher levels of carbon and nitrogen. This points to a layer of epoxy being left on the surface, which in the case of the red areas is enough to almost completely mask the presence of the aluminium oxide layer. The degree to which XPS is surface sensitive means that this layer could still be extremely thin, but what appears visually to be an interfacial failure is in fact in the epoxy layer. It is worth remembering that these measurements are the average results over an area 1x5mm and so we can say little about the uniformity of the epoxy layer. However if we compare the results of the dry green areas with those obtained from the wet specimen we see that the aluminium and oxygen levels are even higher on the wet specimen with a corresponding drop in the amount of carbon and nitrogen. This suggests that there is still a layer of epoxy on the dry green areas but that it is even thinner than the red areas of the specimen. This also suggests that the specimens taken from the wet sample are closer still to a truly interfacial failure. Without the XPS analysis from both side of the failure (i.e. both the adhesive and adherend sides) it is difficult to determine the absolute locus of failure, however the comparison between the specimens still gives insight into the type failure. Comparing the results from the two sections taken from the wet sample we can see that there are noticeable differences in all of the elements that were monitored. We see that the aluminium/oxygen levels are highest for the section taken from strip 7. Figure 3.25 shows that strip 7 had greater toughness loss than strip 1. This is suggesting that the failure is either closer to aluminium oxide layer, or potentially in the layer itself. The trend is certainly clear in that the closer the failure is to the interface, indicated by higher concentrations of aluminium, the weaker the bond.

3.4.6 Results from original two-layer PAA specimen

Although not covered in detail the results from a two-layer PAA specimen which was made during the early stages of the work are presented in Figure 3.27 and Figure 3.28. The most interesting result obtained from this specimen was the appearance of a narrow line under the epoxy layer after 48 days immersion in water. The reason for not showing a complete set of scans for this specimen was due to the epoxy layer bowing and peeling away from the aluminium plate after this exposure time. The reason for this very rapid failure is partially thought to be due to the polishing of the free epoxy surface. This was done to enable a better view of the line which is visible under the epoxy in Figure 3.27 (b). However once the epoxy had peeled away from the aluminium the line was still visible on the failure surface, and so a small section was cut and placed in the scanning electron microscope and the images shown in Figure 3.27 (c) and Figure 3.28 (a-c) were produced. From Figure 3.27 (c) it can be seen that the line width is only of the order of 100μm wide. This may be a strong reason for this line not being detected ultrasonically as this is close to the resolving power of the probe used.

The SEM images shown in Figure 3.28 (a) show both the failure surface and the edge of the specimen where it was cut to enable a cross-section of the line to be seen. The following micrographs show a cross-sectional view of the line defect. Here it can be seen that the line is a small covering layer of epoxy. Relatively high resolutions were required to make this detail clear, and so it was not possible to include both edges of the line in the same photo. However inspection of the line the S.E.M. revealed the line to be similar either side. This is a similar feature to that seen on the grit-blast specimen shown in Figure 3.6. Although on the grit-blast specimen the appearance is quite different, the epoxy covering seems to run just across the height of the roughness on the specimen. Therefore the difference in appearance is largely due to the large difference in the roughness height between the PAA and grit-blast surfaces. The implication again is that the line is a flaw in the epoxy layer, which is why some epoxy remains on the surface when the epoxy layer is removed.

3.4.7 Summary of results from PAA specimen

The results from the PAA specimens had many similarities with the grit-blast specimen.

- edge disbonds - the edge disbonds on the PAA specimen are fundamentally the same as seen on the grit-blast specimen. The major differences is in the rate at

which the disbond expands, approximately half that of the grit-blast specimen. Figure 3.19 best shows the progression of the edge disbonds.

- small spots - there were considerably fewer spots on the PAA specimen than the grit-blast specimen. They were more common nearer to the edges of the specimen. Again the detection of these defects was largely governed by size. This spots were also seen to change with time, starting as disbonds and changing into corrosion pits (discussed in 3.4.1).

- line defects - there were only the faintest traces of lines on the failure surface of the PAA specimen discussed in sections 3.4.1-3.4.5. However the specimen discussed in 3.4.6 showed a clear line defect, which was identified as a thin covering of epoxy much like that seen on the grit-blast specimen.

- The mechanical test results from these specimens showed a general drop in toughness (see section 3.4.4), which was of a similar magnitude to that seen on the grit-blast specimen. There was also evidence that the edge strips nearest the unsealed edge had a greater loss of toughness than the rest of the specimen.

- The surface analysis from this specimen showed that the locus of failure changed with toughness, becoming closer to the bulk adherend as toughness dropped. It was not possible to say whether the failure actually occurred within the oxide or at the interface between oxide and epoxy.

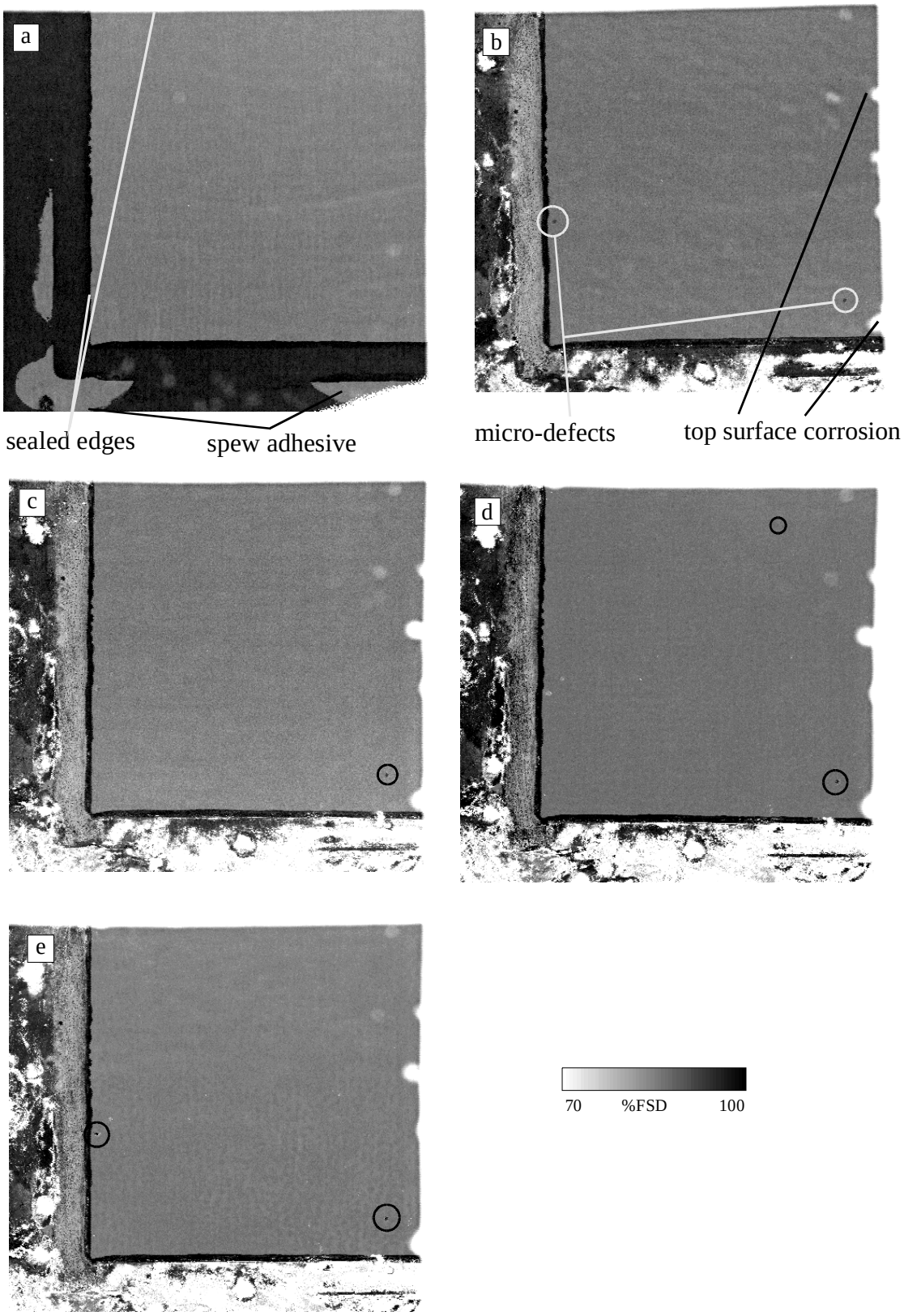

Figure 3.19 Normal incidence scans from 2-layer PAA specimen after (a) 0 (b) 63 (c) 102 (d) 143 and (e) 181 days in water.

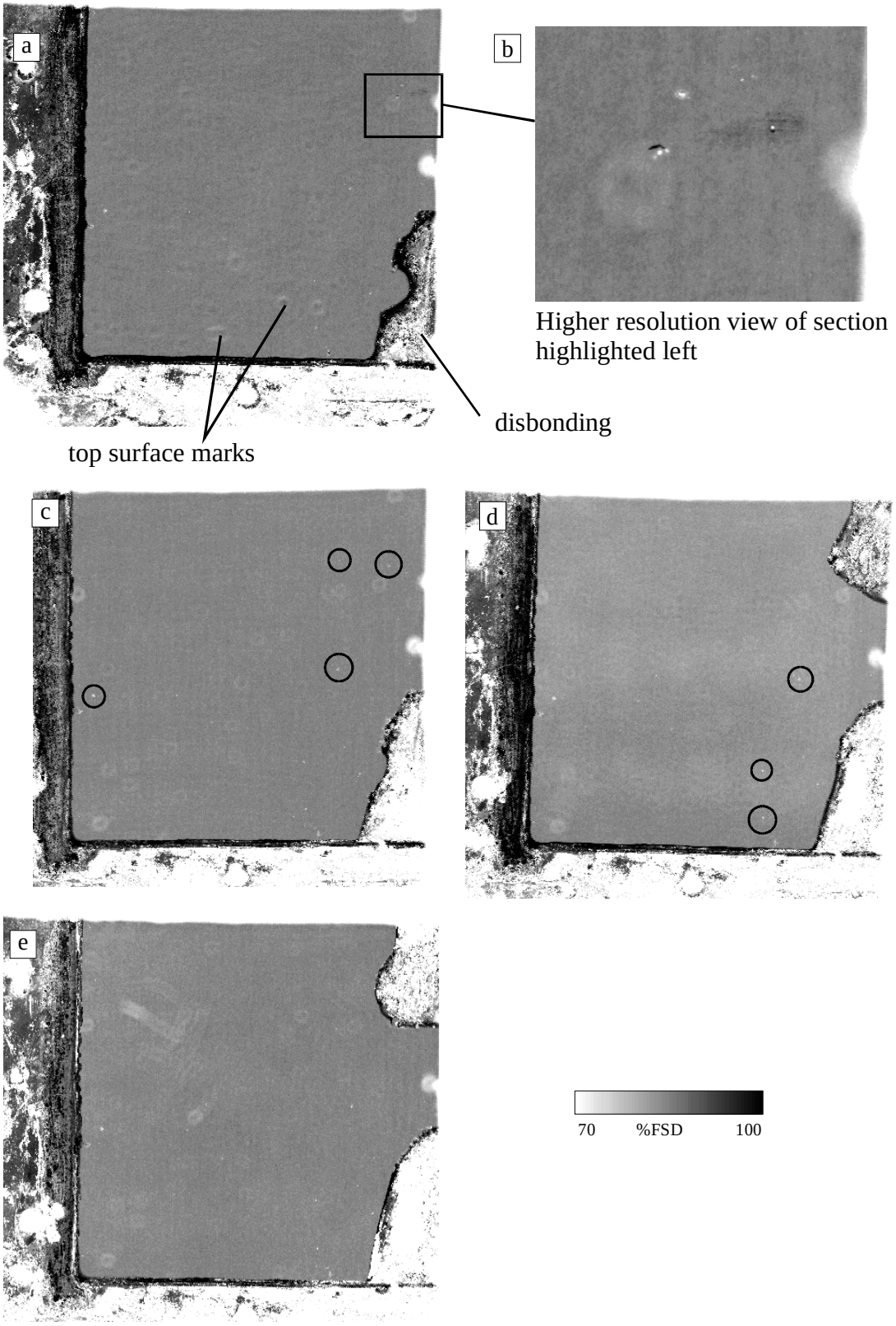

Figure 3.20 Normal incidence scans from 2-layer PAA specimen after (a) 237 (b) 237 (c) 287 (d) 343 and (e) 393 days in water.

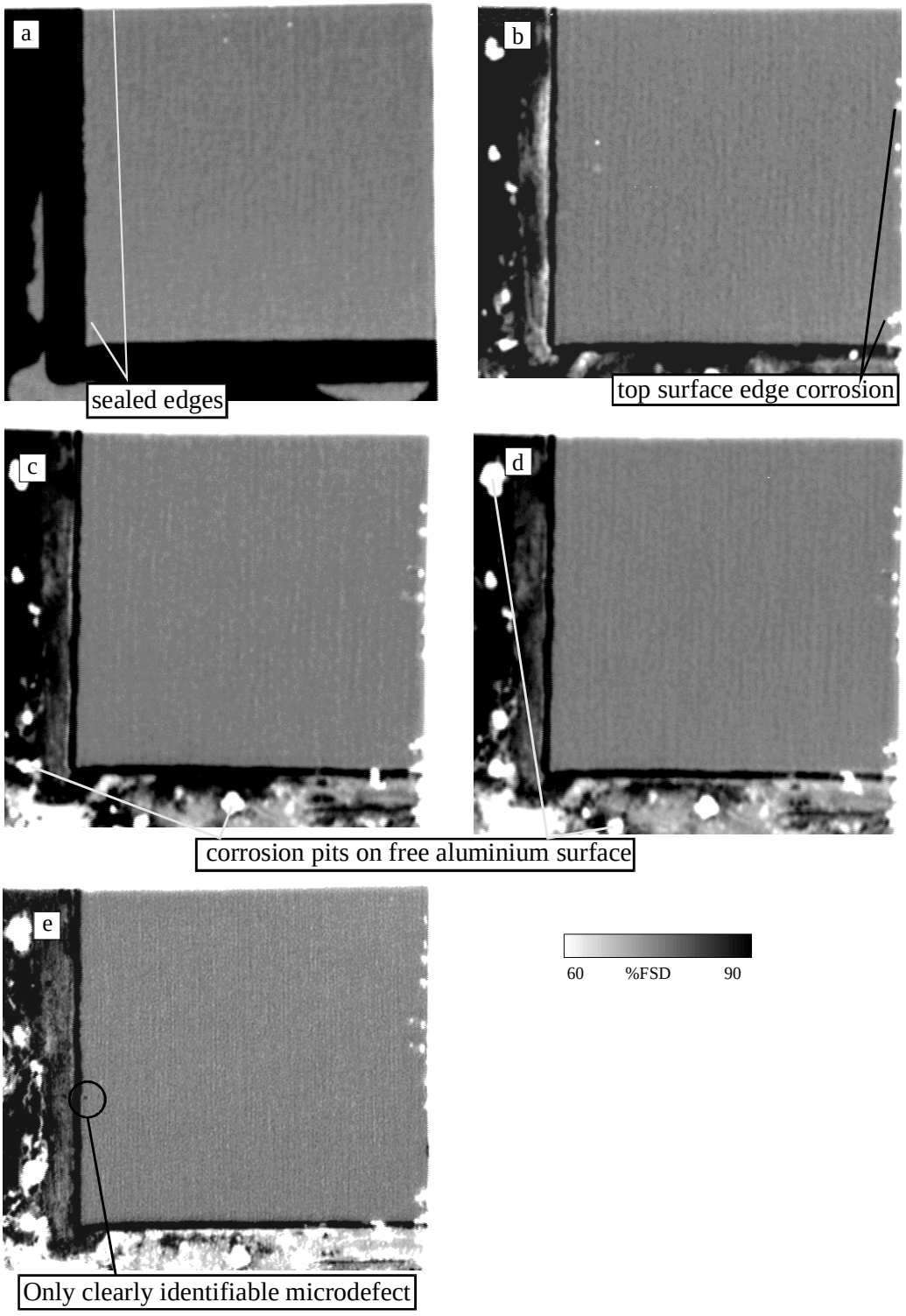

Figure 3.21 Oblique incidence scans from 2-layer PAA specimen after (a) 0 (b) 63 (c) 102 (d) 143 and (e) 181 days in water.

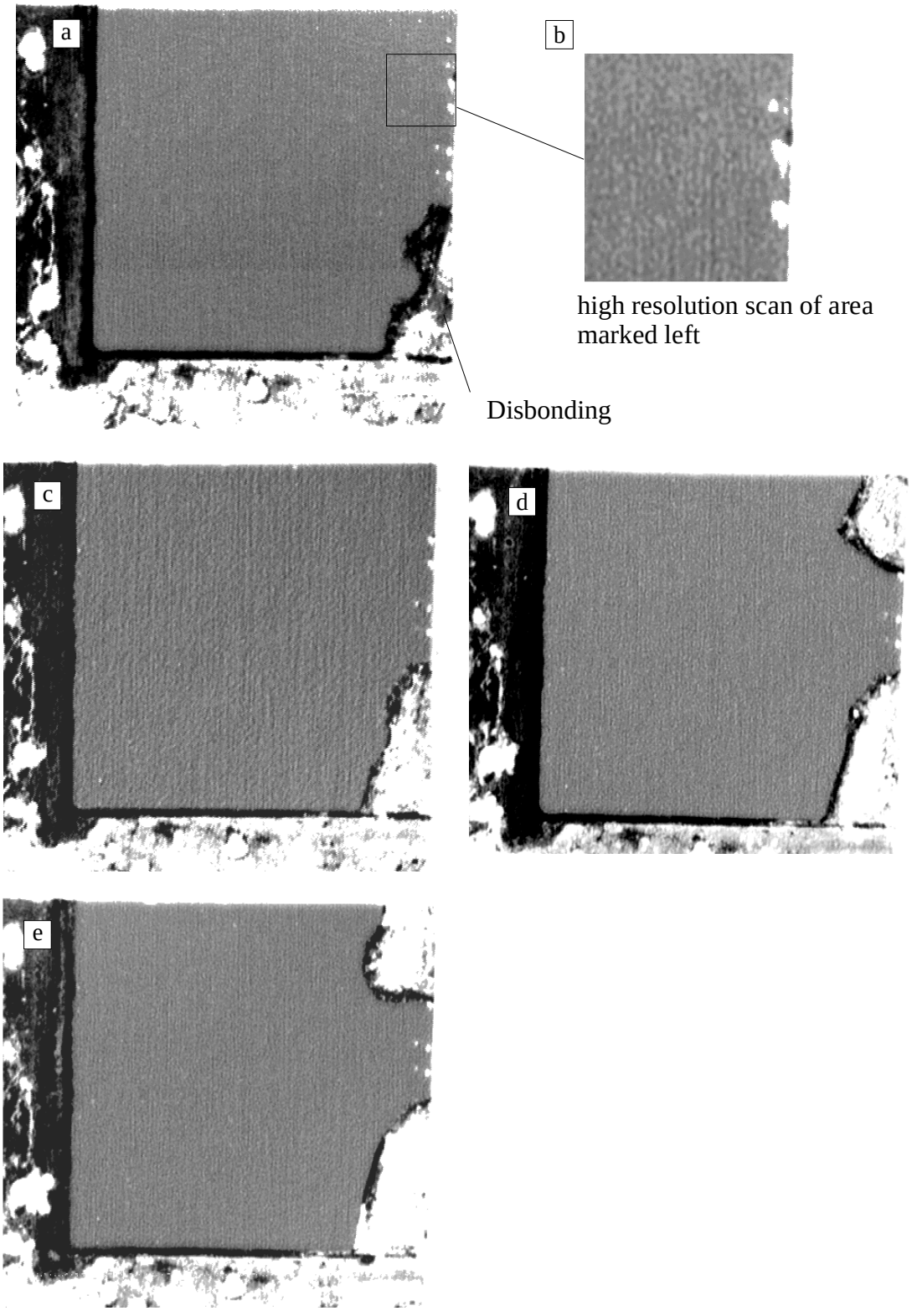

Figure 3.22 Oblique incidence scans from 2-layer PAA specimen after (a) 237 (b) 237 (c) 287 (d) 343 and (e) 393 days in water.

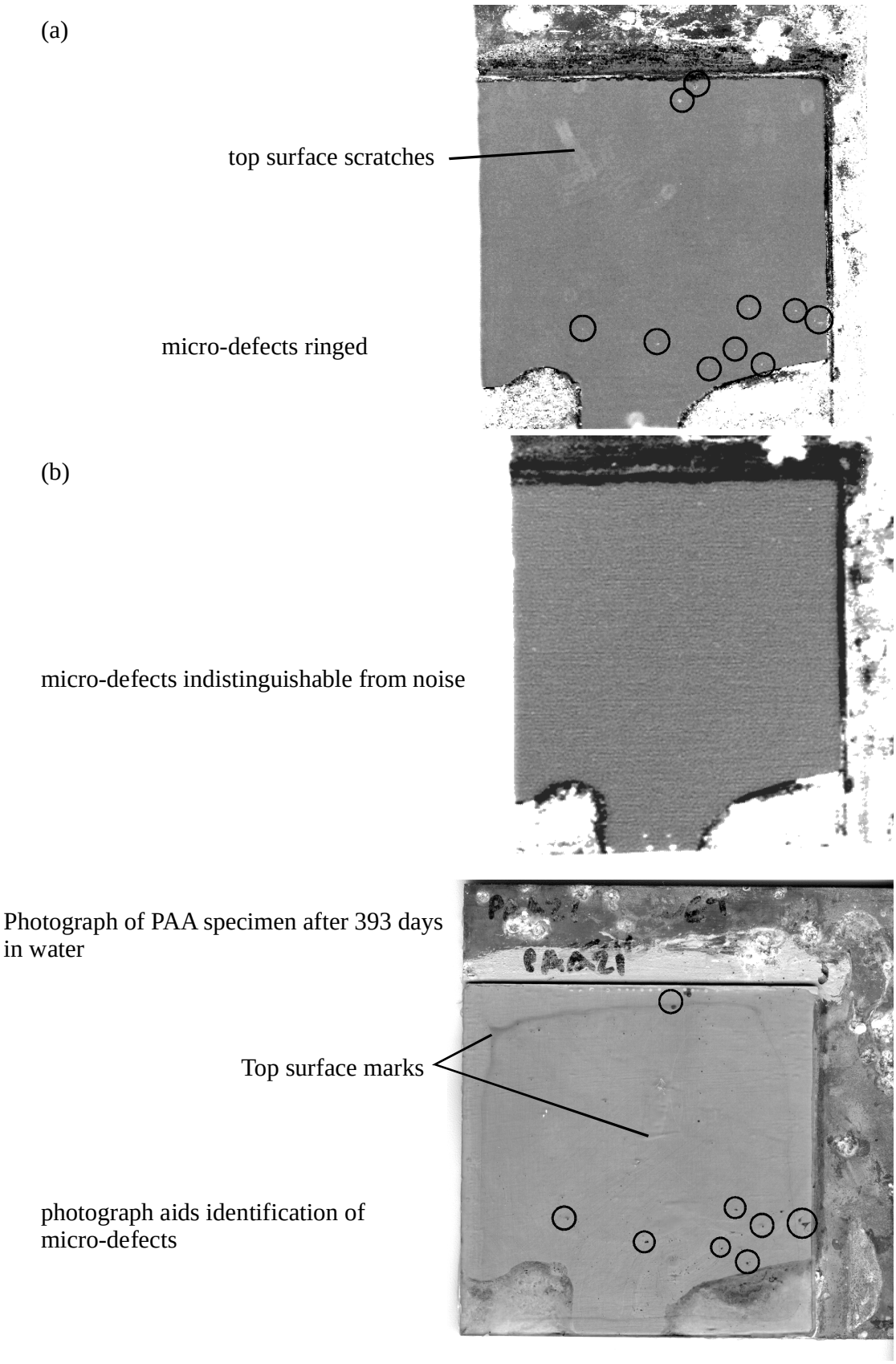

Figure 3.23 Comparison of (a) normal and (b) oblique incidence scan with (c) photograph of specimen.

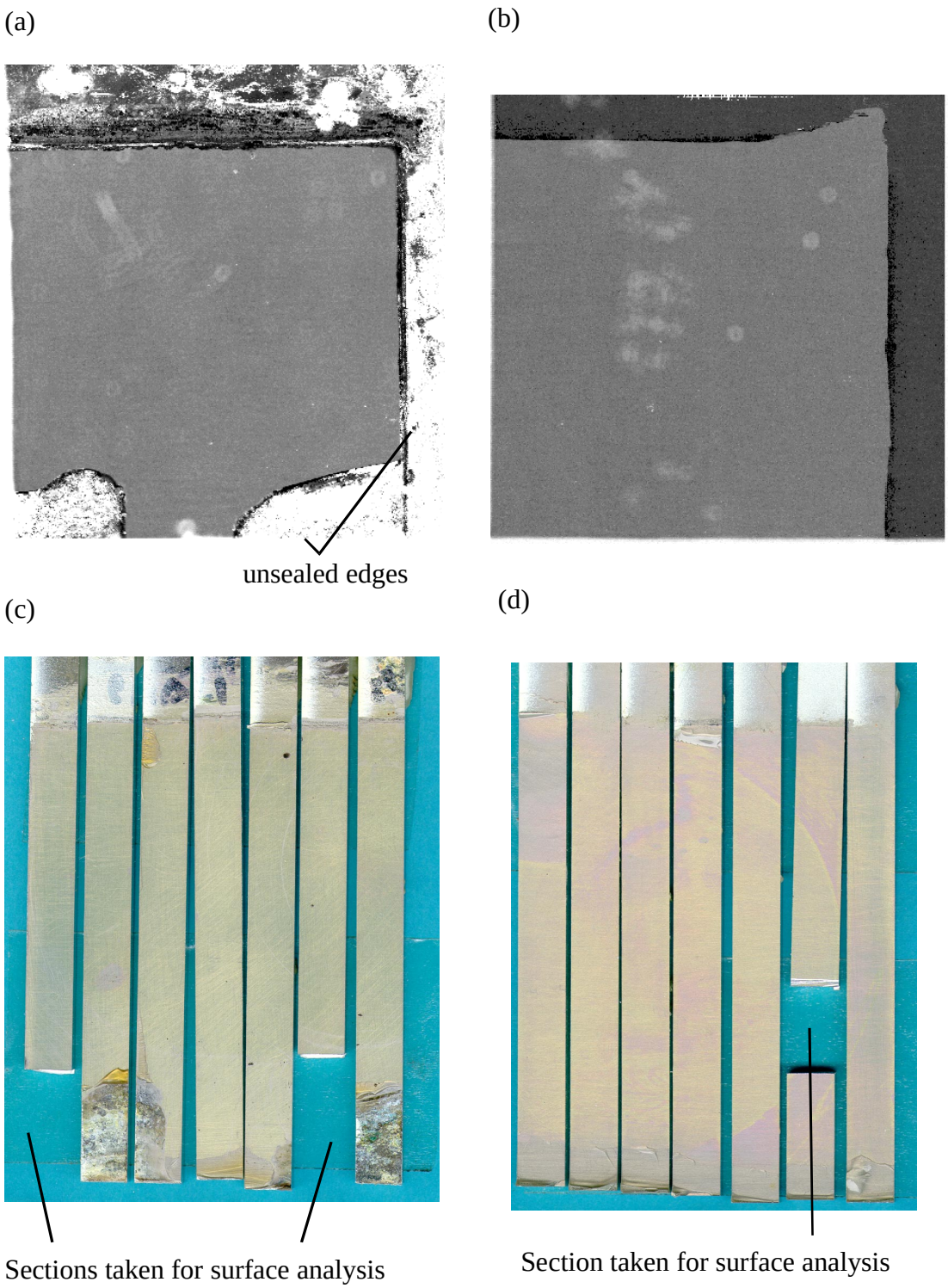

Figure 3.24 Comparison of final scans from (a) wet and (b) dry PAA specimens with photograph of failure surface from (c) wet and (d) dry specimen.

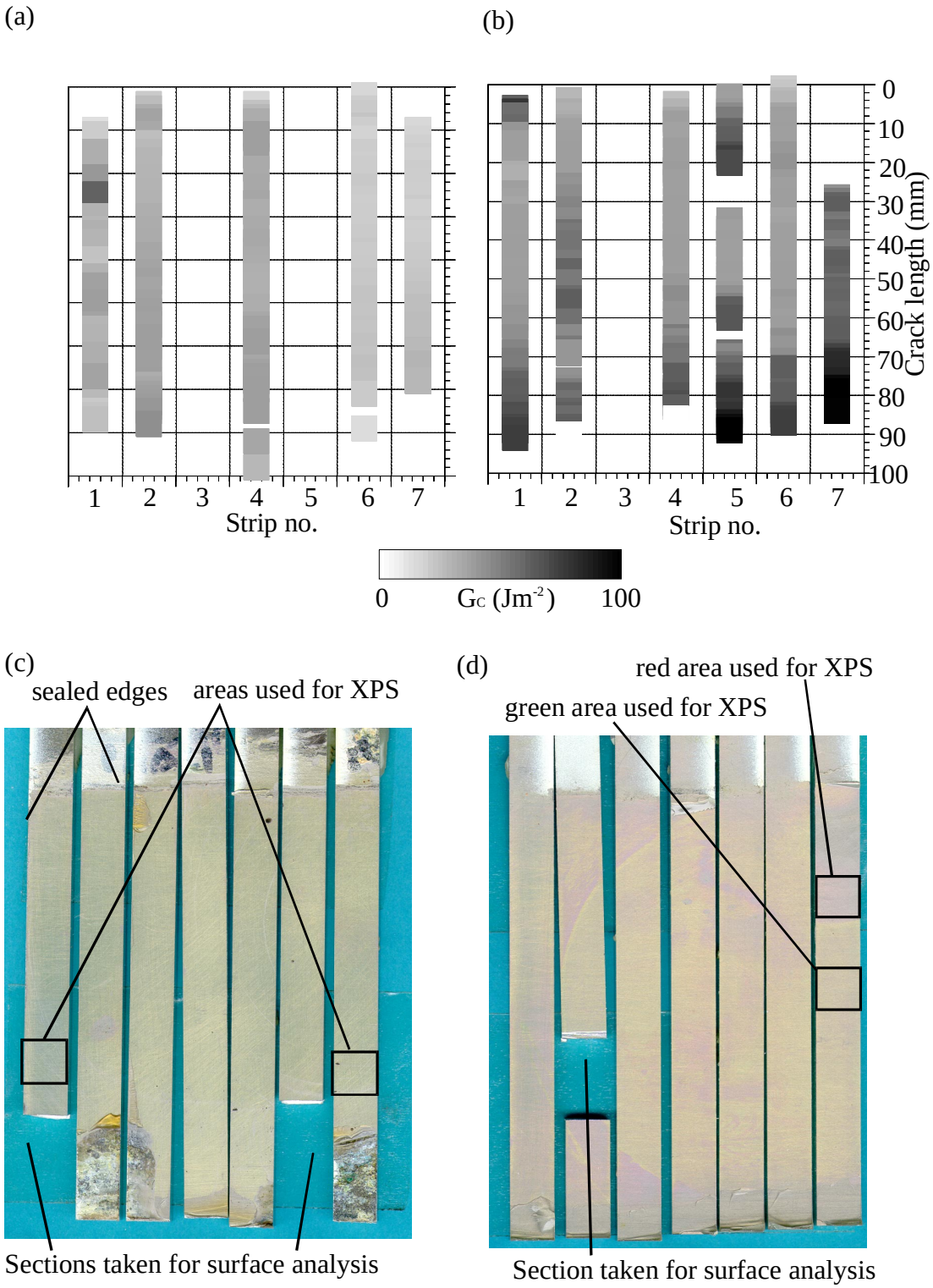

Figure 3.25 Comparison of fracture toughness maps from (a) wet and (b) dry 2-layer PAA specimen with (c) wet and (d) dry failure surfaces.

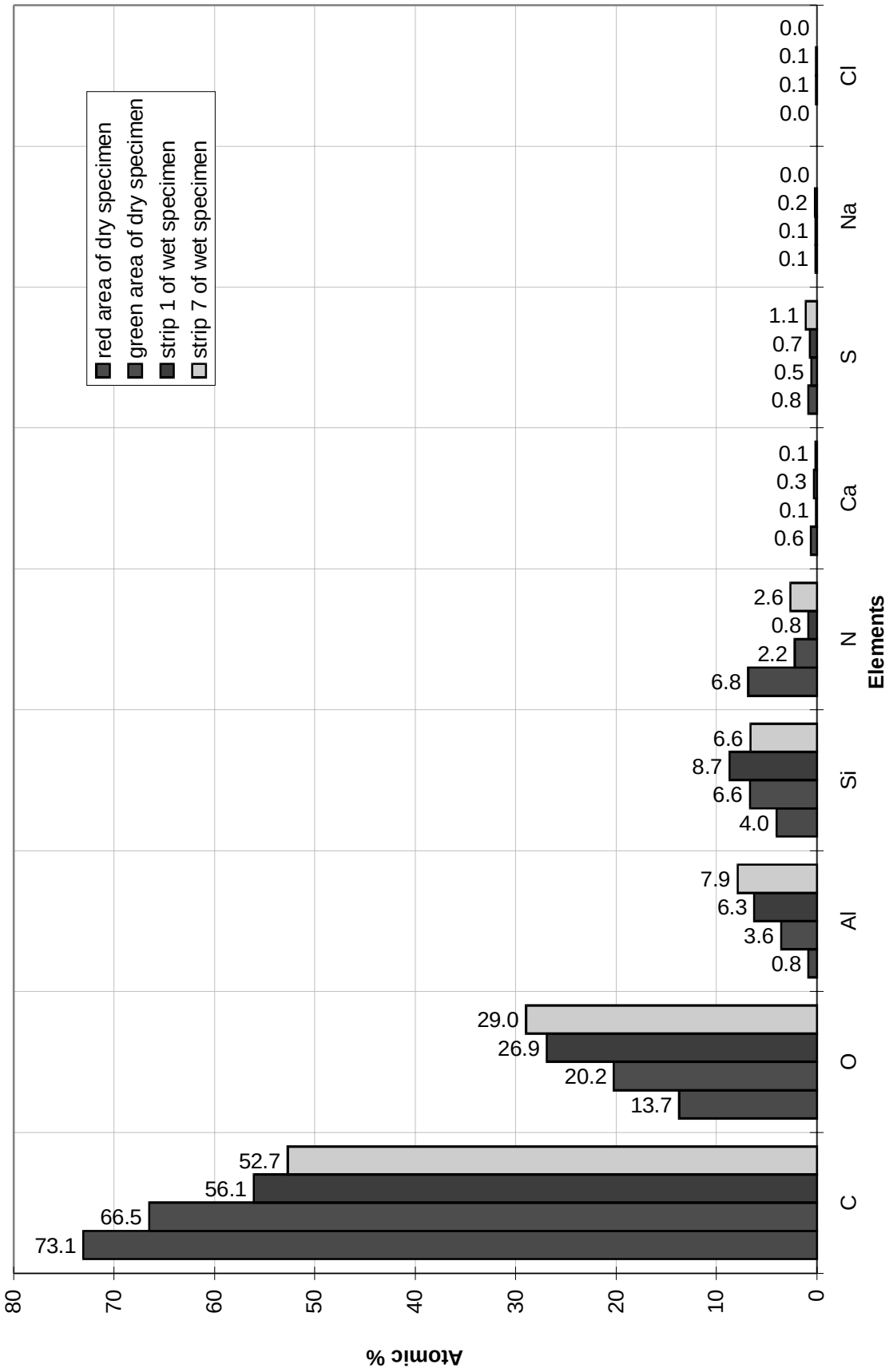

Figure 3.26 XPS results from 2-layer paa specimens.

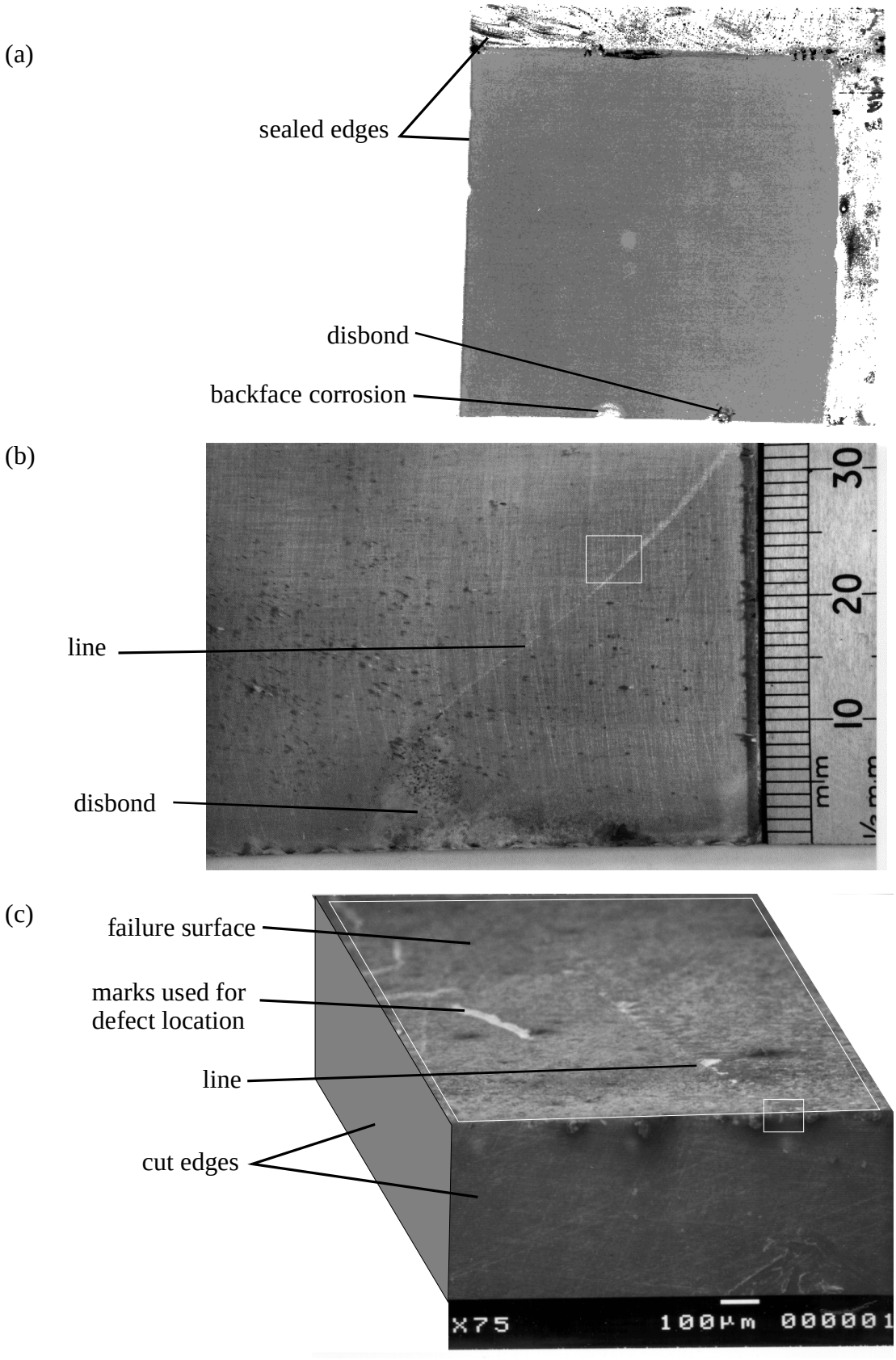

Figure 3.27 Results from early two-layer PAA specimen showing (a) 50MHz normal incidence scan (b) photograph through epoxy layer (c) low magnification SEM picture of failure surface.

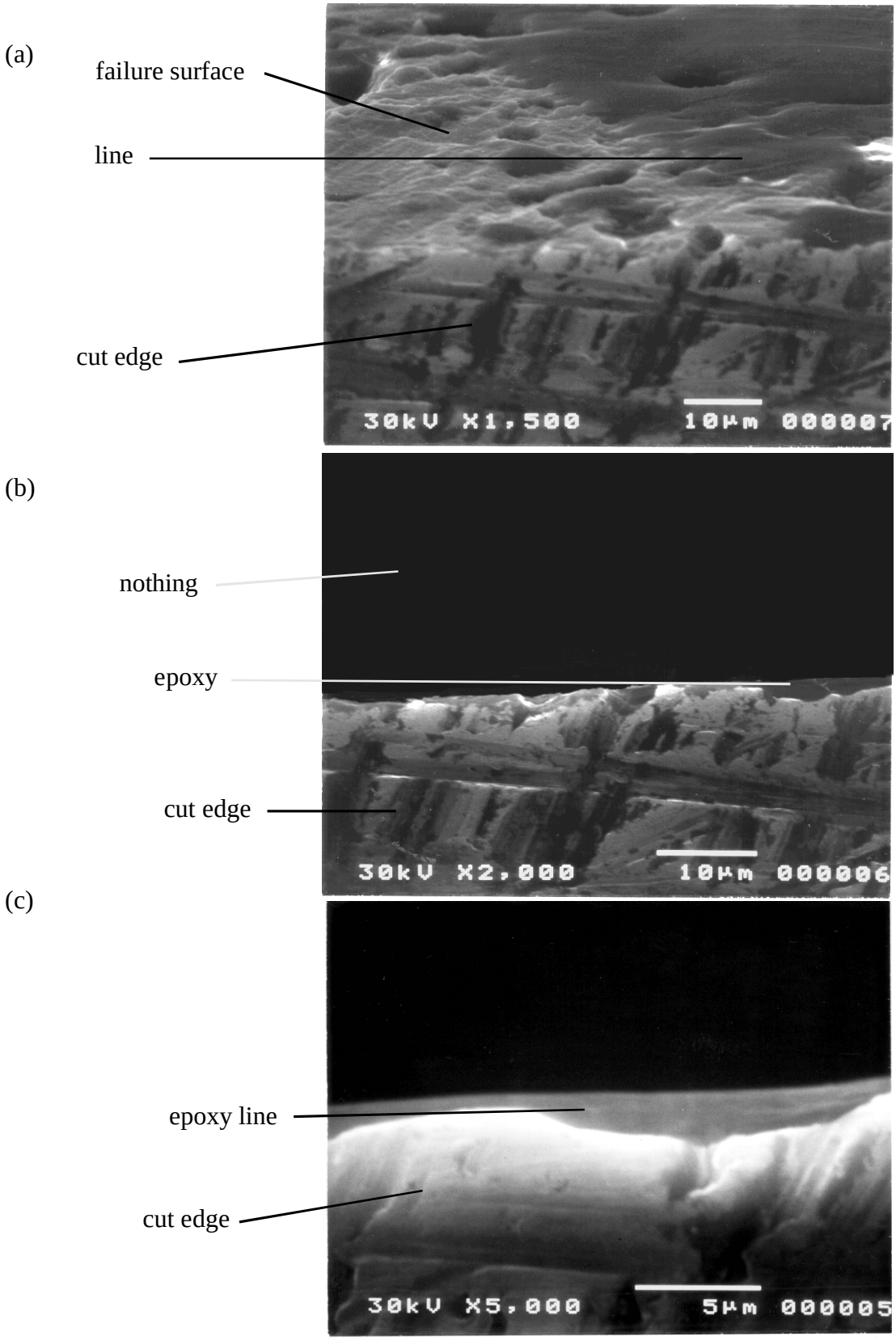

Figure 3.28 S.E.M. micrographs from early two-layer PAA specimen showing (a) failure surface and end of section (b) 2,000x end on view and (c) 5,000x end of view of line on failure surface.

3.5 Chromic Acid Anodise

3.5.1 Normal incidence ultrasound

Figure 3.29 and Figure 3.30 show the progression of degradation for a 2-layer CAA specimen obtained using normal incidence scans. The initial scan from this sample appears different to subsequent scans, and those seen from other specimens. This is due to the scan being performed using the older scanning system mentioned in Chapter 2. Following the sequence of scans there is a clear progression of a single disbond initiating on the unsealed flush edge. There is also the growth of a corrosion pit on the unsealed recessed edge which undercuts the epoxy as time progresses. This sample differs from the previous samples in that at no point is there the appearance of any micro-defects, either visually or from the ultrasonics, at any time during the 465 days that this sample was in water (longer than any other two layer sample).

The higher resolution scan shown in Figure 3.29d after 103 days of exposure shows a detailed view of the disbond. This shows that there is a sharp edge between disbond and what appears as untouched epoxy. As seen on other specimens, corrosion around disbonded regions soon leads to a reduction in signal amplitude. The high resolution scan of this disbond shows regions where this roughened surface is immediately adjacent to a well bonded region. The manner in which the disbond on this sample progresses is noticeably different from other samples in that it has produced a much tighter radiused crack front, so that the disbond appears to have burrowed its way into the specimen as opposed to levering the epoxy away. It could be inferred from this that the interface in the regions around this disbond are tougher than similar areas on other specimens, in that if we consider the corrosion products to be producing a point displacement under the epoxy, then the weaker the interface the further the crack front would be from the displacement point and the bigger the radius of the crack front produced.

3.5.2 Oblique incidence ultrasound

The oblique incidence scans for this sample are shown in Figure 3.31 and Figure 3.32. The first scan produced of this specimen at oblique incidence was done using plane 20MHz probes as opposed to the focused probes that have been used for all of the other scans shown so far. As was discussed in Chapter 2 this type of scan suffered from large amounts of variability because of problems with alignment. All of

the other scans from this sample have been performed using the focused probes. The scans shown in these two figures show the same defects as seen in the normal incidence scans. The higher resolution scan shown for the sample after 359 days in water shows the same information as was seen in the high resolution normal incidence scan, in that the disbond is sharp edged to the limits of the resolution attainable, with no sign of a gradual change in properties away from the disbond. This sample shows the same graining as has been seen in oblique incidence scans from all other specimens, thought to be due to scattering from within the aluminium.

3.5.3 Comparison of scans with visual appearance

Figure 3.33 shows a comparison of the final normal and oblique incidence scans with a photograph of the specimen. This confirms both the normal incidence and oblique incidence scans discussed above in that there is no sign of any defects except the corrosion disbond initiating at the unsealed flush edge. There are some marks visible along the left hand side of the specimen, but these are merely marks in the top epoxy surface, careful examination by eye revealing no marks at the interface. The photograph of the specimen also shows that around the disbond there are cracks in the epoxy running through its thickness. This suggests that as corrosion products are forcing the epoxy away from the aluminium it easier for the crack to run through the epoxy than along the interface. This indicates that the interfacial toughness of the specimen in regions immediately adjacent to disbonded regions is still good.

3.5.4 Mechanical test results

Figure 3.34 compares the failure surface from the wet and dry two layer CAA samples with the final normal incidence scans from each of the specimens. Examination of the failure surface for the wet specimen shows no more sign of any micro-defect than had been detected on any scan or seen visually. The large disbond on the lower right corner of the specimen can be seen to have corroded heavily. This agrees with the observations taken before mechanical testing of the sample in that there is quite serious corrosion extending to the edge of the disbonded region prior to testing. The rest of the failure surface on this specimen and also the dry specimen is very uniform, with only a few areas showing some epoxy left on the surface to break the uniformity. Comparisons of these failure surfaces with the mechanical test results are shown in Figure 3.35. Comparing the wet and dry mechanical tests results shows that for the majority of the specimen the wet sample is tougher than the dry. However, on the wet specimen, the two strips adjacent to the unsealed recessed edge appear less tough than the rest of the specimen, falling back to approximately the level of the dry

sample. The average fracture toughness for the whole wet specimen was 98 Jm^{-2} with a standard deviation of $\pm 31\ Jm^{-2}$, and for the dry specimen the average fracture toughness is 78 Jm^{-2} with a standard deviation of $\pm 18\ Jm^{-2}$. However if we separate the rest of the results from the wet sample from the two strips closest to the unsealed edge we see that the average for strips one to six is 108 Jm^{-2} and for strips seven and eight it is 66 Jm^{-2}. The standard deviations are also reduced by splitting the results in this manner to $\pm 28\ Jm^{-2}$ for strips one to six and $\pm 15\ Jm^{-2}$ for strips six and seven. This gives the edge strips a toughness slightly below that of the dry sample.

The missing strips from the dry sample are due to the crack not initiating between the epoxy and aluminium when being tested but rather between the epoxy and the base plate to which the specimens were bonded, which resulted in plastic deformation of the beam.

3.5.5 Failure surface analysis

Figure 3.36 shows the XPS results from both the wet and dry two-layer CAA specimens. The mechanical test results from these specimens showed a number of features that we wished to explain with the XPS results. The results from the wet sample showed in general very little evidence of joint degradation, and potentially an increase in toughness for much of the joint. However it was seen that the strips closest to the unsealed edge showed a reduction in toughness. The sections that were used for the XPS measurements are shown in Figure 3.35. Comparison of the two XPS measurements taken from the wet sample show that the most significant difference in the results from this sample is that the strip which had a loss in toughness (strip 7) is the only strip from the CAA specimens to show traces of calcium, sodium and chlorine. This is evidence that the degradation of the joint is affected by the presence of water which has carried in salts in solution. We know from the diffusion calculations that a specimen with a 2mm epoxy layer that has been immersed in water for 465 days will have a near saturated epoxy layer. However it was only the strips next to the unsealed edge which exhibited a loss of toughness, with the corresponding traces of calcium, sodium and chlorine.

Comparison of the section from strip one of the wet sample (caa3 1), and the section and the dry sample (caa2 1) show that there are still differences in the failure surfaces despite there being no obvious degradation of the bond. It can be seen that there is more aluminium and oxygen present on the surface of the wet sample, with the carbon and nitrogen levels being higher from the dry sample. This is suggesting

that there is some epoxy remaining on the surface of the dry sample. It is known that the mechanical properties of the adhesive will change in the presence of moisture, tending toward more plastic behaviour. This may well have pushed the failure closer to the interface for the wet sample, with the dry sample behaving much the same as other dry samples that we have seen, in that the failure is fractionally into the epoxy layer.

3.5.6 Summary of results from CAA specimens

The wet CAA specimen is the one which stands out from the rest in its overall performance.

- Edge disbond - the wet CAA specimen had the slowest overall rate of disbond growth compared with all other pre-treatments, (see Figure 3.29 and Figure 3.30).

- Small spots - there were no small spots detected on this specimen at any point either visually or ultrasonically, before or after the mechanical tests despite the overall exposure time being higher than any other specimen.

- Line defects - there were no line defects present on this specimen either before or after the mechanical tests.

- The mechanical tests from these specimens showed that in general the wet sample had suffered no toughness loss and that plasticisation of the epoxy had increased the fracture toughness. However the two strips taken from the unsealed edge of the specimen were less tough than the dry sample (see Figure 3.35.)

- The XPS results from the wet specimen showed small traces of sodium, calcium and chlorine on the least tough of the strips taken from the specimen. There also appeared to be a small difference in the locus of failure between the toughest wet strip and the strip taken from the dry sample. (see Figure 3.36)

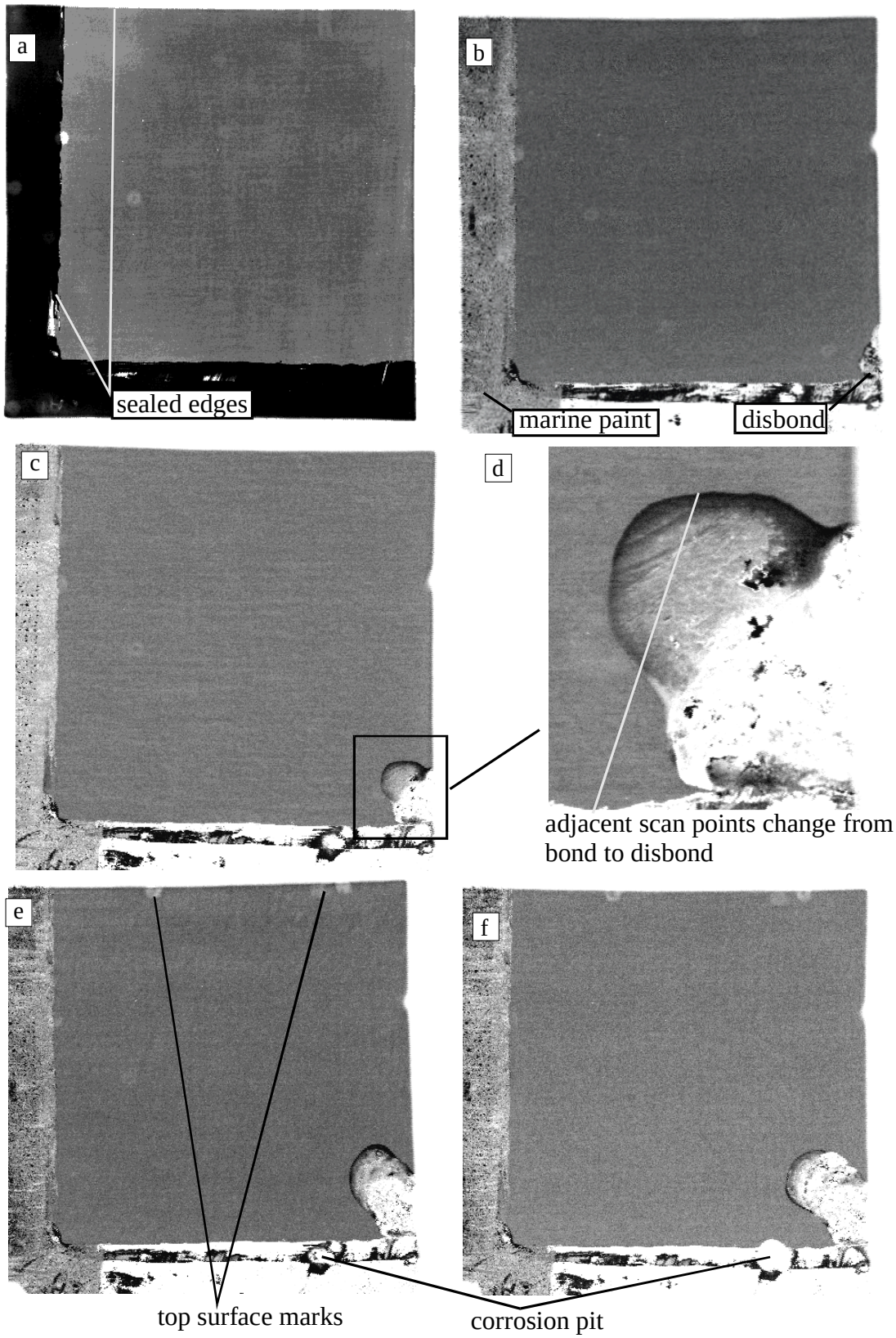

Figure 3.29 Normal incidence scans from 2-layer CAA specimen after (a) 0 (b) 64 (c) 103 (d) 103 (e) 135 and (f) 175 days in water.

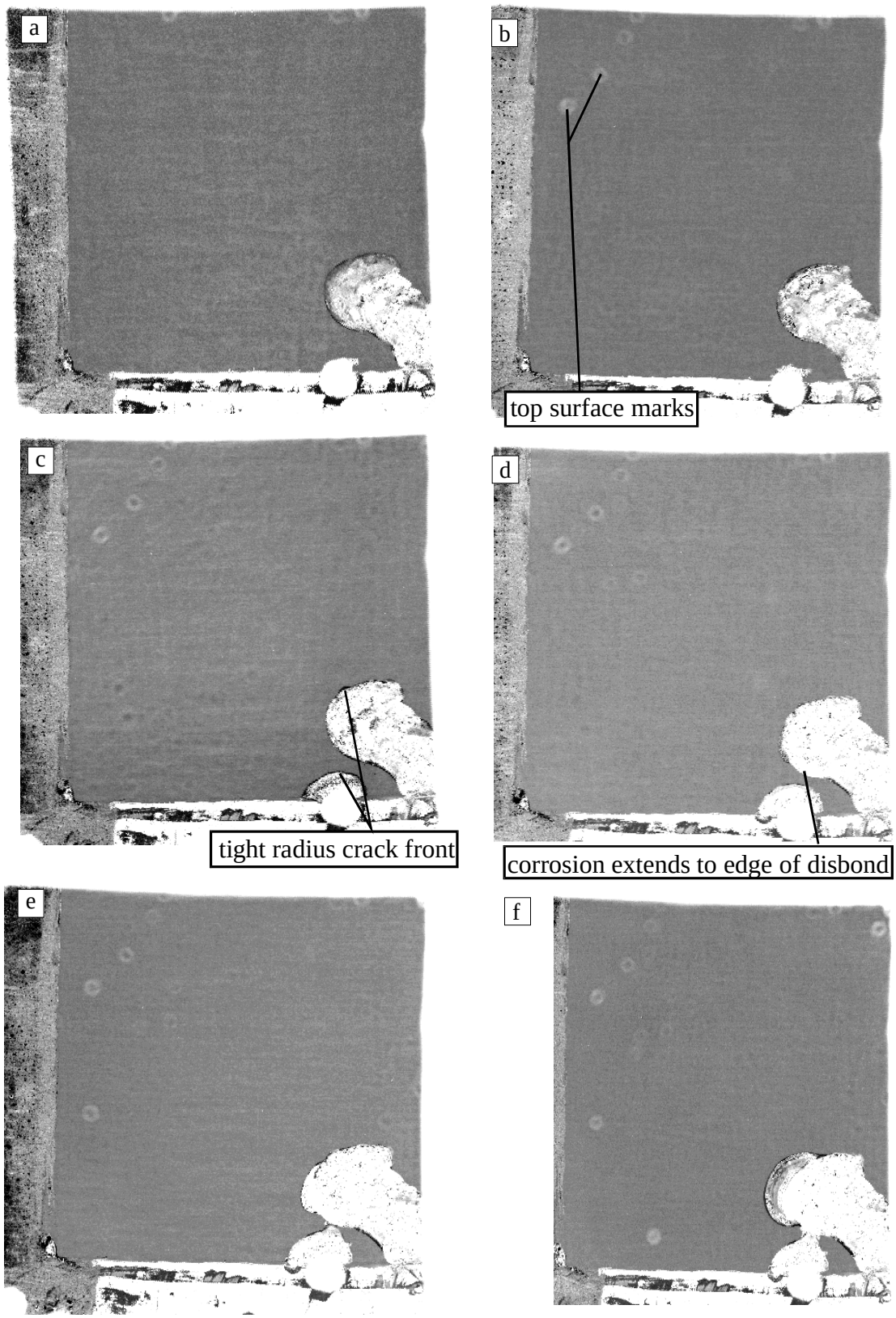

Figure 3.30 Normal incidence scans from 2-layer CAA specimen after (a) 216 (b) 254 (c) 309 (d) 359 (e) 415 and (f) 465 days in water.

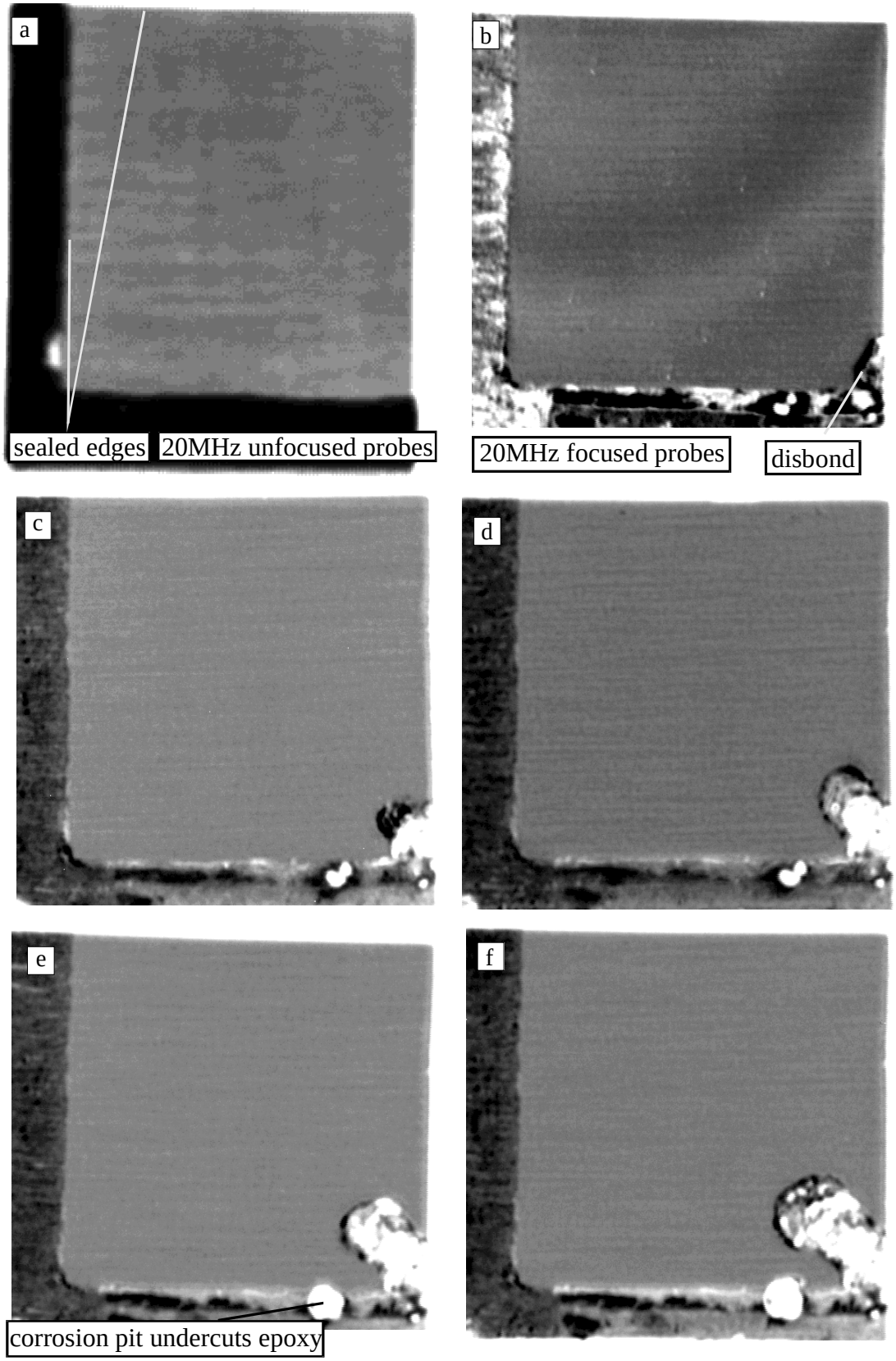

Figure 3.31 Oblique incidence scans from 2-layer CAA specimen after (a) 0 (b) 64 (c) 103 (d) 135 (e) 175 and (f) 216 days in water.

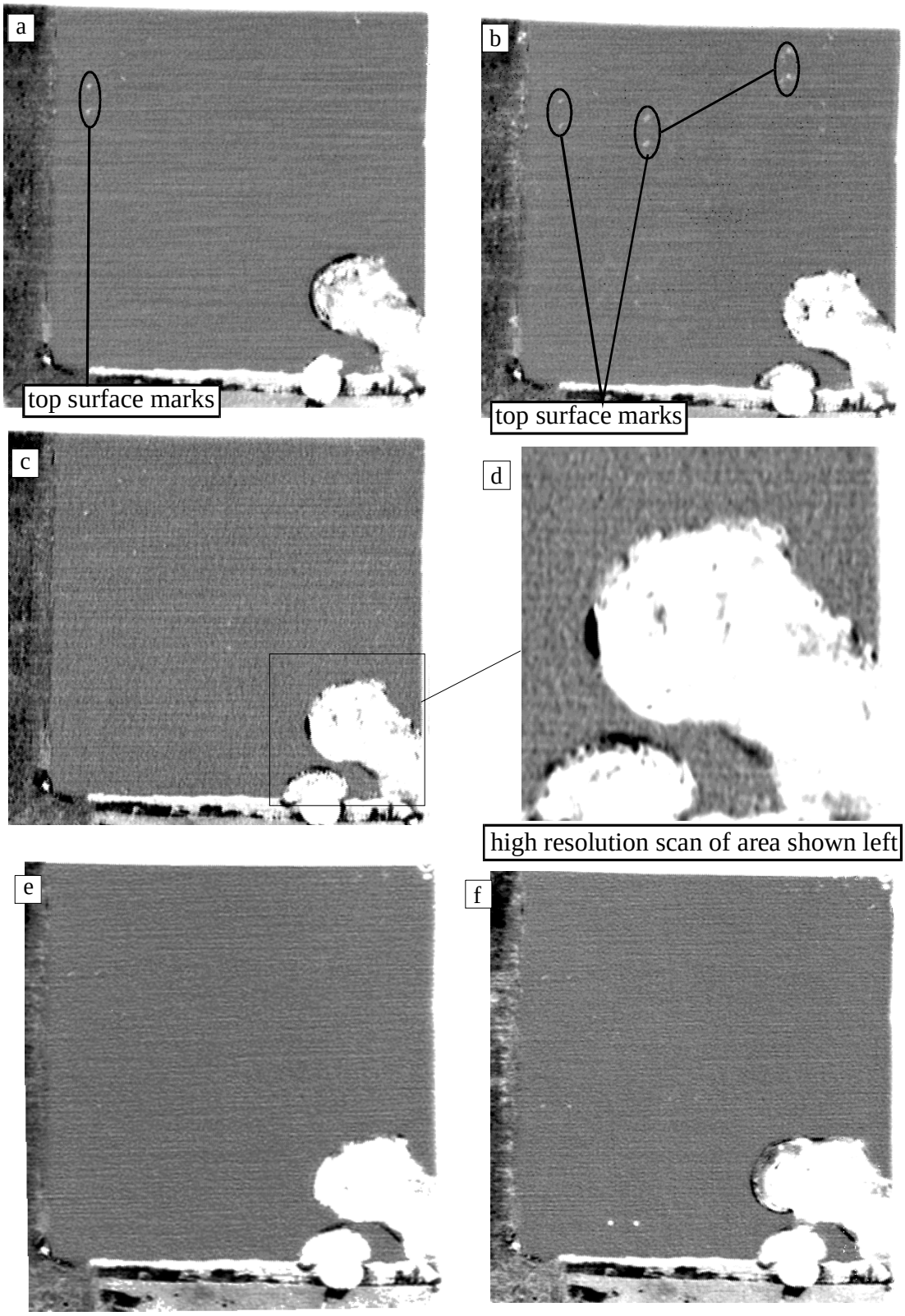

Figure 3.32 Oblique incidence scans from 2-layer CAA specimen after (a) 254 (b) 309 (c) 359 (d) 359 (e) 415 and (f) 465 days in water.

(a)

Some top surface corrosion spots interfere with scan

Large corrosion induced disbond detectable, difference between recent disbond and corroded areas apparent

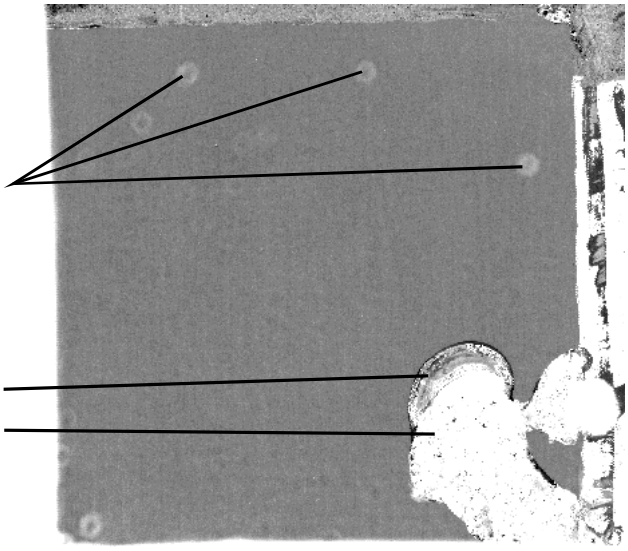

(b)

Top surface corrosion pits leave double shadows on interface scan

Corrosion induced disbond easily detected

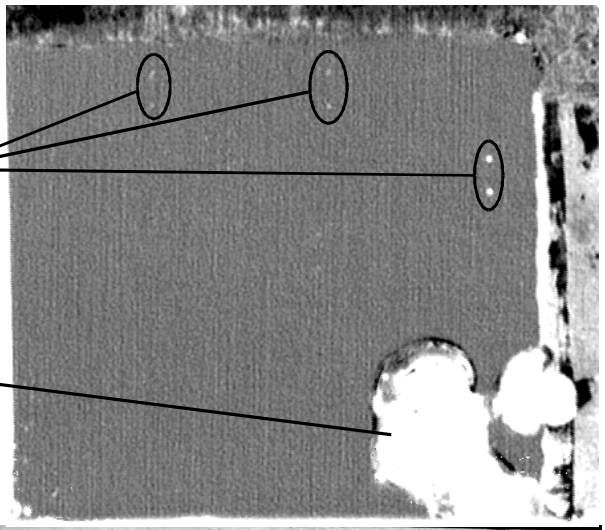

(c)

Free epoxy surface marks, not at interface

Cracks through thickness of the epoxy layer

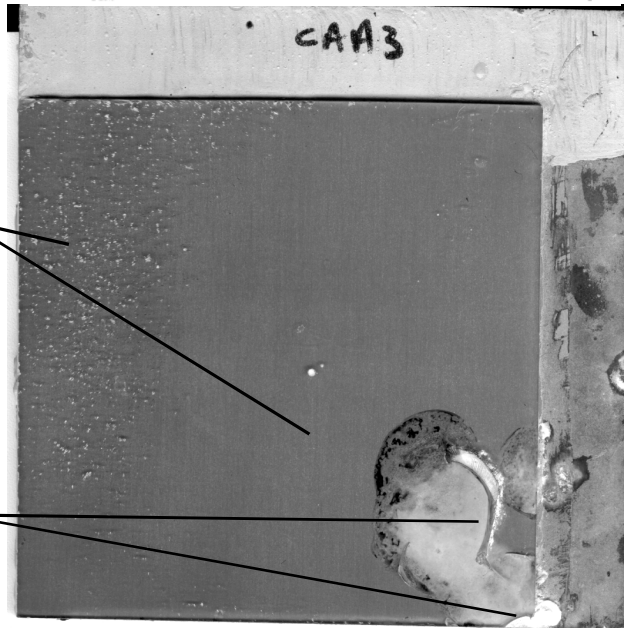

Figure 3.33 Comparison of (a) normal and (b) oblique incidence scans with (c) photograph of 2-layer CAA specimen.

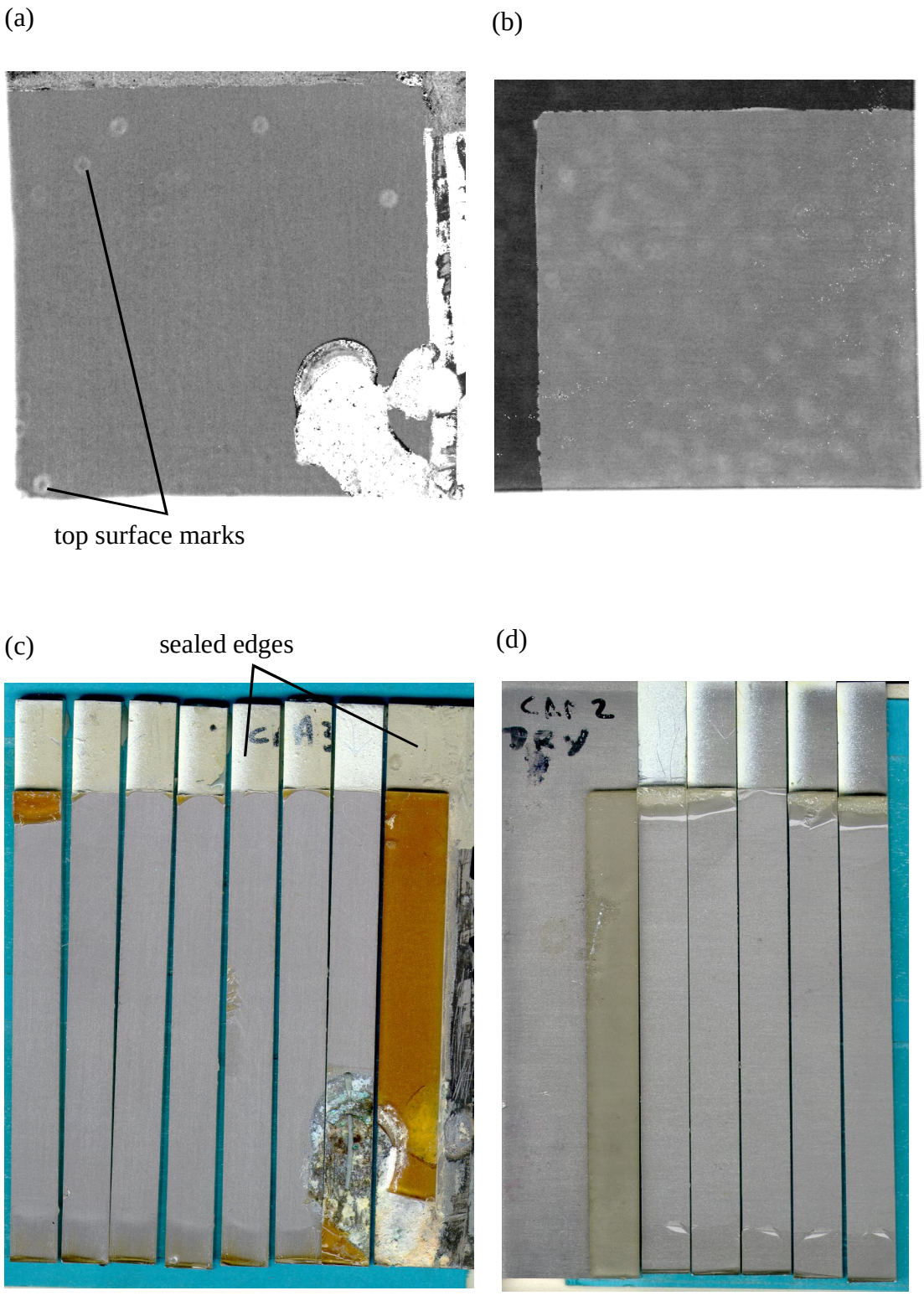

Figure 3.34 Comparison of final normal incidence scans from (a) wet (b) dry 2-layer CAA specimens with photographs of (c) wet and (d) dry failure surfaces.

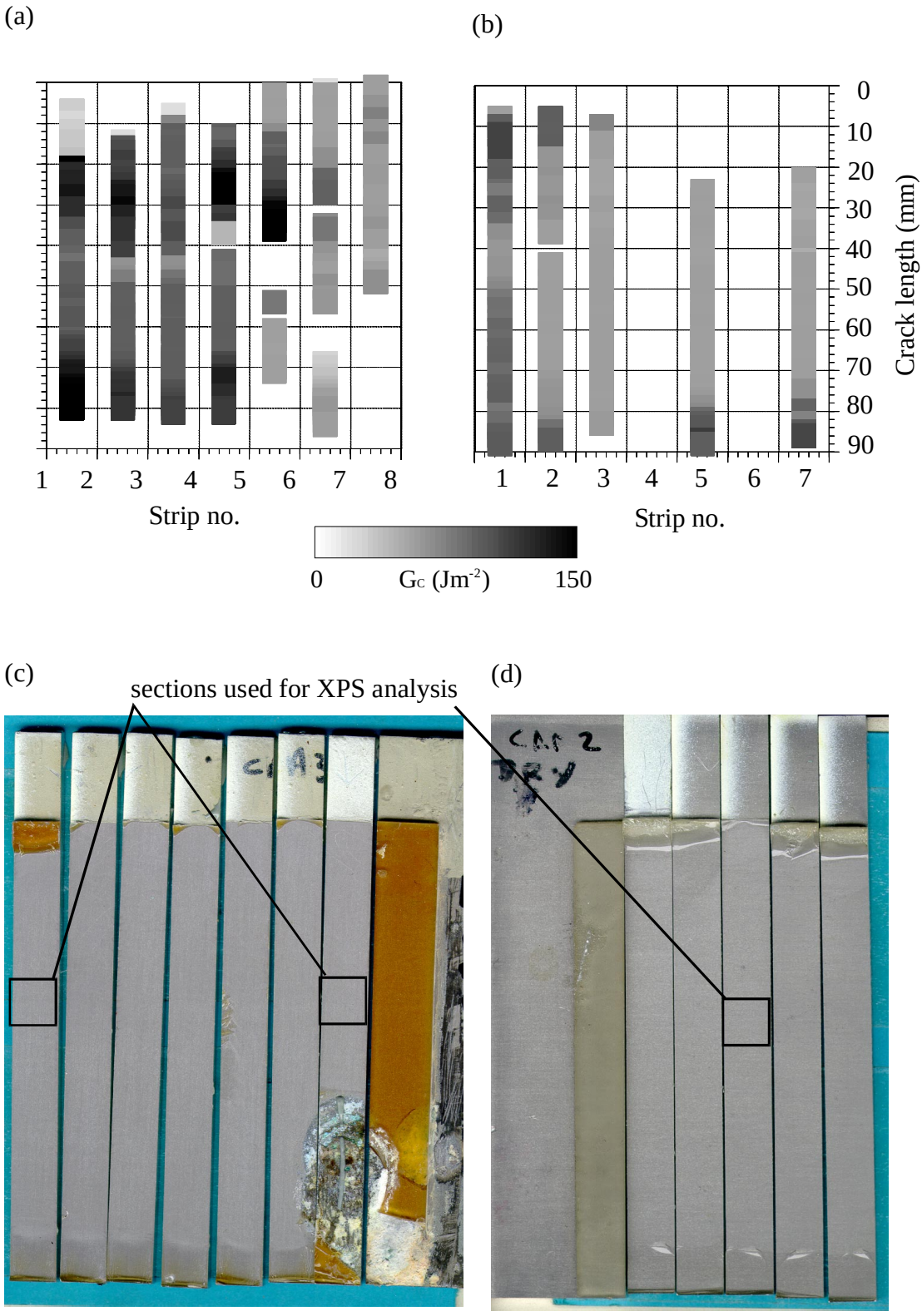

Figure 3.35 Comparison of mechanical test results from (a) wet and (b) dry 2-layer CAA specimen with photographs of (c) wet and (d) dry failure surfaces.

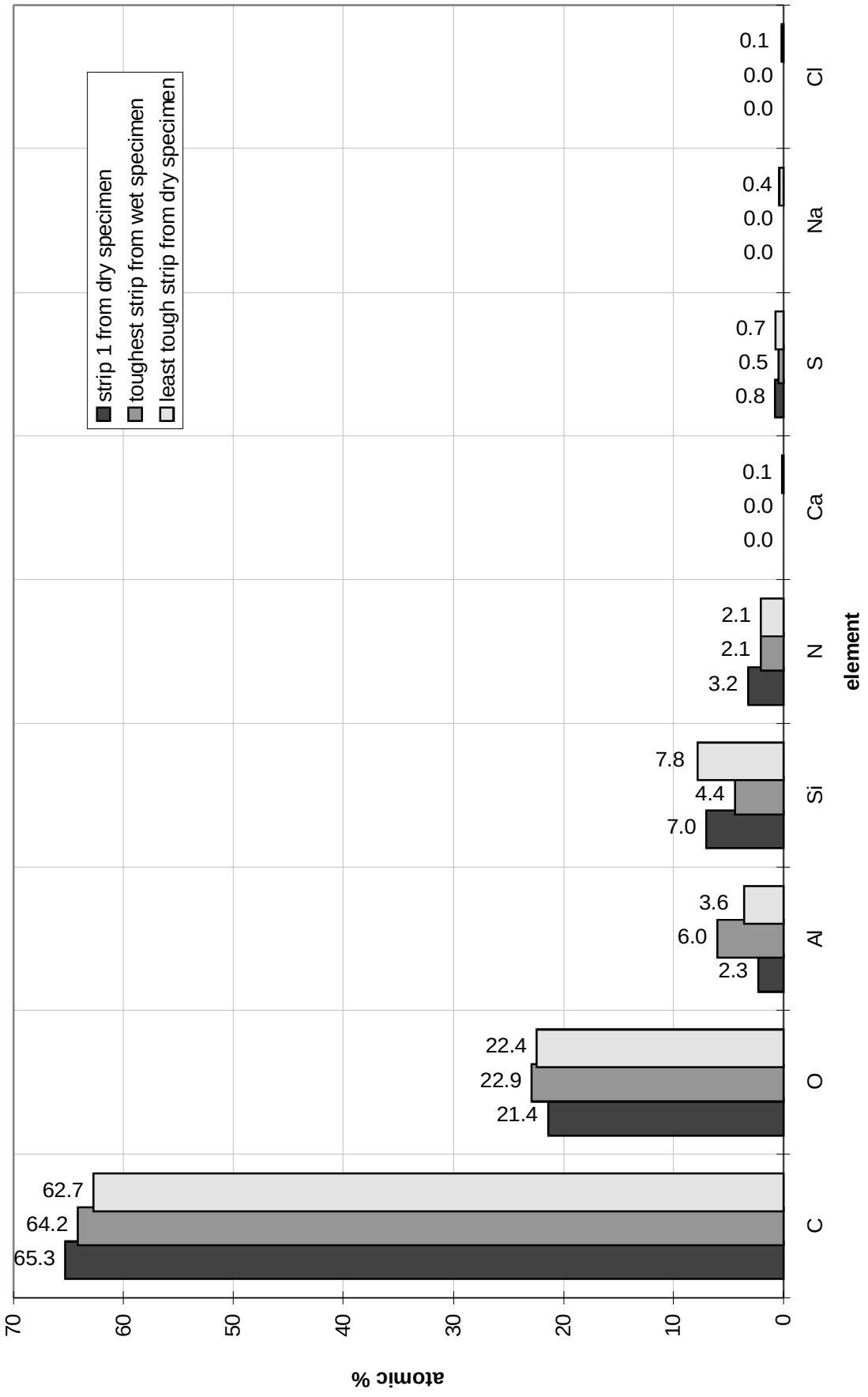

Figure 3.36 XPS results from 2-layer CAA specimens.

3.6 Brief discussion of two layer specimen results

3.6.1 Introduction

The results that have been presented here are discussed in greater detail and compared with the results from the three-layer specimens in Chapter 5, after the three-layer results have been presented in Chapter 4. However there are connections that can be made between the results seen from the two-layer specimens with different pre-treatments. Table 3.1 shows a summary of the results from the two-layer specimens.

Table 3.1 Summary of results from two layer specimens

Specimen	Exposure time (days)	Disbond Area (mm^2)	Rate (mm^2/day)	Micro defects	G_C wet Jm^{-2}	G_C dry Jm^{-2}
Grit Blast	223	1464	6.6	V. many	42(±24)	55(±12)
CAE	194	1958	10.1	Many	-	-
PAA	393	1274	3. 2	Average	30(±7)	55(±17)
CAA	465	1013	2.2	None	98(±31)	78(±18)
Grit Blast (ii)	145	700	4.8	Many	28 (±7)	61(±8)
CAE repeat	185	685	3.7	V. few	99(±17)	103(±78)

3.6.2 Results from N.D.T.

The scans performed on these specimens showed several important results. The normal incidence scans showed all of the defects that could be identified through visual assessment of the specimen (with some exceptions) if they were greater than the resolving power of the probe. Typically 0.25mm was sufficient for detection of the small spots, this best illustrated by Figure 3.2 but this can also be seen from the comparison of scans and photographs from most of the specimens. The exceptions are the detection of some of the line defects, this can be seen from Figure 3.12 and Figure 3.15. This showed some line defects that by eye appeared large enough for detection but were not apparent from the scans. The hypothesis for this is that the disturbance to the interface was not as great as visually inspection may have suggested.

The large edge disbonds seen on all of the specimens were easily detected by both the normal and oblique incidence techniques, with the extent of disbonding comparing exactly with the visual assessment of the specimen. The only possible exception to this is the lack of ability of either ultrasonic technique for scanning to the very edge of the specimen as discussed in Chapter 2, section 2.3.3. Neither technique showed any signs of more subtle damage extending ahead of the disbonds.

The oblique incidence technique has shown no advantages over the normal incidence technique from the results from these specimens. The oblique incidence technique was hoped to be more sensitive to the properties of the interface layers, (discussed in 2.3.2), which might have been expected to change due to such mechanisms as water diffusing through the epoxy or travelling along the interface. The fact that this has not been seen does not suggest that this has not occurred, simply that we have been unable to detect it.

3.6.3 Summary of defects.

The results seen across the range of pre-treatments for these two layers specimens have shown a number of common features. In general all the specimens have shown two distinct types of defect (these were discussed in detail in section 3.2.7 page 79. We have seen that there is the development of disbonding starting almost exclusively from the unsealed flush edge. There has also been the appearance on most of the specimens of other, much smaller defects, away from the edges of the specimens and apparently not connected to any open edge. These small defects have taken the form of small corrosion spots as well as narrow lines. Whether these small defects have been detected has largely been a factor of the resolution of the scanning method being used, the higher the resolution the better the chance of detection.

We have seen that the pre-treatments that offer the poorest corrosion protection are the ones which have shown the greatest number of these “micro-defects” as well as the highest rate of edge disbonding. This is best illustrated by comparing Figure 3.4 and Figure 3.33 which show the final scans compared with a photograph of the specimen from the grit-blast and CAA specimens. These two pre-treatments are the extremes in terms of the corrosion protection as was discussed in Chapter 1, section 1.5. The difference in the rate that the edge disbonding progresses is apparent (especially when the difference in exposure times is considered, 223 days for the grit-blast specimen and 465 for the CAA specimen), with the rate for the CAA being approximately a third that of the grit-blast specimen. However the difference in

the appearance of the small spots and lines is even more striking, with the grit-blast specimen having a huge number present and the CAA specimen showing none of these defects.

The CAE and PAA specimens are between the grit-blast and CAA specimen in terms of the appearance of these two specimen types. The two sets of CAE specimens used for this work show considerable difference in performance. This first specimen had a higher rate of edge disbonding than the grit-blast specimen, with a many micro-defects being apparent. However the second CAE specimen had a lower rate of edge disbonding and virtually no micro-defects. The PAA specimen showed an edge disbonding rate of 3.2 mm^2/day which falls between the grit-blast and CAA specimens. The number of micro-defects was small compared with the grit-blast specimen, but there were more than ten clearly identifiable small spots distributed across the specimen.

3.6.4 Mechanical test results

The toughness values that have been shown in the table have been calculated as an average value, with no value being taken for the areas of large scale disbonding which have always had no measurable toughness. This implied that both the G_c value and the disbond area need to be considered when ascertaining the overall extent of degradation. The standard deviation for the data from each specimen is shown as the number in brackets next to the toughness value. The highest standard deviations are generally due to places on the specimen where the crack arrested and the apparent toughness was much higher when the crack re-initiated, this was particularly apparent for the dry CAE repeat specimen, the results from which are shown in Figure 3.17.

We have seen on a number of specimens a noticeable drop in toughness for the strips taken adjacent to an unsealed edge. The extent to which this data is reliable has varied, but the grit blast (Figure 3.8), PAA (Figure 3.25) and CAA (Figure 3.35) specimens have all exhibited this to some extent. Only the mechanical tests from the CAE specimen have shown no sign of a greater loss of toughness around the unsealed edge, but this specimen showed no toughness loss any where. There has not been a significant indication that the edge strips should be less tough either visually or ultrasonically (except perhaps a slightly higher occurrence of micro-defects around these edges, however this is not a strong connection).

We have seen from the grit-blast, first CAE and PAA specimens that the loss of toughness has been accompanied by the appearance of micro-defects (or vice versa). The specimens that showed no micro-defects (the second CAE and CAA specimens) showed excellent residual toughness.

3.6.5 XPS results

The XPS analysis obtained from the failure surfaces of the two-layer specimens has in many cases helped explain differences in the mechanical performance of the specimens and differences in the appearance of the failure surfaces. This has enabled a connection between certain elements present on the failure surface of specimens and loss in toughness. The most important connection has been that the clearest losses of toughness have occurred when there have been detectable traces of elements such as chlorine, sodium and calcium. These elements produce a strong connection with the presence of bulk water. The strongest evidence for this has come from the CAA specimen, see Figure 3.35 for the mechanical test results and Figure 3.36 for the XPS results. This specimen also suggests that the presence of moisture via diffusion through the epoxy has not been sufficient to produce a loss of toughness in the specimens. Indeed, for the majority of this specimen it has been seen that the effect of water on the joint has been to increase the toughness of the interface.

The results from the surface analysis of the PAA specimen has helped explain differences both in the mechanical performance and the appearance of the failure surface. It was seen from Figure 3.25 and Figure 3.26 that the tougher areas of the specimen had a covering layer of epoxy, and the weakest areas from the wet specimen were much closer to the bulk adherend, although it was impossible to say whether this failure was in the oxide layer.

3.7 Concluding remarks

We have seen from the non-destructive examination defects, both along unsealed edges, and also distributed throughout the interface of the joint. These distributed defects have been seen to correlate with a general loss of toughness throughout the specimen. There has also been no advantage of the oblique incidence technique over normal incidence. The surface analysis results have shown variations in the locus of failure for the different specimens and these have correlated with the

mechanical test results. These specimens have shown variations in durability in line with what is expected for specimens with this variation in pre-treatments, with the grit-blast being the least durable, with the CAE specimen being next best followed by the PAA and then CAA. The better performance of the CAA specimen appears to be due to the better corrosion protection offered by the pre-treatment.

The following chapter contains the results for the three-layer specimens. These are presented in the same order as was used in this chapter for the two-layer specimens. The comparison of the results from both the two and three-layer specimens are then presented in Chapter 5.

4. Three-layer Specimen Results

4.1 Introduction

The results from the three layer specimens are presented in fundamentally the same form as those from the two layer specimens. However the introduction of the second adherend and thinner epoxy layer has introduced some differences both in the mechanical tests and also the ultrasonic scans, as has been discussed in Chapter 2. For the ultrasonic scans it has been possible to monitor three parameters from each specimen (this has only applied since the introduction of the new scanning system, and so some of the early scans from the oldest specimens do not have all the possible data). The three parameters measured have been the two amplitudes of the reflection from both the first and second aluminium/epoxy interfaces and also the time delay between these signals (i.e. the thickness/velocity ratio of the epoxy layer). Scans produced monitoring the reflection from the interface between the top aluminium plate and the epoxy are referred to as first interface scans. The scans produced mapping the amplitude of the reflection from the interface between the epoxy and the lower aluminium plate are referred to as the second interface scan. It should be remembered that scans obtained through multiple layers will show the effects that preceding layers have had on the signal amplitude. This has already been seen for the case of top surface pitting in the two layer specimens, but when a disbond exists in an adhesive joint this may result in virtually no energy propagating into subsequent layers.

4.2 Grit blast specimens

4.2.1 Normal incidence ultrasound

The results obtained from normal incidence scans of a 3-layer grit blast specimen are shown in Figure 4.1. The results obtained from each gate are shown for both the initial scan and also the scan taken after 67 days in water. This specimen shows significant amounts of scattering as indicated by the white specs which can be

seen from Figure 4.1 (a) and (b). It also shows one of the problems not encountered with the two layer specimens, that of trapping air in the epoxy layer. These air voids also indicate the shadowing effect generated by total reflection as the white spots appearing in the scan from the second interface indicate no energy propagating that far. There are two types of air void present in some of the samples. Very small voids are usually present in the epoxy before pouring and are generally contained within the thickness of the epoxy; these are minimised by degassing the epoxy after mixing the resin and hardener. The much larger voids are caused by trapping air between the epoxy and the second aluminium plate as it is brought in contact with epoxy while producing the joint. These voids are generally present at the interface.

The scan from the second interface, Figure 4.1 (c), shows that there has been some cracking around the edge of the adhesive where one of the shims has been removed after curing. The time of flight scan, Figure 4.1 (e), shows that there is a significant variation in the thickness of the epoxy layer. The thickness scale shown with this figure has been calculated based on a epoxy velocity of $2610ms^{-1}$. The variation in thickness is due to slight curvature in the plate, and is almost unavoidable with this size and thickness of plate. The first interface scan taken of the specimen after 67 days in water, Figure 4.1 (b) shows that a disbond has started along the unsealed flush edge. The fact that it appears black on the first interface scan and white on the second indicated the disbond is between the top adherend and the epoxy. The following scans shown in Figure 4.2 (a),(c) and (e) are the scans obtained from the specimen after 252 days in water. After approximately another six months in water the disbond along the unsealed flush edge appears to have changed very little, however we can see the appearance of a new disbond along the unsealed recessed edge. Comparing Figure 4.1 (d) and Figure 4.2 (c) there is no sign of change at the second interface. Similarly comparing Figure 4.1 (f) and Figure 4.2 (e) there is no evidence of thickness change in the specimen.

Unlike the two layer specimens, where a visual assessment of the specimen was generally sufficient to determine whether further damage had occurred, a scan was needed after sectioning to determine the final state of the specimen before mechanically testing, these are shown in Figure 4.2 (b),(d) and (f). It should be noted that between Figure 4.2 (a),(c),(e) and (b),(d),(f) there has been no further exposure to water. After sectioning it can be seen that there are a number of new disbonded regions, all of which appear as interfacial cracks, with several appearing at the first interface, and one at the second interface. Dry test specimens had been produced and sectioned to determine whether specimens could be sectioned without damaging the

joint. The dry test specimens were sectioned without damaging the joint. This led to the suspicion that this wet grit blast specimen was less tough than the test specimens.

4.2.2 Oblique incidence ultrasound

The oblique incidence scans taken from the same grit blast specimen are shown in Figure 4.3. In this case only one of the interfaces has been examined. The longer time domain signals obtained at oblique incidence from the three layer specimens would often lead to unsatisfactory results due to the overlapping of various reflections from within the bondline if images from the second interface were to be produced. The scans shown here are taken at the same intervals as have been shown for the normal incidence scans. The major details that are evident from the normal incidence scans are also present in the oblique incidence scan. However there is less influence of scattering from roughness, making the scan easier to interpret.

The effects of the longer wavelength can also be seen in the appearance of the crack caused by the removal of the shim. From the normal incidence scan taken from the first interface there appears to be only a small amount of the crack, however from the oblique incidence the crack influences the scan over a larger area. This is in closer agreement with the second interface scan produced using normal incidence. These oblique incidence scans show similar signs of internal scattering as was seen from the two layer specimens, evident by the grainy striping of the scans. There is also a visible difference between the initial and subsequent scans that is best described as less well focused. This is somewhat surprising given the reproducibility of most of the scans obtained at oblique incidence but serves to highlight the difficult of reliably producing accurate oblique incidence results. The unsealed recessed edge shows increasing numbers of corrosion pits as the exposure time increases, while the sealed edge remains unchanged, giving confidence that the sealant worked satisfactorily.

4.2.3 Mechanical test results

The comparison of the mechanical test results with a photograph of the failure surface is shown in Figure 4.4. The failure in this specimen was visually assessed as interfacial, by which is meant that the bulk of the adhesive has remained attached to only one of the adherends. This is not to say that there is definitely no epoxy remaining on the adherend surface, but if there is any there it is only at a microscopic level. The areas that can be seen from the figure to have epoxy covering them are where the interfacial failure has switched to the opposite interface. Figure 4.5 compares the failure surface and the final C-scan from this specimen. We can see that

the voids that were present on the scan have left a small amount of epoxy on the surface. The disbond that was detected along the unsealed recessed edge can be seen as a light corrosion patch on the failure surface. It is interesting to note that the pitting caused by this corrosion is as nothing compared with the corrosion patch on the two-layer grit-blast specimen. The disbonds that were detected along the unsealed flush edge are not seen on the failure surface, as the specimen was cut into uniform strips and then the edge of each strip was fly cut to produce a smooth edge. This preparation for the mechanical tests removed the edge disbond.

The comparison of the results from two dry grit blast specimens with the result obtained from the wet specimen are shown in Figure 4.6. The fracture toughness values do not appear vastly different, 48 Jm^{-2} for the wet specimen, 61 Jm^{-2} for the dry specimen which was not post cured and 49 Jm^{-2} for the post cured dry specimen. However there is a major difference in the locus of failure. The two dry specimens failed clearly cohesively, with the crack running along the centre of epoxy layer. The difference that post cure has on these specimens can be seen from the mechanical test results. The effect is not only in the measured fracture toughness, but also in the way the specimen fails. The post cured specimen fails relatively smoothly with the crack not growing more than a few millimetres at a time. The specimen that was not post cured fails with large jumps by the crack. This is the reason for the large gaps in the data. The wet specimen however failed apparently totally interfacially. This is in many ways the defining characteristic of environmental attack [1].

It is important to stress that this failure is across the entire specimen. With two aluminium adherends sandwiching the epoxy there are two possible ways for water to have entered the joint. Water may have entered by diffusion through the epoxy layer or by travelling along the interface. The possibility of diffusion through the epoxy has already been discussed in Chapter 2. The diffusion calculations indicate there is no significant concentration of water more than 10mm into the joint. Therefore either the diffusion coefficient is highly inaccurate or water is entering the joint by another path. There is also the possibility that water may also travel through flaws in the epoxy layer. The scans that were produced from this specimen show nothing that suggests that there is water moving along the interface. However the failure surface shows possible signs of water ingress along the interface. Careful examination reveals staining on the surface, which traverses most of the specimen, and if caused by water would certainly offer access to the central regions of the specimen. If this is the case then we need to determine why the ultrasonic scans did not reveal the presence of

moisture at the interface. Reasons for this are discussed in Chapter 5 in the light of the evidence from the other specimens.

4.2.4 Failure surface analysis

Figure 4.7 shows the XPS results obtained from sections taken from one edge strip and one strip from the centre of the wet specimen discussed above. These are the sections labeled in Figure 4.4. The sections were taken from the adherend side of the failure (not the one that had all of the epoxy layer on it).Only the wet specimen was suitable for surface analysis as the dry specimens failed cohesively, leaving a thick layer of epoxy in the surface. The results for these two sections show only minor variations in the concentrations of the elements present on the surface. Unlike the two-layer CAA specimen there is no sign of sodium, chlorine or calcium that could be associated with the presence of bulk water. However the similarity of the elements present on the surface suggest that the failure was relatively uniform across the specimen, which is in agreement with the mechanical test results.

4.2.5 Summary of results from grit-blast specimen

As was the case with the two-layer specimens, these grit-blast specimens can be expected to be the ones that degrade the quickest. A number of key parameters can be drawn from the results and comparisons made with the specimens with different pre-treatments.

- edge disbonds - there were two areas of edge disbonding on this specimen totaling 25 mm^2. This is much smaller than any of the two-layer specimens.

- line defects - only the failure surface showed any sign of “line defects”, with none being detected ultrasonically

- mechanical tests - the wet specimen failed interfacially across the whole area of the joint. The two dry specimens also showed large variations in toughness due to post curing, but both failed cohesively.

- surface analysis - simply showed that the failure from the edge of the specimen to the centre appeared very similar.

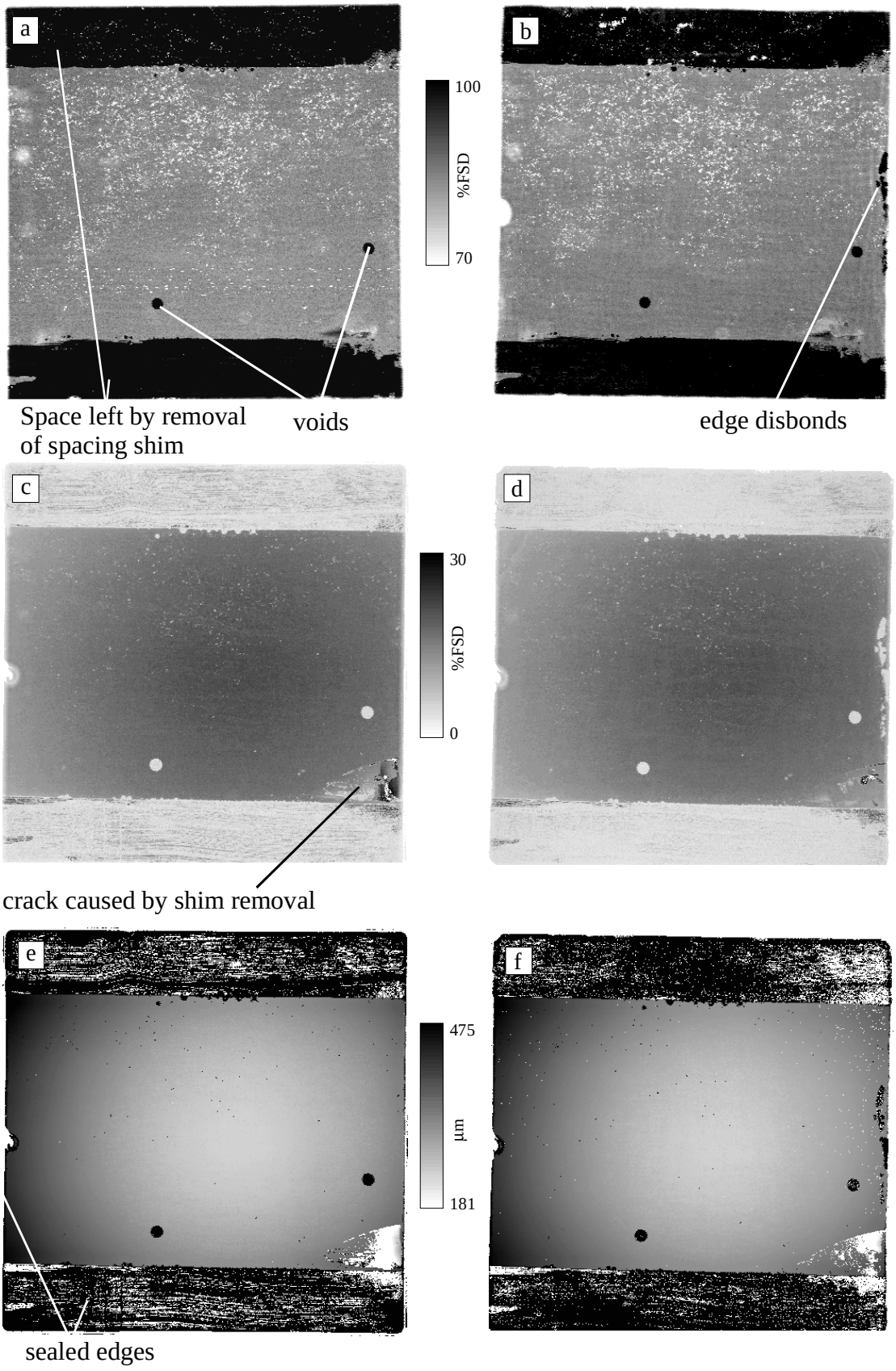

Figure 4.1 Three-layer grit blast specimen scans from first interface after (a) 0 and (b) 67 days, second interface after (c) 0 and (d) 67 days, and time of flight scan after (e) 0 and (f) 67days.

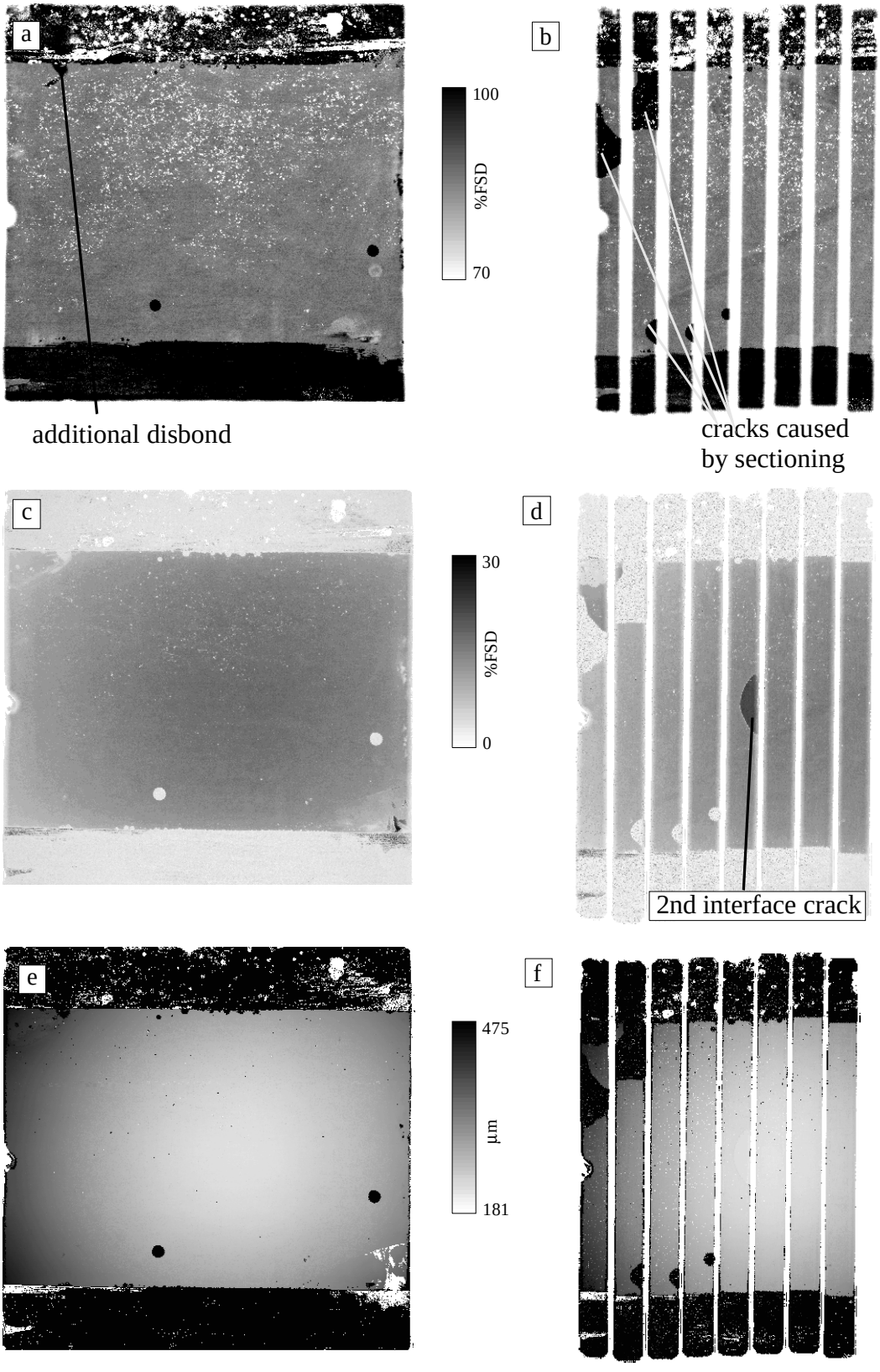

Figure 4.2 Threeo-layer grit blast specimen scans from first interface after (a) 252 days and (b) sectioning, second interface after (c) 252 days and (d) sectioning, and time of flight scan after (e) 252 days and (f) sectioning.

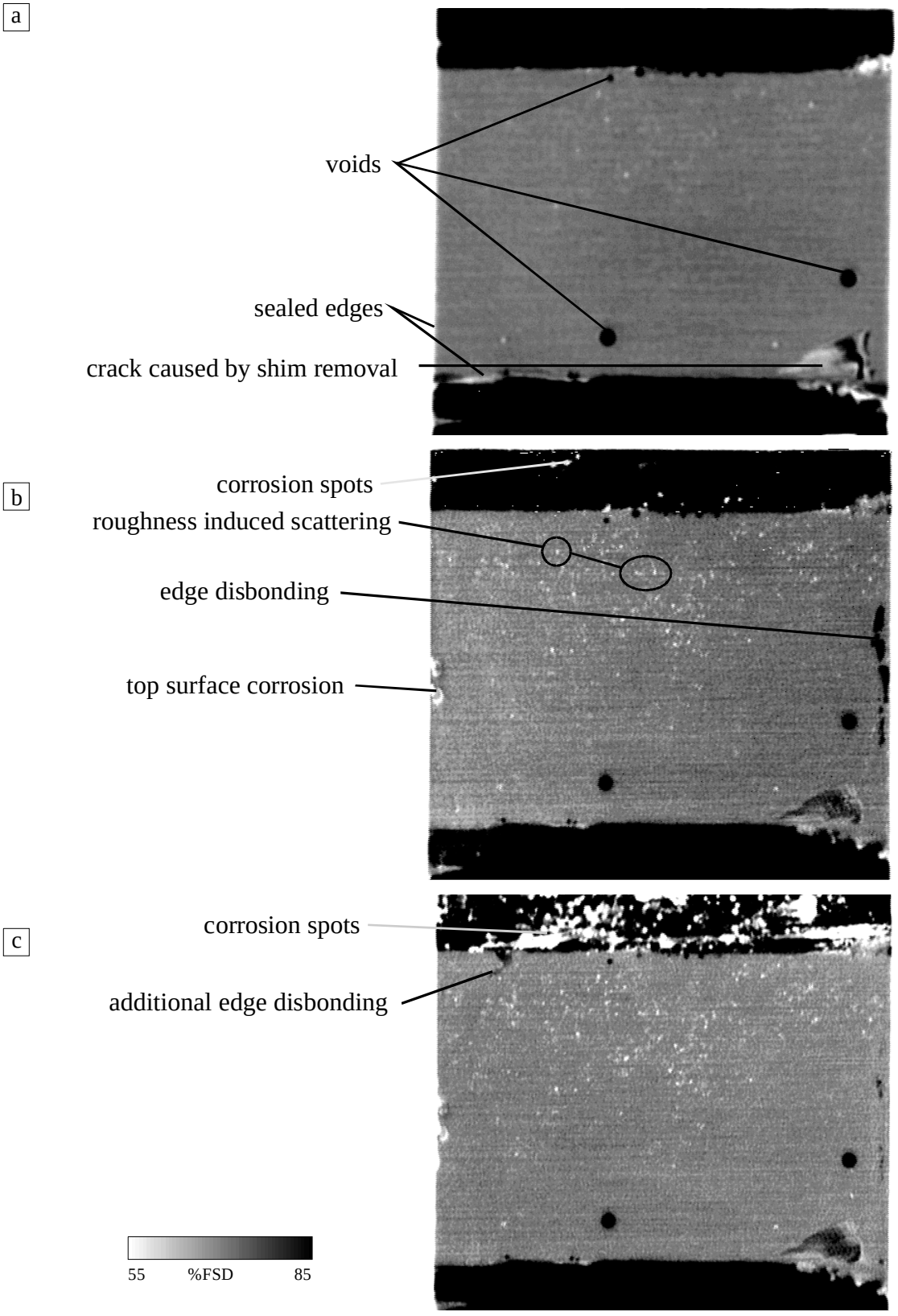

Figure 4.3 Oblique incidence scans from 3-layer grit blast specimen after (a) 0 (b) 67 and (c) 252 days in water.

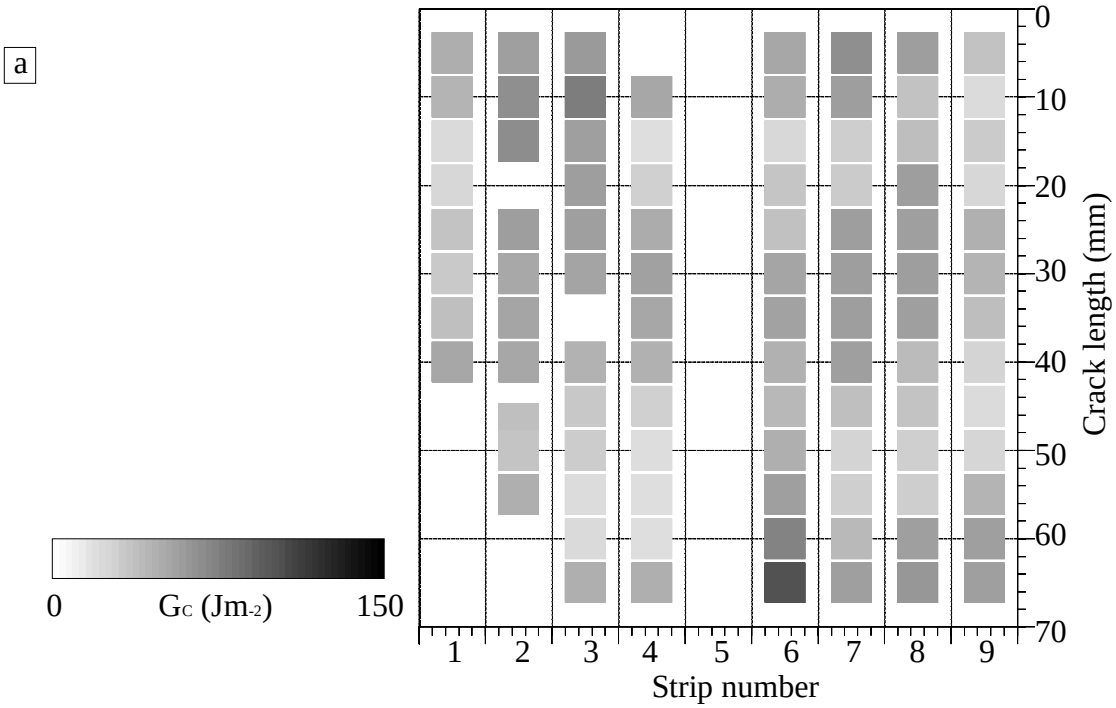

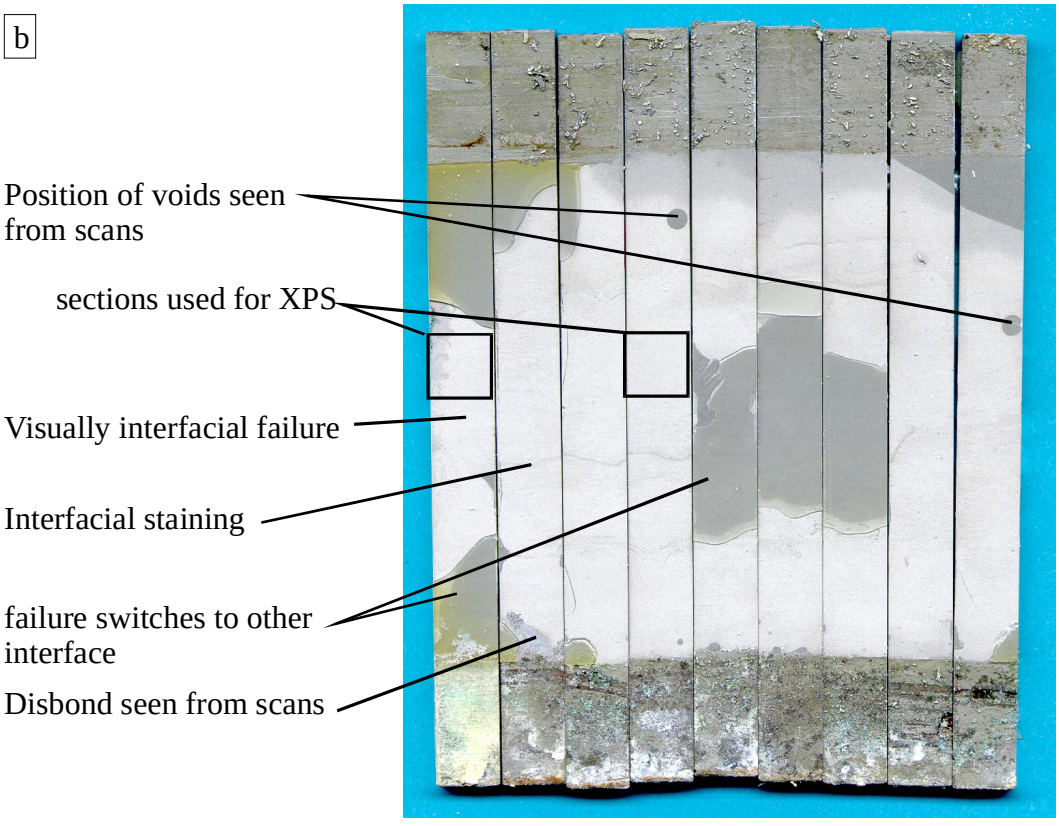

Figure 4.4 Comparison of (a) mechanical test result and (b) failure surface from three layer grit blast specimen.

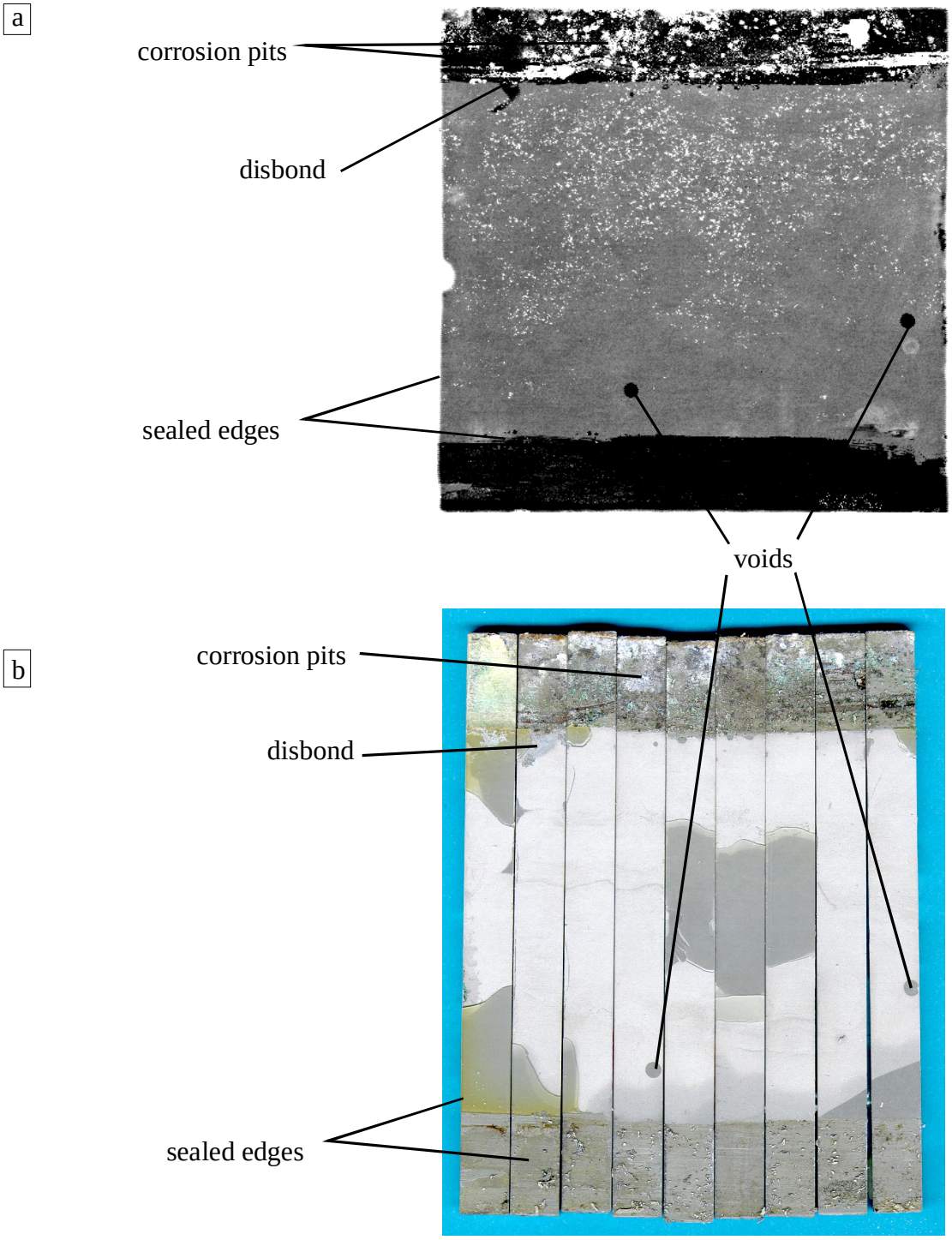

Figure 4.5 Comparison of (a) normal incidence scan and (b) failure surface from a three layer grit blast specimen.

a

Failure totally interfacial

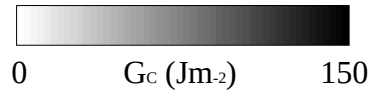

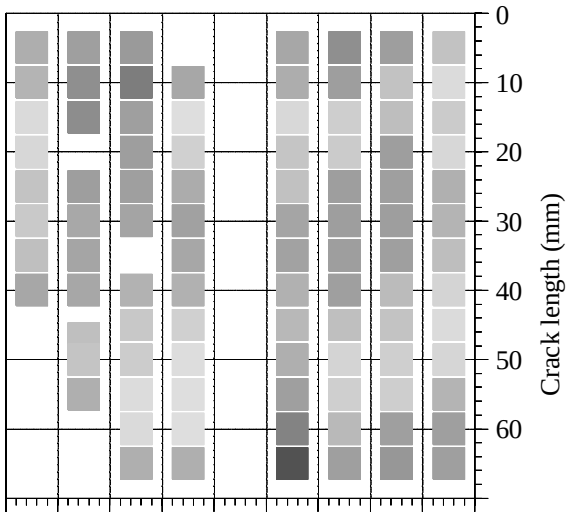

b

Failure totally cohesive

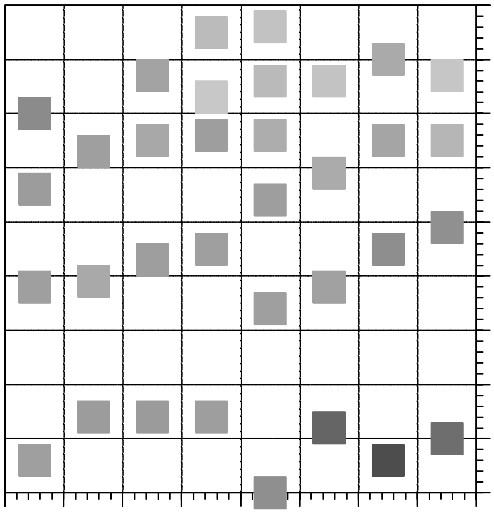

c

Failure totally cohesive

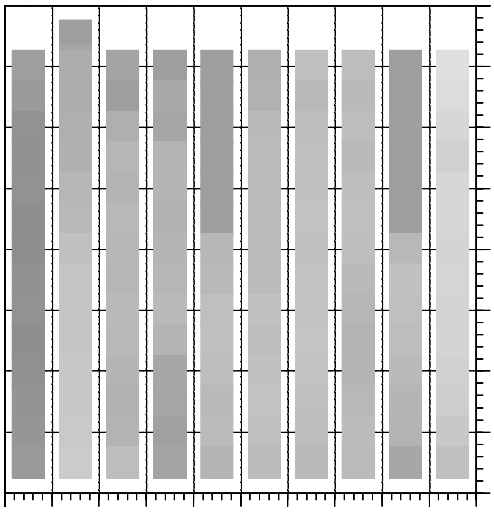

Figure 4.6 Three layer grit blast mechanical test results from (a) wet (b) dry and (c) dry post cured specimens.

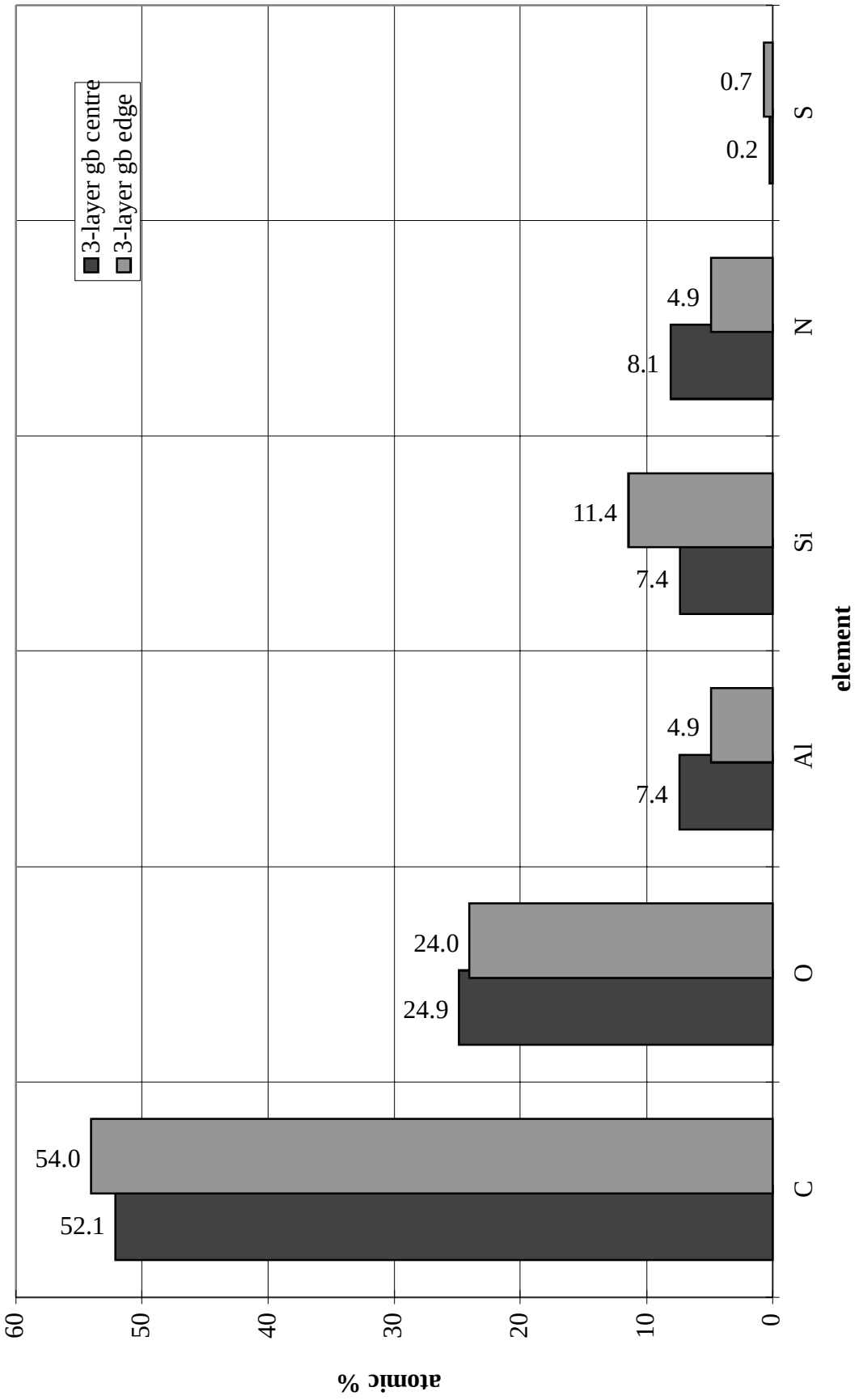

Figure 4.7 XPS results from wet three-layer grit-blast specimen.

4.3 Chromic acid etch

4.3.1 Normal incidence ultrasound

This specimen was produced earlier than the grit blast specimen discussed above, and appears slightly different in the scans shown in Figure 4.8. The difference is the position of the shims used both to control the bondline thickness and also to generate the recessed edges. The change was made to make manufacture easier, and the use of one less shim made sealing the edges easier and reduced the risk of cracking the epoxy while removing the shims. The first scan from this sample shows that there was some air trapped during manufacture. The difference between the first and second interface scans shows that some of the larger voids are present at, or very close to the interface, as they appear on the first interface scan, Figure 4.8(a). The smaller voids appear as the white areas on the second interface scan, Figure 4.8(b), where they are reflecting energy before the wave reaches the second interface. Reflectors at or close to the second interface will appear as darker areas, such as the one shown near the position of the small shim.

Comparing the initial scan with the one produced after 44 days in water we can see that the only detected change is the appearance of a narrow line. Figure 4.9 (a-c) shows the first interface scans from the same specimen after 90, 133 and 411 days in water. From these the progression of disbonds from the flush edges can be seen. Although initially this is from the unsealed edge, we also see disbonding from the flush sealed edge. This was accompanied by an undercutting of the sealant along this edge. We can also see the poor performance of the sealant on this specimen as there are corrosion pits along the recessed sealed edge as well as the unsealed edge. However there are no further signs of smaller defects within the central portions of the specimen. The second interface scan is also shown from the final scan of the specimen, after 411 days in water Figure 4.9(d). There are no further signs of defects on the other interface, just the appearance of the shadowing from the disbonds of the first interface.

4.3.2 Oblique incidence ultrasound

The oblique incidence scans from this specimen, seen in Figure 4.10, are similar to those seen from oblique incidence scans from other specimens. All of the detail that has been detected with normal incidence scans is also detected using the

normal incidence technique if the defects occupy a sufficiently large portion of the focal zone of the transducer. In this case the only defect which is close to the limit of detectability is the narrow line defect, which can be seen to be less clear than when the scans are performed using the 50MHz normal incidence probe. As was seen with the normal incidence scans there are areas of disbonding on this specimen spreading from the flush edges. After 411 days in water there are no further signs of defects other than the continued expansion of the edge disbonds. These scans do highlight the fact that it is possible to scan closer to the edge of a plate when the two probes are aligned parallel with the edge. The footprint of these probes on the plate surface can be considered as a long elliptical zone, and so one edge of the plate can be better interrogated than the ones perpendicular to it. This can be seen more clearly in Figure 4.11 where the final normal and oblique incidence scans are shown together. The pair of light spots that indicate a top surface mark in the oblique incidence scan has been shown. This indicates the alignment of the probes. With the probes in this arrangement the edges aligned in the same direction can be interrogated closer to the edge, hence the disbond on the left-hand edge appears larger from the oblique incidence scan. Consequently the disbond along the top edge appears smaller at oblique incidence compared to the normal incidence scan.

4.3.3 Mechanical test results

The results of the mechanical tests and a photograph of the failure surfaces from both the specimen discussed above and those obtained from a dry CAE specimen are shown in Figure 4.12. This dry specimen was produced at the same time as the wet specimen, but stored in a dessicator at room temperature. The most significant observation for both of these specimens is that they failed almost entirely cohesively. The only exception to this is the areas that were seen to be disbonded from both the normal and oblique incidence scans. The left-most strip seen in the photograph of the wet specimen failure surface failed during sectioning, and so no mechanical test data is presented for this. The observation that can be made about this strip is that the ultrasonic data failed to show the full extent of the damage due to the proximity of the edge of the plate. The failure surface indicated that the disbond had spread around 10mm into the specimen along the entire length.

Comparison of the mechanical test results shows that the wet specimen has a lower fracture toughness than the dry specimen. However the results also show gaps in the results from the dry sample. This is due to the brittle nature of the adhesive, which produced a crack that grew in stages, in a stick-slip manner. This was not the

case for the specimen which had been kept in water at 50° C for 411 days. This period in water has the effect of an extended post cure which is liable to change the properties of the adhesive. To verify this a specimen was produced and given an extended post cure of 4 weeks at 50° C but kept dry. The results from this specimen compared to the wet specimen are shown in Figure 4.13. It can be seen that after post curing the specimen that was kept dry, there has a been a drop in toughness which has reduced the measured toughness to below that of the wet sample. The post curing also produced a specimen that failed in the same manner as the wet specimen, in that the crack grew in a near continuous manner with none of the slip stick of the dry specimen not given a post cure. However it can also be seen that the right most edge strip did not fail in the same uniform manner as the rest of the specimen. This appeared to be because of inconsistencies at the edge of the epoxy layer during manufacture which affected the crack growth.

The results from the mechanical tests for these specimens are shown Table 4.1. The failure type for all these specimens was cohesive, which implies that differences seen are due to changes in the properties of the epoxy. This shows how significant the effects of heat are on the measured toughness of these specimens.

Specimen	**failure type**	**fracture toughness (Jm^{-2})**
dry, no post sure	cohesive	127(±37)
dry, post cured	cohesive	61(±5)
wet	cohesive	84(±19)

Table 4.1 Mechanical test results from three-layer CAE specimens

4.3.4 Summary of results from CAE specimen

The non-destructive examination of these specimens appeared very similar to the grit-blast specimen, but there were several important differences in the mechanical tests.

- edge disbonds- 300 mm^2 of edge disbonds were detected on this specimen which was considerably more than seen on the grit-blast specimen.

- line defects - the ultrasound scans from the wet CAE sample showed the appearance of a small line defect after 44 days in water. This was an isolated case, and appeared to have little consequence to the mechanical performance of the joint.

- mechanical tests - all the samples tested failed in a cohesive manor, except the areas the could already be seen as disbonded from the ultrasound scans. Differences in the post curing of specimens lead to a large difference in the measured fracture energies.

- XPS - the cohesive failure of all of the specimens resulted in no XPS measurements being performed.

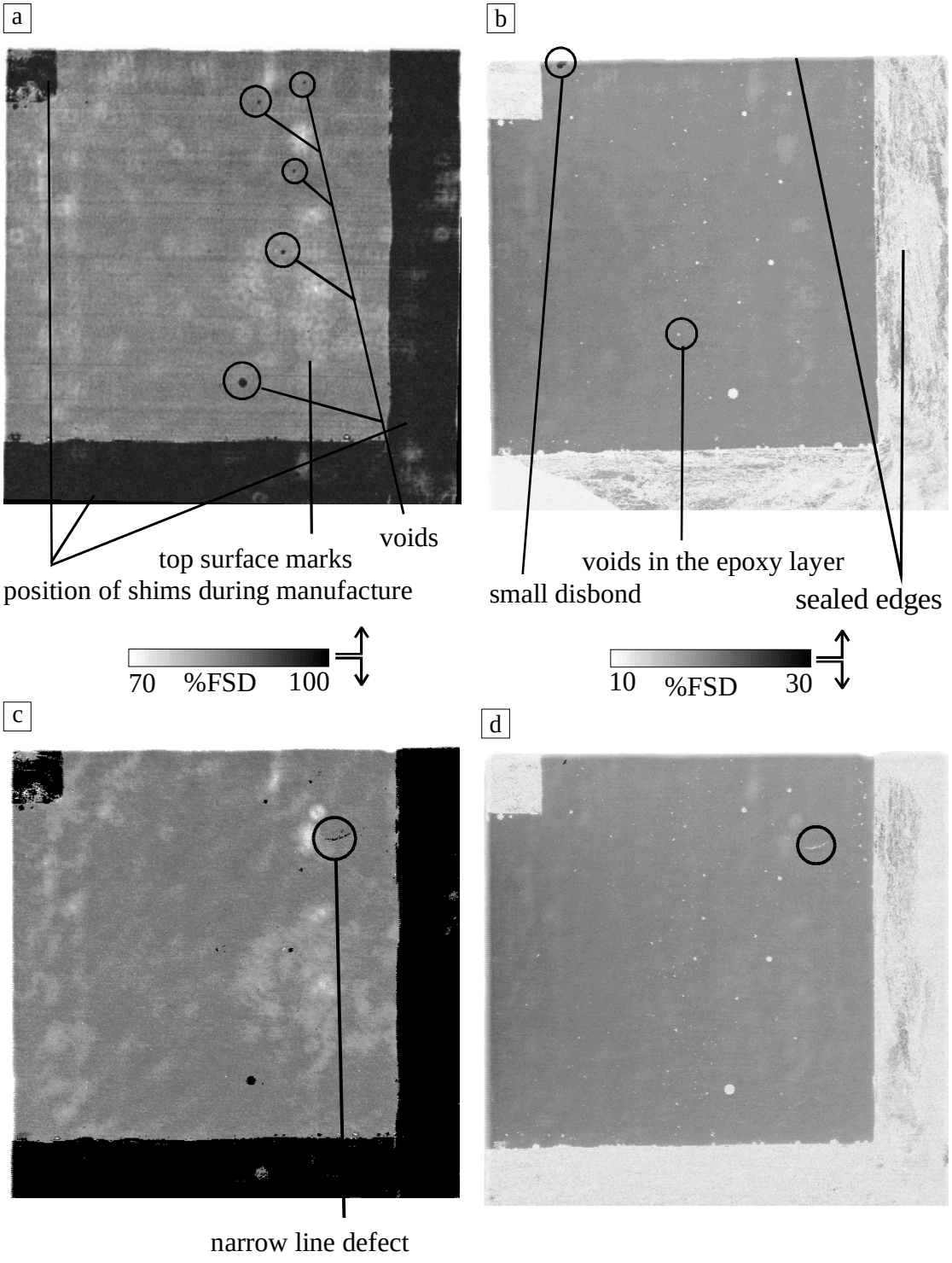

Figure 4.8 Normal incidence scan from three layer CAE specimen (a) initial first interface scan (b) initial second interface scan (c) first interface scan after 44 days (d) second interface scan after 44 days.

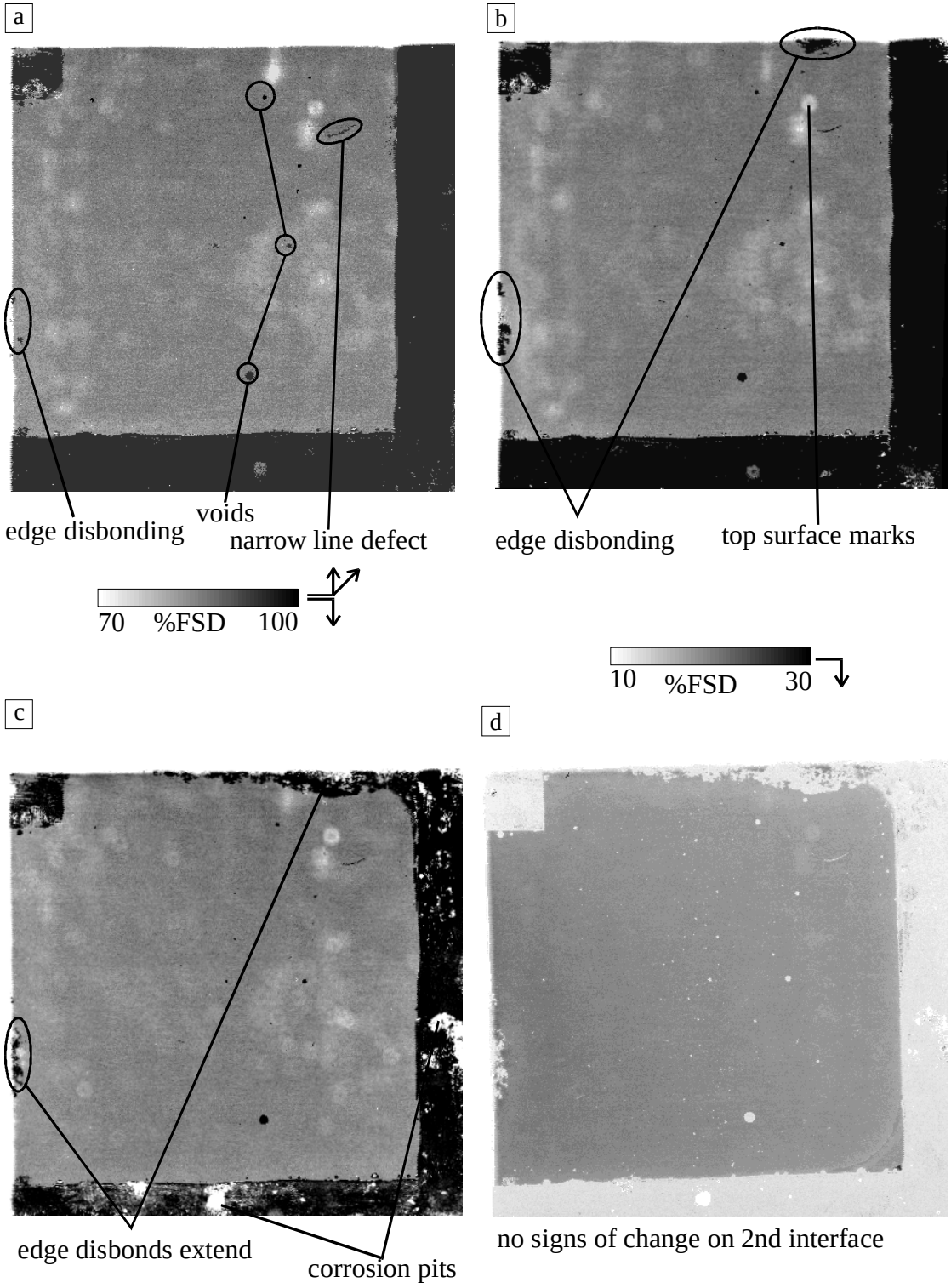

Figure 4.9 Normal incidence scan from three layer CAE specimen from first interface after (a) 90 (b)133 and (c) 411 days in water and (d) from the second interface after 411 days in water.

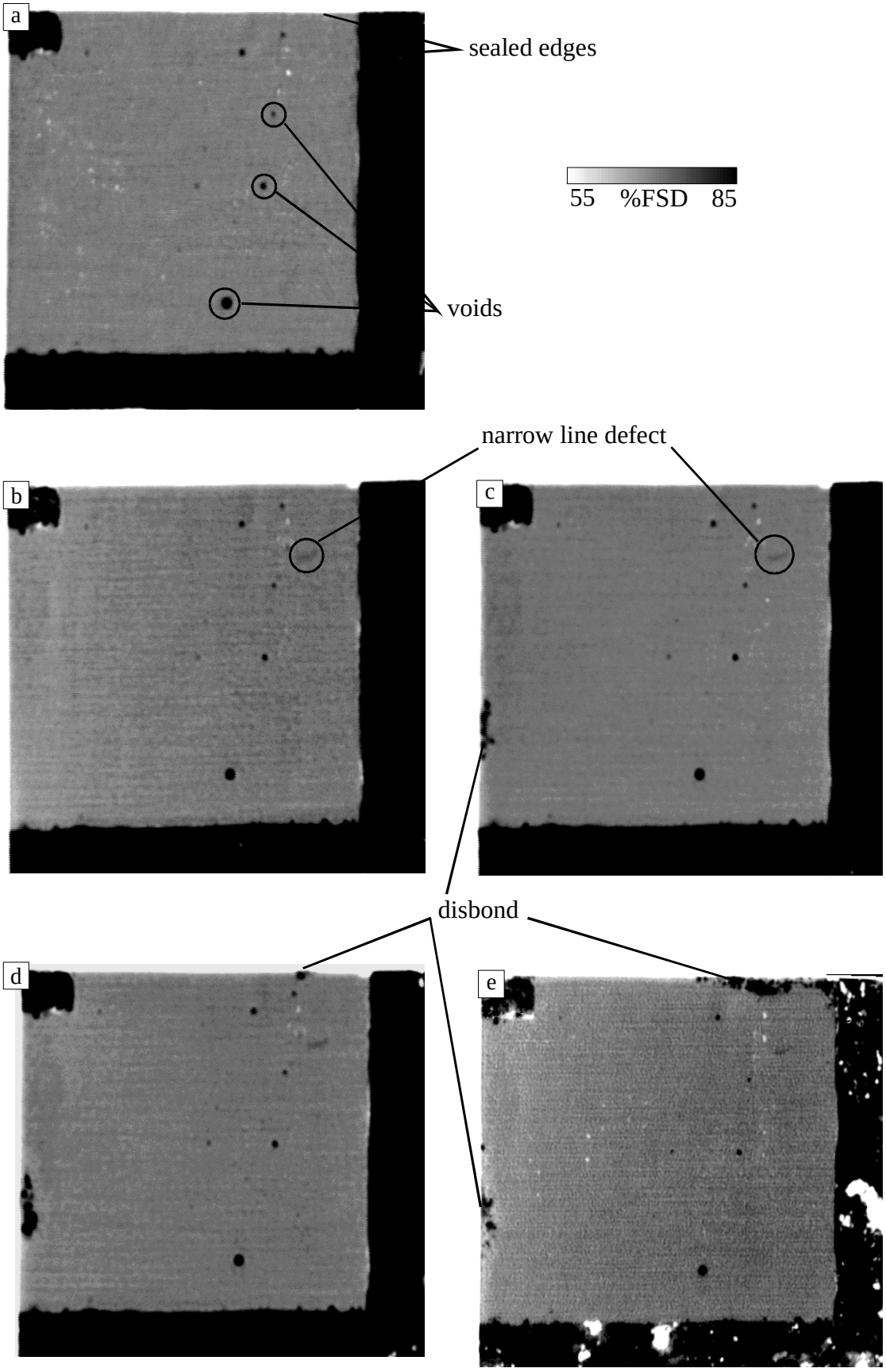

Figure 4.10 Oblique incidence scans from a three layer CAE specimen after (a) o (b) 44 (c) 90 (d) 133 and (e) 411 days in water.

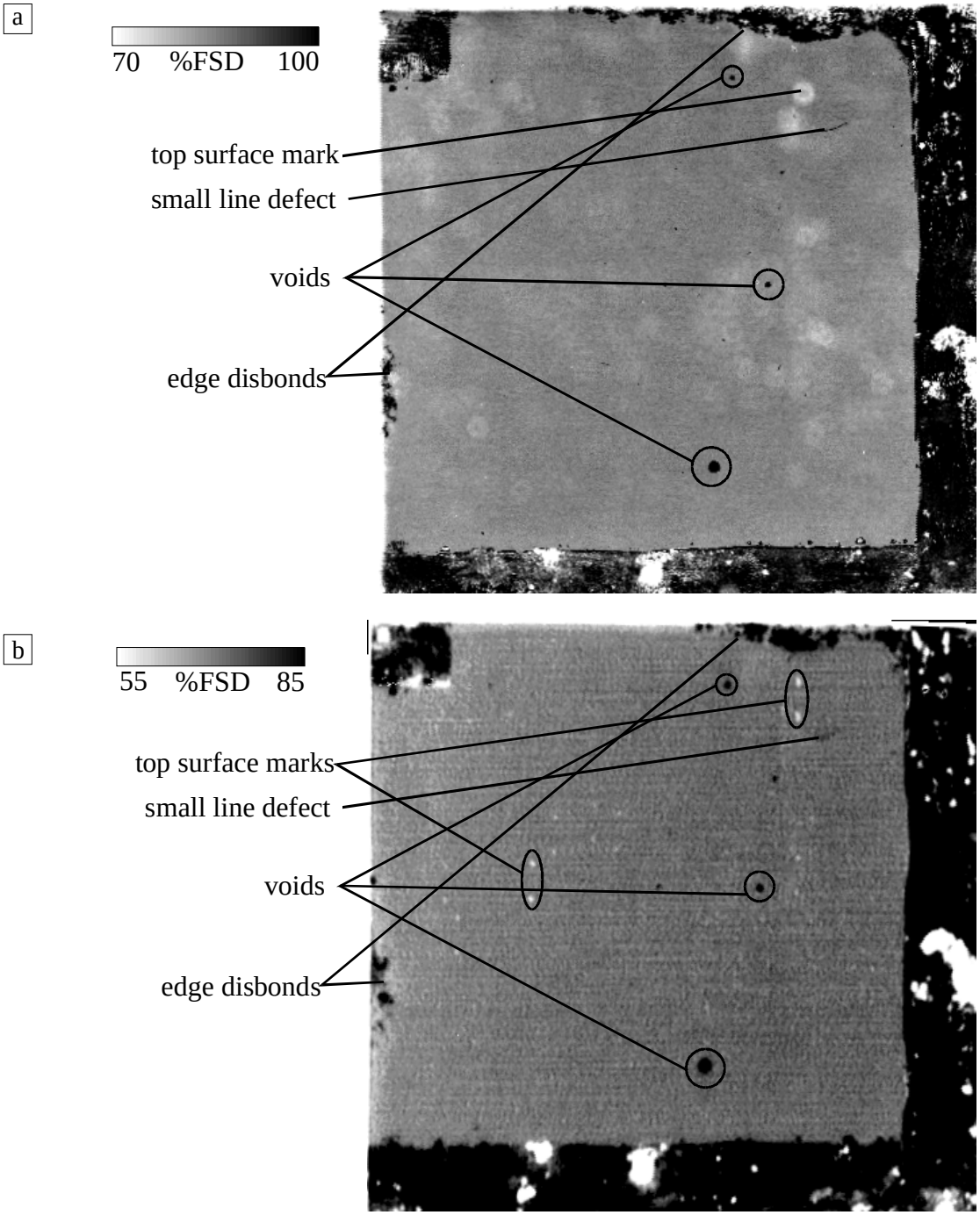

Figure 4.11 Comparison of final scans from three layer CAE specimen using (a) normal incidence and (b) oblique incidence.

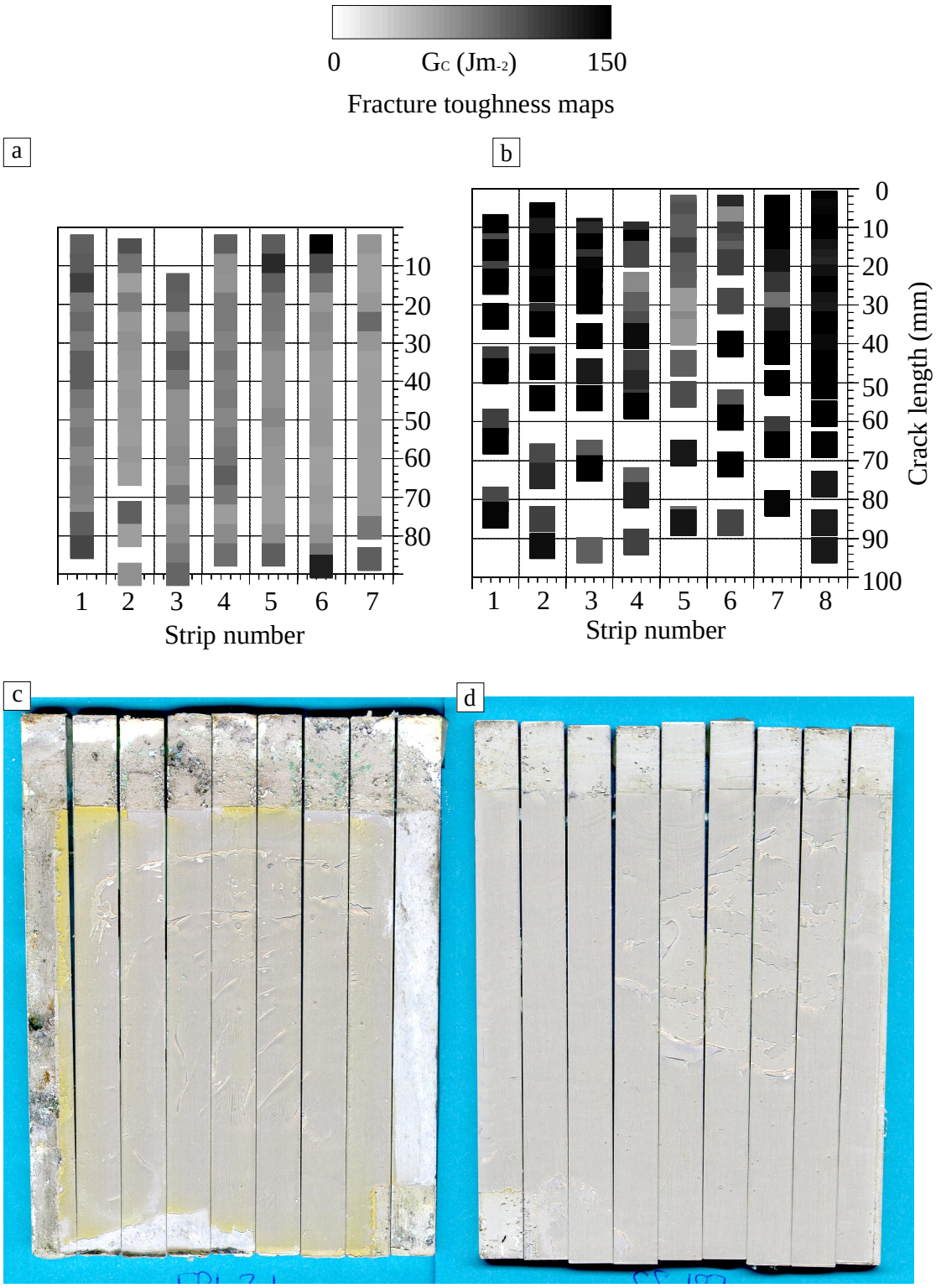

Figure 4.12 Comparison of fracture toughness maps from (a) wet and (b) dry CAE specimens with failure surface from (c) wet and (d) dry failure surface.

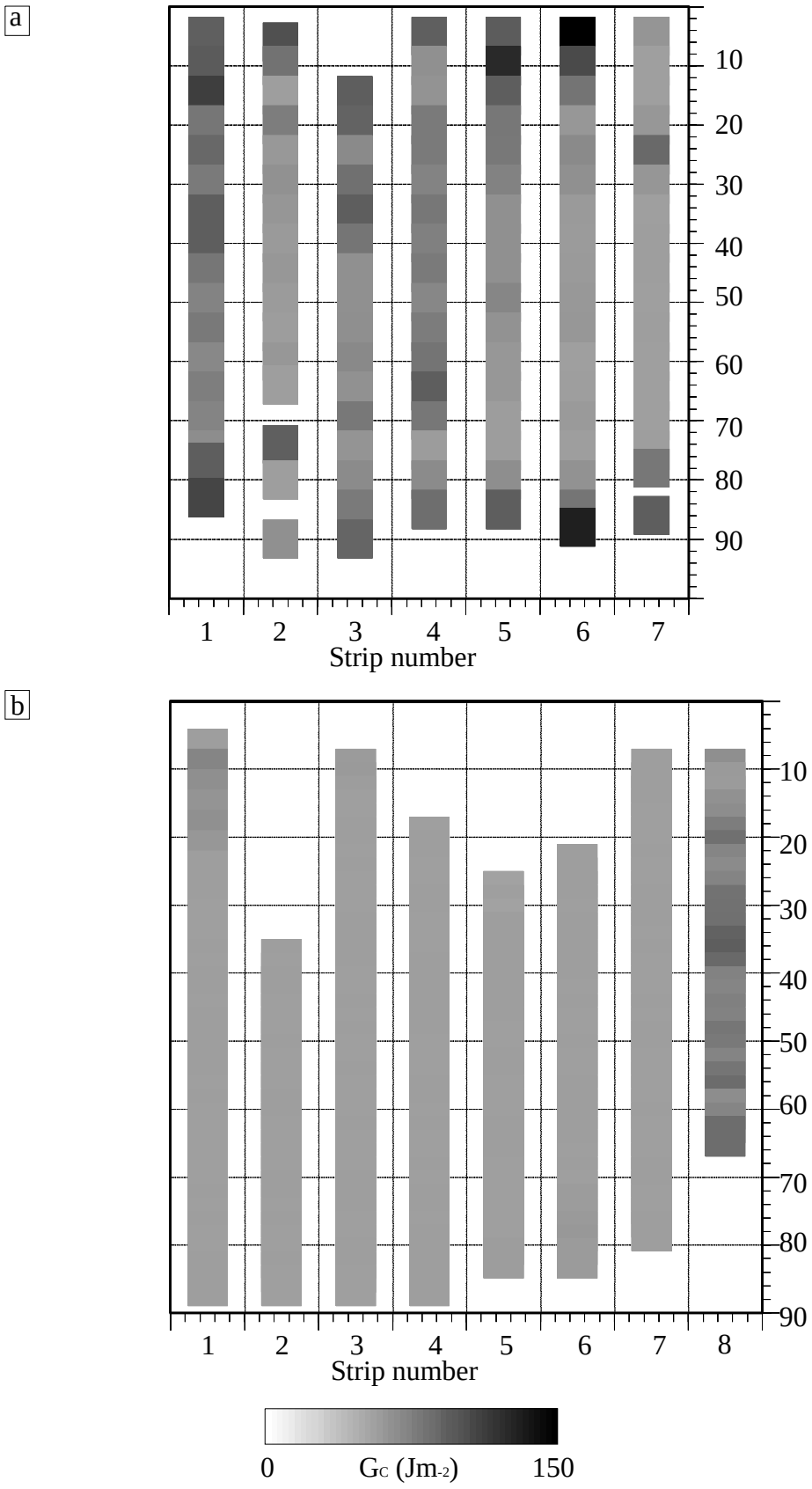

Figure 4.13 Comparison of fracture toughness maps from (a) wet and (b) dry post cured three layer CAE specimens.

4.4 Phosphoric Acid Anodised

4.4.1 Normal incidence ultrasound

The normal incidence scans from a wet three layer PAA specimen are shown in Figure 4.14. This is one of the specimens where the initial scans were performed using the older scanning system. This makes a significant difference to the appearance of the scan. The initial scan of the second interface could not be produced at the same time as that from the first interface, but is directly comparable with the scans shown later in the figure produced using the newer system. The initial scan from the first interface shows that there was a single large interfacial crack produced while removing a spacing shim, and for this reason this edge was sealed. There are also three voids visible from this scan. There is also some evidence of near interface cracks, which are more clearly visible in Figure 4.14b. (The locus of these cracks zigzags through the epoxy layer, getting close to the interface in places. These are the areas on the first interface scan that appear white where the thickness of epoxy left on the adherend is small enough to cause destructive interference with the reflection from the aluminium/epoxy interface.) There is also evidence of some line defects within the epoxy layer from Figure 4.14b. These are defects that were present immediately after manufacture.

It required 103 days of immersion before any change was detectable for this specimen, seen in Figure 4.14c, and is only a very small disbond along the unsealed flush edge. No further signs of degradation are visible from the second interface scan. The scans from this sample after a total of 410 days in water can be seen in Figure 4.14e and f. These show no sign of further degradation despite an additional 307 days in water. There is an increase in the amount of top surface pitting. In general across this specimen there has been very little sign of degradation.

4.4.2 Oblique incidence ultrasound

The oblique incidence scans for the same specimen are shown in Figure 4.15. The initial scan from this sample was performed using the older scanning system, with plane probes, as opposed to the focused ones used in subsequent scans. Figure 4.15b was performed using 10MHz focused probes with Figure 4.15c using 20MHz focused probes. Also, there are only the top interface scans shown for this specimen due to the difficulty in obtaining reliable second interface scans at oblique incidence. The major

features appear similar to those seen in the normal incidence scans, but there are significant differences in the detail. These differences are greatest for the initial scan which used plane probes, and so suffered from the effects of alignment that were discussed in chapter 2. The amplitude scale used in all three scans is the same, but it can be seen that there is a large variation in amplitude across the initial scan, compared with the later scans. This variation is hiding detail that we know to be present from the normal incidence scans. For example the voids that are clear from the normal incidence scans in Figure 4.15a and also Figure 4.15b are not clear in Figure 4.15a.

There is also the appearance of a line defect in Figure 4.15b, that cannot be seen clearly in a, which from the normal incidence scans is a defect in the epoxy layer. This highlights an effect that has been seen before in that it is more difficult to determine the defect's depth from the oblique incidence scans due to the longer wavelengths. Defects that are in the epoxy, but close to the interface may appear on the interfacial scans at oblique incidence, when from the normal incidence scans they are clearly in the epoxy. This suggests that the line defect in the epoxy that appears in both Figure 4.14b and b is not at a constant depth as only a small section of the line is apparent from the oblique incidence interfacial scan. The comparison of the normal and oblique incidence scans for this specimen also show that the poorer spatial resolution of the oblique incidence scans prevented the small edge disbond from being detected after 103 days in water, but was apparent after 156 days. (Not all scans from either the normal or oblique incidence have been presented, just those showing significant detail being shown.) The final oblique incidence scan from this specimen is shown in Figure 4.15c, which shows no signs of any further degradation from the specimen, although there is the appearance of some shadowing from top surface pitting.

4.4.3 Mechanical test results

A comparison of the failure surfaces and the second interface scan from both wet and dry PAA specimens are shown in Figure 4.16. The ultrasonic scans from these specimens show some defects, but these are comparatively few and were generally present after manufacturing the joint. As has been discussed there was very little sign of defects appearing after prolonged exposure to water. However there is an immediately obvious difference in the failure surfaces from these specimens in that the dry specimen failed almost entirely cohesively and the wet one failed almost entirely interfacially. The failure surface from the wet specimen shows the presence of

epoxy, but with the exception of a small area this is simply where the failure jumped from one interface to the other. These small areas of cohesive failure are close to the centre of the specimen.

Comparing the ultrasonic scan with the failure surface from the wet specimen it can be seen that the narrow line defects that appear within the epoxy layer are visible on the failure surface, but as apparently thin layers. The finer detail from the failure surface shows the appearance of fine lines running along the surface, Figure 4.16c, covering large areas of the specimen. They appear similar to defects that have been encountered on the two layer specimens, with the important difference that at no point was there any evidence of these lines from the ultrasonics. There is a combination of reasons for these lines not being detected ultrasonically. First, the lines are generally less than 0.5mm in width, often being considerably less than this. Secondly the geometry of the three layer specimen will make it more difficult for a gap to open between the epoxy and the aluminium in the event of a small disbond, as the combination of epoxy layer and aluminium plate is considerably stiffer than the 2mm epoxy layer as would be prevent the separation of the surfaces seen in the case of a two layer specimen. This increased stiffness would also reduce the rate at which water could travel along the defects, slowing subsequent damage.

The results of the mechanical tests are shown in Figure 4.17 along with the failure surfaces for both wet and dry PAA specimens. The fracture energy maps show that there has been a significant decrease in the toughness from the dry to the wet specimen, and that it is relatively uniformly distributed across the specimen. The small area of cohesive failure that was highlighted for the wet specimen in Figure 4.17 shows as being a small area of higher toughness in the centre of the wet specimen. There are also a few small areas of interfacial failure visible from the failure surface on the dry specimen that also appear as areas of reduced toughness on the fracture toughness map. The ultrasonic scans of these specimens show nothing that would suggest any difference in behaviour either of these specific areas of the specimens or the difference between the wet and the dry specimen, more detailed discussion of reasons for this are given in Chapter 5.

The average fracture toughness values from these two specimens show a value of 120 Jm^{-2} ($\pm$ 26 Jm^{-2}) for the dry specimen and half that for the wet specimen, 60Jm^{-2}($\pm$ 25 Jm^{-2}). To determine whether this large decrease in fracture energy was simply a function of the crack having run along the interface for some reason, an additional PAA specimen was produced and this was mechanically tested in a similar

manner to the two layer specimens. One arm of the beam was bonded to a solid base, and this produced a crack which ran predominantly along the interface. The fracture toughness for this interfacial failure in a dry three layer specimen was found to be 185 Jm^{-2}, indicating that the wet specimen had undergone genuine interfacial degradation across the majority of the specimen and that it was not simply a case of some minor defect changing the failure mode and reducing the apparent toughness.

Figure 4.18 shows the failure surface, both the macroscopic view seen in the previous figure and also that taken from an optical microscope. This shows that the line left on the surface of the sample was a thin line of epoxy, and is at the limit of what can be detected using ultrasonics, and this is without considering what might be a small difference in the impedance between the line and the surrounding epoxy. However it is clear that this line of epoxy left on the failure surface suggest that there are possible flaws or weaknesses in the epoxy layer. This is a possibility that is discussed in detail, with the results from all of the other specimens being considered, in Chapter 5.

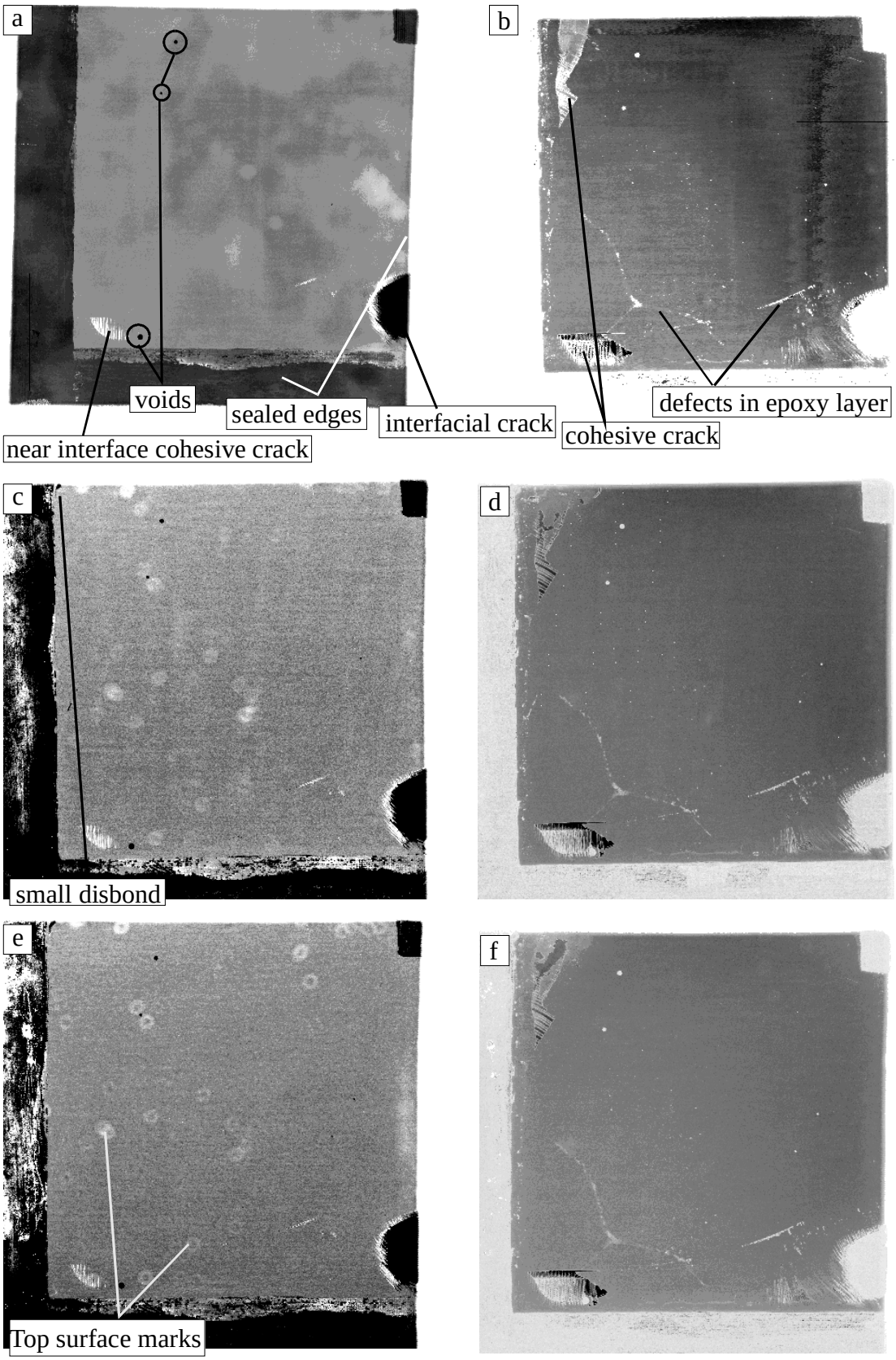

Figure 4.14 Normal incidence scans of three layer PAA specimen of (a) first interface and (b) second interface after 0 days (c) first interface and (d) second interface after 103 days and (e) first interface and (f) second interface after 410 days.

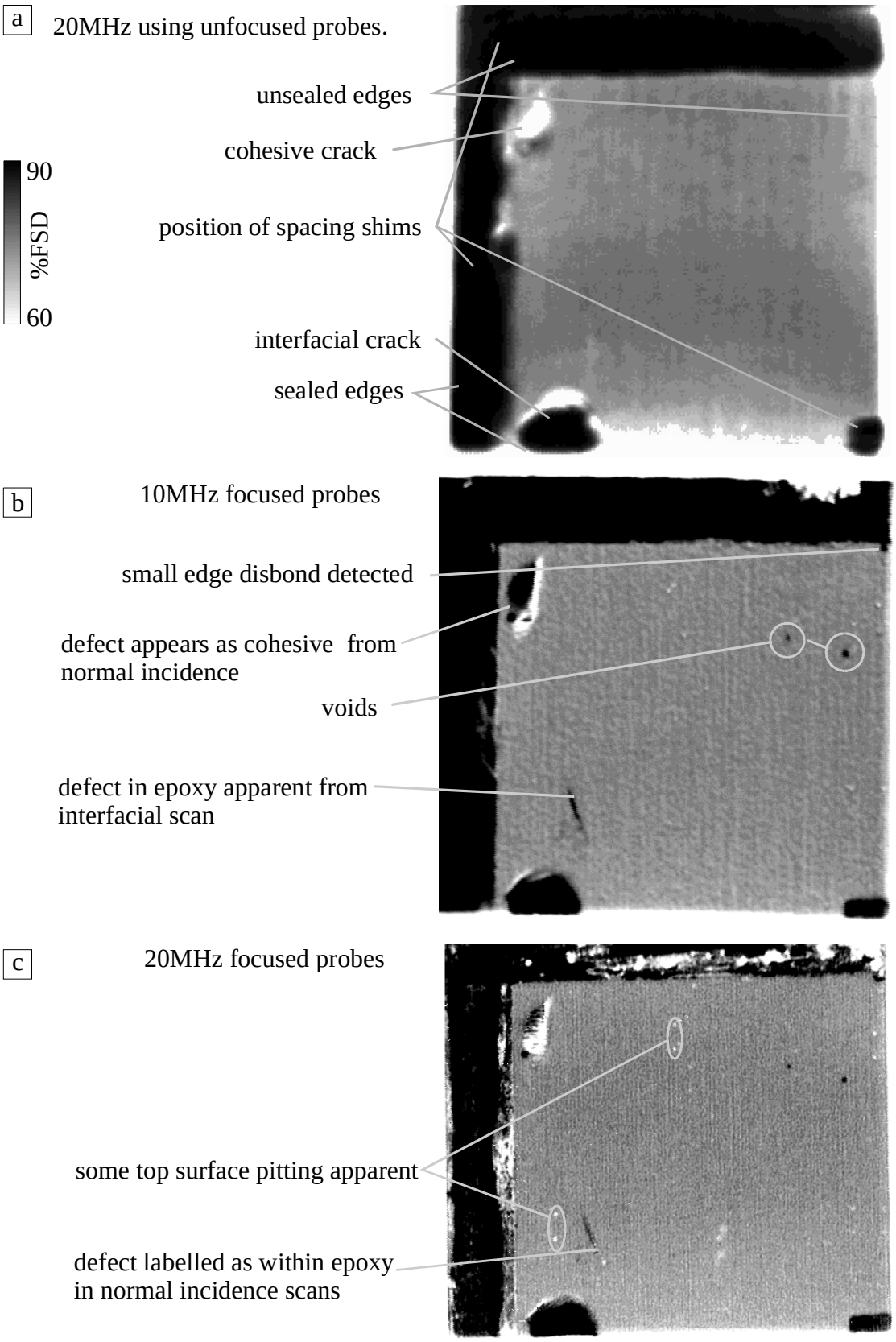

Figure 4.15 Oblique incidence scans from three layer PAA specimen after (a) 0 (b) 156 and (c) 566 days in water.

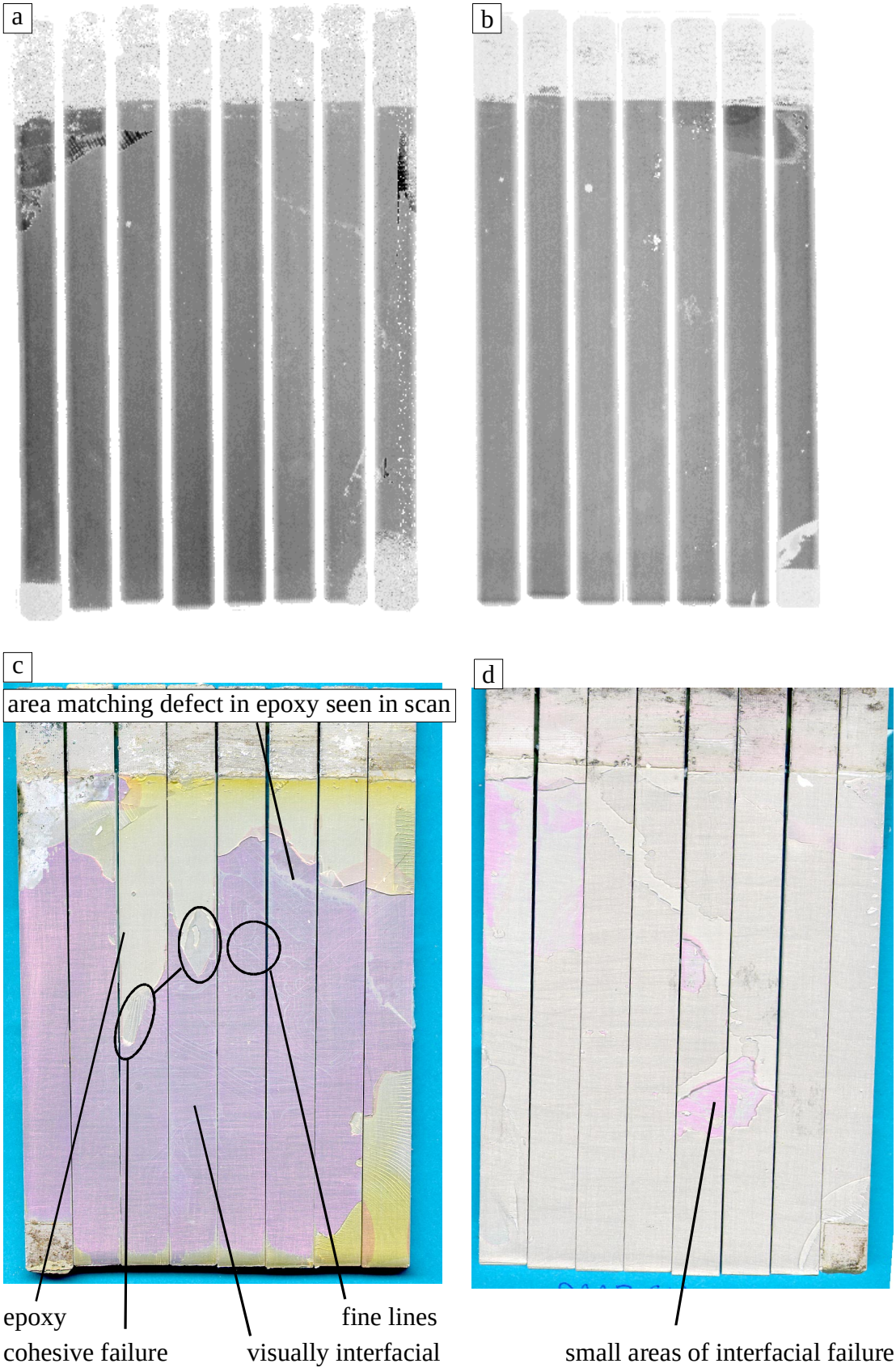

Figure 4.16 Comparison of second interface scans from (a) wet and (b) dry, three layer PAA specimens with (c) wet and (d) dry failure surfaces.

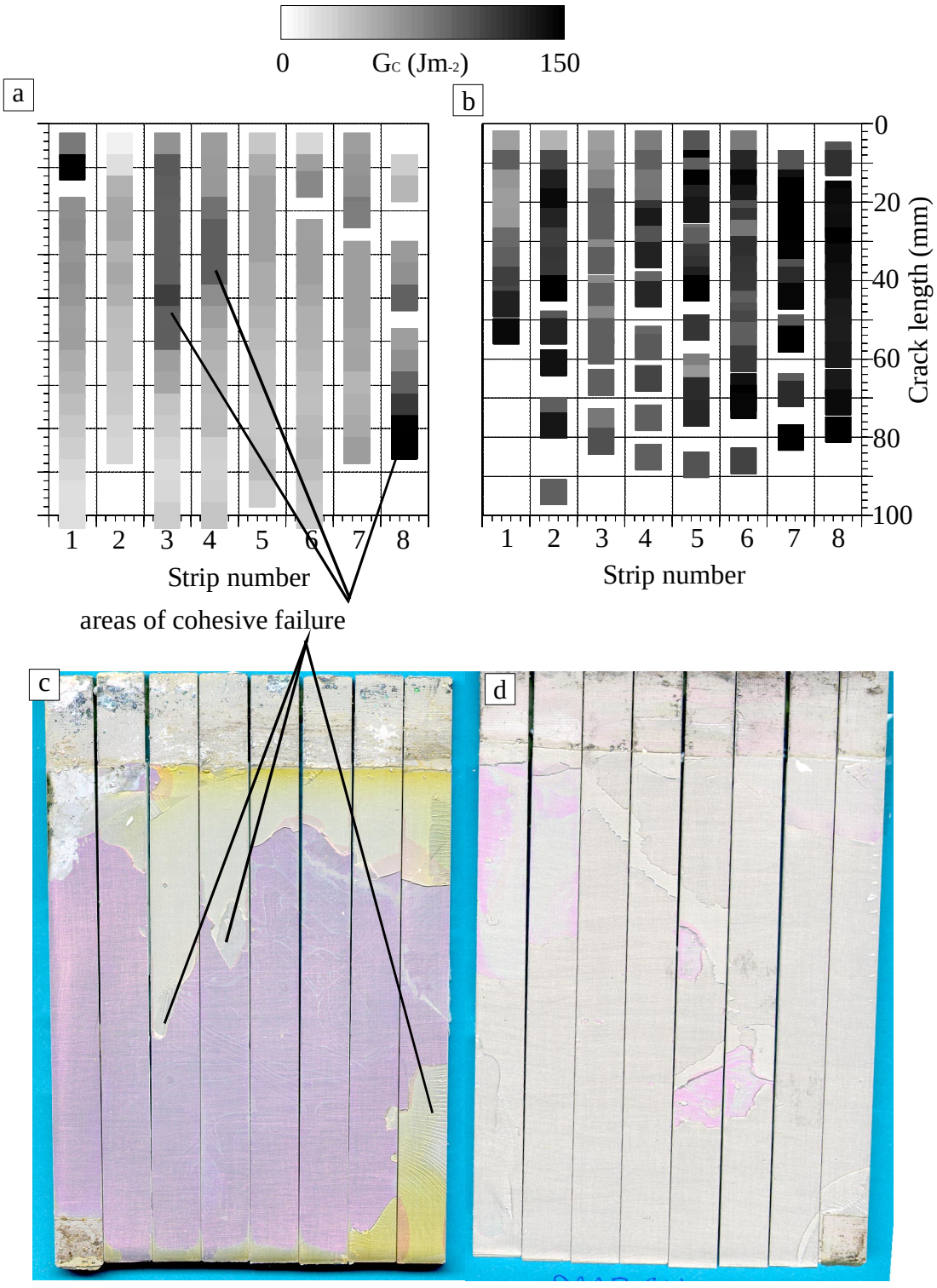

Figure 4.17 Comparison of fracture toughness maps from (a) wet and (b) dry, three layer PAA specimens with (c) wet and (d) dry failure surface.

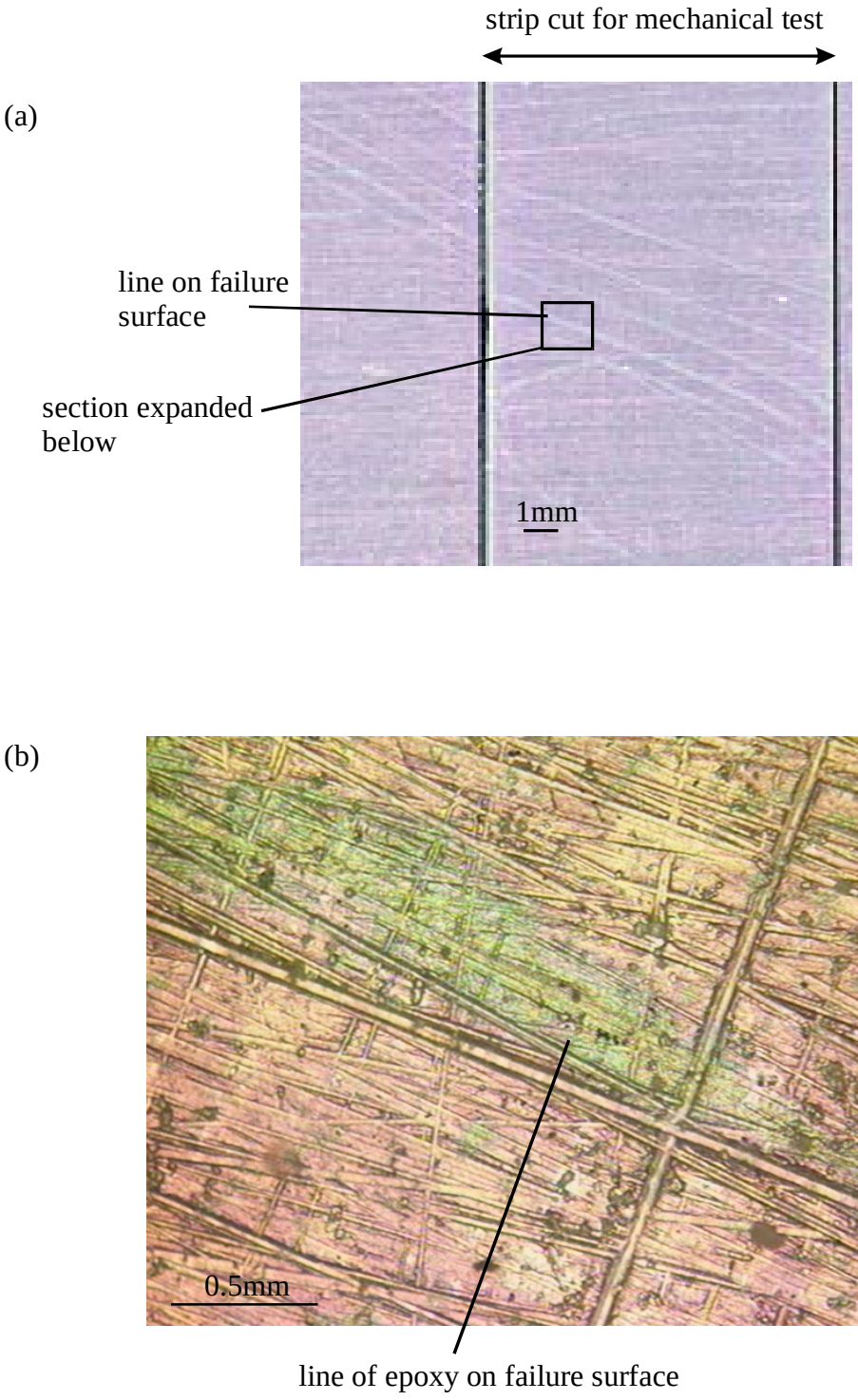

Figure 4.18 Failure surface from three-layer PAA specimen showing (a) macroscopic view and (b) optical micrograph.

4.5 Chromic Acid Anodised specimen

4.5.1 Normal incidence ultrasound

Initial normal incidence scans for a CAA specimen and after it has been exposed to water for 567 days are shown in Figure 4.19a-d. Only two scans for different exposure times are shown for this specimen, with both the first and second interface scans being shown. This is because this specimen has shown virtually no change from the initial to final scan. There is a difference in the appearance of these scans due to the change in scanning system during the lifetime of the specimen, but there has been no fundamental change in the ten scans made from this sample at intervals during the 567 days. Figure 4.19a shows the initial first interface scan from the sample. There are some interfacial cracks along the lower edge (determined as interfacial because of the increase in signal amplitude) caused by removing the spacing shims, so this edge was sealed, as was the right hand edge. The second interface scan, Figure 4.19b, shows that there is also some cohesive cracking present (determined as cohesive because there is no defect at the first interface, and no energy is propagating to the second interface). These cohesive cracks appears slightly different in Figure 4.19d due to the difference in the positioning of the gates for the old and new scanning system, but the detail is essentially the same but slightly better defined with the new system.

4.5.2 Oblique incidence ultrasound

The oblique incidence scans from this specimen are shown in Figure 4.20a-c. Being one of the earliest produced specimens the oblique incidence scans show the evolution of this technique through three stages. The initial scan was conducted using the 20MHz plane probes, and because of this suffers from poor spatial resolution, and inconsistent signal due to bowing of the plate. The second scan, after 38 days in water, Figure 4.20b, was performed using 10MHz focused probes. This shows more detail than the plane probe scan, and comparison with the normal incidence scans for this sample, Figure 4.19a-b, shows that these defects were present at joint manufacture, but were not easily identifiable using the unfocused oblique incidence technique. It can also be seen that the signal level is more consistent using the focused probes. The final scan, Figure 4.20c, was performed using 20MHz focused probes. This shows the improvement in resolution that the higher frequency has allowed, this most noticeable by the size of voids that can be identified from the 20MHz scan when compared to the

10MHz scan. Figure 4.20c also highlights the problem that scattering introduces at higher frequencies, with the increase in noise in the image. There are also several marks due to top surfaces pitting present on this scan. However there is no further information available from this scan than was seen in the normal incidence scans from this sample.

4.5.3 Mechanical Tests

Figure 4.21 shows the comparison of the fracture toughness map and failure surface for both the wet and dry CAA specimens. Perhaps the most important point to highlight from the mechanical tests is whether the sample failed interfacially or cohesively. In this case both wet and dry specimens failed in a cohesive manner. The fracture toughness maps for the wet and dry specimens show that the wet sample has a lower toughness, but as has been seen on other three-layer specimens this is most likely to be due to the extended post curing effect of being in hot water. (This was covered in more detail in 4.3.3) The spaces in the mechanical test results for the dry specimen indicate where the crack has been jumping, and these are not present in the wet sample. The average fracture toughness values for these sample were 131 Jm^{-2} ($\pm$20 Jm^{-2}) dry, and 85 Jm^{-2} ($\pm$28 Jm^{-2}) wet. These are very similar values that have already been seen for the CAE three-layer specimens.

An interesting point that can be clearly seen from the photograph of the failure surface from the wet sample is the change in colour of the epoxy layer, with the edges being more yellow than the central areas. This appears to represent the extent of water diffusion into the specimen. This has been seen on other three-layer specimens, whereas for the two-layer specimens the entire epoxy layer had discoloured. This gives a qualitative agreement with the predictions based on Fickian diffusion, see Chapter 2. The sealant that was used around the edge of these specimens was an epoxy based marine sealant that can be expected to have similar diffusion properties to the resin used in the joint. The sealant works by preventing the access of bulk water. The edge of the specimen closest to the bottom of the page was sealed and it can be seen that the yellowing of the epoxy has advanced only slightly less than on the left hand edge of the specimen.

4.5.4 Summary of results from CAA specimen

As was seen from the two-layer specimens the CAA pre-treatment has endowed the specimen with greater durability than the other pre-treatments

- Edge disbonds - there was no sign of any edge disbonds on this specimen, either from the ultrasonic scans or from the failure surfaces.

- Line defects - there were signs of a some line defects in the epoxy on this specimen, but present aftermanufacture

- Mechanical tests - the mechanical test results from these specimens showed no sign in a reduction in interfacial toughness, with both wet and dry specimens failing cohesively. The wet sample showed a slightly lower fracture energy due to the extended post-cure of being in hot water.

- XPS - there were no failure surfaces suitable for examination using XPS due to all specimens failing cohesively.

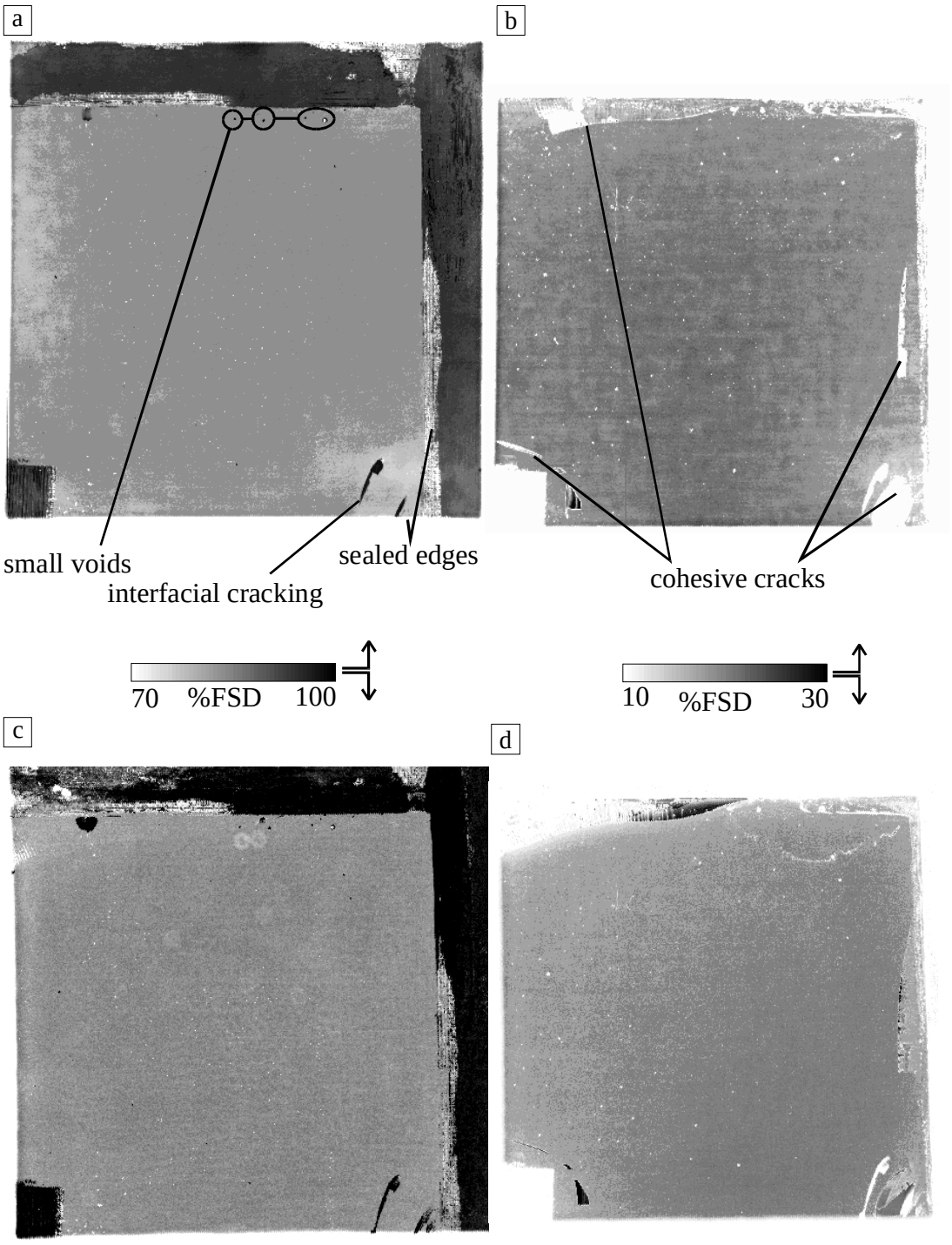

Figure 4.19 Normal incidence scans of wet three layer CAA specimen from (a) first interface (b) second interface after 0 days and (c) first interface and (d) second interface after 567 days in water.

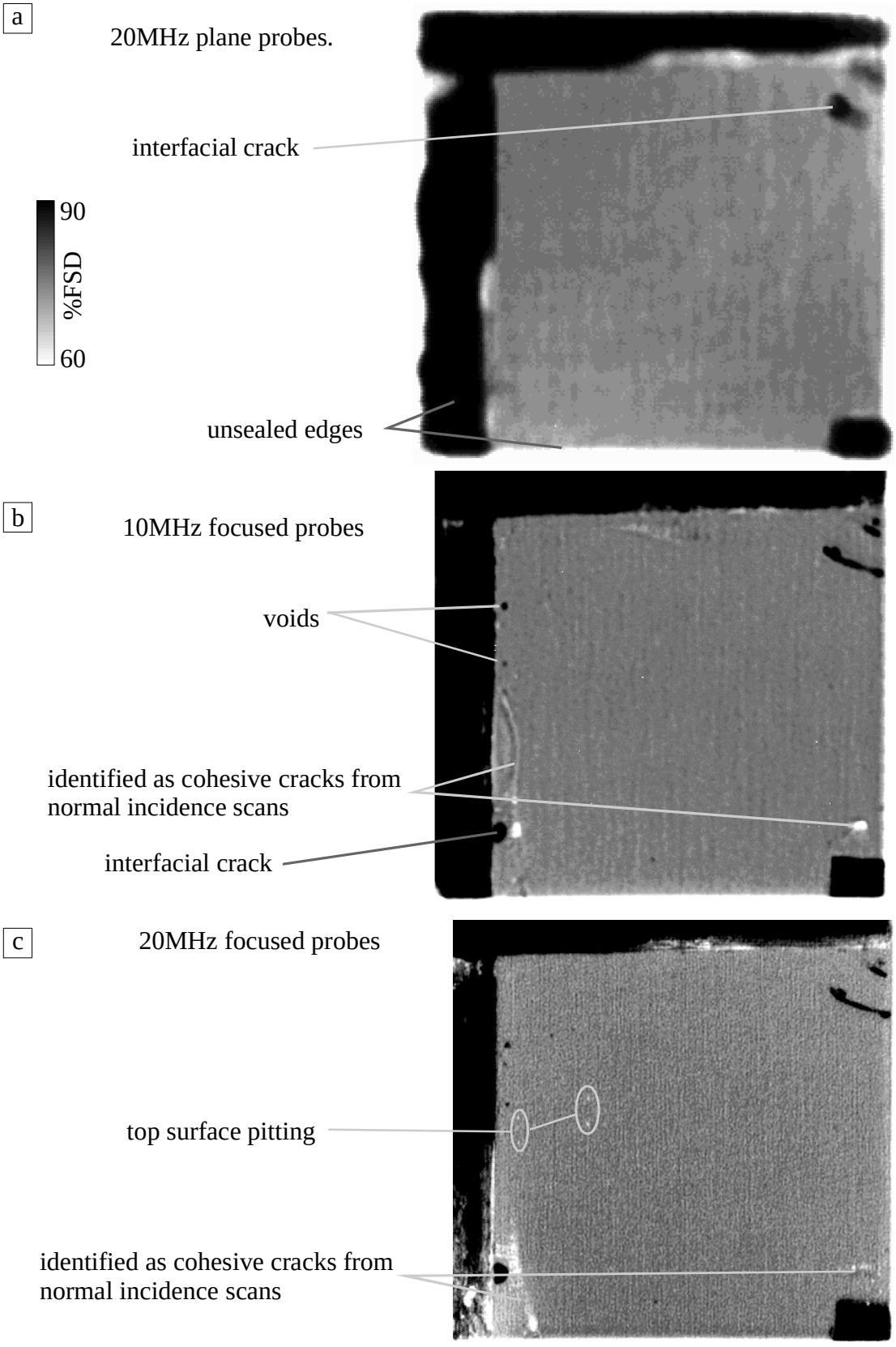

Figure 4.20 Oblique incidence scans from three layer CAA specimen after (a) 0, (b) 38 and (c) 567 days in water.

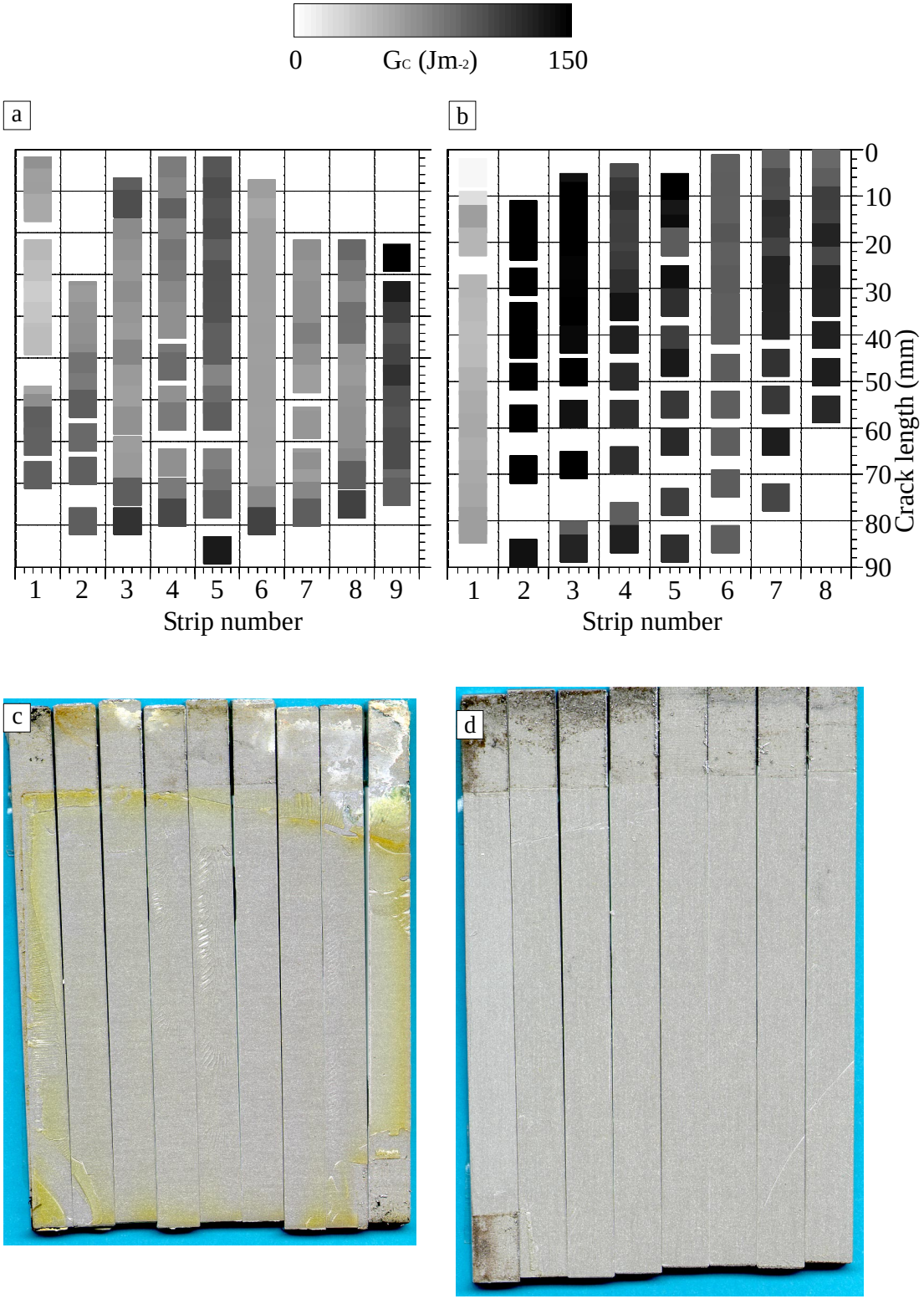

Figure 4.21 Comparison of fracture toughness maps for (a) wet and (b) dry three layer CAA specimen with (c) wet and (d) dry failure surfaces.

4.6 Brief discussion of results from three-layer specimens

4.6.1 Introduction

The following sections give a brief discussion of the results obtained from all of the three-layer specimens covering all of the pre-treatments. The comparison of the results from the two and three-layer specimens is covered in the following chapter. A summary of the results obtained from the three-layer specimens is shown in Table 4.2. There have been significant differences between these three-layer specimens and the two-layer specimen results presented in the previous chapter. These three-layer specimens are in many ways more important than the two-layer specimens in that they represent something much closer to what is likely to be found in a structural adhesive joint. The difference in geometry has had an important effect on the non-destructive methods used, but perhaps more importantly on the mechanical tests, which have

Specimen	Exposure time (days)	Disbond Area (mm^2)	"wet" locus of failure**	G_C Wet Jm^{-2}	G_C Dry Jm^{-2}
Grit Blast	251	25	Interfacial	48 (±16)	61(±18) *49(±11)
CAE	411	300	Cohesive	84(±19)	127(±37)
CAE extended dry post cure	28	0	Cohesive	-	61(±5)
PAA	566	~0	Interfacial	55(±25)	120(±26)
PAA dry+ interfacial	-	0	Interfacial	-	185(±40)
CAA	566	~0	Cohesive	95(±28)	131(±20)

Table 4.2 Summary of results from 3-layer specimens

+ *generated by forcing crack along interface in a similar manner to two-layer specimen mechanical test*

* Result for grit-blast specimen maintained dry at 50°C.

** All dry specimens failed at least 90% cohesively.

shown a clear distinction between the majority of specimens that have failed cohesively and the wet grit-blast and PAA specimens that failed interfacially. Perhaps the single most important piece of information is that the specimens that have failed interfacially have done so not only near edges, where there is evidence of water diffusion into the epoxy layer, but rather across the entire area of the specimens.

4.6.2 Results from N.D.T.

The non-destructive examination of these specimens has shown significant differences from the two-layer specimens. Whereas in the two-layer specimens we have seen small defects distributed throughout the interface region of the joint, which has given some indication of degradation, the three-layer specimens have shown no sign of this type of defect. The non-destructive examination of the three layer specimens has been restricted to ultrasonic methods, whereas in the two-layer specimens visual inspection has proved to be very useful.

The scans produced from these specimens showed that the least durable pre-treatments (grit-blast and CAE) showed the most disbonding around the unsealed edges, with the two-anodise treatments showing no edge disbonding. As was seen with the two-layer specimens it was the flush edges that were the ones to show most disbonding, with the related problems of scanning close to the specimen edges.

There were no advantages in the use of oblique incidence ultrasound compared with normal incidence. The most useful information that could be extracted from the scans involved defects that were best described using high frequency well focused scans. For example, determining whether cracks were interfacial or cohesive was easier from the normal incidence scans than the oblique, this is demonstrated by comparing Figure 4.14 and Figure 4.15, from the PAA specimen. It can also be seen that identifying voids in the epoxy layer is clear with normal incidence, for example comparing Figure 4.9 and Figure 4.10 from the CAE specimen. However at no point on any specimen were small spot disbonds in the central regions of the specimen apparent, like those seen on the two-layer specimens (most obviously the two-layer grit-blast specimen).

4.6.3 Mechanical test results

The most notable results from the mechanical tests concern the wet grit-blast and PAA specimens. There two specimens failed almost entirely interfacially, whereas every other specimen failed cohesively. The PAA specimen had a very small area in

the centre of the specimen that failed cohesively. The failure surface of both of these specimens showed signs of lines on the surface. These were similar to those seen on almost all of the two-layer specimens (the exceptions were the CAA specimen and repeat CAE specimen). Microscopic examination of the PAA specimen revealed that these lines were thin epoxy covering layers. The width of these lines would have made detection with ultrasound difficult even if these lines were complete voids in the epoxy, however it is possible that they were lines of weakness.

The XPS results from the failure surface of the grit-blast specimen (Figure 4.7) showed virtually no difference in the failure surface from the strips closest to the unsealed edge and those from the centre of the specimen. This suggests that by what ever mechanism the specimen was being degraded 252 days were sufficient for the process to have extended across the whole specimen. This is supported by the mechanical test results (Figure 4.4) which shows the fracture toughness for the specimen was uniform.

These specimens have also shown significant variation in the mechanical performance due to changes in the epoxy layer. Specimens which were maintained dry at room temperature failed in a very brittle manner whereas those that were kept at elevated temperature showed lower fracture toughness but a much less brittle failure. The best example of this can be seen from the CAE results that compare two dry specimens, one maintained at 50°C and the other at room temperature.

The diffusion of water into the wet specimens could also be seen after the mechanical tests with the appearance of yellow halo around the edges of the specimen. This also showed that the sealant did not prevent water diffusion, but was generally adequate to prevent disbonding along the edges where it was applied. There was no connection in the mechanical test results from any specimen with the diffusion of water into the joint.

4.7 Concluding remarks

Although the N.D.T. results have less detail than those seen in Chapter 3 they are none the less extremely important. The following chapter discusses the results, making links between the results from the two specimen types, allowing a more complete understanding of the mechanisms of degradation that have occurred and the

implications that these have on the non-destructive evaluation of adhesive joints subject to hostile environments.

5. Discussion of Results

5.1 Introduction

The purpose of this chapter is to draw together all the results that have been presented in the previous two chapters. The chapter is divided into five sections; the introduction; second is the section concerning the ultrasonic results, with this being divided between the normal and oblique incidence techniques followed by a comparison of the two techniques; the third section discusses the effect that varying pre-treatment has had on the performance of the specimens, again this is divided into sections for the two and three-layer specimens followed by a comparison of the two; section four deals with the mechanisms of attack, divided into sections concerning the kinetics of attack and also the actual degradation mechanisms; the fifth section is an overview discussing the role of ultrasonic techniques in the detection of degradation of adhesive joints.

5.2 Ultrasonics

5.2.1 Introduction

Chapter 3 contained all of the results that were obtained from the two-layer specimens, with the results from the three-layer specimens being presented in Chapter 4. The following sections discuss the results obtained using the normal incidence technique from both the two and three-layer specimens, and then the results obtained using the oblique incidence technique, followed by a comparison of the results obtained here and those published by others.

5.2.2 Normal incidence

Normal incidence ultrasound is the most common application of ultrasound in the inspection of structures, including bonded joints, and is used because it is relatively simple and well understood. The only improvement that the work presented

here was likely to show was due to the higher frequency and hence smaller focal spot that was used in comparison with that generally used for inspection purposes, coupled with the inspection being specifically focused on the interface and not being used as a global joint inspection. Defects that were expected to be detectable were disbonds and voids. Nagy [20] also suggests that kissing bonds are more likely to be detected when using highly focused transducers.

Disbonds and voids were seen and easily identified using the 50MHz normal incidence scans. Disbonds initiating at the edges of the specimen were seen on every two-layer specimen; examples of this type of disbond are highlighted in Figure 3.1, Figure 3.11, Figure 3.19 and Figure 3.29 which cover all of the pre-treatments from the two-layer specimens. Voids were only seen on the three-layer specimens, with examples of this being seen in Figure 4.1, Figure 4.8, Figure 4.14 and Figure 4.20 which show the normal incidence scans from the three-layer specimens. Only the grit-blast and CAE showed edge disbonds amongst the three-layer specimens (Figure 4.1 and Figure 4.8).

The normal incidence technique showed sufficient resolution to discriminate between interfacial and cohesive failures to within a few tens of microns. A crack in the epoxy layer may appear the same from an ultrasonic scan as an interfacial failure if the crack is close to the interface. Shorter wavelengths give more separation in time between cracks at the interface and cracks in the epoxy. The clearest indication of this was from the three-layer PAA specimen, Figure 4.14, but the reason for this is best explained in section 3.3.1, which discusses the appearance of thin layers of spew adhesive. The most prevalent of the defects detected across all of the specimens were disbonds extending from the unsealed (usually flush) edge. These were easily detected, with the only significant shortcoming being the inability to examine close to the edge of the specimen. In some specimens this resulted in a significant amount of disbonding not being detected, most particular the wet three-layer CAE specimen. This can be seen by comparing the scans seen in Figure 4.11 and the failure surface of the wet specimen shown Figure 4.12. This shows that the edge of the right most strip was disbonded across almost half of its width but only the furthest encroaching disbond was detected from the scans.

However what was not expected was the appearance of the very small disbonds that appeared in many of the two-layer specimens (these defects along with the narrow line defects, whose detection appears to be largely determined by spatial resolution have been termed micro-defects). The detection of these was largely a

question of resolution. Small spots of the order of 0.5mm were detectable and these would almost certainly be missed using a conventional scanning system operating at typical frequencies of 10MHz. However in many cases there was no apparent reason for these spots occurring as the joint in adjacent areas appeared unchanged from joint manufacture. The assumption is that the small spots were corrosion sites, and as such water was expected to be present, however, reflection coefficient measurements on such small targets are not very reliable so the presence of water could not be confirmed. Indeed some of these small spots can be seen to alter their appearance in the scans as time progresses, changing from areas of lower impedance to scatterers, this can be seen from Figure 3.19 and Figure 3.20 which show scans from a wet two-layer PAA specimen. A reflection coefficient measurement allowing for an unknown geometry would be required if an accurate assessment were to be made of the composition of these small spots.

It was not possible to detect the paths by which water was accessing the small spot corrosion sites. In the case of the two-layer specimens this could be via diffusion through the epoxy layer. The ultrasonic detection of changes in the epoxy properties due to water uptake in the epoxy was discussed in detail by Pialucha [26] for this adhesive, and it was found that the change in properties was virtually undetectable using ultrasound. This is not the case for all adhesives. Some adhesives change their properties sufficiently to allow easy identification of water uptake. However in the case of the two-layer grit-blast specimen micro-defects were detected before any significant level of water would have reached the interface via diffusion through the epoxy. The water concentration at the interface after 28 days in water would only be a few percent of saturation.

However it is possible that water was travelling along the interface of the joints (particularly in the case of the three-layer PAA and grit-blast specimens, discussed in sections 4.4 and 4.2 respectively, both of which failed almost entirely interfacially). There have been no signs of this using normal incidence ultrasound. The other possibility, discussed in section 5.4.2.4, is that water could travel in flaws in the epoxy layer. The evidence for this type of flaw comes from the appearance of lines of epoxy on the failure surface of several specimens. The following paragraph considers the detection of this type defect. The lines left on the surface of the three-layer PAA specimen (Figure 4.18), thought to be due to flaws in the epoxy, are less than 0.5mm wide. This is difficult enough to detect purely from a size perspective, but if we consider a thin water channel in epoxy the impedance difference between it and the surrounding epoxy would be extremely small, making it virtually undetectable. The

normal incidence reflection coefficient at 50MHz for a 1μm thick water layer between semi-infinite layers of epoxy is 23%, if the layer is only 0.1μm thick this is reduced to 2.4%. The increase in reflection coefficient from a 1μm water layer between layers of aluminium and epoxy compared to an aluminium/epoxy interface is 8.5%, and this reduces to 0.12% if the water layer is only 0.1μm thick. Layers of this thickness are more than sufficient for the transport of bulk water. (Leidheiser [33] suggests that 50 molecules of water is sufficient to be considered as aqueous phase water.)

In general the normal incidence ultrasound scans have performed very much as expected. The results have also placed stronger emphasis on maximising the spatial resolution of the technique. There have been detectable signs of joint degradation in the case of the two-layer specimens in the form of micro-defects and edge disbonding has been detected from both specimen types. The only areas that have been seen to have a total loss of adhesion (disbonds) have all been detected using the normal incidence technique.

5.2.3 Oblique incidence

The predictive modelling that preceded the use of this technique (see Chapter 2), both by the group at Imperial College [44] [26] and others [52, 67] [50], suggested a considerable improvement in the sensitivity of the oblique incidence technique to the properties of interface layers in adhesive joints when compared to the normal incidence method. This has been discussed in detail in Chapter 2. However the question remained whether it was sensitive enough to detect any change in a real joint exposed to a degrading environment, prior to disbonding. One of the assumptions that was made about the form that degradation would take is that it would proceed in a relatively uniform manner if water were to gain access in a uniform manner. This was hoped to be the case when using the two-layer specimen geometry. The results have shown that it is questionable whether this occurs. There is far more evidence that degradation occurs when water enters the joint from unsealed edges and via flaw lines in the epoxy layer. There is little evidence of degradation of the interface due to water diffusion through the epoxy layer alone. These results have put much greater emphasis on the spatial resolution of the technique, and ideally we would like to be able to combine the best spatial resolution with good sensitivity to interlayer properties and low sensitivity to misalignment. However the oblique incidence technique is never going to be able to achieve the spatial resolution of the normal incidence method.

To improve the application of the oblique incidence technique to the scanning of the two specimen types it was found that the use of focused probes gave a large improvement in the consistency of the results obtained. The results from the three-layer PAA and CAA specimens demonstrate this (Figure 4.15 and Figure 4.20 respectively), where both the unfocused and focused probes have been used. It was seen from these figures, and also from section 2.3.3 that the use of focused probes gave far less sensitivity to curvature of the specimens, allowing defects to be detected far more easily. These figures also show the effect of increasing the frequency of the scans from 10 to 20 MHz. The 20 MHz scans show improved spatial resolution. However they also show coherent material noise to be one of the limits that has been reached with this form of oblique incidence scanning as the grain of the aluminium plate becomes more apparent at higher frequency.

The defects that were seen using oblique incidence were fundamentally the same as those seen using normal incidence. Large disbonds initiating at the edges of the specimens were easily detected, this is clearly demonstrated for all of the two-layer specimens (Figure 3.3, Figure 3.13, Figure 3.21 and Figure 3.31 show the oblique incidence scans from the two-layer specimens). The lower frequency of the oblique incidence scans resulted in less loss of signal due to surface roughness, including scattering from both top and bottom surfaces of the top adherend. The difference in scattering from roughening at the bondline is small, but can be seen from Figure 3.15, which shows a comparison of the results from both normal and oblique incidence techniques for the two-layer CAE specimen. This most easily seen by comparing the appearance of the exposed aluminium on the unsealed recessed edge, where the roughening caused by corrosion has caused a total loss of signal using normal incidence but there is still a clear signal using oblique incidence. The appearance of top surface pitting is more distinct compared to pits at the adhesive interface. A pair of marks is seen from the oblique incidence scan, whereas the normal incidence scan shows a single larger mark. The best example of this can be seen from Figure 3.33, which shows the normal and oblique incidence scans from the two-layer CAA specimen. This feature was seen on most of the specimens. This is a useful artefact of the oblique incidence scan, allowing rapid discrimination of features seen from the scans.

The more interesting features seen from the normal incidence scans were the “micro-defects”, these being the small spots and lines seen predominantly through the epoxy layer of the two-layer specimens. As was seen with the normal incidence results, detection of these appeared to be resolution limited. Due to this the oblique

incidence scans would not show as many of the small defects as the normal incidence scans. This is best illustrated from the specimen that had the most micro-defects, the two-layer grit-blast specimen. Figure 3.4 in chapter 3 shows the normal and oblique incidence scans from this specimen. In this case there are still signs of degradation from the oblique incidence scan for large areas of this specimen, but lacking the detail of the normal incidence scan (and to an even greater extent the visual appraisal). However the absence of detail is more important in cases where the extent of the micro-defects is much less. This can be seen from the scans of the two-layer PAA specimen (Figure 3.23), where the micro-defects are fewer and more isolated. None of the oblique incidence scans were able to detect the presence of any line defects.

If we consider the hypothesis that water gained access to the central portions of the specimens (particularly the three-layer grit-blast and PAA specimens) by travelling through flaws in the epoxy layer, then it is important to know if we could expect to detect this mechanism of water ingress using oblique incidence. The evidence that we have for this mechanism is the narrow lines of epoxy remaining on the failure surface after the mechanical tests and also the lines that have been observed from some of the two-layer specimens. This suggests that the flaws in the epoxy layer are generally narrow, frequently less than 0.5mm. This immediately makes them difficult to detect using oblique incidence as they will occupy a small percentage of the focal zone of the probes. With little information about the form that these epoxy layer flaws might take it is difficult to be quantitative about the effect they will have on the obliquely incident ultrasound. However it is clear that they have not been detected. Further discussions of the line defects is shown in section 5.4.2.4.

It has also been seen that the minimum detectable variation that could reliably detected using the oblique incidence technique is limited by the coherent noise generated by the grain structure of the aluminium. The maximum frequency that could be used would increase for a thinner adherend, with typical aircraft structures often being less than 2mm thick; however this would require increasingly accurate alignment which becomes difficult if we consider that many of the structures of interest are not likely to be flat. This would also be a problem using normal incidence, and to take advantage of higher resolutions would require a mechanical system capable of high resolution indexing, and this would produce huge amounts of data to be analysed and stored when considering an aircraft structure.

5.2.4 Conclusions and comparisons with published results

The simplest conclusion that can be drawn from the results presented in this thesis is that the normal incidence technique has been shown to be better than oblique incidence for the inspection of adhesive joints for the detection of degradation. The reason for this is the superior resolution that the normal incidence technique offers over oblique incidence, coupled with the simpler experimental arrangements and excellent repeatability. The importance of maximising the resolution of the scans is due to the appearance of what have been termed micro-defects, these being small spots and lines at or near the interface of the joints, with dimensions frequently less than 1 mm. Moidu and Sinclair [68] have shown the formation of micro-defects during the degradation of a two part epoxy adhesive when exposed to a water at 67° C, with there defects being similar to the defects seen in many of the specimens used for this work. Moidu and Sinclair used a very similar two-layer specimen design and reported the appearance of micro-defects which were identified as small debonds between 30-150 μm in size. Leidheiser [33] reports a similar phenomenon for a polymer glass interface, with water collecting in discrete circular regions. The normal incidence scans also have been more versatile in scanning the three-layer specimens because the shorter pulse length has allowed separation of reflections from the front and back of the adhesive layer, allowing better characterisation of detected defects.

The oblique incidence technique was investigated because many of the models that were used to predict the response of the interface of adhesive joints showed that at oblique incidence there was greater possibility of detecting weak bonds. This was particularly the case if a weak bond was modelled as a thin layer with fluid-like properties. The models used generally considered the weak layer to be infinite in the plane of the joint. However the results that have been presented in this thesis have shown that the changes that are occurring in joints as they degrade have been dominated by effects which are spatially discrete. This can include the edge disbonds which expand towards the central regions of the joint, as well as the appearance of small spots. This is particularly relevant when results that have been obtained from a point measurement using a large diameter probe, where the area of the joint being interrogated may include some edge disbond and other smaller defects. The importance of detecting and accurately measuring the extent of edge disbonds should not be underestimated, as it is the edges of the joint that carry the greatest stress if it is loaded [69].

The use of a spring model has been shown to give good agreement with experimental results for the reflection of ultrasound from partially contacting surfaces [70] [71]. Tattersall [45] modelled the interface of an adhesive joint as a spring, with the stiffness of the spring being related to the state of the bond. An infinitely stiff spring was a perfect bond, and a zero stiffness spring was a complete debond. His experimental technique involved a transmitting and receiving transducer attached to an aluminium test block against which bonds were made with varying preparations. He then attempted to relate bond strength to the ultrasonic response of the interface. He found interpretation of the results difficult due to a number of factors, amongst these being flaws in the bondline that would lead to failures at lower loads, varying degrees of contact between the adhesive and aluminium due to gaseous contamination of the interface and also that the failures invariably started at the edges of the specimen which were outside the area interrogated by the probe. These are problems which are in many ways answered through the use of high resolution scanning, where edge debonds and small scale contamination of disbonds can be characterised. Similar modelling of bonds was used by Pilarski [49], who reported a correlation between the reflection coefficient and the mechanical strength of the bonds. Again the experimental method used a fixed single probe to interrogate the bond.

Much of the work using oblique incidence has concentrated on measuring the properties of the interface layers of adhesive joints. With the durability of adhesive bonds to metals being so dependent on good surface preparation (see Chapter 1), measurement of this interface region has been considered as important in assessing joint performance. Rokhlin [22] and Pialucha [72] have both modelled the interface as a thin layer. With particular application to the bonding of aluminium, the measurement of aluminium oxide properties were also performed by Rokhlin using obliquely incident ultrasound [58]. However the work on measuring properties of oxide layers has invariably been done using artificially thick oxide layers, or layers to which there is free access without the need to measure through an adherend. The problem with the pre-treatments used in the preparation of adhesive bonds is that the oxide layers are at most a few microns thick, 3.5 μm for a CAA oxide, with the CAE oxide being only 40 nm thick. This makes detection of these layers almost impossible, and with the possibility that only a small percentage of the oxide layer needs to degrade for the bond to fail, the probability of detection is even smaller. A direct measurement of varying properties of the oxide layer is considered by the author to be impossible for the oxide layers used in the preparation of aluminium bonds, given the limitations of adherend and oxide thickness.

However although direct measurement of oxide properties is not considered possible, this does not detract from the possible benefits of using oblique incidence. Rose et al. [53] found that 20MHz oblique incidence scanning was able to detect areas of weak bond that normal incidence scans could not. One major difference between that work and the results shown in this thesis is that simulated defects were used. The resolutions of the scans obtained by Rose et al was poor in comparison with the results shown in Chapters 3 and 4. This leaves the possibility that areas with large numbers of small spot disbonds similar to those seen most notably in the two-layer grit-blast specimen (Figure 3.4) may have been present, but not seen directly due to the lower resolution.

5.3 Effects of Pre-treatments

5.3.1 Introduction

As was discussed in Chapter 1, the different pre-treatments endow the specimens with a range of durabilities. The following section is divided into two major parts where the results from the two and three-layer specimens are discussed in turn. Each of these is then sub-divided by pre-treatment. The effect of the different pre-treatments can be gauged by several parameters; the extent of edge disbonding detected ultrasonically, (or visually for the two-layer specimens) and measured from the failure surface; the appearance of small spots and lines; and the fracture energy measured from the mechanical tests.

5.3.2 Two-layer Specimens

5.3.2.1 Grit-blast

The grit-blast specimens were in many ways used as a reference as they were expected to be the least durable of all of the specimens [24]. The most obvious change seen on specimens with this pre-treatment after exposure to a hot-wet environment was the growth of corrosion driven disbonds. Corrosion was seen as the driving force behind these debonds purely from the amount of corrosion product that could be seen under the epoxy layer. This was accompanied by rapid corrosion of the exposed aluminium edges. The rate at which the disbonds progressed and the appearance of corrosion pits and surface roughening can be seen from Figure 3.1. This shows that after only 27 days in water there was the development of edge disbonding and substantial corrosion of the exposed aluminium. This figure also shows the other

major feature seen on these specimens, the appearance of small spot disbonds. Figure 3.2 shows that there are also line defects that could be detected both visually and ultrasonically on this specimen, with the visual assessment showing more detail than either form of ultrasound scan. After 117 days most of the small defects that were present on the final scan had been detected, but the disbonds can be seen to grow in a relatively uniform manner.

A repeat grit-blast specimen was also produced and this showed similar results to the first specimen. Both showed the appearance of micro-defects and substantial edge disbonds. The mechanical tests of both showed a large loss in toughness compared to dry grit-blast specimens. The results from these specimens are summarised in Table 3.1, page 132. The XPS analysis from the adherend side of the failure surfaces of these specimens showed little difference between the wet and dry specimens but in all cases a significant amount of aluminium was present (between 8% and 16%) suggesting that the failure was at or very close to the interface.

5.3.2.2 CAE

As with the grit-blast specimen, two wet CAE specimens were produced. The first of these showed rapid growth of edge disbonds, and the appearance of many micro-defects, shown in Figure 3.11. The rate of growth of the edge disbonds was higher than the grit-blast specimen, but the number and extent of micro-defects that appeared was smaller. This specimen was not mechanically tested as it self-destructed, with the epoxy layer peeling away from the aluminium. This suggests that the interface of this specimen was poor. The second CAE specimen was considerably different showing a much slower rate of edge disbonding (3.7 mm^2/day). However this specimen showed no micro-defects and the mechanical tests showed excellent retention of toughness, 99(±17) Jm^{-2} wet and 103(±78) Jm^{-2} dry. The results from both sets of wet and dry CAE specimens are shown in Table 3.1, page 132. These two CAE specimens make a particularly strong connection between the appearance of micro-defects and loss of toughness. More detailed discussion of this is included in the following section concerning mechanisms of attack. The XPS analysis of the adherend side of the failure surface from the second wet CAE surface when compared to the grit-blast specimen (Figure 3.18) showed more carbon and less aluminium and oxygen on the adherend side of the failure, suggesting a thin (or thinner) epoxy layer being present on the surface.

5.3.2.3 PAA

The results shown in Table 3.1, page 132, show that the PAA specimen had an edge disbond rate half that of the first grit-blast specimen. The progression of these disbonds can be seen in Figure 3.19 and Figure 3.20. These also show that the number of micro-defects appearing on this specimen were considerably less than the seen on the grit-blast specimen. However there were at least twelve identifiable defects seen in Figure 3.23, and the appearance of lines at the interface of the specimen, best seen from Figure 3.24, which shows the failure surface of the specimen. The mechanical tests from the PAA specimens show a substantial loss of toughness from 55(±17) Jm^{-2} dry to 30(±7) Jm^{-2} wet. The XPS analysis of the failure surfaces from the PAA specimens, Figure 3.26, showed that there was a trend for the failure to be closer to the adherend the weaker the joint. However it was not possible to say whether the failure had occurred at the epoxy/oxide interface or in the oxide.

5.3.2.4 CAA

The CAA specimen was the one to show the least number of defects, the edge disbond rate was the lowest at 2.2 mm^2/day, and showed no micro-defects (Figure 3.33). This was reflected in the mechanical performance with the wet specimen showing an increase in average toughness (Figure 3.35). The XPS results from the CAA specimens (Figure 3.36) showed little difference in the failure between the dry specimen and sections taken from the most and least tough sections of the wet sample. However the strip to show a reduction in toughness from the mechanical test was the only one to show any traces of sodium, calcium and chlorine, albeit very small quantities of each. The relevance of this is discussed in more detail in the following section regarding mechanisms of degradation.

5.3.3 Comparison of pre-treatments based on two-layer specimen results

The results from the specimens showed large variations in performance due to the different pre-treatments as was expected. Three factors that can be used to grade the performance of the specimens; the edge disbond rate, the appearance of micro-defects and residual toughness, largely agree with each other for the rank that each implies about the durability of the specimens. In all cases the CAA specimen is the most durable. The characteristic of this pre-treatment over the others is the thickness of the oxide layer and the greater corrosion protection that it offers [24].

5.3.3.1 Edge Disbonds

Disbonds growing from the unsealed edges of specimens were the largest of the defects seen in the specimens. The growth of the defects can be related to two parameters. Firstly corrosion must be initiated and the swelling of the corrosion products will tend to drive the crack along the interface. For the disbond to expand, the bonds at the interface must be ruptured. The pre-treatments that offered the least corrosion protection, grit-blast and CAE, can be seen to have edge disbonds starting from an early stage (Figure 3.1 and Figure 3.11 for grit-blast and CAE respectively), 27 days for the grit-blast and 32 days for the CAE specimen. The poor corrosion protection of these pre-treatments can be seen by how quickly the exposed edges of the specimen corrode. The CAA and PAA specimens take considerably longer for disbonds to develop, 64 and 237 days respectively (the CAA specimen is not directly comparable as the edges of the specimen were machined, as described in section 2.2.3, page 39), whereas the PAA specimen was not machined. However despite the longer time to initiate the disbond, the PAA specimen still had a faster disbond rate overall compared with the CAA specimen, see Table 5.1.

Specimen	Exposure time (days)	Disbond Area (mm^2)	Time to initiate disbond (days)	Mean rate (mm^2/day)	Mean G_C wet Jm^{-2} (σ)
Grit Blast	223	1464	27	6.6	42(±24)
CAE	194	1958	32	10.1	-
PAA	393	1274	237	3. 2	30(±7)
CAA	465	1013	64	2.2	98(±31)
Grit Blast(ii)	145	700	na	4.8	28 (±7)
CAE repeat	185	685	na	3.7	99(±17)

Table 5.1 Summary of edge disbond results from two-layer specimens.

The rate of disbonding can then be related to the toughness of the bond remaining. This may appear inaccurate, particularly for the PAA specimen, but if we subtract the time for initiation from the overall exposure time of the disbond the disbond rate increases to around $8mm^2$/day, making it faster than the grit-blast specimen. The rank of disbond rates then agrees with the rank of the toughness of the remaining bond. This is obviously an over-simplification but the trend of the results shows that the disbond rate can be related to the toughness of the joint. The

comparison of the disbond rate (adjusted for time to initiate the disbond) compared to the mean fracture toughness is shown in Figure 5.1. This shows that the specimens with the lowest mean adhesive fracture toughness were the ones with the highest disbond rate. These results can be considered as showing variations solely due to the variation in pre-treatments as factors such as diffusion of water through the epoxy layer would have been the same for all of these specimens. The kinetics of water in these joints are discussed in section 5.4. The toughness of the bond in the CAA specimen was high enough to force the crack to run through the epoxy in some areas as opposed to along the interface, see Figure 3.33.

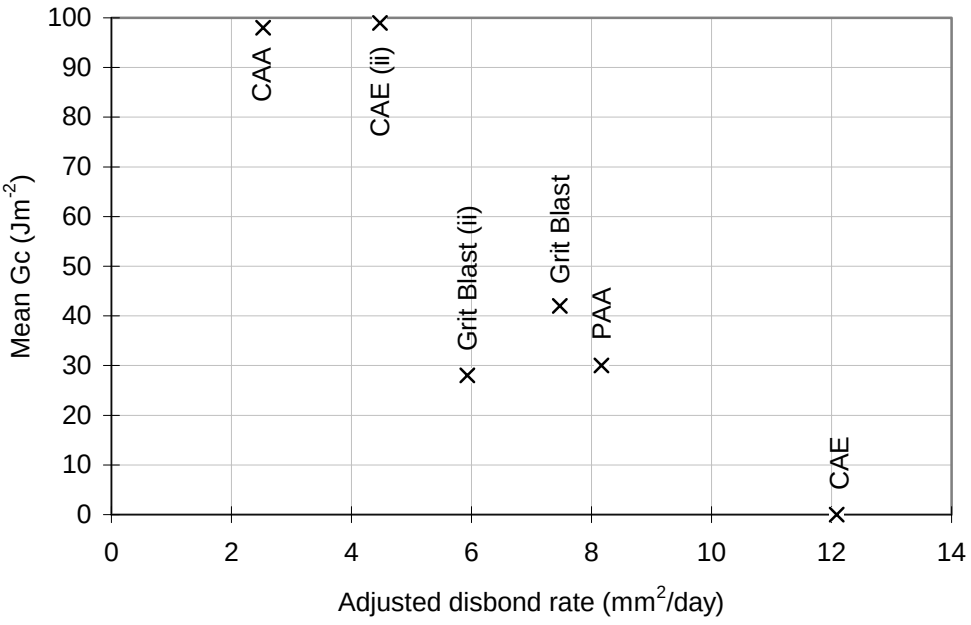

Figure 5.1 Comparison of disbond rate and fracture toughness.

The performance of the PAA appears worse than may have been expected, Brewis states that the usual order of durability is grit-blast < CAE < CAA < PAA, however in the case of these specimens the CAA has clearly outperformed the PAA. The major difference between the CAA and PAA oxide layers is that the CAA oxide is thicker and denser. The PAA oxide, having a more open structure, is more likely to allow water penetration along the interface of the joint if the pores are not filled by adhesive. Davis and Venables [31] show results where an epoxy based primer enters the pores of the oxide filling them to the bottom. They attribute the good durability of the PAA oxide to the interlocking of adhesive/primer with the pores. However if this does not occur this may leave the oxide more susceptible to environmental attack.

Indeed the XPS results suggest that degradation of the oxide may have occurred as the mechanical test of the wet PAA specimen (Figure 3.25) show that the strips closest to the unsealed edge are the ones to suffer greatest loss of toughness. The XPS results from both the wet and dry PAA specimen (Figure 3.26) show that the greater the toughness loss, the closer to the failure to the aluminium. This could easily be a failure at the epoxy/oxide interface but the XPS analysis was not performed on the epoxy side of the failure to check for the presence of aluminium oxide, making this difficult to prove. Brewis on the other hand attributes the good durability of the PAA treatment to the greater resistance of the oxide to hydration compared to other oxides. However the results shown here suggest that this has not been sufficient, and appears to have been overtaken by the rate at which water has penetrated along the interface. (This will be discussed further, both after discussion of the three-layer specimen results and also in the section about mechanisms of attack.)

Brewis also reports more scatter in durability test results from joints using CAE pre-treatment compared with PAA treatment. This may explain the large difference in the results from the two set of CAE specimens, see Table 3.1, page 132. However an important difference between these two specimens was the period in water between inspections. The first specimen was inspected at shorter time intervals than the second, and a simple explanation could be that the cyclic nature of the exposure of the first specimen compared with the second resulted in faster corrosion. With corrosion being the driving factor behind the disbonds this may explain much of the difference between the specimens. Similar results were found between the first and second grit-blast specimens, with the rate of disbond growth being slower for the second specimen which was inspected less frequently.

5.3.3.2 Micro-defects

The appearance of what have been termed micro-defects, small spots and lines distributed throughout the area of the specimen, was one of the reasons for the normal incidence technique being judged as better than the oblique incidence technique. However we need to determine the significance of the micro-defects. The simplest answer to this comes when we compare the appearance of micro-defects with the toughness of the specimen. This comparison is shown in Table 5.2. The connection is clear, in that the specimens that have micro-defects (grit-blast specimens, first CAE specimen and PAA specimens) have experienced a loss in toughness, and those that have not lost significant toughness have not had any micro-defects (CAA and second CAE specimen). However the degree of toughness loss does not correlate directly

with the number of micro-defects. The PAA specimen did not have as many micro-defects as the grit-blast specimen but the toughness loss was greater. It appears that the micro-defects can only be considered as signs of degradation in the joint, but are not the only damage occurring.

Specimen	Exposure time (days)	Micro defects	Mean G_C wet Jm^{-2} (σ)	Mean G_C dry Jm^{-2} (σ)
Grit Blast	223	V. many	42(±24)	55(±12)
CAE	194	Many	-	-
PAA	393	Average	30(±7)	55(±17)
CAA	465	None	98(±31)	78(±18)
Grit Blast (ii)	145	Many	28 (±7)	61(±8)
CAE repeat	185	V. few	99(±17)	103(±78)*

Table 5.2 Comparison of micro-defects and mechanical test results.

* high σ due to erratic crack growth jumping between epoxy and interface.

The other important observation concerning the micro-defects is how rapidly they have appeared in the specimens. The grit-blast specimen, which showed the most micro-defects, showed detectable features after just 27 days (Figure 3.1), with these being at least 10 mm into the specimen. The first CAE specimen showed micro-defects more than 20 mm into the specimen after 32 days in water (Figure 3.11). The PAA specimen had a few micro-defects detected after 63 days (Figure 3.19) but these were close to the edges of the specimen; it required in excess of 100 days to show any defects more than 10 mm into the specimen. This suggests that the different pre-treatments affect the rate at which water is penetrating the joint. This is evidence suggests the possibility of water movement along the interface of which will be discussed in detail in the section 5.4.2.5.

5.3.3.3 Mechanical Test Results

The results from the mechanical tests reveal the same trend as was seen both in the edge disbonding of the specimens and also the appearance of micro-defects. However the mechanical tests were not able to link specific areas of toughness loss with, for example, areas with micro-defects. The results tend to show an average result for the specimen. However the second grit-blast, PAA and CAA specimens

(Figure 3.8, Figure 3.25 and Figure 3.35 respectively) all showed greater toughness loss in the strips closest to the unsealed edge. The average toughness results give a good overview of the relative performance of the specimens; these are shown in Table 5.2. These results show that the PAA and grit-blast specimens were the least durable of the specimens, with the CAE and CAA specimens showing no loss of toughness away from the regions of obvious disbonding. The exception to this must be the first CAE specimen. Although no mechanical test results were obtained for this specimen it is clear that it had suffered a large loss in interfacial integrity due to the speed with which the epoxy layer peeled from the aluminium due to residual stresses in the epoxy layer.

5.3.3.4 Conclusions

The pre-treatments that were used on these specimens appear to have affected the durability of the specimens in two key ways; first is the degree of corrosion protection that the pre-treatment affords the adherend; second is the extent to which water weakened the interface. Both anodise pre-treatments were more effective corrosion protection than the etch or grit-blast treatments. The PAA showed the longest time for a disbond to initiate, but the CAA specimen appeared to be worse than might have been expected due to the exposure of alloy caused by the machining of the edges. The CAA specimen appeared the most effective at resisting the effects of water, showing no toughness loss across the majority of the specimen. The second CAE specimen also showed little sign of toughness loss. This resistance to attack by water was also seen by the absence of micro-defects in the CAA and second CAE specimens. However both the grit-blast and PAA specimens showed significant loss of toughness across the whole specimen, accompanied by the appearance of micro-defects.

5.3.4 Three-layer Specimens

The following sections summarise the performance of the different pre-treatments used on the three-layer specimens. Their performance is then compared. The comparisons that are used for the three-layer specimens concern the development of edge disbonding and the mechanical test results.

5.3.4.1 Grit-blast

The results from the three-layer grit-blast specimens are discussed in section 4.2 page 137 and summarised in Table 4.2. The only defects detected from the N.D.T.

of the wet specimen was a small area of edge disbonding (25 mm^2). However the mechanical tests showed (Figure 4.6) a change in the failure type from cohesive (dry) to interfacial (wet). The interfacial failure was across the entire specimen, and not restricted to the edge where water had diffused through the epoxy. The failure surface from this specimen had a streaky appearance (Figure 4.4), suggesting that water had penetrated along the interface (or in the epoxy very close to it). The XPS results from the edge and centre of this specimen showed no discernible variation across the area of the joint.

5.3.4.2 CAE

The results from the three-layer CAE specimen show a greater extent of edge disbonding than the grit-blast specimen, (comparing Figure 4.2 and Figure 4.9). However the results from the mechanical test showed that the entire specimen failed in a cohesive manner, except for the area of disbonding that had been detected ultrasonically. Differences in the mechanical performance of the wet and dry specimens were attributed to variations in the properties of the adhesive and the effects of post-curing, see section 4.3.3.

5.3.4.3 PAA

The wet three-layer PAA specimen showed no sign of edge disbonding. All of the ultrasonic scans from this specimen showed no change despite a total of 566 days in water (Figure 4.14 and Figure 4.15). However the mechanical testing of this specimen showed an almost total interfacial failure (Figure 4.17). This was accompanied by a reduction in toughness of more than 50% when compared to the dry PAA specimen (Table 4.2)

5.3.4.4 CAA

The wet CAA specimen, like the PAA specimen, showed no signs of change from the ultrasonic scans (Figure 4.19 and Figure 4.20) after 566 days in water. The mechanical test results showed a slight reduction in toughness, but like the CAE specimen, this was attributed to changes in mechanical properties of the epoxy. The failure of the wet CAA specimen was entirely cohesive.

5.3.5 Comparison of pre-treatments based on three-layer specimen results

The results from the three-layer specimens can be compared in a similar manner to the two-layer specimens, with the exception that there were no micro-defects detected ultrasonically.

5.3.5.1 Edge disbonds

Only two of the three-layer specimens showed any sign of edge disbonds, those being the grit-blast and CAE specimens. The CAE specimen was considerably worse than the grit-blast, effectively disbonding an entire edge strip used for the mechanical tests. However there was not enough disbonding across all the specimen for any inference on the performance of the whole specimen to be made, as was shown for the two-layer specimens.

Both of the anodise pre-treatments showed no edge disbonds despite the exposure times being greater than any other specimen tested. This was aided by the fact that neither the CAA or PAA specimens had any machining of edges, leaving a protective oxide layer on all exposed edges.

5.3.5.2 Mechanical tests

In many respects the mechanical test results can be considered the most important of all of the results that have been generated. It is ultimately the mechanical performance of joints which is the main concern and the three-layer specimens are the ones that are closest to a structural adhesive joint. The specimens effectively split into two sections; the specimens which failed cohesively, and those which failed interfacially.

The two specimens which failed interfacially (grit-blast and PAA) did so across almost the entire area of the joint. The two specimens that failed cohesively (CAA and CAE) only showed very small areas of interfacial failure where disbonds were detected from N.D.T. The difference in the performance of these specimens based upon pre-treatment suggests that the pre-treatment is responsible for the change in locus of failure. One explanation for this difference would be that the different pre-treatments vary in the rate at which water can move along the interface. This implies that the grit-blast and PAA specimens allow rapid ingress of water along their interfaces. The fact that the interfacial failure in both grit-blast and PAA specimens

extended to the centre of the specimen discounts water diffusion through the epoxy (see following section regarding kinetics of degradation). If this is the case then the CAA and CAE pre-treatments prevent water ingress along the interface.

The other possibility is that water also penetrated the CAA and CAE specimens but had no discernible effect. The presence of lines was seen from the failure surface of both PAA (Figure 4.18) and grit-blast (Figure 4.5) specimens. In the case of the PAA specimen this was clearly identified as a thin layer of epoxy on the surface. This suggests the possibility that there were lines of weakness in the epoxy along which water could travel (further discussion of this is contained in the following section about mechanisms of attack). However this suggests that water may have penetrated the joint through the epoxy layer close to the interface and only in the case of the PAA and grit-blast specimen was there a reduction in joint toughness. If lines were present in the epoxy close to the interface of the three-layer CAE and CAA specimens they would be difficult to see as a thick layer of epoxy was left on the failure surfaces. Either way the difference between the two failure types must be attributed to the pre-treatment.

5.3.5.3 Conclusions

Two areas of the specimen performance were identified as being influenced by the pre-treatment of the three-layer specimen, the edge disbonding and the mechanical test performance. The extent of edge disbonding was very small in the three-layer specimens and was not sufficient to allow any correlation with the mechanical test results. We have seen that the different pre-treatments have had a large effect on the mechanical test results of the three-layer specimens with the PAA and grit-blast specimens failing interfacially and the CAA and CAE specimens failing cohesively. It has not been clear if the differences in the pre-treatments have affected the rate of water ingress or whether water ingress has been the same for all pre-treatments but the grit-blast and PAA specimens degraded where the CAA and CAE specimens did not.

5.3.6 Comparison of two and three-layer specimens

If we consider the different defect types that have occurred on both the two and three-layer specimens then it is possible to compare the two specimen types.

5.3.6.1 Edge disbonds

The rates of edge disbonding were very different between the two and three-layer specimens but the rank of durabilities implied by this for each pre-treatment was the same. The anodise treatments produced bonds with the lowest rate of disbonding with the grit-blast and CAE specimens having the highest disbond rate. In the case of the three-layer anodised specimens there was no edge disbonding. From the two-layer specimens it was seen that the PAA specimen performed well because of the length of time before a disbond was initiated, as opposed to the rate at which the disbond spread thereafter.

5.3.6.2 Micro-defects

Only the two-layer specimens had micro-defects detected from the ultrasonic scans. However the pre-treatments where the two-layer specimens showed micro-defects were the same ones where the three-layer specimens showed lines on the failure surface. This shows that the appearance of micro-defects was not only related to a loss of toughness in the two-layer specimen but also to the interfacial failure of the three-layer specimen with the same pre-treatment. The exception to this is the first two-layer CAE specimen which showed many micro-defects which would have suggested an interfacial failure of the CAE three-layer specimen. However the second two-layer CAE specimen had virtually no micro-defects and the three-layer CAE specimen failed cohesively. The fact that the three-layer specimens which failed interfacially had lines on the surface similar to those seen in the two-layer specimens suggests that similar mechanisms may be at work in both specimen types. This would suggest that a two-layer specimen could be used as a quicker way of determining the performance of different pre-treatments.

5.3.6.3 Mechanical tests

The relative performance of the joints with the same pre-treatment from the different specimen types showed good agreement. From both sets of specimen types the grit-blast and PAA specimens showed the greatest toughness loss. Similarly the CAE and CAA specimens showed excellent residual toughness in both the two and three-layer specimens.

The mechanical tests from the two-layer specimens with all pre-treatments except CAE showed a reduction in the toughness of the strips closest to the unsealed edge; however this was not something that was seen in any of the three-layer

specimens. A possible reason for this is that in the three-layer specimens a weakening of the interface would only be detected if it was sufficient to change the failure type from cohesive to interfacial, therefore small changes in the interfacial integrity of the three-layer specimens would not be seen. The PAA and grit-blast specimens that had clearly suffered from degradation failed interfacially across almost the whole specimen, with the few areas of cohesive failure appearing tougher that the rest of the specimen (Figure 4.17). It should be noted that the toughness of the edge strips of the three-layer PAA and grit-blast specimens were not noticeably different than the strips from the centre of the specimen.

5.3.7 Conclusions

The different pre-treatments used for this work in general performed much as would have been expected, following the description of the pre-treatments in Chapter 1. The major differences between the expectation and the results was the comparatively poor performance of the PAA treatment and the better than expected performance of the CAE treatment. The PAA specimens showed good resistance to the initiation of disbonds but showed a considerable drop in toughness of the intact bond after exposure to moisture. This trend was seen in both two and three-layer specimens. The CAE specimens generally showed poor performance with regards to the growth of disbonds, but showed excellent toughness in the areas of bond still intact. These results may not be as different from published results as they at first appear to be, as disbonds around the edge of a specimen will degrade the performance of the joint in a mechanical tests that simply records a failure stress far more than disbonds in the centre of the specimen. With the mechanical tests used here the fracture toughness is measured on a point by point basis across the whole specimen, and so is not influenced by areas of disbonding. Thus with a mechanical test that measures a stress to failure the CAE joints may appear to perform less well than PAA joints because of the better resistance of the PAA specimen to the formation of disbonds. The worst overall pre-treatment was grit-blasting showing poor resistance to the formation of disbonding and poor residual toughness. The best overall performance was seen from the CAA specimens which showed excellent resistance to the formation of disbonds and little loss of toughness over the remaining bonded area.

5.4 Kinetics and Mechanisms of Degradation

5.4.1 Introduction

The degradation of an adhesive joint in a hostile environment can be divided into two sections; the mechanism through which water enters the joint (kinetics); and the process by which the performance of the joint is degraded.

5.4.2 Kinetics

5.4.2.1 Introduction

The performance of adhesive joints has been seen to be largely dependent on the interface regions of the joint. This was discussed in detail in Chapter 1, and the variation in the performance of specimens with different pre-treatments is clear evidence of this. The kinetics that are of interest are those which describe how water gains access to the interface between the adhesive and the adherend. Four possible mechanisms have been identified, and these are discussed in the following sections.

5.4.2.2 Water entering via corrosion driven disbonding

The design of the specimens was deliberately such that some areas of the specimen would see the ingress of water faster than others. This was achieved through the use of a marine epoxy based paint along two of the edges to seal them against the ingress of bulk water. The variation in edge conditions of the joint could then be investigated and their significance determined. This could be considered successful as there were significant differences in the rate of degradation experienced by the different edges of the specimens. This can be almost entirely explained as a corrosion driven mechanism when we see that the areas of disbonding experienced by almost all specimens extended from the unsealed edges (this can be seen in all of the normal incidence scans from the two-layer specimens in Chapter 3). Only the anodised three-layer specimens did not suffer from this form of degradation (see PAA and CAA results, Chapter 4). It can be seen from the results that the specimens that suffered the most from this were the two-layer specimens with the least corrosion resistant pre-treatments i.e. the grit-blast and CAE specimens (sections 3.2 and 3.3 respectively). The disbonding usually started at the flush edge, and was initiated by a corrosion patch which undercuts the epoxy layer. Swelling of corrosion products force open the interface to allow water entry to the joint. This is shown schematically in Figure 5.2.

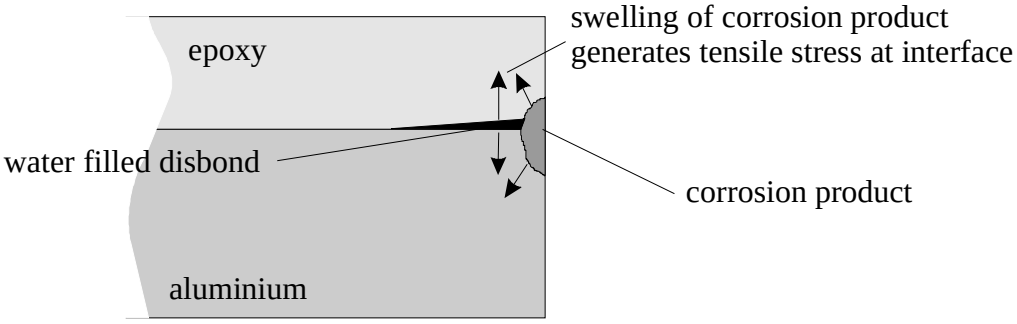

Figure 5.2 Water ingress caused by swelling of corrosion production.

This mechanism of water ingress can be seen to depend heavily on the corrosion protection offered by the pre-treatment and also the overall joint stiffness. Hence the specimens most susceptible to this form of attack have been the two-layer grit-blast and CAE specimens. The swelling of the corrosion products imparts a tensile stress on the interface and once disbonded, only the stiffness of the epoxy layer holds the two layers together. The interface is then easily opened up by the corrosion products, thus allowing water further access and the process continues. This has been clearly seen on all of the two-layer specimens where a smooth-faced water filled disbond develops in places along the unsealed edge and after some time corrosion roughens the failure surface (see Figure 3.1, Figure 3.11, Figure 3.20 and Figure 3.29). The considerable improvement in corrosion protection of the CAA pre-treatment over simple grit-blasting explains the large difference in the failure rates seen for the specimens with these pre-treatments. There is another significant difference in the performance of the two-layer CAA specimen. The growth of the disbond in the CAA specimen had a small radius crack front and in some places the crack jumped into the epoxy as opposed to continuing along the interface (see Figure 3.33). All of the other two-layer specimens had a larger radius crack front and the failure always continued along the interface. This is strong evidence for the interface of the CAA specimen being considerably tougher than the other specimens, as was discussed in the section 5.3 regarding the effects of pre-treatment.

5.4.2.3 Diffusion of water through epoxy layer

In the past much work has concentrated on the diffusion of water into a joint via the epoxy layer, as epoxy is known to be hygroscopic [25]. Kinloch and Gledhill [73], proposed that diffusion of water into the adhesive layer may be the rate determining factor in the degradation of adhesive joints. The calculation of diffusion rates has already been discussed in Chapter 2. When examining the possible effects of diffusion, there is a clear distinction to be made between the two and three-layer

specimens. Part of the reason for the design of the two-layer specimens was to allow water to saturate the epoxy layer in a reasonable time, as the three-layer specimen design would take tens of years to saturate. This is due to a diffusion path of around 50mm to reach the centre portion of one of the three-layer specimens, however the diffusion path for the two-layer specimens was only 2mm. The open epoxy layer of the two-layer specimen was considered to allow saturation of the epoxy adjacent to the interface in a uniform manner. The concentration of water present at the epoxy/aluminium interface for a two-layer specimen is shown in Figure 5.3. In this figure the level of water in the epoxy at the interface has been normalised to saturated epoxy.

If we first consider the diffusion of water into the two-layer specimens. All of the specimens that were tested had been exposed to water for a minimum of 100 days, which is sufficient to allow greater than 55 % of saturation of the epoxy adjacent to the interface, with most specimens being immersed in water for considerably longer than that. The epoxy adjacent to the interface was calculated to be 99 % saturated in the CAA specimen, which was exposed to water for the longest time.

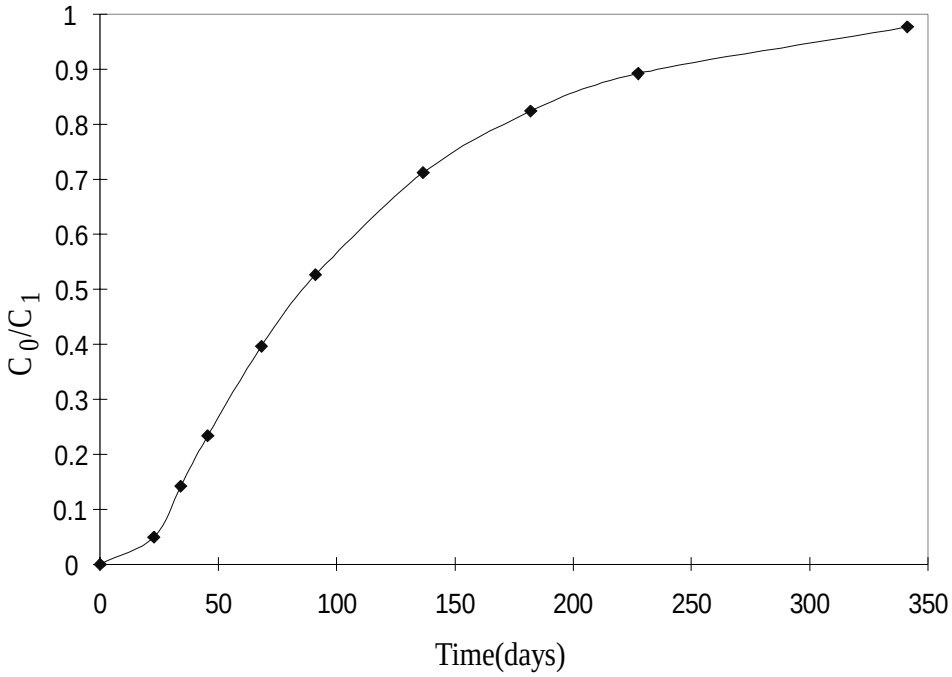

Figure 5.3 Water concentration at aluminium interface through 2mm of epoxy.

We can divide the results from the two-layer specimens between those with a significant degree of degradation and those without. Those without were the CAA and the second CAE specimen. The fact that the wet CAA specimen exhibited higher toughness than the dry specimen was attributed to water plasticising the epoxy. This

suggests that water diffusion was occurring as expected in the two-layer specimens, but diffusion of water alone into the specimen was not sufficient to degrade the joint. This is further evidenced by the lack of degradation of the second CAE specimen (section 3.3.4). From the two-layer specimens we have seen evidence of the greatest degradation occurring closest to the unsealed edges. This is supporting evidence that water diffusion into the epoxy is not our primary concern as the diffusion into the two-layer specimens should occur in a uniform manner. Further evidence against diffusion being the primary mechanism of water penetration is the appearance of micro-defects on the two-layer grit-blast and PAA specimens (Figure 3.1 and Figure 3.19) sooner than diffusion of water through the epoxy layer should allow.

The results from the three-layer specimens can be seen to support the diffusion calculations. Figure 5.4 shows the concentration of water in the epoxy layer of a three-layer specimens after 700 days in water. This prediction is for a simple, one dimensional diffusion path, which was considered accurate enough given the size and impermeable nature of the adherends. The curve is shown corresponding to the

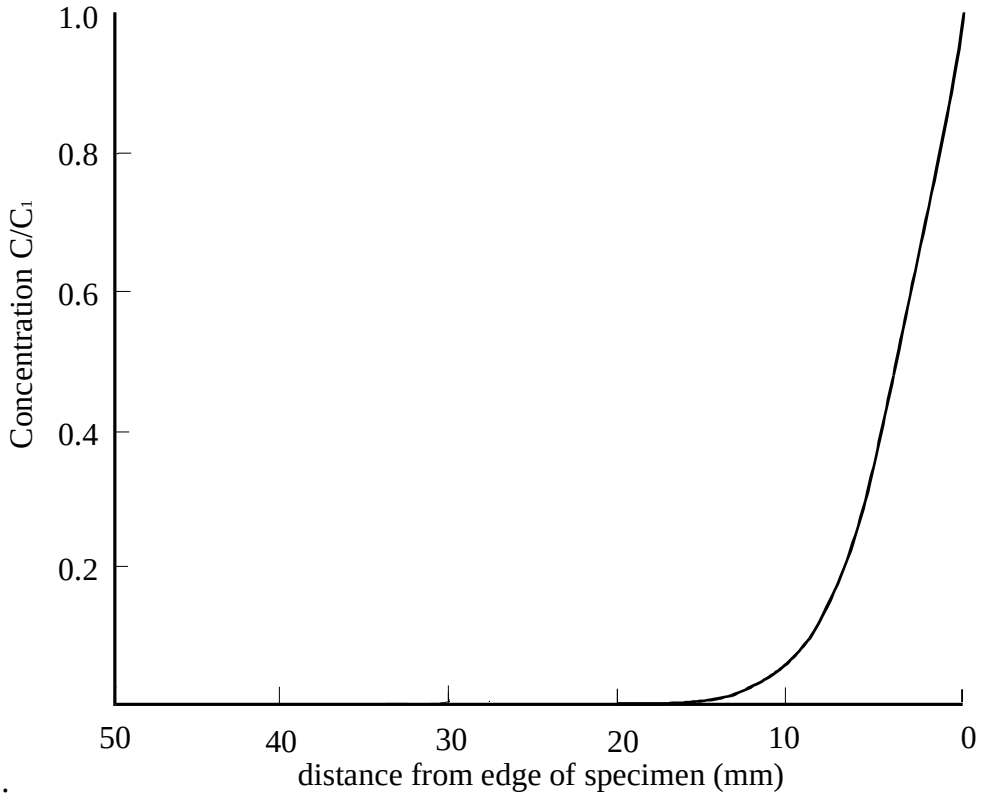

Figure 5.4 Concentration of water in epoxy layer of three-layer specimen after 700 days in water.

smallest value of Dt/l^2 taken from Figure 2.6, as this shows the distribution of water in

the epoxy after 700 days which is slightly longer than the exposure seen by the three-layer CAA and PAA specimens. Examining the failure surfaces shows an area of discolouration around the edge of the specimen; this is best seen from the three-layer CAA specimen (Figure 4.21). The epoxy used in all of these specimens yellows as it absorbs water. All of the epoxy in the wet two-layer specimens could be seen to have yellowed but with the three-layer specimens this only extends a short way into the specimen. Comparison of Figure 5.4 and Figure 4.21 shows good agreement between the predicted water concentration and the yellowing of the epoxy. This shows that no significant level of water has penetrated more than 10 mm into the specimen (this being the width of one of the strips cut for the mechanical tests. The mechanical test results show no correlation between loss of toughness and this area of diffused water, however evidence that water had penetrated much further into the specimen than the diffusion calculations suggest is clear from the interfacial failure suffered by the grit-blast and PAA specimens. Even these three-layer specimens that failed interfacially showed no greater loss of toughness in the areas with diffused water. This is further evidence that we need to detect more than water diffusion in the epoxy if we are going to detect joint degradation.

5.4.2.4 Water penetration through channels in the epoxy layer

There are several pieces of evidence that suggest that flaws existed in the epoxy layer, and that these flaws may have been the path for rapid water transport into the specimen. It is unlikely that these flaws existed in the specimen immediately after manufacture as they were relatively easily detected by visual assessment of the specimen after a short time in water. From the two-layer specimens fine lines were seen in the grit-blast specimen (Figure 3.4), the first CAE specimen (Figure 3.15) and the PAA specimen (Figure 3.23). The connection between these lines and the transport of water is strongly suggested by the increased appearance of the small spot disbonds in the vicinity of the lines (Figure 3.4). These lines were difficult to detect ultrasonically, but were detected for both the grit-blast and CAE specimens, (Figure 3.4 and Figure 3.15), with many more lines being detected visually than ultrasonically. The best evidence for these being flaws in the epoxy layer and not simply along the interface was seen from the failure surface of the grit-blast specimen (Figure 3.6), which showed a clear line of epoxy remaining on the surface of the aluminium. An almost identical feature was also seen on the surface of a two-layer PAA specimen (section 3.4.6), where a much thinner epoxy layer was seen. The difference between the appearance of these lines on the failure surface was thought to be due to the large

difference in the roughness of the grit-blast and PAA surfaces. A schematic showing the form that a flaw in the epoxy layer might take is shown in Figure 5.5.

Similar lines were seen on the failure surface of both the grit-blast and PAA three-layer specimens (Figure 4.4 and Figure 4.18 respectively). The lines seen on these failure surfaces extend across all of the specimen. If water is able to travel in these flaws then this would help explain the rapid degradation of these three-layer specimens. If this is the case then the major concern is the inability of the ultrasonic scans to detect them. Discussion on the detection of line defects has been presented in section 5.2.2. Comyn [25] discusses the possibility of the formation of cracks in epoxy adhesives due to the action of heat and moisture. He cites several examples of cases where water may exist in micro-cavities in the adhesive layer, these being in the form of either cracks or voids. It is therefore possible that these types of defect are responsible for water transport in these samples, with the water then degrading the joint in a relatively uniform manner, which then accounts for the mechanical test results from these samples (Figure 4.4 and Figure 4.17).

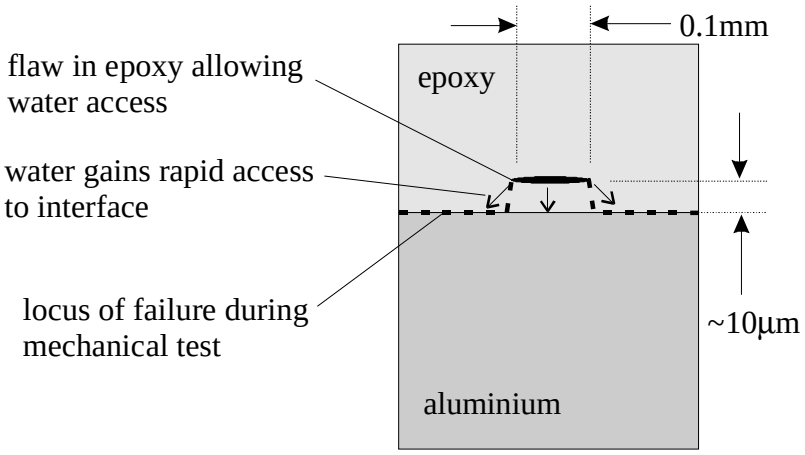

Figure 5.5 Schematic of flaw in epoxy layer.

Possibilities also exist that these flaw lines are formed to release either swelling or contraction stresses in the adhesive layer. The fact that they have appeared in specimens after so little time in water (see two-layer grit blast and CAE specimens) suggests that is more likely to be the effects of heat than from swelling due to water uptake. However they have only been seen on samples exposed to water and not in samples that have been kept in a dry heat, suggesting that water is at least partially responsible for their appearance. A factor that may have bearing on this phenomenon is that extremely brittle nature of the adhesive used, which may contribute to the appearance of these flaws.

5.4.2.5 Degradation of edge strips

There is evidence to suggest that edge disbonds, diffusion and water moving through flaws in the epoxy layer may not be the only mechanisms of water transport present. The mechanical test results from the two-layer grit-blast, PAA and CAA specimens (Figure 3.8, Figure 3.25 and Figure 3.35 respectively) show a greater loss of toughness adjacent to one of the unsealed edges. This is despite there being no evidence either visually or from the ultrasonic scans of any greater extent of damage in these areas compared with the rest of the specimen. Micro-defects, which appear to be indicators to degradation of the interface, were no more prevalent on any of the strips that were less tough than other strips from the same specimen. Water diffusion through the epoxy layer in the two-layer specimens should occur in a uniform manner and so would appear not to be the cause of the degradation of the edge strips. The greater loss of toughness around the unsealed edges point to the movement of water along the interface of the specimen as this toughness loss occurred along the unsealed edges and not the sealed.

Two other results which suggest that water may be moving along the interface are the three-layer grit-blast and PAA specimens which suffered interfacial failures across virtually the whole specimen. The previous section discussed the presence of flaws in the epoxy layer to explain the result. We need to understand the reason why only the grit-blast and PAA specimens were affected. Two possible reasons for this are that either water penetrated the CAA and CAE specimen but failed to degrade the joint or, water was entering along the interface of the PAA and grit-blast specimens due to the more open nature of the interface (on a microscopic scale), where the CAA and CAE specimens resisted this form of water penetration. The appearance of the lines on the failure surface of the grit-blast and PAA specimens could then be explained simply as flaws in the epoxy layer which caused the failure to divert into the epoxy layer for a small distance, but they were not responsible for the transport of water. As the failure of the CAA and CAE specimens were cohesive, flaws in the epoxy layer may be present near the interface, however there presence is not detected as the failure is some distance from them.

The loss of toughness of the edge strips appears to be a real effect but it is not possible to identify the reason for this. Water penetration along the interface has been suggested as one possibility but there are many problems with this argument. If we assume that this mechanism is the same in both two and three-layer specimens then we would expect to see greater toughness loss in the edge strips in the three-layer

PAA and grit-blast specimens. This has not been seen. This is clearly an issue that requires further investigation.

5.4.2.6 Conclusions

Four possible mechanisms of water penetration into the specimens have been identified. The edge disbonding has been easily detected and the extent to which it has been present on the different specimens has been clearly seen, with the grit-blast and CAE specimens being the worst affected. The diffusion of water into the epoxy layer of the specimens has been considered, but cannot be considered responsible for the majority of toughness losses seen in the mechanical test results. The two remaining mechanisms, water penetration through flaws in the epoxy layer and water permeating along the interface are considered to be highly important in explaining the results from the specimens. It has not been possible to determine which of these mechanisms is the most prevalent. However it is clear from the interfacial failure of the three-layer grit-blast and PAA specimens that whichever mechanism dominates, it progresses at a rate far faster than the diffusion of water through the epoxy layer. From the evidence available so far water moving through flaws in the epoxy has been the most strongly suggested.

5.4.3 Degradation Mechanisms

So far we have discussed mechanisms by which water may enter an adhesive joint. The following sections discuss how the presence of water will reduce the performance of the joint. Comyn [25] highlights four processes by which weakening may occur; altering the properties of the adhesive in a reversible manner, altering the properties of the adhesive in a non-reversible manner, attacking the interface either by displacing the adhesive or hydrating the metal or metal oxide surface of the adherend and inducing swelling stresses in the adhesive. Of these, only the irreversible changes in the epoxy and the attack on the interface of the joint have been investigated to any extent here. Reversible changes in the epoxy were not measured as the mechanical tests were performed in a dry environment several months after the specimens were removed from water. The possibility of swelling stresses induced by the adhesive would only have been detected (if they changed the thickness of the epoxy layer) using the time of flight measurements in the three-layer specimens, but no change was detected.

5.4.3.1 Changes in the adhesive properties

Two fundamental changes in the properties of the adhesive were seen. The clearest of these was a reduction in the fracture energy of the adhesive after exposure to heat. This was seen in the three-layer grit-blast, (Figure 4.6), CAA (Figure 4.21) and CAE specimens, (Figure 4.12 and Figure 4.13) all of which failed cohesively. However this effect was explained to be an effect of heat and not of moisture, as specimens exposed to dry heat produced very similar results to those exposed to hot water (Table 4.1).

From the two-layer specimens the only effect which was attributed to changes in the properties of the adhesive was the increase in toughness of the wet CAA sample compared with the dry sample (Figure 3.35). This was thought to be due to plasticisation of the epoxy by the ingress of moisture.

5.4.3.2 Attack on the interface of the joint

Brewis [24] identifies mechanisms by which aluminium bonded joints may be weakened through attack of the interface; displacement of the adhesive from the substrate surface, weakening of the aluminium oxide and reduction of ion-pair interactions across the oxide/polymer interface. The changes seen on the specimens used for this thesis are divided between those which could be detected prior to the mechanical tests and those seen either during or after the mechanical tests.

Detected changes

The degradation of the interface that has been detected either visually or ultrasonically before the mechanical tests can be divided into two areas; the edge disbonds and small spot disbonds.

- edge disbonds - these have been seen on all the two-layer specimens and were discussed in section 5.4.2.2. This mechanism is driven through the swelling of corrosion products which impart a tensile force on the interface in the presence of bulk water. This is not an effect of gross corrosion of the adherend. The corrosion does however provide the driving force for the crack and allows water immediate access to the interface.

- small spot disbonds (micro-defects) - these appear to be fundamentally the same as the edge disbonds but they are considerably smaller, and they develop very

slowly. In the case of the two-layer PAA specimen (section 3.4) their appearance changes from areas of low acoustic impedance to scattering defects, suggesting that initially they are smooth-faced disbonds which develop into pits with the passing of time. In the case of the two-layer grit-blast specimen (section 3.2) the number of small spots detected at the interface of the specimen might appear sufficient to explain the loss in toughness (Table 3.1). However the number present in the two-layer PAA specimen (Figure 3.23) would appear to be too few to explain the loss of toughness (Figure 3.25).

Changes detected from or after the mechanical tests

The suspicion of changes to the interface region of specimens, other than those detected prior to the mechanical tests, have come from the mechanical test results. The XPS results can help to explain these changes.

The clearest evidence of a change in the properties of the interface of a joint have come from the XPS analysis of the failure surfaces from the wet and dry two-layer PAA specimens (section 3.4.5). These results showed that the amount of aluminium and oxygen present on the failure surface of the PAA specimens was highest for the weakest areas of the joint, with the aluminium and oxygen quantities decreasing as toughness increased. This suggests that the failure was closer to the adherend for areas with the poorest toughness. Although it was not possible to determine whether the failure was in the oxide or at the oxide/epoxy interface, this represents the best evidence for a change in the properties of the oxide layer being responsible for the loss of toughness in the specimen.

The mechanical test results from both two and three-layer grit-blast and PAA specimens showed far greater loss of toughness than either the CAA or second CAE specimens (results summarised in Table 3.1 and Table 4.2). The ultrasonic scans from the three-layer grit-blast (Figure 4.1 - 4.4) and PAA samples (Figure 4.14 - 4.15) did not reveal anything to indicate that this should be the case. The lines on the surface of these specimens (discussed in section 5.4.2.4) may explain how water gained access but do not explain what changes occurred to reduce the joint toughness.

5.4.4 Conclusions

Four mechanisms for the penetration of water into adhesive joints were identified; entering through edge disbonds, diffusing through the adhesive, travelling

in flaws in the adhesive layer and wicking along the interface of the joint. Of these, the growth of edge disbonds and the diffusion of water through the adhesive layer are the two that can either be detected or predicted with reasonable accuracy. However it is the movement of water along the interface or through flaws in the adhesive that appear to be key to the degradation of PAA and grit-blast three-layer specimens which suffered interfacial failures.

The degradation of the joint was divided into two groups, changes in the adhesive and changes at the interface. Two changes were seen in the adhesive; first was the increase in toughness due to plasticisation in the two-layer CAA specimen (section 3.5.4), and second was a reduction in the adhesive fracture toughness and also brittle failure in grit-blast, CAE and CAA three-layer specimens. The latter was found to be due to the effects of heat and not moisture. Changes at the interface of the specimens was also divided into two categories, those that were detected prior to mechanical tests and those identified after mechanical tests. Thus we have seen evidence of change at the interface of some specimens without detection of the mechanism of degradation.

5.5 Concluding remarks

This chapter has discussed the results obtained from all of the specimens. Several key areas were examined: the performance of the ultrasonic techniques employed, the effect of different pre-treatments and the kinetics and mechanisms of degradation. The main conclusions are:

- Ultrasonic techniques - high resolution normal incidence scans have proved to be the most useful for detecting environmental degradation of the specimens used, but in many cases loss of toughness was accompanied by no detectable change.

- Pre-treatment - from both specimen types, the CAA treatment was shown to give the most durable specimens, with grit-blasting producing the least durable specimens. The results showed that the PAA specimens performed worse than would have been expected, though it should be noted that a primer was not used when it commonly would be with the PAA pre-treatment.

- kinetics - four possible means of water penetration into an adhesive joint were identified. Water entering from edge disbonds and through diffusion were

quantified but it was not possible to quantify the extent by which water entered the specimens through flaws in the epoxy or through permeating along the interface. These last two mechanisms are the greatest concern for non-destructive testing as they were not detected.

- degradation - the displacement of the adhesive was seen both from large edge disbonds and from the smaller spot defects, however the changes that occurred in other areas of the specimen to generate loss of toughness were not detected. Surface analysis results suggested that in the case of the two-layer PAA specimens the variation in toughness was due to changes in the properties of the oxide layer.

The following chapter discusses the implication of these results for the non-destructive evaluation of environmental degradation of adhesive joints. The best possible approach for N.D.T. of adhesive joints is discussed and recommendations for further work are made.

6. Conclusions

Chapter 1 of this thesis contained a summary of the problem to be solved. This stated that we wished to find a technique that was able to determine the serviceability of an adhesive joint after exposure to degrading environments. Specifically we were concentrating on the type of bonding found in the aerospace industry, i.e. the bonding of aluminium adherends using epoxy based adhesives. Part of finding a solution for this problem involved developing an understanding of the mechanisms responsible for the degradation of the joint. Ultrasonic techniques were identified as being the most promising for solving this problem, particularly as it was thought that measurement of the interfacial properties of the adhesive joints (and subsequent changes in these) would be most suitable for determining environmentally induced problems with the interface of the adhesive joint. The conclusions have been divided into three sections; the suitability of ultrasonic techniques for detecting degradation of joints, the mechanisms of degradation and suggestions for future work.

6.1 Ultrasonic inspection of adhesive joints

6.1.1 Normal incidence

The key points from using the normal incidence technique for the scanning of adhesive joints can be summarised as follows;

- Excellent repeatability of results was obtained (±3%), with the experimental set-up being simpler than oblique incidence.

- The spatial resolution of the normal incidence scans was found to be approximately 0.2 mm using the 50MHz focused transducer.

- Large disbonds extending from the edges of specimens were easily detected.

- Small spot disbonds and lines were detected from two-layer specimens, however not every defect that could be found through visual appraisal of the two-layer

specimens was detected ultrasonically with the limiting factor appearing to be the spatial resolution attainable.

- From the three-layer specimens, no micro-defects were detected and no change was seen away from the edges of the joints, despite the PAA and grit-blast three-layer specimens suffering almost completely interfacial failure.

- There was no evidence to suggest that any kissing bonds or areas of near zero toughness existed, except for the detected disbonds, however large toughness loss of the three-layer PAA specimen was seen with no detected change.

- Significant loss of toughness was measured from the mechanical tests, particularly along the edge strips of most of the two-layer specimens, with NO associated change in the appearance of the ultrasound scans.

6.1.2 Oblique incidence

The oblique incidence technique was used and refined to produce reliable scans from adhesive joints. The following key observations were made about the use of the oblique incidence technique.

- The use of focused probes instead of unfocused probes was found to decrease the sensitivity of the oblique incidence scans to misalignments caused by slight curvature of the specimens, which is minimal using focused probes. (The signal amplitude variation across the two-layer CAA specimen was 30% using unfocused probes and 4% using focused probes.)

- Defect detection was comparable to normal incidence scans but slightly poorer resolution resulted in some defects not being detected using oblique incidence that were seen using normal incidence.

- No additional changes were detected using oblique incidence scans compared with normal incidence scans.

- 20MHz was found to be the highest reasonable frequency to test at oblique incidence for this thickness of adherend due to the coherent noise generated by the grain of the aluminium plate.

6.1.3 Guidelines for most reliable use of ultrasound to inspect joints

The results have shown that one of the best ways of detecting signs of environmental attack is to look for changes on a small scale. This is perhaps a different way of looking at the problem in that most models of degradation have looked at subtle changes occurring in a uniform manner over a significant area. However it appears that finding much grosser changes on a small scale gives us more chance of detecting degradation. However it is not only changes at the interface of the joint that we need to inspect for as the results suggest that much of the degradation is due to flaws in the epoxy layer that are responsible for water accessing the central regions of the specimen. It is problems associated with this that may be the key to determining whether a joint is fit for service.

Problems of joints disbonding due to corrosion around the edges are well known, which is why care is taken to adequately seal the edges of the joint to protect them from harsh environments. Moreover in the event of the sealant failing it is relatively simple to inspect the joint to find disbonds around the edge (albeit with problems associated with scanning close to the edge of the adherends). The major concern is rapid degradation occurring in the central regions of the joint due to water gaining access, either through flaws in the epoxy or wicking along the interface, thus causing the bond to degrade. This was seen in the case of the three-layer PAA and grit-blast specimens and the problems of detecting this are apparent from the lack of any indication of defects from the ultrasonic scans. The performance of these specimens could be discounted on grounds of the surface preparations being insufficient to endow a joint with adequate durability for a safety critical joint. In the case of grit-blasting this would never be used alone for a safety critical joint exposed to a harsh environment, and a PAA treated surface would be used in conjunction with a primer to ensure the porous oxide is filled to prevent water ingress along the interface. However a desirable feature of any N.D.T. technique would be to ensure that the joint had been properly constructed before entering service, and this something that normal incidence ultrasound alone could not achieve. Whether the application of a primer could be detected using normal incidence ultrasound has not been investigated (and is highly unlikely due to the primer and epoxy properties being so similar), but it is certain that the presence of a PAA oxide layer could not be detected as the frequency that would be required for a 0.6μm oxide layer (of the order of 2 GHz) is far higher than can be used through a useful thickness of aluminium adherend.

In order to optimise the spatial resolution of normal incidence ultrasound relatively simple guidelines need to be followed. The highest attainable frequency should be used that allows adequate transmission through the adherend. In most aluminium aircraft structures this will be around 100MHz, with 50MHz being readily achievable for adherends 4mm thick. The focal length of the probe used should be kept as short as possible to obtain a minimum of water path between the probe and the test piece whilst keeping the interface of interest in the focal zone of the probe. This can be reduced to the point that the probe is coupled to the structure via a bead of water. The diameter of the probe then needs to be determined by considering a number of points. With a short focal length the angle of incidence generated around the edge of the probe could be oblique enough to generate surface waves in the aluminium and this could easily lead to confusion of signals. Also the broader the footprint of the probe on the top surface of the test piece, the further the probe must be kept away from the edge of the specimen in order to produce a reliable signal.

The guidelines discussed above optimise the probe for the finest resolution; however this still leaves many problems in the engineering of a system for scanning structures to take advantage of this high resolution. This would involve a system capable of scanning at considerably sub-millimetre resolutions while maintaining probe alignment and stand-off over almost arbitrary shaped structure. To detect environmental degradation also implies that the joints that need to be inspected will be in service, and so in-situ inspection would be needed with a minimum of disruption to the operation of the structure under examination. This, coupled with the analysis and storage of the quantities of data that would be generated from all of the bonded structure in an aircraft would generate significant, though solvable, problems. This approach is feasible in the aerospace industry where the tolerances that are applied to joints is small compared with other industries, such as automotive, where large variations in adherend and adhesive thickness may occur.

6.2 Effect of pre-treatment on durability

The performance of the specimens was considerably different for the two specimen types, however the durability endowed by the different pre-treatments was generally consistent between the two and three-layer specimens. The results showed that the grit-blast and PAA specimens suffered from the greatest degradation. The CAE and CAA specimens were the most durable, with the better corrosion protection of the CAA pre-treatment being responsible for the better durability of joints with this

pre-treatment compared with all other specimens. The key points concerning the effect of pre-treatment are as follows;

- For both specimen types the CAA pre-treatment produced joints that suffered the least degradation.

- The time to initiate edge disbonds appeared to be related to the corrosion protection of the pre-treatment.

- The rate at which edge disbonds expanded was correlated with the measured fracture toughness of the remaining bond, which was seen to vary for different pre-treatments. However only the two-layer specimens showed a significant level of edge disbonding against which to relate the toughness of the remaining bond.

- The possibility of water penetrating along the interface with grit-blast and PAA pre-treatments was suspected as a possible reason for the poor mechanical test results from the three-layer specimens with these pre-treatments.

6.3 The kinetics and mechanisms of degradation

6.3.1 Water ingress

Four possible mechanisms were identified:

- Water penetrating through edge disbonds. In the specimens used for the work presented in this thesis this has largely been a corrosion driven effect. This has been detected using both normal and oblique incidence techniques.

- Diffusion of water through the epoxy layer. The quantities of water in both two and three-layer specimens has been predicted. The diffusion of water has been seen by the discolouration of the epoxy in the three-layer specimens (after mechanical tests) and this compared well with predictions. With the adhesive used in the specimens there has been no ultrasonically detectable sign of water diffusion.

- The penetration of water through flaws in the epoxy layer. The failure surfaces of several specimens have shown lines of epoxy left on the surface (most clearly the

two-layer grit-blast and three-layer PAA specimens). This has been considered as one possible explanation for the interfacial failure of the three-layer grit-blast and PAA specimens which cannot be explained by the diffusion of water through the epoxy layer. Line defects have been detected using ultrasound in the case of two-layer grit-blast and CAE specimens, but not in any three-layer specimens. The results from the two-layer specimens suggest that the lines develop after the specimens have been immersed in water, as they are not visible immediately after manufacture, and were not seen in any of the samples kept in the desiccator.

- Water ingress along the interface of joints. This is an alternative explanation for the interfacial failure of the three-layer grit-blast and PAA specimens. Grit-blast, PAA and CAA two-layer specimens all showed greater toughness loss along strips adjacent to the unsealed edge suggesting that water may have penetrated along the interface. However why this should have occurred in the two-layer specimens and not the three-layer specimens requires further investigation.

The penetration of water into the specimens through edge disbonds and via diffusion through the epoxy was either detected or calculated satisfactorily, however it has not been possible to determine to what extent the other two water ingress mechanisms have occurred. Indeed the difference in the interface properties endowed by the different pre-treatments may make the processes highly dependent on the surface preparation.

6.3.2 Mechanisms of degradation

The following key points were made concerning the degradation of the joints:

- The reduction of toughness in the two-layer specimens could be related to the appearance of micro-defects. The relationship between the appearance of micro-defects and loss of toughness was not a direct one, as the number of micro-defects was not always proportional to the extent of toughness reduction. However they were certainly clear signs that degradation had occurred, but only in the two-layer specimens were these detected non-destructively.

- The presence of water in the epoxy layer adjacent to the interface alone is not sufficient to degrade the joint performance.

- Surface analysis using XPS of the two-layer PAA specimens indicated a reduction in joint toughness associated with a change in the locus of failure from within the epoxy towards the oxide layer, which indicated degradation of the oxide or oxide/epoxy interface.

- XPS from the two-layer CAA specimen showed a connection between calcium, chlorine and sodium on the failure surface of the strip adjacent to the unsealed edge and a loss of toughness. This suggests that water diffusion through the epoxy does not give the same results as water that has gained access through other means. The exposure time for this specimen was sufficient to allow saturation of the epoxy layer, and yet it was only the strips next to the unsealed edge which showed the presence of calcium etc. and a loss of toughness. This suggests that water diffusion will not transport certain ions, whereas the ingress of bulk water may.

6.4 Future work

Many of the findings here are based on what are essentially model specimens, particularly the two-layer specimens. Even the three-layer specimens differ from joints that would be seen in service in many ways. It is not clear that the mechanisms of attack that have been identified here will be as significant or indeed exist in joints made using the adhesive systems that are in place in the aerospace industry. However joints that are in service will undergo loading which will generally aid the detection of defects and weakness in the bonding of the structure. Such loading will help to open up areas of significant toughness loss, making detection much easier. The thin and consistent bondlines will also make the imaging of defects in the epoxy layer easier. It is the opinion of the author that a very important piece of work will be to undertake similar experimental work to that reported here but using identical bonding technology to that in service in aircraft today using specimens that are loaded while in degrading environments. It would also be important to determine the effect of primers and external paint to the overall characterisation of bondline parameters and the detection of degradation.

This work has highlighted the possibility of flaws in the epoxy layer being a potential mechanism for the rapid transport of water into the central regions of the joints. This could be investigated in more detail, with specimens designed specifically for studying this. There are several useful ways of doing this. One would be to use a

two-layer specimen design but with a much thinner epoxy layer than used in the specimens used here. A very thin, clear and well polished epoxy layer would allow investigation of the epoxy layer using optical microscopy along with ultrasonic techniques. This might well help the quantifying of the effects of water gaining ingress through the epoxy layer. Another useful specimen design would be to produce a three-layer specimen using one aluminium adherend and varying the pre-treatment as before, but making the second adherend glass, while still using a thin clear adhesive layer. This would allow rapid correlation of visually obtained results with those from a thin epoxy two-layer specimen helping to ascertain if the mechanisms of water ingress are the same for the two and three-layer specimens. It would also be useful to investigate a technique that would allow verification of the paths taken by water to enter the joints. With the two-layer specimens a simple die might be adequate if the water is travelling as rapidly as some of the results in this thesis suggest.

The adhesive used for the work presented in this thesis would not be used in a structurally important joint due to its highly brittle nature. Due to the possibility of water ingress through the epoxy layer it is considered essential to investigate a number of different adhesives that are used in structural bonding to determine what effect they have on the mechanisms of attack and how this may affects the ultrasonic interrogation of the joint. There is also the strong possibility that water would penetrate along the carrier used in many film adhesives, therefore it is considered important to investigate adhesives which use a carrier film.

References

1. Kinloch, A.J., *Durability of Structural Adhesives*. 1983: Applied Science Publishers.

2. Roberts, S.S.J. Dawson, J., and Yates T., *Sensing techniques for the detection of water in adhesives,* . 1994, AEA Technology.

3. Stone, D.E.W., *Non-destructive methods of characterising the strength of adhesive-bonded joints - A review, 86058,* 1986, Royal Aircraft Establishment.

4. Temple, J., *Inspection of adhesive joints : a review,* 1992, Theoretical Studies Department Harwell Laboratory, U.K.

5. Guyott, C.C.H., P. Cawley, and R.D. Adams, *The non-destructive testing of adhesively bonded structure : a review.* Journal of Adhesion, 1986. **20**: p. 129-159.

6. Smith, R.A., *Non-destructive evaluation for corrosion in ageing aircraft.* Insight, 1995. **37**(11): p. 884-891

7. Hung, Y.Y., *Shearography : a new optical method for strain measurement and non-destructive testing.* Optical Engineering, 1982. **21**(3): p. 319-395.

8. Reynolds, W.N. and Wells, G.M. *Video-compatible thermography.* British Journal of Nondestructive Testing, 1984. **26**: p. 40-45.

9. Rosenthal, D. and Trolinger, J. *Holographic nondestructive testing.* Materials Evaluation, 1995. **53**(12) p. 1353-1355.

10. Zoughi, R., *Microwave and Millimeter Wave Nondestructive Testing: A Succinct Introduction.* Materials Evaluation, 1995(april 1995): p. 461-462.

11. Kuhn, W., *NMR Microscopy - Fundamentals, Limits and Possible Applications.* Angewandte Chemie, 1990. **29**(1): p. 1-19.

12. Adams, R.D., *A review of defect types and nondestructive testing techniques for composites and bonded joints.* NDT International, 1988. **21**(4): p. 208-221.

13. Hayward, D., Affrossman, S. and Pethrick, R.A. *The application of dielectric relaxation measurements to the non-destructive examination of adhesively bonded joint structures.* Non-destructive Testing Evaluation, 1991. **6**: p. 45-63.

14. Cawley, P., *The sensitivity of mechanical impedance method of non-destructive testing.* NDT International, 1987. **20**(4): p. 209-215.

15. Taylor, J. *Advanced Inspection of Thermal Protection Systems*. in *Review of Progress in Quantitative Nondestructive Evaluation.* 1997. San Diego, CA. USA: Plenum Press.

16. Newman, J.W., *Shearographic inspection of aircraft structure.* Materials Evaluation, 1991. **49**: p. 1106-1109.

17. Challis, R.E., *et al., Viscoelasticity of thin adhesive layers as a function of cure and service temperature measured by a novel technique.* Journal of Applied Polymer Science, 1992. **44**: p. 65-81.

18. Dewen, P. and Cawley, P., *An ultrasonic scanning technique for the quantitative determination of the cohesive properties of adhesive joints*. in *Review of progress in Quantitative NDE*. 1992: Plenum Press, New York.

19. Pialucha, T. and Cawley, P. *The detection of a weak adhesive/adherend interface in bonded joints by ultrasonic reflection measurements.* in *Review of Progress in Quantitative NDE*. 1991: Plenum Press, New York.

20. Nagy, P.B., *Ultrasonic detection of kissing bonds at adhesive interfaces.* Journal of Adhesion Science Technology, 1991. **5**(8): p. 619-630.

21. Cawley, P., Pialucha, T. and Lowe. M. *A comparison of different methods for the detection of a weak adhesive/adhered interface in bonded joints*. in *Review of Progress in Quantitative NDE*. 1993: Plenum Press, New York.

22. Rokhlin, S.I., Wang, W. and Wang, Y.J. *Ultrasonic evaluation of interphasial properties in adhesive joints*. in *Review of Progress in Quantitative NDE*. 1990: Plenum Press, New York.

23. Wang, W. and Rokhlin, S.I. *Evaluation of interfacial properties in adhesive joints of aluminium using angle-beam ultrasonic spectroscopy*. Journal of Adhesion Science Technology, 1991. **5**(8): p. 647-666.

24. Brewis, *Aluminium Adherends*, in *Durability of Structural Adhesives*, A.J. Kinloch, Editor. 1983, Applied Science Publishers: York. p. 215-254.

25. Comyn, J., *Kinetics and Mechanisms of Environmental Attack*, in *Durablility of Structural Adhesives*, A.J. Kinloch, Editor. 1983, Applied Science Publishers: York. p. 85-131.

26. Pialucha, T.P. and Cawley, P. *The detection of environmental degradation in adhesive joints by ultrasonic reflection measurements*, 1992, Imperial College. MOD Agreement 2037/385/RAE(F).

27. Cawley, P. and Pialucha, T.P. *The quantitative determination of the ultrasonic reflection coefficient from interlayers in adhesive joints*. in *Review of Progress in Quantitative NDE*. 1994: Plenum Press, New York.

28. Zinin, P., *et al. Cut-off properties of leaky surface waves for the evaluation of adhesive-adherend interlayers by acoustic microscope*. in *Proceedings of the IEEE Ultrasonics Symposium*. 1996. San Antonio, TX, USA.

29. Albericci, P., *Aerospace Applications*, in *Durability of Structural Adhesives*, A.J. Kinloch, Editor. 1983, Applied Science Publishers: York. p. 317-350.

30. Bishopp, J.A. and G.E. Thompson, *The role of electron microscopy in the study of adhesion to aluminium substrates.* Surface and Interface Analysis, 1992. **20**: p. 485-494.

31. Davis, G.D. and J.D. Venables, *Surface and Interfacial Analysis,* in *Durability of Structural Adhesives*, A.J. Kinloch, Editor. 1983, Applied Science Publishers: York. p. 43-84.

32. Davies, R.J., *The Durability of Adhesively Bonded Aluminium Alloy,* Ph.D. Thesis, Mechanical Engineering Dept. Imperial College: University of London.1989,

33. Leidheiser Jr, H. *Mechanisms of de-adhesion of organic coatings from metal surfaces*. ACS Symposium Series. 1986. p. 124-135 ACS, Washington, DC, USA

34. Crank, J., *The mathematics of diffusion*. 2 ed. Oxford University Press, 1975.

35. Bikales, N.M., *Mechanical Properties of Polymers*, ed. N.M. Bikales. 1971.

36. Gazit, S., *Dimensional Changes In Glass-Filled Epoxy Resin As A Result Of Absorption Of Atmospheric Moisture.* Applied Polymer Science, 1978. **22**(12): p. 3547-3558.

37. Hunter, M.S., Towners, P.F. and Robinson. D.L. *Hydration of Anodic Oxide Films*. in *American Electroplaters*. 1959.

38. Pialucha, T.P., *The reflection coefficient from interface layers in NDT of adhesive joints*, Ph.D. Thesis, Mechanical Engineering Dept. Imperial College: University of London.1992,

39. Lamb, H. *On waves in an elastic plate*. in *Conference of the Royal Society*. 1917. London.

40. Brekhovskikh, L.M., *Waves in layered media*. 1980: Academic Press, New York.

41. Krautkramer, J. and Krautkramer, H. *Ultrasonic Testing of Materials*. 1983: Springer-Verlag Berlin Heidelberg New York.

42. Arrowsmith, D.J. and Moth, D.A. *Pore penetration by adhesive in anodised aluminium.* Transactions of the Institute of Metal Finishing, 1986. **64**(4).

43. Pialucha, T. and Cawley, P. *The detection of thin embedded layers using normal incidence ultrasound.* Ultrasonics, 1994. **32**(6): p. 431-440.

44. Cawley, P., Zeller, B.D. and Pialucha, T.P. *Characterization of oxide layers in adhesive joints using ultrasonic reflection measurements.* Proceedings of the Royal Society of London, Series A: Mathematical, Physical and Engineering Sciences, 1996. **452**(1951): p. 1903-1926.

45. Tattersall, H.G., *The ultrasonic pulse-echo technique as applied to adhesion testing.* Journal of Applied Physics D: Applied Physics, 1973. **6**: p. 819-832.

46. Baik, J.M. and Thompson, R.B. *Ultrasonic scattering from imperfect interfaces : a quasi-static model.* Journal of Non-destructive Evaluation, 1984. **4**(3/4): p. 177-196.

47. Lavrentyev, A.I. and Rokhlin, S.I. *Ultrasonic spectroscopy of imperfect contact interfaces between a layer and two solids.* Acoustical Society of America, 1998. **103**(2): p. 657-664.

48. Alers, G.A., Flynn, P.L. and Buckley, M.J. *Ultrasonic techniques for measuring the strength of adhesive bonds.* Materials Evaluation, 1977. **35**(4): p. 77-84.

49. Pilarski, A., *The coefficient of reflection of ultrasonic waves from an adhesive bond surface.* Archives of Acoustics, 1983. **8**(1): p. 41-54.

50. Jiao, D. and Rose, J. *An ultrasonic interface layer model for bond evaluation.* Journal of Adhesion Science & Technology, 1991. **5**(8): p. 631-646.

51. Pilarski, A. and Rose, J.L. *Ultrasonic oblique incidence for improved sensitivity in interface weakness determination.* NDT International, 1988. **21**: p. 241-246.

52. Rokhlin, S.I. and Marom, D. *Study of adhesive bonds using low-frequency obliquely incident ultrasonic waves.* Journal of the Acoustical Society of America, 1986. **80**(2): p. 585-590.

53. Rose, J.L., Dale, J. and Ngoc, T.D.K. *Ultrasonic oblique incidence experiments for interface weakness.* British Journal of Nondestructive Testing, 1990. **32**(9): p. 449-452.

54. Haskell, N.A., *The dispersion of surface waves on multi-layered media.* Bulletin of the American Seismological Society, 1953. **43**: p. 17-34.

55. Lowe, M., *Matrix techniques for modelling ultrasonic waves in multilayered media.* IEEE Transactions on Ultrasonics, Ferroelectrics and Frequency control, 1995. **42**(4): p. 525-542.

56. Nielsen, L., *Elastic properties of two-phase materials.* Materials Science and Engineering, 1982. **52**: p. 39-62.

57. Rokhlin, S.I. and Wang, W. *Measurements of elastic constants of very thin anisotropic plates.* Journal of the Acoustical Society of America, 1993. **94**(5): p. 2721-2730.

58. Rokhlin, S.I. and Wang. W. *Ultrasonic Characterisation of a Thin Layer of Anodized Porous Aluminium Oxide*. in *Review of Progress in QNDE*. 1990: Plenum Press, New York.

59. Zeller, B.D., *Adhesive/Adherend Interlayer Property Measurement by Acoustic Microscopy*, . 1999. (Personal Communication)

60. NTSB, *NTSB\AAR-89/03*, . 1989, National Transport Safety Board: Washington, USA.

61. Duer, R., *et al., Comments on mixed-mode fracture in adhesive joints.* Internation Journal of Fracture, 1995. **75**: p. 157-162.

62. Blackman, B., *et al.*, *The calculation of adhesive fracture energies from double-cantilever beam test specimens.* Journal of Materials science letters, 1991. **10**: p. 253-256.

63. Centre, B.S.C.I., *SEM/EDS : Scanning Electron Microscopy with X-ray microanalysis*, . 1999, Buffalo South Campus Instrumentation Centre. *www.sdm.buffalo.edu/research/scic/sem-eds.html*

64. VGScientific, *What is XPS*, . 1998. *www.vgscientific.com*

65. Adler, L., Achenbach, J.D. and Roberts, R. *Reflection from a boundary with periodic roughness : theory and experiment.* Journal of the Acoustical Society of America, 1983. **74**(3): p. 1025-1032.

66. Nagy, P.B. and Adler, L. *Surface roughness induced attenuation of reflected and transmitted ultrasonic waves.* Journal of the Acoustical Society of America, 1987. **82**(1): p. 193-197.

67. Huang, W., Wang, Y.J. and Rokhlin, S.I., *Oblique scattering of an elastic wave from a multilayered cylinder in a solid. Transfer matrix approach.* Journal of the Acoustical Society of America, 1996. **99**(5): p. 2742-2754.

68. Moidu, A.K., Sinclair, A.N. and Spelt, J.K. *Adhesive Joint Durability Assessed Using Open-faced Peel Specimens.* Adhesion, 1998. **65**: p. 239-257.

69. Broding, W.C., *Criteria for Designing Adhesive Bonded Joints.* Product Engineering, 1953. **October**.

70. Drinkwater, B., Dwyer-Joyce, R. and Cawley. P. *A study of the transmission of ultrasound across real rough solid-solid interfaces*. in *Review of Progress in Quantitative NDE*. 1995: Plenum Press, New York.

71. Margetan, F.J., *et al.*, *The interaction of ultrasound with imperfect interfaces : experimental studies of model structures.* Journal of Non-destructive Evaluation, 1992. **11**: p. 109-126.

72. Pialucha, T., Lowe, M. and Cawley. P. *Validity of different models of interfaces in adhesion and diffusion bonded joints*. in *Review of Progress in Quantitative NDE*. 1993: Plenum Press, New York.

73. Gledhill, R.A., Kinloch, A.J. and Shaw, S.J. *A Model for Predicting Joint Durability.* Adhesion, 1980. **11**: p. 3-15.

Appendix A

Pre-treatments

Grit-blast

Process Step	Method	Time (minutes)	Temp (C)
Solvent Degrease	Trikolene Bath	15	-
Dry	Warm air dryer	30	-
Grit Blast	Grit blaster, until uniform finish obtained	-	-
Solvent Degrease	Trikolene Bath	15	-
Dry	Warm air dryer	30	-

Chromic Acid Etch

Process Step	Method	Time (minutes)	Temp (C)
Solvent Degrease	Trikolene Bath	15	-
Dry	Warm air dryer	30	-
Alkaline Clean (if plate condition dictates)	Non silicate cleaner	-	-
Rinse	Clean tap water	5	ambient
	Distilled water	3	ambient
Inspect	Inspect for water breaks on surface, repeat above steps on rejects	-	-
FPL (CAE) etch	In Chromic acid etch bath	10	68
Rinse	Clean tap water	5	ambient
	Distilled water	3	ambient
Inspect	Inspect for water breaks on surface	-	-
Dry	Warm air specimen dryer	-	-

Chromic Acid Anodise

Process Step	Method	Time (minutes)	Temp (C)
Solvent Degrease	Trikolene Bath	15	-
Dry	Warm air specimen dryer	30	-
Alkaline Clean	If plate condition dictates, follow manufacturers instructions	-	-
Rinse	Clean tap water Distilled water	5 3	Ambient Ambient
Inspect	Inspect for water breaks on surface, repeat above steps on rejects	-	-
FPL (CAE) etch	In Chromic acid etch bath	10	68
Rinse	Clean tap water Distilled water	5 3	ambient ambient
Inspect	Inspect for water breaks on surface	-	-
Anodise	5% Chromic acid in distilled water Apply current, raise to 40V Maintain 40V Raised to 50V Maintain 50V	 10 20 5 5	38-42
Rinse	Clean tap water Distilled water	5 3	ambient ambient
Inspect	Inspect anodic film for uniformity, scratching, burning etc.	-	-
Dry	Warm air specimen dyer	30	-

Phosphoric Acid Anodise

Process Step	Method	Time (minutes)	Temp (C)
Solvent Degrease	Trikolene Bath	15	-
Dry	Warm air specimen dryer	30	-
Alkaline Clean	If plate condition dictates, follow manufacturers instructions	-	-
Rinse	Clean tap water Distilled water	5 3	Ambient Ambient
Inspect	Inspect for water breaks on surface, repeat above steps on rejects	-	-
FPL (CAE) etch	In Chromic acid etch bath	10	68
Rinse	Clean tap water Distilled water	5 3	ambient ambient
Inspect	Inspect for water breaks on surface	-	-
Anodise	Phosphoric acid 9-12% by weight Apply voltage, raise to 10V Switch off	25	21-28
Rinse	Clean tap water Distilled water	5 3	ambient ambient
Inspect	Inspect anodic film for uniformity, scratching, burning etc.	-	-
Dry	Warm air specimen dyer	30	-

Appendix B

Investigation of FM1000 adhesive

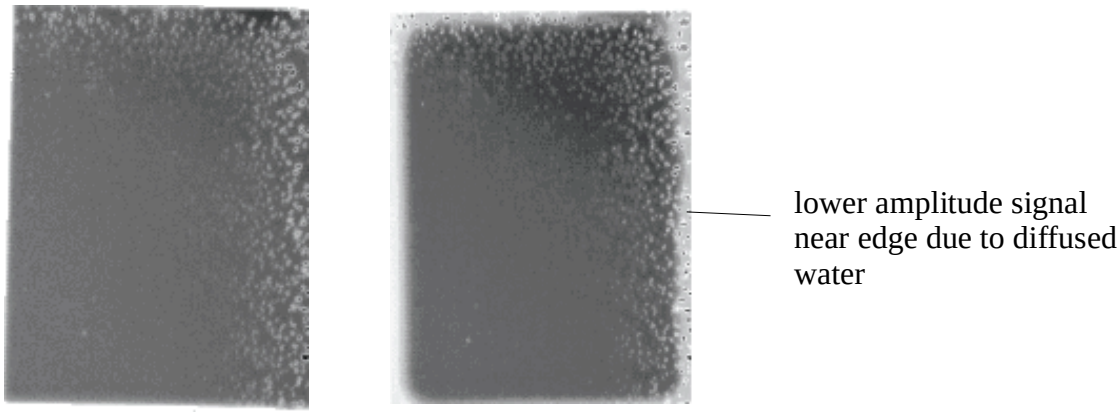

(a) (b)

Figure B.1 2nd interface scan from three-layer PAA specimen with FM1000 adhesive showing (a) initial scan and (b) scan after 5 months in water.

The effect of water uptake in some adhesives results in an increase in attenuation. An example of this is shown in figure 1, which shows the ultrasonic scans taken from a joint made using FM1000 adhesive. FM1000 is a nylon-epoxy adhesive produced by American Cyanamid.. The scan was performed using a 50 MHz focused transducer operating in pulse echo mode at normal incidence. The images were produced by gating the reflection from the back of the bondline. The initial scan shows that there was significant voiding in the adhesive layer. After 5 months in water the scan shown in figure B.1 (b) was obtained. This shows a halo effect around the edge of the specimen where water has diffused into the adhesive. This lighter shade of grey represents a lower signal amplitude showing an increase in the attenuation of the adhesive.

Appendix C

Calculation of fracture toughness from mechanical tests

The raw data that was used to calculate the fracture toughness came from two sources. The displacement data was obtained from the software controlling the Instron® mechanical testing machine in the form of an ASCII file. This gave displacement against load. The mechanical test were performed using a constant rate displacement of 0.5mm/min. The crack length data was obtained from a video recording of the mechanical test, which yielded crack length against video clock time. To combine the two, the ASCII file of load against displacement was imported into a spreadsheet, where the displacement was converted into a time. This was done from knowing the start and end times and displacement of the test. The displacement was then converted into the time that appeared on the video clock, which was also recorded on the tape. From the spreadsheet the corresponding load at anytime during the test was known. The conversion from displacement to time could be verified when

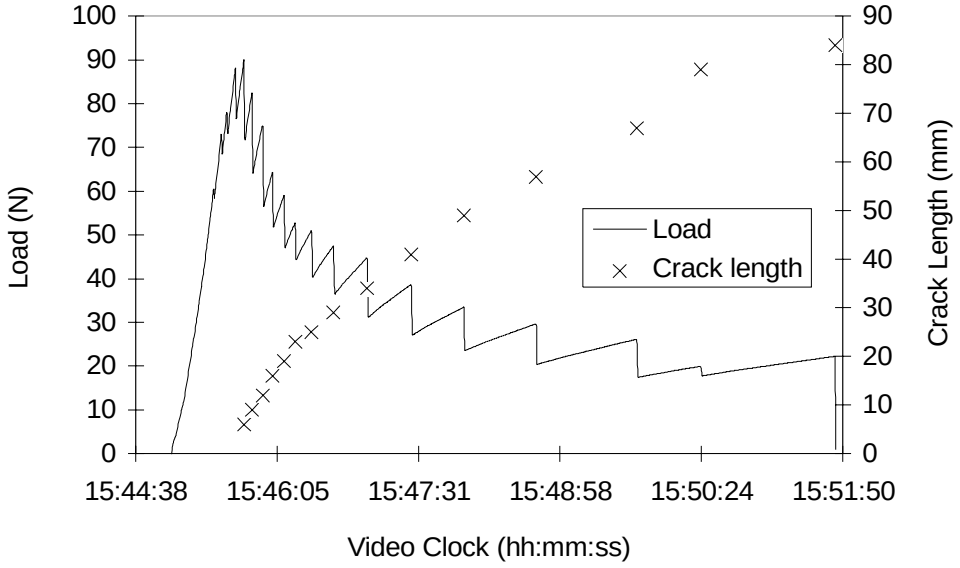

Figure C.1 Load and crack length versus video clock from mechanical test of one strip from a three-layer CAA specimen.

the failure was brittle as there was a clear step change in the load which was due to the crack jumping, and the crack jumping could clearly be seen from the video.

Figure C.1 shows the graph of this results for one strip taken from a three-layer CAA specimen. The accuracy of the calculation of load against time can be seen from this graph, as the crack progressed in a stick-slip manner, which gave many points where the load could be related to the growing of the crack. The crack length data points were taken just prior to the jumping of the crack as determined from the video. It can be seen that these points correspond exactly to steps in the load displacement curve. In this case the load was taken just before the crack jumped, and so a crack initiation value of G_c would subsequently be calculated.

Knowing the beam geometry, the load and the crack length the fracture toughness for each point could then be calculated, as described in Chapter 2, section 2.4, using equation (2.8)

$$G_c = \frac{12a^2P^2\delta}{b^2t^3E}$$

where a is the crack length, P is the load, δ is used to correct for the stiffening effect of the end block, b is the specimen width, t is the thickness of the adherend and E is the Young's modulus of the adherend. For this specimen the following values were used;

δ = 1.8, b = 10 mm, t = 4 mm and E = 70 Gpa and the crack length and load from figure C.1 were used, giving the results shown in figure C.2

The same procedure was used for all of the other strips in a specimen, and these were then displayed together to produce the fracture toughness maps that have been used to display the mechanical test results in this thesis.

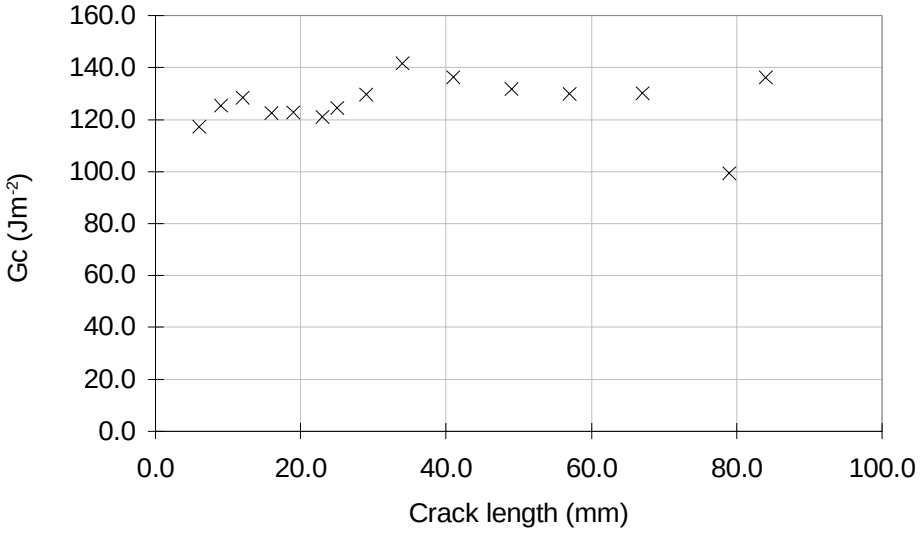

Figure C.2 Fracture toughness for single strip from three-layer CAA specimen.